Gas Condensate Flow around Hydraulically Fractured / Perforated Wells

By

Hojjat Mahdiyar

Submitted for the degree of **Doctor of Philosophy** in

Petroleum Engineering

Heriot-Watt University

Institute of Petroleum Engineering

April 2009

ACADEMIC REGISTRY
Research Thesis Submission

Name*:*	Hojjat Mahdiyar		
School/PGI:	Institut of Petroleum Engineering		
Version: *(i.e. First, Resubmission, Final)*	Final	Degree Sought (Award **and** Subject area)	**PhD** of Petroleum Engineering

Declaration

In accordance with the appropriate regulations I hereby submit my thesis and I declare that:

1) the thesis embodies the results of my own work and has been composed by myself
2) where appropriate, I have made acknowledgement of the work of others and have made reference to work carried out in collaboration with other persons
3) the thesis is the correct version of the thesis for submission and is the same version as any electronic versions submitted*.
4) my thesis for the award referred to, deposited in the Heriot-Watt University Library, should be made available for loan or photocopying and be available via the Institutional Repository, subject to such conditions as the Librarian may require
5) I understand that as a student of the University I am required to abide by the Regulations of the University and to conform to its discipline.

* *Please note that it is the responsibility of the candidate to ensure that the correct version of the thesis is submitted*.

Signature of Candidate*:*		Date:	

Submission

Submitted By *(name in capitals):*	HOJJAT MAHDIYAR
Signature of Individual Submitting:	
Date Submitted:	

For Completion in Academic Registry

Received in the Academic Registry by *(name in capitals):*			
Method of Submission *(Handed in to Academic Registry; posted through internal/external mail):*			
*E-thesis Submitted (**mandatory for final theses from January 2009**)*			
Signature:		Date:	

ABSTRACT

Gas condensate flow, which is very different from the conventional two-phase (oil and gas) flow, shows more complicated behaviour around the wellbore owing to condensate buildup and the different velocity effects on relative permeability (k_r) of these low IFT fluid systems. This is especially true for complex wellbore completions, such as hydraulically fractured or perforated wells.

This research programme has two separate parts. The first part is about gas condensate flow around hydraulically fractured wells (HFWs). In this part of the study, different in-house simulators have been developed by the author. These simulators account for the changes in fluid properties with pressure, phase change, coupling (increase in k_r as IFT decreases or velocity increases) and inertia (decrease in k_r when velocity increases) when it is required to do so. The simulators have been used to investigate the effect of different important geometrical and flow parameters on the performance of a HFW. The new developed formulae for accurate estimation of effective fracture conductivity, fracture skin factors (mechanical and flow) and effective wellbore radius are the main practical outcomes of this part of the study.

The author has also provided a new convenient method for the optimization of fracture dimensions for a given fracture volume, in gas condensate reservoirs.

The second part of this research is about the study of gas condensate flow around perforated wells. Here the previously developed simulators by the Gas Condensate Research group have been used to develop a new method for estimation of mechanical perforation skin. The introduction of a method for calculation of effective wellbore radius of a perforated well by which the flow skin is negligible is another important result of this part.

The new formulae introduced in this work can be used as a useful tool for estimation of well productivity/injectivity. They are also very useful in reservoir simulation, because having the effective wellbore radius for a complex wellbore geometry- such as a perforated well or hydraulically fractured well - provides an opportunity to define a simple open-hole system instead of the real wellbore. This eliminates the need for a costly and cumbersome fine grid exercise, which otherwise would be required to capture accurately the variation of flow parameters around these types of wellbores.

To: ***my mother, my wife***

and
the lights of my life,

Hadis, Hasti and Darya

Acknowledgements

I wish to express my sincere appreciation to my supervisor, Dr Mahmoud Jamiolahmady, for his technical guidance and valuable comments during this research program. This work would certainly not have been completed without his professional support and encouragement.

I would especially like to pay my profound respects to my former supervisor, the late Professor Ali Danesh, who sadly died in September 2007. I believe he did not teach me different ideas, but he taught me how to create a new idea. It was an honour for me to be his last PhD student. May God bless him.

My special thanks are due to Professor Dabir Tehrani and my second supervisor, Dr Mehran Sohrabi, for their great support and valuable comments.

I am privileged to be a member of the Gas Condensate Recovery Project Team at Heriot-Watt University. Hence the contribution of all members in this project is appreciated.

Thanks go my colleagues Mrs Panteha Ghahri, Mr Masoud Riazi, Mr Alireza Emadi and Mr Yousef Rafiei and all other my dear friends in Heriot Watt University.

The financial support of the National Iranian Gas Company and Ministry of Science, Research and Technology through the award of their full scholarship to conduct this work is sincerely acknowledged.

My final and especial deepest gratitude is due to my mother and my wife for their outstanding kindness and patience.

Table of Contents

List of Figures

List of Tables

List of Symbols

Nomenclature

A	a parameter, showing the effect of fracture penetration ratio on effective wellbore radius at SS.
A_{eff}	effective area (m^2)
B	a parameter, showing the effect of fracture penetration ratio on effective wellbore radius at PSS.
B_g	gas formation volume factor
C_{1-7}	Constants
C_1	Methane
C_4	Butane
C_{10}	Decane
C_{fD}	dimensionless absolute fracture conductivity
C_{fD-eff}	dimensionless effective fracture conductivity
D	D-factor (s/m^3).
f_{1-5}	function
f_A	function of A
f_B	function of B
F_{ND}	non-Darcy function
F_{SS}	steady state function
F_{PSS}	pseudo-steady state function
$g(\lambda)$	geometrical function, defined in the paper of Meyer and Jacot (2005)
h	formation thickness (m)
h_p	the distance between two successive perforation (m)
I_X	Fracture penetration ratio
J_D	Dimensionless productivity index
k	absolute matrix permeability (mD)
$\bar{\bar{k}}$	permeability tensor
k_d	absolute damaged matrix permeability (mD)

k_f	absolute fracture permeability (mD)
$k_{f,ck}$	absolute choked zone permeability (mD)
k_h	horizontal permeability (mD)
k_v	vertical permeability (mD)
k_r	relative permeability(mD)
L_p	perforation length (m)
$\dot{m}$	mass flow rate (kg/s)
n	number of data points
N	perforation density (Shot per meter)
N_C	capillary number
N_G	geometrical dimensionless number
N_K	permeability dimensionless number
N_p	Propped number
NY	number of block rows
P	Pressure (pa)
PR	productivity Ratio
q_w	volumetric production rate at bottomhole conditions (m^3/s)
Q	volumetric production rate at standard conditions (Sm^3/s)
Q_D	Dimensionless flow constant
ref	reference
R	flow resistance ($Pa.s/m^3$)
RX	flow resistance at x-direction ($Pa.s/m^3$)
RY	flow resistance at y-direction ($Pa.s/m^3$)
Re	Reynolds number
r	Radius (m)
r_w'	effective wellbore radius (m)
S	skin factor
S_F	flow skin
S_G	geometrical skin
S_k	permeability skin
S_M	mechanical skin
$S_{H,V,wb}$	Horizontal, vertical and wellbore skin, defined in Karakas-Tariq method
S_p	perforation skin
S`	pseudo skin factor

S'_f	pseudo fracture skin factor
S_{ck}	Choked skin
S_{fD}	face damage skin
V_f	facture volume per unit height of the fracture (m/s)
$\|v\|$ *or* v	velocity (scalar value) (m/s)
$\vec{v}$	velocity vector (m/s)
x_j	mass fraction of component j in liquid phase
x_{ck}	the length of choked zone in each fracture wing (m)
x_e	Half length of the square reservoir (m)
x_f	Half length of the fracture (m)
y_j	mass fraction of component j in vapour phase
w_f	fracture width (m)
w_d	face damage thickness (m)
z_j	mass fraction of component j in the mixture of liquid and vapour
Z_m	The value predicted from modelling
Z_e	The value estimated by a proposed formula

Greek Letters:

γ_g	gas specific gravity
δ	A parameter defined in Equations 3.36 and 3.37
λ	aspect ratio of drainage area
λ_{av}	average distance covered by the fluid in the perforated zone
μ	Viscosity (Pa.s)
M	relative mass mobility (s/m^2)
MR	relative mass mobility ratio
β	inertia factor (scalar value) (m^{-1})
$\overline{\overline{\beta}}$	inertia factor (tensor) (m^{-1})
φ	porosity
ρ	density (kg/m^3)
σ	weighting factor
θ	phasing angle (degree)
ξ_∞	the ratio of fracture half length to the effective wellbore radius of the fractured well with infinite fracture conductivity.
Ψ	pseudo pressure ($kg/(m^3.s)$)

Subscript

av	average
b	base
c	condensate
cr	crushed zone
d	damage
D	dimensionless
e	exterior
eq	equivalent
eff	effective
f	fracture
fz	fractured zone
g	gas
h	horizontal
HFSZ	horizontal flow sub-zone
m	matrix
mz	unfractured/unperforated zone
OH	open-hole
opt	optimum
p	perforation
perf	perforated
r	relative
s	standard
t	total
v	vertical
VFSZ	vertical flow sub-zone
w	wellbore
wb	wellblock

Abbreviations

AAD%	Average Absolute Deviation (percentage)
1D	one dimensional

2D	two dimensional
3D	three dimensional
OH	Open-Hole
EOH	Equivalent Open-Hole
EOS	Equation Of State
GTR	Gas Total Ratio (volumetric fractional flow of gas)
IFTR	Interfacial Tension Ratio
HFW	Hydraulically Fractured Well
HFWS	Hydraulically Fractured Well System
HW	Heriot-Watt
IFT	Interfacial Tension
IPE	Institute of Petroleum Engineering
PR	productivity Ratio
PR3	3 parameter Peng Robinson EOS
PSS	Pseudo-steady state
SEE	Standard Error of Estimate
SS	Steady state
UFD	Universal Fracture Design

Chapter 1 Introduction

The negative impact of condensate build-up, when bottomhole pressure drops below the dew point pressure, in addition to the dependency of gas condensate relative permeability to velocity and interfacial tension makes gas condensate flow around the wellbore a complex subject. This fact, in addition to the importance of the accurate estimation of well productivity, has made *'gas condensate flow around the wellbore'* an attractive subject for many investigators (such as: Danesh *et al.,* 2004, Jamiolahmady *et al.,* 2005, Saleh and Stewart, 1996 and Wang *et al.*, 2000).

Normally in gas or gas condensate reservoirs around the wellbore, as a result of the decrease in flow area, velocity is too high. As a result the simple Darcy law, where pressure drop is linearly proportional to superficial velocity, can not describe the flow. In the absence of the gravity effect in single phase gas flow systems, the competition between inertia and viscous force controls the flow regime, whilst in gas condensate systems the complex competition between viscous, inertia and capillary force presents different velocity effects.

The description of unique characteristics of gas condensate flow around the wellbore becomes more difficult to capture around complex flow systems such as perforated well completions or hydraulically fractured wells. In perforated wells, 3-dimensional flow geometry makes the flow complex. In hydraulically fractured wells, the presence of very different flow conductivity in the fracture and in the matrix is the source of the flow complexity.

The investigation of gas condensate flow around hydraulically fractured wells and

perforated wells has been defined as the main purpose of this research programme. The major practical purpose is to introduce methods of defining equivalent open-hole systems of these types of wellbores in gas condensate reservoirs.

The term 'Equivalent Open-Hole' (EOH) means a homogenous open-hole well model which, under a certain drawdown, provides the same production as the real wellbore completion.

One of the main applications of defining EOH system is in reservoir simulations. When modeling a reservoir, it is almost impractical to use very fine grid blocks to catch up the significant variations in flow parameters around each wellbore. For instance, the diameter of perforations or the thickness of a hydraulic fracture is in the range of inches, and using this type of block dimension in a reservoir simulator is too cumbersome.

On the other hand, the accurate estimation of the production/injection rate of each well is one of the main purposes of reservoir simulation, which is strongly dependent on the accurate definition of each wellbore in the model.

Therefore many studies have been done so far in order to formulate skin factor or effective wellbore radius of different types of wellbore completions. These parameters - in addition to their application for estimation of well productivity - can be used as a useful tool for a reservoir engineer to model a simple open-hole well instead of the complex real wellbore completion system.

There are some methods available in the literature for estimation of perforation skin or effective wellbore radius of a hydraulically fractured well. However, to the best of the author's knowledge, they are applicable only for single-phase Darcy flow systems, whilst for gas condensate flow systems; the well performance could be totally different as the result of condensate build-up and complex velocity effects.

Thus in this study, attempts have been made to develop new methods for defining the EOH system of a hydraulically fractured well or perforated well in gas condensate reservoirs.

In the development of these methods the following important points have been considered:

1- The methods should be applicable for both single-phase (gas) flow and two-phase (gas condensate) flow systems. In a gas field, switching from single-phase to two-phase can be done simply as the result of dropping the pressure below the dew point. Thus the developed method should have this generality to be applicable for both cases.

2- The method should be dependent on the available parameters. In the petroleum industry, preparing data can be very expensive. Attempts were made, therefore, to ensure that the developed formulae do not need data that are either unavailable or difficult to obtain.

3- The formulae should be developed based on the physics of flow. In the development of the formulae, the author has tried to develop the methods and their dimensionless numbers or correlations based on a sound physical approach. Although, there are some coefficients or exponents that have been adjusted based on matching the results of numerical simulator and the developed formulae.

In this manuscript before presenting the main discussions some of the important basic concepts about gas condensate fluid system, hydraulic fracturing and perforation will be discussed very briefly in Chapter 2. The chapter starts with the discussion about the condensate build-up around a producer well. Then the velocity effects on relative permeability will be explained, which will be followed by a short discussion about a generalized relative permeability correlation which expresses the combined effect of coupling (i.e. the increase in relative permeability by an increase in velocity or a decrease in IFT) and inertia (i.e. the decrease in relative permeability by an increase in velocity) with universal parameters. Brief descriptions of hydraulically fractured wells and perforated wells will be provided in the last two sections of this chapter.

This research programme can be separated into two parts. The first part, which is the bigger part, is about gas condensate flow around hydraulically fractured wells. The second part is about the study of gas condensate flow around perforated wells.

Hydraulic Fracturing is one of the most widely used and accepted methods for enhancing well performance. Figure 1.1 schematically shows a hydraulically fractured well. The fracture has two symmetrical wings that have penetrated along the maximum horizontal stress. Proppants are used to withstand the stress and prevent complete fracture closure.

Chapter 3 is aimed at the investigation of gas condensate flow around the hydraulically fractured wells, including the impact of condensate liquid drop-out, coupling and inertia. One of the main outcomes of this exercise is the development of a method for calculation of the effective wellbore radius for a hydraulically fractured well (HFW) in a gas condensate reservoir.

Since large data banks are required to investigate the effects of pertinent parameters on the well performance and develop the formulae covering a wide range of variation of parameters, the author has developed and used his own in-house simulators.

The basic theory, governing equations and numerical methods of the in-house simulator, is discussed in section 3.2.

In section 3.3, single-phase Darcy flow around hydraulically fractured wells is studied. First the impact of important flow parameters, i.e. fracture conductivity and fracture penetration ratio on the flow and pressure distribution around the wellbore, is investigated. One major part of this section is devoted to a discussion on the differences between the performance of an HFW operating at steady state or pseudo-steady state conditions. The main outcomes of Section 3.3 are the formulations of effective wellbore radius at SS and PSS conditions. In the last subsection, the effects of fracture face damage and choked damage on the HFW performance will also be investigated. The result of this latter part is the introduction of two new correlations for more accurate estimation of these two damaged skins.

Inertial effect inside the fracture can decrease fracture conductivity significantly. There are several formulae available for predicting the extent of this effect. Although all investigators are in agreement on the significant negative impact of inertial effect on the HFW performance, there is not such agreement on the proposed formulae expressing this effect. This subject is investigated in detail in section 3.4, to clarify these reports and identify the correlation that can be used for accurate estimation of this effect.

Two-phase flow can decrease the conductivity in both matrix and fracture, albeit to a different extent. To the best of the author's knowledge, in all the developed methods for estimation of the productivity of a HFW in gas condensate reservoirs, two-phase flow in the fracture has been neglected, and condensate build-up around the fracture has been treated as a fracture face damage for the single-phase flow. The weak points of this approach will be made clear in Section 3.5.

The variation of condensate saturation and volumetric fractional flow of gas (GTR) around the wellbore, as well as the variation of relative permeability in both fracture and matrix, is investigated in Section 3.5 as well. Subsequently the author will propose a new method for the estimation of effective fracture conductivity in gas condensate systems.

The main practical outcomes of Sections 3.2-3.5 are the development of the formula for calculation of effective fracture conductivity and also the formulation of wellbore radius at steady state as well as pseudo-steady state.

The results of an exercise conducted to verify the integrity of these formulations for different cores, fluids and operating pressures will be presented in section 3.6. In this section, the method will be verified for both steady state and pseudo-steady state conditions. It will also be shown that the use of these correlations can be extended to transient state conditions. This chapter ends with a summary of conclusions of this exercise.

An optimised design for hydraulic fracturing is of great importance, especially with the growing demand for this method as a means for production enhancement from tight gas reservoir. The first optimum fracture design (OFD) approach, which maximizes well productivity for a certain fracture volume, was introduced for single-phase Darcy flow

systems by Prats in 1960. This method, which was later modified and presented in the form of Unified Fractured Design (UFD) charts by other investigators, is widely used in the petroleum industry, even for gas condensate systems. Recently some methodologies have been proposed; these consider the two-phase region around the fracture as a damage zone with reduced permeability. In Chapter 4 it will be explained that the results of these very difficult methods are not reliable. They also require information which is not readily available, in particular concerning pressure profile (the two-phase boundary) around the wellbore.

Finding the optimum fracture half length, in the presence of gas condensate flow complexities, is the main purpose of chapter 4. In this chapter, the developed formulae in chapter 3 will be utilized to find the optimum geometry of a Hydraulic Fracture (HF) with a given volume. In Section 4.3, two sets of formulae for estimation of optimum fracture conductivity and optimum fracture length for SS and PSS will be developed. These formulae, which are applicable for gas condensate square reservoirs, are developed mathematically, based on the maximization of an effective wellbore radius for a fixed fracture volume.

The developed formulae will be verified in Section 4.4, where several different illustrations confirm their applicability for finding an optimum fracture design at different operating conditions.

The second part of this study is about the investigation of gas condensate flow around perforated wells. The Gas Condensate Recovery group at Heriot-Watt University had started the investigation of flow around perforated wells four years before the start of this PhD programme. The developed 3D perforated well simulator and some valuable results about gas condensate flow around the perforated rock and perforated wells were the results of those studies. The author of this study, taking advantage of previous results, is trying to complete the study, and is suggesting new ideas to introduce practical approaches for defining the equivalent open-hole system of a perforated well as described in chapter 5.

The main purpose of this chapter is the development of a convenient method for defining the Equivalent Open-Hole (EOH) system of a perforated well in gas condensate flow systems: single-phase or two-phase. This method could be adopted as a

useful tool in a commercial reservoir simulator (like ECLIPSE) as well as well performance simulators (like INFLOW software) to calculate well-flow without the need of the simulation of complex flow around perforations.

Darcy flow around perforated wells is the subject of Section 5.3. In this section, pseudo perforation skin, based on an open-hole at the tip of perforations which can represent flow resistance in the perforated zone, will be defined. As this parameter presents a physically meaningful parameter, i.e. flow resistance, correlating that to the other pertinent parameters is a more straightforward task, as described in this section.

Single phase non-Darcy flow around perforated wells will be discussed in Section 5.4. The effects of production rate and geometrical parameters on the well performance are investigated in this section. A similar investigation for gas condensate systems has been done by Jamiolahmady and his co-authors (2006 and 2007). The important conclusions of these papers will be provided in Section 5.5.

In Section 5.6, a new method will be developed for defining an EOH system in which flow behaviour is very close to that in the real system. The main advantage of this method is that flow skin is negligible and there is no need for its calculation.

One of the main approaches for taking the inertial effect into account is the use of the D-factor. This method could be used for open-hole completions only. However, in practice, it is mistakenly used for perforated wells, which can cause major errors in the estimation of well productivity. In Section 5.7, how the D-factor of perforated wells in single-phase flow systems should be calculated will be shown, so that the non-Darcy effect, and consequently well-productivity, can be calculated correctly using this approach.

The last chapter contains the main conclusions of this study and the author's recommendations for further investigations.

REFERENCES

Danesh, A, Tehrani, D.H., Henderson G.D., Jamiolahmady, M., Ataei, R. and Carvajal, G.: Gas condensate recovery studies: Flow in perforated zone and fractures, Proceedings of 25th IEA Annual Workshop & Symposium on Enhanced Oil Recovery, Stavanger, Norway. September 2004.

Jamiolahmady, M., Danesh, A., Rezaei, A., Ataei, R. and Sohrabi, M.: "Calculation of productivity of a gas condensate well: application of skin with rate dependent pseudo-pressure" SPE 94718, presented at Proceedings of the SPE European Formation Damage Conference, May 2005.

Prats M.: "Effect of Vertical Fractures on Reservoir Behaviour-Incompressible Fluid Case", SPE Journal, **222**, pp. 105-118, June 1961.

Saleh, A.M., and Stewart, G.: "New approach towards understanding of near wellbore behaviour of perforated completions", SPE 36866, presented at SPE European Petroleum Conference, Milan, Italy, 1996.

Wang X., Indicate S., Valdo P.P and Economides, M. J.: "Production Impairment and Purpose Built Design of Hydraulic Fracture in Gas Condensate Reservoirs," SPE 64749, presented at International Oil and Gas Conference and Exhibition, Beijing, China, November 2000.

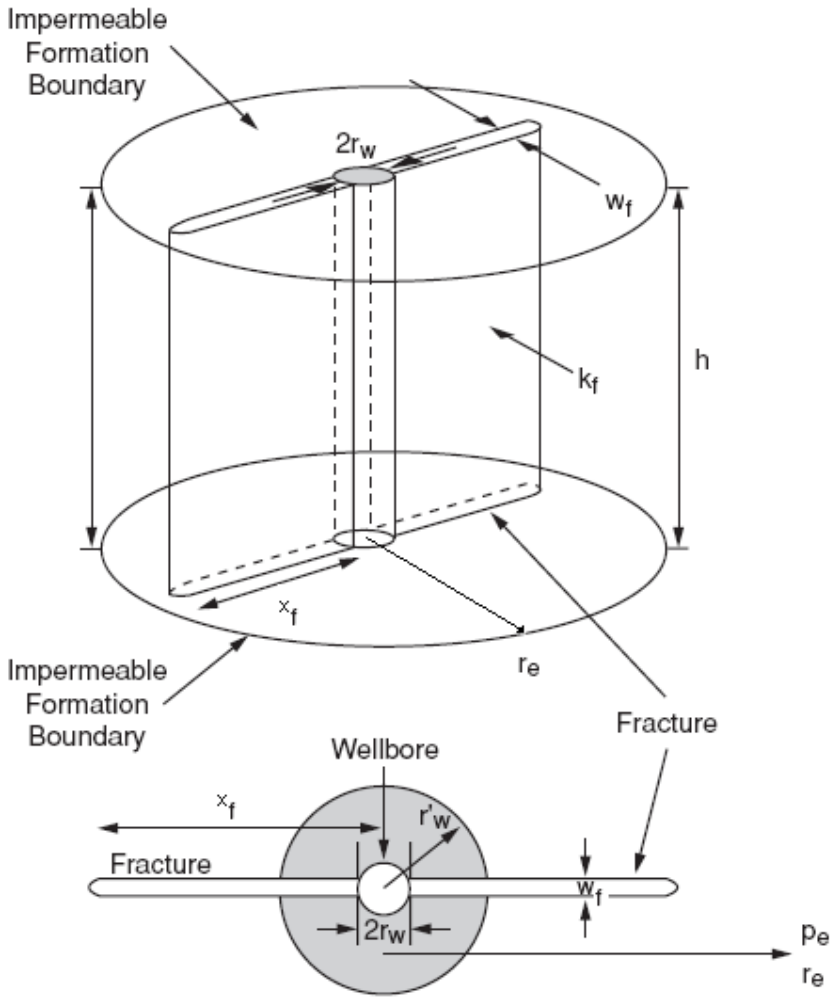

Figure 1.1: A hydraulically fractured well in the centre of a cylindrical drainage area, (Lecture Note of Production Technology II published by HW University (2002)).

Chapter 2 Gas Condensate Reservoirs

2.1 Introduction

The fluid and flow behaviour of gas condensate systems are fundamentally different from those of conventional gas oil system. According to production characteristics, a reservoir is considered as a gas condensate reservoir when the Gas Oil Ratio (GOR) of the production is between 8,000 and 70,000 scf/bbl. The produced liquid (condensate) has an API of up to 60 and its appearance is water white or slightly coloured (Cronquist, 1973).

Figure 2.1 shows a typical phase envelope of a hydrocarbon mixture. Between the bubble-point curve at which the first vapour bubble is formed, and dew-point curve at which the first liquid drop is produced, the hydrocarbon fluid is in the two phase region. The lines of constant liquid percent meet at a critical point, at which a phase boundary ceases to exist (Danesh, 1998). In Figure 2.1, the critical point is shown with C.

Cricondentherm, the maximum temperature at which two phases can exist, is also shown. Between the critical temperature and cicondentherm and below the dew point pressure, there is a retrograde region where isothermal pressure reduction results in condensation and a larger liquid percentage. This zone is the called retrograde condensation region (Danesh, 1998).

When the reservoir temperature is in the between of the critical temperature and cricondentherm, then as long as the pressure amongst the whole reservoir is above the dew point pressure there is only single phase gas within the reservoir. However, when the

pressure falls below the dew point, there are both gas and condensate in the reservoir. Figure 2.2 shows schematically a pressure profile around a producing well. The constant fluid dew point pressure is also shown, based on the assumption of constant composition and temperature inside the reservoir. In this figure, the pressure at the exterior boundary is kept constant and above the dew point, where there is only a single phase of dry gas. However, owing to flow, there is a pressure drop towards the wellbore which results in pressure decline below the dew point. In the region where pressure is less than the dew point pressure, there are both gas and condensate. Thus in this example there are two regions in the reservoir: single-phase region and two-phase region. The presence of condensate leads to a significant drop in the well productivity. The impact of critical condensate saturation, above which the condensate is mobile, also has a significant impact on the flow calculation in this region.

There is also a possibility that the whole reservoir pressure has fallen below the dew point pressure. It is also likely that the pressure drops further, entering the vaporization zone (the zone below the condensation zone in Figure 2.1) at which further declining pressure results in more vaporization.

Therefore, the performance of a gas condensate reservoir, in addition to other important parameters such as drawdown, rock and fluid property is also dependent on the pressure profile along the drainage area.

The relative permeability of these low IFT systems, are also a function of interfacial tension and velocity. This further complicates the flow behaviour of gas condensate reservoirs compared to conventional gas oil system. In ordinary gas or oil reservoirs, increasing velocity decreases effective permeability owing to the high velocity inertial effect; however, in gas condensate reservoirs, an increase in velocity can increase relative permeability because of a coupling effect. At high velocities gas condensate relative permeability is affected by both coupling and inertia simultaneously (Henderson *et al.*, 2001).

In this chapter, some of the important basic points about gas condensate reservoirs which are related to the main topic of this study, available in the literature or the reports of the Gas Condensate Research Group at Heriot-Watt University, will be discussed very briefly.

The discussion is concerned first with the condensate buildup around a producer well. Then the velocity effects on relative permeability will be explained, and this will be followed by a short discussion about a generalized relative permeability correlation which expresses the combined effect of coupling and inertia with universal parameters. Brief descriptions of hydraulically fractured wells and perforated wells will come in Sections 2.5 and 2.6.

2.2 Condensate build-up

In Figure 2.2, before the start of production, pressure within the whole reservoir is P_i greater than the dew point pressure; thus, in addition to connate water, there is only a gas phase within the pores. After the start of constant-rate production, bottomhole flowing pressure starts declining, and when it drops below the dew point condensate starts forming. The studies of the Gas Condensate Research Group at Heriot-Watt University have proved that critical condensate saturation is around zero: i.e. condensate flows even at very low condensate saturations (Danesh *et al.*, 1991). However, at low condensate saturations, the condensate relative permeability is very much smaller than the gas relative permeability; therefore the majority of the formed condensate stays inside the pore. The accumulation of condensate carries on and condensate saturation increases until at each location the total rate of condensate generation plus inflow to that location becomes equal to the rate of condensate outflow from that location.

Afterwards, the condensate saturation does not change with time but remains steady, although it could be very different from the condensate fractional flow. At steady state, the flow composition becomes constant in the whole drainage area of the producing well and equal to the production composition. However, the flow composition could be very different from the total composition of local residual fluid inside the pore.

The time required to reach the steady state depends on many items such as fluid and rock properties, production rate and pressure distribution. For very tight cores, this time could be very long as the laboratory studies at HW University show that even for a small cylindrical core (height=30 cm, diameter=5 cm, k=0.1mD) the required time to reach steady state is about 3 weeks.

During the condensate build-up, gas relative permeability decreases continuously until achieving the steady state when at a certain pressure condensate saturation and thus its relative permeability reaches the maximum possible value, and gas relative permeability is at its minimum value.

In gas condensate reservoirs, velocity (Danesh *et al.,* 1994) and interfacial tension (Bardon 1980) can have significant effects on gas relative permeability. Normally the relative permeability is measured in the laboratory at low velocity and high IFT. This curve referred to as base relative permeability. However, it could be very different from the true relative permeability affected by velocity and interfacial tension. Predicting relative permeability from base relative permeability, velocity and IFT is an important issue, which will be discussed briefly in Section 2.4.

2.3 Velocity Effects in Gas Condensate Reservoirs

Darcy's law states that the pressure drop inside the porous media varies linearly with fluid velocity. That is to say, the viscous force, which is linearly proportional to velocity, controls fluid energy loss.

However, with increasing velocity in addition to viscous force, other forces become important. In other words, if for simplicity the effect of gravity force is ignored, the inertia and/or capillary forces could play key roles and control the flow behaviour.

The subsequent acceleration and deceleration of fluid through the tortuous pores, with variable cross section, provides an extra energy loss which is called the inertial effect. The impact of chaotic motion of fluid particles could also be a contributing element to inertia. According to the Forchheimer equation, the inertial effect is proportional to the velocity squared (Forchheimer, 1914).

The competition between inertia and viscous forces can be characterized by the Reynolds number, defined in Section 3.3, which is the ratio of the inertial to viscous forces.

For single phase systems, based on the Forchheimer equation, when the Reynolds number is about 0.01, the inertial effect can reduce the effective permeability only by

1%; thus at Reynolds number less than 0.01, the inertial effect can be neglected safely (see Section 3.3).

Danesh et al. (1994) were first to report the increase in relative permeability of condensing systems as the result of an increase in velocity by conducting steady-state relative permeability measurements at realistic near wellbore condition. The increase in relative permeability of such low IFT systems as velocity increases and/or IFT decreases, known as the coupling effect, has been attributed to the simultaneous coupled flow of the gas and condensate phases with intermittent opening and closure of gas passage by the condensate at the pore level (Jamiolahmady, 2000). The increase in velocity, especially at high condensate saturations, can keep the passage of gas open for longer periods.

In order to gain a better understanding of the nature of gas condensate flow and prevailing mechanisms, Jamiolahmady (2000) followed a combined experimental (flow visualisation experiments using micro-models) and a theoretical study at the pore level. In this study the observed simultaneous two-phase flow of gas and condensate with intermittent opening and closure of gas passage by condensate occurring within a single pore was simulated. The effect of multiple pores was included for this cyclic flow pattern through a network modelling exercise (Jamiolahmady *et al.,* 2003).

Figures 2.3-6 show the effect of velocity on gas relative permeability of a typical core (Gas Condensate Research Group, 1999-2002 Final Report).

In Figure 2.4, different curves of gas relative permeability versus condensate saturation at several low velocities are shown. In this figure, the improvement of the relative permeability as the result of the coupling effect - which is more pronounced at high condensate saturation - is clearly shown.

With further velocity increases, shown in Figures 2.5 and 2.6, the inertial effect also becomes dominant. Inertia has its maximum effect for single phase systems at zero condensate saturation, and it becomes less effective with the increase in condensate saturation. At a certain level of condensate saturation (about 11% in Figure 2.5), there is no net velocity effect, and after that the coupling improvement effect outweighs the inertial effect.

The velocity effect in gas condensate systems is a complex function of core type, fluid properties and flow rate; thus there is not a straightforward formula for identifying the flow regime or estimation of the dominancy of inertia or coupling effect. However, in general it can be said that the coupling effect is more pronounced at low to moderate velocities - especially at higher condensate saturations - whilst the inertial effect is dominant at high velocities and its effect is more intensive at lower condensate saturations, Figures 2.3-2.6.

2.4 Gas Condensate Relative Permeability

Usually relative permeability is measured in the laboratory at steady state, very low velocity and high interfacial tension, The result is called the base relative permeability. However, in practice and especially near the wellbore, fluid and flow properties could be very different from those in the laboratory conditions. Thus, the estimation of the relative permeability at the local reservoir conditions using base relative permeability as measured in the laboratory has been one of the most important subjects in gas condensate studies.

There are several empirical correlations available in the literature and commercial simulators accounting for positive coupling effect as a function of capillary number (ratio of viscous over capillary forces). Here it is not the intention to go through the details of these correlations as it is a vast subject and beyond the scope of this summarized chapter. It is sufficient to say that all the available correlations, except that recently developed by Jamiolahmady et al. (2006), express the effect of coupling and inertia separately and require core specific constants. This latter requirement means that expensive relative permeability measurements are needed for the core under study to estimate its relative permeability accurately using the old version correlations.

The generalized relative permeability correlation developed by Jamiolahmady *et al.* (2006) is based on gas total ratio (GTR). GTR which is also called fractional flow of gas is the volumetric ratio of gas flow over total flow. In the generalized correlation, first the base gas relative permeability curve, measured in the laboratory, and the miscible relative permeability, a linear function of GTR, are corrected for the effect of inertia. Then the relative permeability is interpolated between the corrected base and miscible relative permeability curves. The generalized interpolating parameter of this method has been correlated to commonly available petrophysical rock properties. This is one of the

main advantages of this correlation; i.e. it does not require specific core exponents. Moreover, condensate relative permeability is simply related to gas relative permeability, and there is no need for an extra correlation for its determination.

The estimation of the inertial effect based on a single-phase non-Darcy factor is another advantage of this correlation. In old versions of relative permeability correlations, inertia has not been included in relative permeability and it must be calculated individually using a two-phase non-Darcy factor. It is very difficult to measure this parameter accurately in the laboratory.

Jamiolahmady and his co-authors in another study showed that the estimation of relative permeability would be more accurate if the independent variable is the gas total relative permeability ratio: $k_{rgtr} = k_{rg} / \left(k_{rg} + k_{rc}\right)$ (Gas Condensate Research Group 2002-2005 Final Report). This modified version of generalized relative permeability correlation is due for implementation in ECLIPSE 2009 release.

2.5 Hydraulically Fractured Wells

Figure 2.7 schematically shows a hydraulically fractured well in the centre of a cylindrical drainage area. In the lecture note of Production Technology published by HW University (2002) it is stated that 'Propped hydraulic fracturing consists of pumping a viscous fluid at a sufficiently high pressure into the completion interval so that a two winged, hydraulic fractured is formed. This fracture is then filled with a high conductivity, proppant which holds the fracture open (maintains a high conductivity path to the wellbore) after the treatment is finished. The propped fracture can have a width between 5mm and 35mm and a length of 100m or more, depending on the design technique employed and the size of treatment. Propped hydraulic fracturing is aimed at raising the well productivity by increasing the effective wellbore radius for wells completed in low permeability carbonate or clastic formations'.

Now the question is *what is the effective wellbore radius of a hydraulically fractured well?* This has been the subject of many studies so far, because the formula for effective wellbore radius can be a very useful tool for a production or reservoir engineer.

In production engineering estimation of well-productivity is dependent on the effective wellbore radius and in reservoir simulation knowing the effective wellbore radius provides this opportunity to model a simple open-hole system instead of the complex real wellbore system, which needs very fine grid blocks.

Obviously effective wellbore radius of a hydraulically fractured well depends on the characteristics of the fracture and reservoir as well as the flow properties. As mentioned in the previous sections, gas condensate flow is more complex than the conventional oil and gas flow systems. This is especially true for flow around hydraulically fractured wells where the significant difference between the conductivity in matrix and fracture provides different velocity effects in them. The first part of this research program is about the study of gas condensate flow around a hydraulically fractured well and the formulation of effective wellbore radius, as described in Chapter 3.

Another important question in this part is about the optimization of fracture geometry. That is, for a given propped volume different fracture length-width combinations can be considered. Selecting a longer fracture or a wider fracture has significant impact on the efficiency of a HFW with a certain fracture volume. In Darcy flow system, there are well established techniques for optimization of fracture dimensions which maximizes well productivity or *provides the maximum effective wellbore radius.* However as will be discussed in Chapter 4 there is little information for optimization of fracture design in gas condensate systems whereby the flow is complicated due to coupling and inertial effect. This will be addressed in Chapter 4.

2.6 Perforated Wells

Figure 2.8 schematically shows a perforated well. In the lecture note of Production Technology published by HW University (2002) perforating operation has been explained as 'In the majority of completions, once the reservoir has been drilled, producing casing or a liner is run into the well and cemented in place. To provide the communication path between the reservoir and the wellbore, it will be necessary to produce holes through the wall of the casing, the cement sheath and the penetration into the formation. This is accomplished by a technique called perforating. The basic operation requires that a series of explosive charges are lowered into the well either on an electric conductor wireline cable, or on tubing or drillstring, and when the charges

are located at the required depth, they are detonated to produce a series of perforations through the wall of the casing and the cement sheath. Since the perforations will hopefully provide the only communication between the reservoir and wellbore, it is necessary to carefully design and execute the perforating operation, to provide the required degree of reservoir depletion control and maximize well productivity/injectivity.'

Here again there is an important question about the estimation of well productivity/infectivity i.e. *what is the productivity/injectivity of a perforated well?*

This question is more difficult for gas condensate reservoirs where complexity of the flow geometry is combined with the complexity of the gas condensate flow characteristics. It is the subject of the second part of this research which will be discussed in Chapter 5.

References

Bardon Charles, D.G. Longeron: "Influence of Very Low Interfacial Tensions on Relative Permeability" SPE 7609, SPE Journal, **20** (5), pp. 391-401, Oct-1980.

Cronquist, C, "Dimensionless PVT Behaviour of Gulf Coast Reservoir Oils", JPT, May 1975, 538.

Danesh A.: PVT and phase behaviour of petroleum reservoir fluids, Elsevier Science B.V., Amsterdam, Netherland, 1998.

Danesh, A., Henderson, G.D., Peden, J.M.: "Experimental investigation of critical condensate saturation and its dependence on connate saturation in water wet rocks" SPE 19695, SPE Journal of Reservoir Engineering, pp.336-342, Aug. 1991.

Danesh, A., Khazam, M., Henderson, G.D., Tehrani, D.H., and Peden, J.M.,: "Gas condensate recovery studies" presented at Proceedings of the UK DTI Improved Oil Recovery and Research Dissemination Seminar, London, June 1994.

Forchheimer, P.: Hydraulik, Chapter15, pp. 116-8, Leipzik and Berlin, 1914.

Gas Condensate Recovery Project (1999-2002) Final Report, IPE, Heriot Watt University, UK, 2002.

Gas Condensate Recovery Project (2002-2005) Final Report, IPE, Heriot Watt University, UK, 2005.

Henderson, G.D., Danesh, A., and Tehrani, D.H.: "Effect of Positive Rate Sensitivity and Inertia on Gas Condensate Relative Permeability at High Velocity", J. Petroleum Geoscience 7, pp. 45-50, 2001.

Jamiolahmady M., Danesh A, Henderson G.D. and Tehrani D.H.: "Variations of Gas Condensate Relative Permeability with Production Rate at Near Wellbore Conditions: A

general Correlation", SPE 83960, presented at SPE offshore Europe Conference, Aberdeen, UK, September 2003.

Jamiolahmady, M., Danesh, A., Tehrani, D.H., and Sohrabi, M.: "Variations of Gas Condensate Relative Permeability with Production Rate at Near Wellbore Conditions: A general Correlation" SPE Reservoir Engineering and Evaluation Journal, **9** (6), pp.688-697, 2006.

Jamiolahmady, M.: Mechanistic Modelling of Gas Condensate Flow in Porous Media, PhD Thesis, Heriot-Watt University, April 2001.

Lecture-note of Reservoir Engineering, IPE, Heriot-Watt University, Edinburgh, UK, 2002.

Lecture-note of Production Technology, IPE, Heriot-Watt University, Edinburgh, UK, 2002.

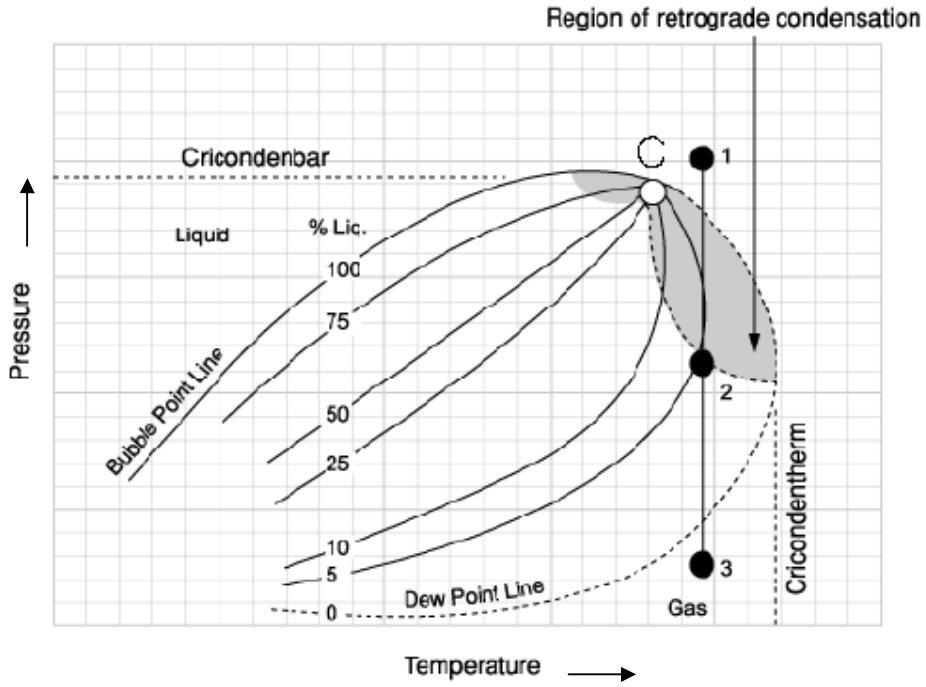

Figure 2.1: Typical shape of a gas condensate phase envelop.
(Lecture Note of Reservoir Engineering, published by HW University (2002)).

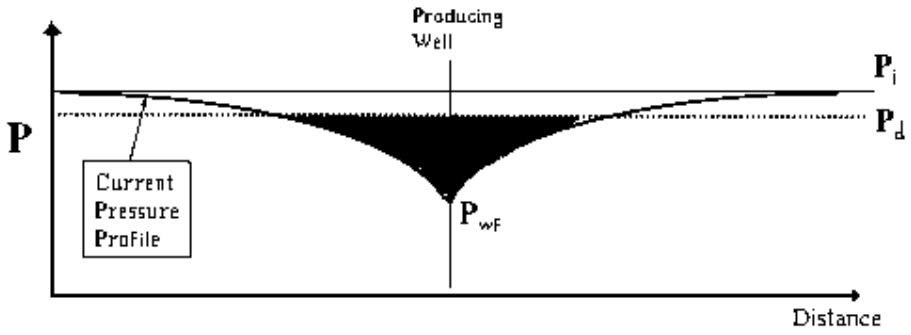

Figure 2.2: A schematic pressure profile around a producing well in a gas condensate reservoir. Shaded area shows two-phase zone, where local pressure is less than the dew point pressure.

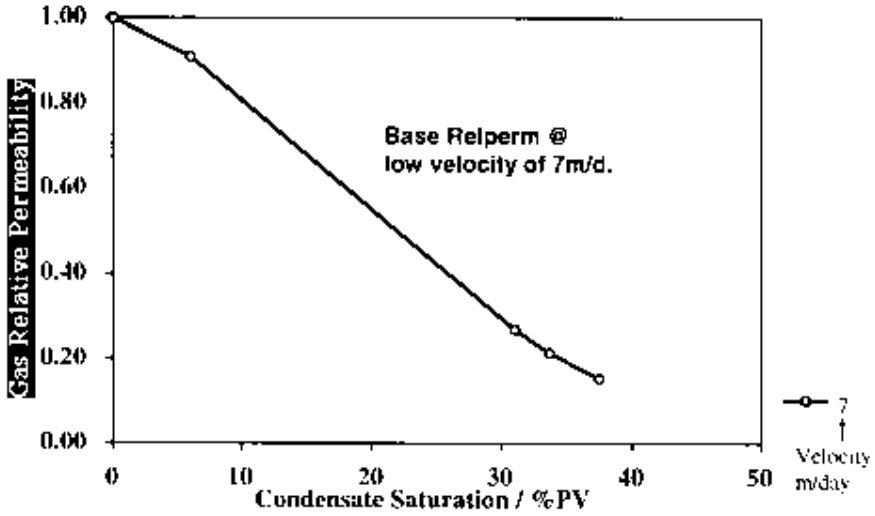

Figure 2.3: Base gas relative permeability curve of a typical core (Clashach). (Gas Condensate Research Group, 1999-2002 Final Report).

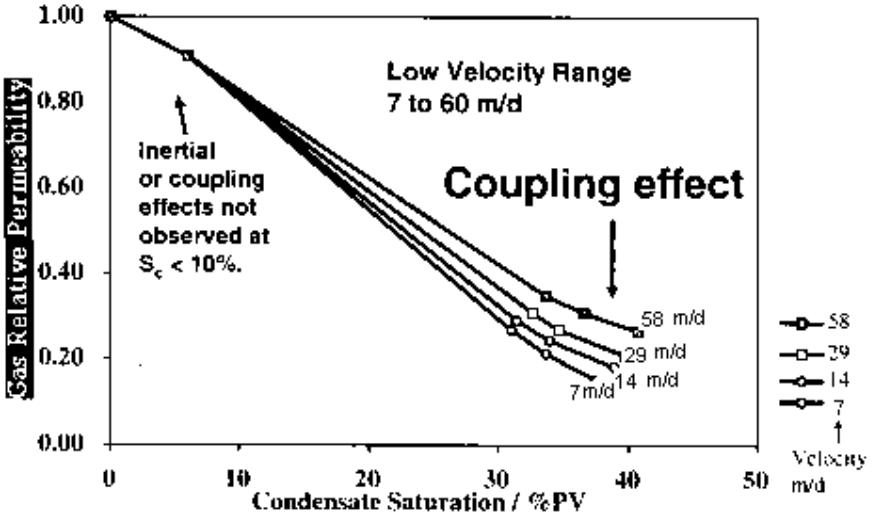

Figure 2.4: Effect of velocity on the gas relative permeability of a typical core (clashach), low velocity range.(Gas Condensate Research Group, 1999-2002 Final Report).

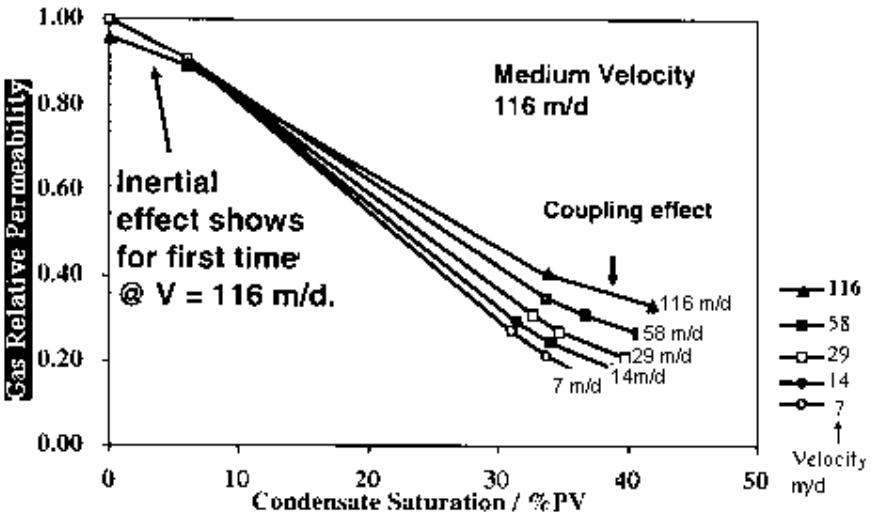

Figure 2.5: Effect of velocity on the gas relative permeability of a typical core (clashach), low to medium velocity range. (Gas Condensate Research Group, 1999-2002 Final Report).

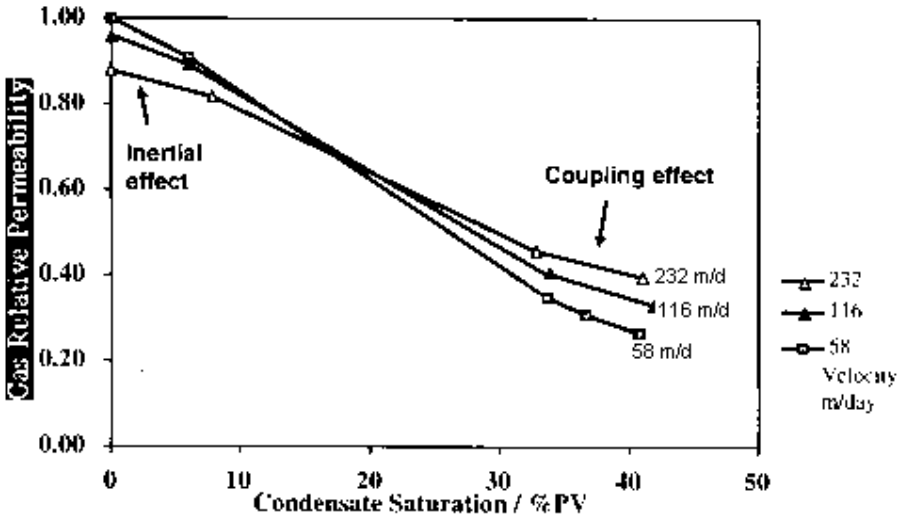

Figure 2.6: Effect of velocity on the gas relative permeability of a typical core (clashach), low to medium-high velocity range. (Gas Condensate Research Group, 1999-2002 Final Report).

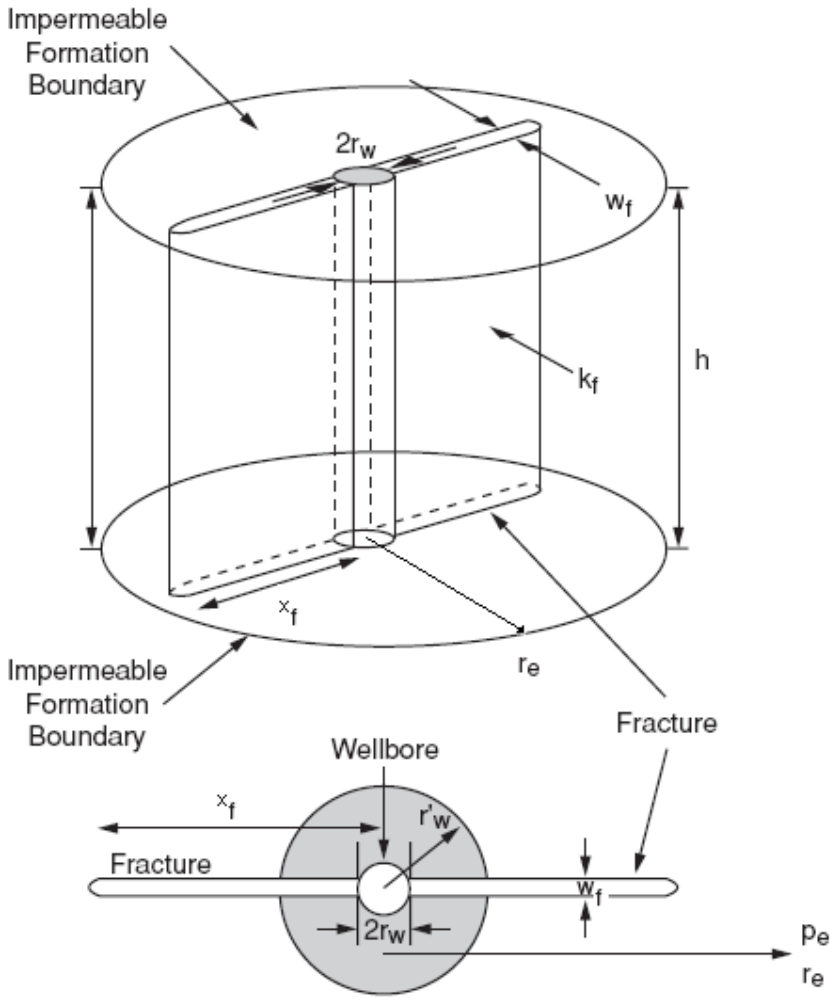

Figure 2.7: A hydraulically fractured well in the centre of a cylindrical drainage area, (Lecture Note of Production Technology II published by HW University (2002)).

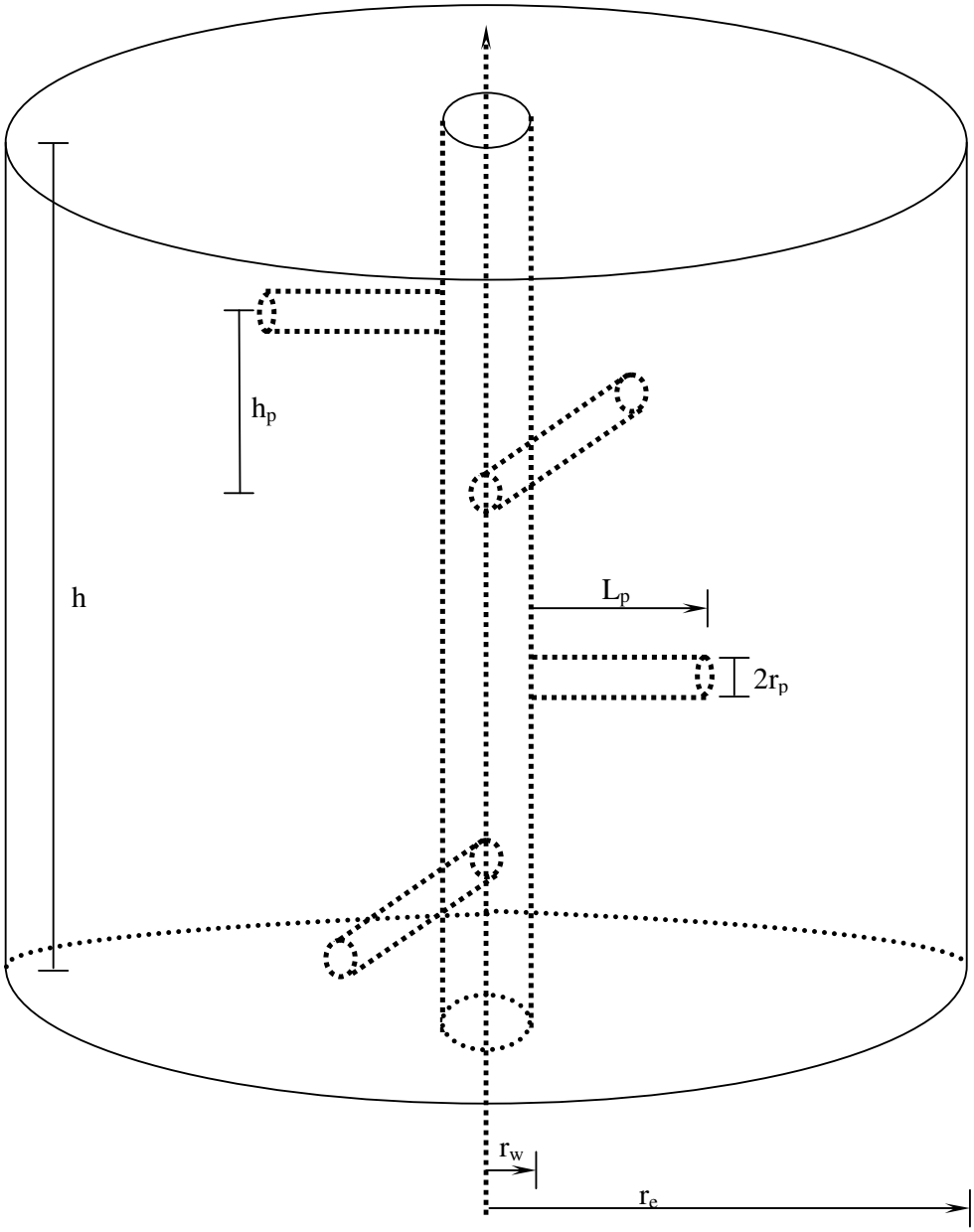

Figure 2.8: A Perforated region with four shots and 90° phasing angle.

Chapter 3 Gas Condensate Flow around Hydraulically Fractured Wells

3.1 Introduction

Hydraulic Fracturing is one of the most widely used and accepted methods for enhancing well performance. Figure 3.1 schematically shows a hydraulically fractured well. The fracture has two symmetrical wings that have penetrated along the maximum horizontal stress. These wings are filled with a high conductivity proppant which holds the fracture open (maintains a high conductivity path to the wellbore).

Figure 3.1 also demonstrates two possible types of damage in a Hydraulically Fractured Well (HFW): fracture face and choked damage. Face damage is caused by infiltration of fracturing fluid into the matrix and the resultant reduction in the permeability of the matrix next to the fracture. Choked damage refers to the decrease in the permeability of the proppant in the fracture, near to the wellbore. Such damage can decrease the productivity of the well as a consequence of increasing the flow resistance in the matrix and fracture respectively.

One of the important phenomena that can significantly decrease the conductivity in the fracture is the inertial effect. At high fluid velocity in the fracture, pressure drop is more than the calculated value by Darcy law. According to the Forchheimer equation, the extra pressure drop is proportional to the velocity squared. This deviation from Darcy flow increases pressure drop in the fracture or, in other words, decreases the fracture conductivity.

Multiphase flow can also change the well performance. In gas condensate reservoirs,

when the well bottomhole pressure falls below the dew point, condensate will build-up around the wellbore, which causes a significant reduction in well production. The condensate buildup in the fracture and in the matrix adjacent to the fracture can change the performance of an HFW significantly.

Moreover, the increase in gas condensate relative permeability caused by an increase in velocity from moderate to high velocities, or a reduction in IFT, could improve the well performance as a result of the coupling effect.

Because of the importance and wide applications of hydraulic fracturing, productivity calculations in such systems have been the subject of interest for many investigators, including McGuire and Sikora (1960), Cinco-ley *et al.* (1977, 1978), Economides *et al.* (2002), Meyer and Jacot (2005) and Mahdiyar *et al.* (2007). These studies were aimed at the determination of improvement in well productivity or optimum fracture design. In these studies, the flow behaviour and pressure distribution around the fracture at steady state or pseudo-steady state conditions have been investigated. The results of these works are in the form of charts or correlations for calculating the well productivity, skin factor or effective wellbore radius.

Most of the available methods in the literature for estimation of fracture skin or effective wellbore radius of a Hydraulically Fractured Well (HFW) were developed for single-phase Darcy flow systems (McGuire and Sikora, 1960; Prats, 1961; Cinco-ley *et al.*, 1977, 1978, Economides *et al.,* 2002; Meyer and Jacot, 2005; Mahdiyar *et al.,* 2007).

McGuire and Sikora (1960) used an electric analogue computer to study the effect of finite-conductivity vertical fractures on the productivity of wells in expanding fluid-drive reservoirs. The result of their study was some curves demonstrating the productivity increase benefited from hydraulic fracturing as a function of fracture length (penetration) and relative fracture conductivity.

Prats (1961) presented an analytical model for the pseudo-steady state behaviour of finite-conductivity vertical fractures. Prats' model was based on a reservoir model divided into two regions of different permeability. Region I represented the fracture domain and region II the formation domain. The two more significant contributions by

Prats were the introduction of the concept of effective wellbore radius and the realization that there is an optimum fracture design, length-width ratio, for a given fracture volume that maximizes productivity. Prats showed that for fractures with infinite conductivity the effective wellbore radius was equal to a quarter of the fracture length.

Raymond and Binder (1967) presented an approximate analytical mathematical model for predicting the productivity ratio increase of finite-conductivity fractures in pseudo-steady state flow in cylindrical drainage areas. Raymond and Binder showed that their model was in reasonable agreement with the McGuire and Sikora curves for fracture penetration ratios less than one-half.

Gringarten *et al.* (1974) studied the unsteady state behaviour of wells intersected by uniform-flux or infinite conductivity fractures. Raghavan *et al.* (1978) also presented a mathematical model based on a constant pressure outer boundary condition for uniform flux and infinite conductivity fractures. Both of these papers illustrated the effect of the fracture penetration ratio on the effective wellbore radius. In the paper of Raghavan *et al.* it was also shown that the performance of an HFW with infinite conductivity depends on outer boundary condition, if the fracture penetration ratio is greater than 0.2.

Cinco-Ley and Samaniego (1981) presented a new technique, using a bilinear flow model, for analyzing pressure transient analysis for HFWs. They also published another paper (1981) that outlined the basic pressure behaviour differences between a finite-conductivity fracture and different types of damaged fracture cases. Cinco-Ley (1982) summarized much of this work and that of his co-authors. The introduction of the pseudo-skin and the presentation of some curves for the dimensionless effective wellbore radius versus fracture conductivity are two important contributions of their studies.

Riley *et al.* (1991) developed an exact analytical solution for elliptical finite-conductivity fractures in infinite reservoirs. Riley's elliptical fracture formulation provides an explicit formula for the effective wellbore radius as a function of fracture conductivity in terms of an infinite sum.

Valko and Economides (1998) represented the correlations between dimensionless productivity index of finite conductivity HFWs as a function of fracture conductivity and fracture penetration ratio at pseudo-steady state conditions.

Meyer and Jacot (2005) presented a new solution methodology for pseudo-steady state behaviour for a well with a finite conductivity vertical fracture, based on reservoir/fracture domain resistivity concept. The resulting pseudo-steady state solution was presented in the form of a dimensionless productivity index, pseudo-fracture and effective wellbore radius. They also improved Gringarten's dimensionless productivity for infinite conductivity vertical fractures in rectangular closed reservoirs.

The importance of the inertial effect on the effective fracture conductivity has also been the subject of some studies.

Holditch and Morse (1976) analyzed the effect of a non-Darcy flow on the behaviour of fractured gas reservoirs. Their results showed that a non-Darcy flow in a fracture could exist for a wide range of formation properties and it can reduce the effective fracture conductivity near wellbore by a factor of 20 or more. Thus it should be considered in the analysis of drawdown tests, pressure build-up tests and history matching of fractured gas wells.

Guppy *et al.* (1982) tried to provide solutions for analyzing pressure data for constant rate HFWs with finite conductivity, producing at high rates to cause non-Darcy flow effects in the fracture. They concluded that, to describe the non-Darcy effect, two physical parameters are required: the dimensionless fracture conductivity and the dimensionless flow rate constant. They also showed how inertial effect can decrease the apparent (effective) fracture conductivity, and developed a correlation between the true (absolute) fracture conductivity, flow rate constant and apparent fracture conductivity.

In another paper, Guppy *et al.* (1982) showed that in buildup tests, the inertial effect on decreasing apparent (effective) fracture conductivity is more significant. Thus they developed another correlation for buildup tests.

Gidley (1991) proposed an approximate correction of the dimensionless fracture conductivity for non-Darcy flow effects, which was dividing the fracture conductivity

by the term (1+Reynlods number), in which the Reynolds number is computed for flow conditions in the fracture at the wellbore.

Settari *et al.* (2002) tried to develop a correlation for the calculation of a non-Darcy flow skin of a producing HFW by simulating a hydraulically fractured well at pseudo-steady state conditions. They compared the results of their simulations with Guppy's build-up correlation, demonstrating that this equation overestimates the non-Darcy effect in a producing well. They also suggested that the non-Darcy skin factor should be a function of two additional parameters (i.e. $k_f w_f$ and k) in addition to absolute fracture conductivity and Reynolds number.

Smith *et al.* (2004) confirmed the Settari's finding that Guppy's buildup correlation overestimates the inertial effect in a producing HFW. Neither of the authors of these two papers has compared their results with the correlation derived for draw-down which can describe their simulations more closely.

Gas condensate flow around HFWs has also been the subject of study. In some of these studies, such as those of Wang *et al.* (2000), Mohan *et al.* (2006) and Rostami *et al.* (2007), for estimation of well productivity or optimization of the fracture, gas condensate flow around the fracture was considered to behave like single-phase flow with a damaged matrix layer, which has a reduced permeability of kk_{rg} and the extent of two-phase region. Some other investigators (Hashemi *et al.,* 2005; Carvajal *et al.,* 2005; Mohan *et al.,* 2006) conducted a series of sensitivity studies on the impact of pertinent parameters.

Carajaval *et al.* (2005) numerically simulated a HFW in a square closed boundary gas condensate reservoir using the ECLIPSE simulator. He showed that compared to radial grid systems a Cartesian grid system better captures the impact of velocity in both single-phase flow of gas affected by inertia and two phase flow of gas and condensate affected by coupling and inertia. He demonstrated that fracture width is very important by reducing the inertial effect, which could be exaggerated by increasing the fracture length. He also concluded that coupling affects flow within the matrix whilst inertia affects flow inside the fracture.

Hence, to the best of the author's knowledge, a method for estimation of skin factor or effective wellbore radius of an HFW in gas condensate reservoirs, correctly accounting for coupling and inertial effects, has not been reported before.

This part of the study is aimed at investigating gas condensate flow around the hydraulically fractured wells, including the impact of condensate liquid drop-out, coupling and inertia. One of the main outcomes of this exercise is the development of a method for calculation of the effective wellbore radius for an HFW which is very useful in the estimation of well productivity. Two other important applications of this method can be summarized as follows:

1. It is impractical to apply very fine grid blocks that are required to simulate accurately a Hydraulic Fracture (HF) using commercial reservoir simulators. The formula for an effective wellbore radius provides the tool to simulate an Equivalent Open-hole (EOH) system instead of the hydraulically fractured well.

2. It can be used to find the optimum design for a given fracture volume. That is, it allows us to calculate (for a constant fracture volume) the optimum fracture length to width ratio, which maximizes the well productivity.

Since large data banks are required to investigate the effects of pertinent parameters on the well performance and develop the formulations covering a wide range of variation of parameters, the author of this study has developed and used his own in-house simulators. He has also used ECLIPSE 300 to study the performance of HFWs at pseudo-steady state conditions.

The basic theory, governing equations and numerical methods of the in-house simulator, is discussed in section 3.2.

In section 3.3, single-phase Darcy flow around the HFWs is studied. Here first the impact of important flow parameters, i.e. fracture conductivity and fracture penetration ratio on the flow and pressure distribution around the wellbore is investigated. One major part of this section is devoted to a discussion on the differences between the performance of an HFW operating at steady state and pseudo-steady state conditions. Then the required formulae for estimation of effective wellbore radius at SS and PSS

conditions will be developed. In the last subsection, the effects of fracture face damage and choked damage on the HFW performance will also be investigated. The result of this later part is the introduction of two correlations for estimation of these two damaged skins.

As mentioned earlier, non-Darcy flow inside the fracture can decrease fracture conductivity significantly. There are several formulae available for predicting the extent of this effect. Although all investigators are in agreement on the significant negative impact of inertial effect on the HFW performance, there is not such agreement on the proposed formulations expressing this effect. This subject is investigated in detail in section 3.4 to clarify these reports and identify the right correlation for estimation of this effect.

Two-phase flow in the matrix can decrease the conductivity in both matrix and fracture, albeit to a different extent. To the best of the author's knowledge, in all studies on gas condensate flow around HFWs, apart from numerical simulation studies such as the one done by Carvajal *et al.* (2005), two-phase flow in the fracture has been neglected and condensate build-up around the fracture has been treated as the fracture face damage in the single-phase flow. The weak points of this approach will be made clear in Section 3.5 and also in the introduction of the next chapter.

The variation of condensate saturation and GTR around the wellbore, as well as the variation of relative permeability in both fracture and matrix, is investigated in Section 3.5 as well. Subsequently the author will propose a new method for estimation of an effective fracture conductivity in gas condensate systems.

The main practical outcomes of Sections 3.2-3.5 are the development of the required formulae for calculation of effective fracture conductivity and effective wellbore radius at steady state as well as pseudo-steady state conditions.

The results of an exercise conducted to verify the integrity of these formulations for different cores, fluids and operating pressures will be presented in section 3.6. In this section, the method will be verified for both steady state and pseudo-steady state conditions. It will also be shown that the use of these correlations can be extended to transient state conditions.

3.2 The In-House Simulators

Flow behaviour around a producing well with constant production rate approaches either steady state or pseudo-steady state, depending on the exterior boundary condition of the drainage area. The system approaches steady state, and the pressure profile does not change with time if the pressure at the exterior boundary is kept constant. However, for a closed boundary drainage area, it approaches pseudo-steady state where the pressure profile around the wellbore is not constant with time but is falling at a constant rate along the drainage area; i.e. the pressure profiles at different time steps are parallel. Whilst for many practical cases there is not a significant difference between the productivity of a well at steady state and that at pseudo-steady state, for special cases where the effective wellbore radius is comparable with the exterior radius of the drainage area the difference could be significant. This could occur in HFW systems with fracture penetration ratio (the ratio of the fracture length over the reservoir length) greater than 0.2 (Raghavan *et al.,* 1978).

The performance of an HFW has been investigated for many different cases using the in-house simulators and ECLIPSE 300, as described in the following sections. The author has developed a couple of simulators to study gas and gas condensate flow around HFWs and 1D open-hole systems at Steady State (SS) conditions. He has also developed a simulator to study single-phase Darcy flow at Pseudo-Steady State (PSS) Conditions. ECLIPSE 300 has also been used to study the transient flow and two-phase flow of gas and condensate at pseudo-steady state conditions.

The in-house simulators automatically generate the required mesh for many prevailing conditions. Performing the same exercise with commercial simulators is time consuming and cumbersome.

Figure 3.2 schematically shows an HFW in the centre of a square, or cylindrical, drainage area. As shown in this figure, the system can be divided into two different zones: fractured zone and unfractured zone. The fractured zone is the cylindrical medium containing both fracture and matrix with the outer radius equal to the fracture half- length, whilst the unfractured zone (behind the fractured zone) contains just the matrix.

In developing the in-house simulators, it has been assumed that:

a) The fracture and matrix are two different porous media but each one is a uniform porous medium.

b) The width of the fracture is constant.

c) The fracture has penetrated symmetrically in both directions.

d) Wellbore flow directly from the matrix is negligible, compared with the flow from the fracture to the well.

e) The effect of perforated casing on the flow regime is negligible.

f) The fracture has penetrated vertically through the whole height of the reservoir.

g) Gravity force is neglected in this 2D system.

3.2.1 Steady state in-house simulators

Governing equations

Continuity equation for gas condensate flow systems at steady state conditions is:

$$\nabla \bullet \left([\rho \vec{v}]_g + [\rho \vec{v}]_c \right) = 0 , \tag{3.1}$$

where ∇ is the gradient operator and subscripts *g* and *c* denote gas and condensate, respectively. The flow-equations for gas and condensate phases in isotropic formations are:

$$\vec{v}_g = -\frac{k k_{rg}}{\mu_g} \nabla P \tag{3.2}$$

$$\vec{v}_c = -\frac{k k_{rc}}{\mu_c} \nabla P \tag{3.3}$$

k_{rg} and k_{rc} are gas and condensate relative permeability, affected by inertia and coupling.

Combining Equation 3.1 with the Equations 3.2 and 3.3 results in:

$$\nabla \bullet \left\{ \left[\frac{\rho_g k_{rg}}{\mu_g} + \frac{\rho_c k_{rc}}{\mu_c} \right] k \nabla P \right\} = 0 \tag{3.4}$$

Now the application of this Equation in the 2D HFW system and 1D open-hole system will be shown.

2D HFW system

In an HFW system with the simplifying assumptions made, the flow will be two-dimensional and Equation 3.4 can be written as:

$$\frac{\partial}{\partial x}\left[\left(\frac{\rho_g k_{rg}}{\mu_g}+\frac{\rho_c k_{rc}}{\mu_c}\right)k\frac{\partial P}{\partial x}\right]+\frac{\partial}{\partial y}\left[\left(\frac{\rho_g k_{rg}}{\mu_g}+\frac{\rho_c k_{rc}}{\mu_c}\right)k\frac{\partial P}{\partial y}\right]=0 \qquad (3.5)$$

Because of the symmetry in both dimensions, a quarter of the system is modelled, as shown in Figure 3.3. The boundaries of x=0 and y=0 in this figure are the symmetrical lines of the original medium, so the pressure gradient along these lines is zero. Thus the boundary conditions required for solving the above differential equation are:

At x = 0 $\quad \frac{\partial P}{\partial x}=0$, (3.6a)

At y = 0 $\quad \frac{\partial P}{\partial y}=0$, (3.6b)

At x=y=0 $\quad P=P_{w,}$ (3.6c)

At $x = x_e$ $\quad P=P_e$, (3.6d)

At $y = x_e$ $\quad P=P_e$, (3.6e)

where x_e is the half-length of the drainage area (the side length of a quarter of the drainage area). Further more as mentioned earlier it is assumed that wellbore flow directly from the matrix is negligible, compared with the flow from the fracture to the well.

In Equation 3.5, relative permeability (which depends also on the rock and fluid properties) gas fractional flow (GTR) and fluid velocities are complex functions of pressure and its gradient.

In gas condensate reservoirs at steady state conditions, the total composition of flow (z_j) within the reservoir is constant, and is equal to the composition of the production. The

following equation is the result of writing mass balance at each location, based on the assumption of an equilibrium state existing between liquid and vapour.

$$z_j = \frac{\rho_g y_j GTR + \rho_c x_j (1-GTR)}{\rho_g GTR + \rho_c (1-GTR)} = const., \tag{3.7}$$

where z_j, y_j and x_j are the mass fractions of component j in the mixture, gas and liquid phases, respectively. Here equilibrium compositions (y_j and x_j) at each point are dependent on the local pressure.

The simulator has been developed using MATLAB as the programming language. And an iterative finite difference numerical method has been used for solving the main highly non-linear partial differential equation, Equation 3.5, and auxiliary equations such as Equation 3.7.

This method can be summarized by the following steps:

1. The pressure distribution in the matrix and fracture grid blocks is assumed.
2. For each grid block, GTR and fluid properties are evaluated.
3. The velocity vector in the fracture and matrix blocks is assumed.
4. For each grid block, using the local values of pressure gradient, velocity, fluid property and upstream value of GTR, gas and condensate relative permeability is estimated.
5. For each block, the velocity vector is calculated.
6. The maximum velocity error is defined and calculated as:- the maximum of the differences between the assumed and calculated values of velocity of each grid block.
7. If the maximum velocity error is less than the accepted value (10^{-7} m/day), the programme proceeds to the next step, otherwise it adjusts the new value for the velocity as the average value of the assumed and calculated values, and returns to step 4.
8. Pressure matrix is solved (using MATLAB matrices solver).
9. The maximum pressure error is defined and calculated as:- the maximum of the differences between the assumed and calculated values of pressure of each block divided by the calculated pressure of that block.
10. If the maximum pressure error is less than the accepted value (10^{-5}), the pressure distribution is accepted as the correct value and well production rate can be calculated;

otherwise the programme adjusts the new assumption for the pressure at each block as the average value of the assumed and calculated values and goes back to step 2.

Gridding

As the numerical method has been used in many studies of HFWs the issue of *appropriate grid size distribution* has been considered by some investigators such as Guppy *et al*. (1982) and Settari *et al.* (2002).

Guppy *et al*. in their paper stated that *'it was observed that at the wellbore the grid size must be extremely small because of the boundary conditions at that point and must continue to be small but increase slightly until the middle of the fracture. This is extremely critical for cases in which the fracture conductivity is small (less than π). This observation is consistent with Cinco-L. et al.'s observation at low fracture conductivities. The irregular grid pattern consisted of 550 blocks (22*25) with 17 grid blocks within the fracture and 8 outside the fracture. For higher conductivities, at the tip of the fracture the grid sizes must be small, although not as small as near the wellbore. The higher-conductivity fractures have the major flow of fluid in the fracture from the farthest half of the fracture. We observed an improvement in the percentage error by changing the value of σ, the weighting factor. The value of σ finally was selected to be 0.5.'*

The author found the above recommendations very useful and used them for developing the grids of the in-house simulator. However, because of the significant advance in the computer speed and memory since the date of Guppy study, to promote the stability the number of gridding was increased to 1000, 40 blocks in x direction (40 rows) and 25 blocks in y direction (25 columns), as shown in Figure 3.4. The fracture length, in x-direction, consists of the first 25 blocks of the first row of blocks. The length of the first block of each row is set equal to 0.2 m and the length of the second to the 17^{th} is equal to the length of the last block times a multiplication factor (1+weighting factor) not greater than 1.4. From the 18^{th} to the 25^{th} block, each block length is equal to the length of the previous block dividing by the same multiplication factor. The length of the remaining blocks, column 26^{th} to 40^{th}, matrix behind the fracture, is set equal to the length of the previous block times the same multiplication factor.

The width of the first row of the blocks is set equal to the fracture half-width ($w_f/2$). Knowing the half reservoir length, number of blocks in y direction (NY=25) and the weighting factor (σ), the thickness of the second row is calculated using the following formula, which is concluded from the formula for the summation of a geometric series:

$$\Delta y(2) = \frac{x_e - w_f}{\left(\frac{(1+\sigma)^{(NY-1)} - 1}{\sigma}\right)} \tag{3.8}$$

The thickness of the 3rd row to the 25th row is equal to the thickness of the last row times the multiplication factor (1+weighting factor).

Therefore, the grid blocks near the well and those near the tip of the fracture are finer than the remaining blocks to capture more accurately the abrupt changes in flow parameters in these areas.

This suitability of gridding was verified extensively by noticing a close conformity between the results of more than 2000 numerical simulations covering a wide range of fracture and reservoir dimensions, with those of an analytical formula (Meyer *et al.* Formula) for the same prevailing conditions. More detail will come in Section 3.3.2.

1D OH System

As mentioned earlier, one of the outcomes of this study is the development of a formula for an effective wellbore radius of an equivalent open-hole (EOH) well to replicate flow in an HFW. The applicability and accuracy of the formulation is verified by comparing the flow production rate predicted by the in-house 2D HFW system simulator with that of an EOH system. To simulate gas condensate flow in the open-hole system, another in-house simulator has been developed. The 1D open-hole system, used in this study, consists of a well in a single layer cylindrical reservoir with external radius of r_e.

The one-dimensional (radial) form of Equation 3.4 is:

$$\frac{\partial}{r\partial r}\left[\left(\frac{\rho_g k_{rg}}{\mu_g} + \frac{\rho_c k_{rc}}{\mu_c}\right) k \frac{r\partial P}{\partial x}\right] = 0 \tag{3.9}$$

Constant pressures at the internal and external radii are the required boundary conditions for solving this non-linear partial differential equation. In the 1D open-hole simulator, there are 50 radially divided grid blocks, with finer blocks near to the wellbore.

The appropriate gridding of an open-hole system has been investigated in the research group of Gas Condensate Recovery at Heriot-Watt University (Gas Condensate Progress Report, September 2006). According to this investigation selecting the number of grid blocks as 50 and weighting factor less than 0.4 promote the stability of finite difference numerical method.

Comparison of in-house simulator with ECLIPSE

The flow in an HFW system, with the same size and grid pattern as those in the in-house simulator, was simulated by ECLIPSE commercial simulator. 64 injection wells with the bottomhole pressure equal to P_e and fluid composition equal to the producing fluid were placed in all the boundary blocks. This was performed to achieve the steady state conditions as soon as possible.

The results of two simulators (at steady state conditions) were compared for many prevailing conditions. The close agreement between the results confirmed the integrity of the structure of the in-house simulator.

Since the in-house simulator automatically generates mesh for the HFW system with any geometry and fracture sizes, it serves as a useful tool for studying gas condensate flow around HFWs for many prevailing conditions. Performing the same exercise with commercial simulators is time consuming and cumbersome.

3.2.2 Pseudo-steady state in-house simulator

At constant production/injection rate, when pressure disturbance meets the exterior boundary if the pressure at the exterior boundary is held constant (e.g. by injecting fluids at the same rate that we produce) the system will reach the steady state conditions. However if there is no flow across the boundary, the system will approach pseudo-steady conditions.

Raghavan (1978) compared the performance of an HFW, with infinite fracture conductivity, in a square drainage area at steady-state with that at pseudo-steady state conditions. He concluded that for small fracture penetration ratios ($I_x=x_f/x_e$) the two performances are almost the same. But with increasing value of I_x, the exterior boundary conditions affect the fracture performance.

In order to investigate the applicability of this conclusion for all ranges of fracture conductivities, the author has developed another in-house simulator that can simulate single-phase Darcy flow at pseudo-steady state conditions. The basic theory and the numerical form of the governing equations are presented in the following section.

Basic theory

As mentioned earlier, a transient system approaches the pseudo-steady state performance if there is no flow across the exterior boundaries; thus the boundary conditions for the quarter of the drainage area (Figure 3.3) at pseudo-steady state are:

$$\begin{aligned} &\text{At} \quad x=0 \quad \text{and} \quad x=x_e \qquad \frac{\partial P}{\partial x}=0 \\ &\text{At} \quad y=0 \quad \text{and} \quad y=x_e \qquad \frac{\partial P}{\partial y}=0 \end{aligned} \tag{3.10}$$

At pseudo-steady conditions, the rate of pressure drop at each point of the reservoir is constant and equal to that of the average pressure drop, therefore by applying mass balance on the drainage area it can be stated that:

$$-\rho_w q_w = V\frac{\Delta\bar{\rho}\varphi}{\Delta t} \Rightarrow \frac{\Delta\bar{\rho}\varphi}{\Delta t} = -\frac{\rho_w q_w}{V}. \tag{3.11}$$

Here V is the reservoir volume. The grid system in this simulator, shown in Figure 3.4, is the same as that used in the SS simulator.

The numerical form of the governing equation can be developed based on the mass balance on each block. That is to say the summation of inflow to each block is equal to the storage or accumulation in that block. This can be written as follows,

$$\frac{P_{(i+1,j)}-P_{(i,j)}}{RX_{(i+1,j)}+RX_{(i,j)}}+\frac{P_{(i-1,j)}-P_{(i,j)}}{RX_{(i-1,j)}+RX_{(i,j)}}+\frac{P_{(i,j+1)}-P_{(i,j)}}{RY_{(i,j+1)}+RY_{(i,j)}}+\frac{P_{(i,j-1)}-P_{(i,j)}}{RY_{(i,j-1)}+RY_{(i,j)}}=h\Delta x_{i,j}\Delta y_{i,j}\frac{\Delta\rho\varphi}{\Delta t} \tag{3.12}$$

For a slightly compressible fluid with constant compressibility, it can be shown that $\frac{\Delta\rho\varphi}{\Delta t}=\frac{\Delta\bar{\rho}\varphi}{\Delta t}$ and therefore substituting from Equation 3.11 into Equation 3.12 gives:

$$\frac{P_{(i+1,j)}-P_{(i,j)}}{RX_{(i+1,j)}+RX_{(i,j)}}+\frac{P_{(i-1,j)}-P_{(i,j)}}{RX_{(i-1,j)}+RX_{(i,j)}}+\frac{P_{(i,j+1)}-P_{(i,j)}}{RY_{(i,j+1)}+RY_{(i,j)}}+\frac{P_{(i,j-1)}-P_{(i,j)}}{RY_{(i,j-1)}+RY_{(i,j)}}=h\Delta x_{i,j}\Delta y_{i,j}\frac{\Delta\bar{\rho}\varphi}{\Delta t}=-h\Delta x_{i,j}\Delta y_{i,j}\frac{\rho_w q_w}{V} \tag{3.13}$$

In this equation, $RX_{(i,j)}$ is the X-directional flow resistance inside a block (i,j) from the block centre to the block boundary, and $RY_{(i,j)}$ is the y-directional form of the same parameter. These values can be calculated as follows:

$$RX_{(i,j)}=\frac{\Delta x_{(i,j)}}{2hk_{(i,j)}\Delta y_{(i,j)}\left(\frac{\rho}{\mu}\right)_{(i,j)}}$$
$$RY_{(i,j)}=\frac{\Delta y_{(i,j)}}{2hk_{(i,j)}\Delta x_{(i,j)}\left(\frac{\rho}{\mu}\right)_{(i,j)}} \tag{3.14}$$

For blocks neighbouring the boundaries, the shape of the equation is slightly different from Equation 3.12 owing to boundary conditions.

Solving this set of equations will give pressure distribution. Subsequently, well productivity can be calculated using the following equation:

$$\dot{m}_w=4\frac{P_{(1,1)}-P_W}{RX_{(1,1)}} \tag{3.15}$$

The in-house simulators discussed so far, are the main tools of the flow study around HFWs, which are discussed in the following sections of this chapter.

3.3 Single-Phase Darcy Flow

The study of single-phase Darcy flow around HFWs can provide very important information about the pressure distribution around the wellbore, and also the effects of physical and geometrical parameters of fracture and matrix on the productivity index. Therefore, in this chapter, the important geometrical and physical parameters in single-phase Darcy flow systems (which can control the HFW performance) are initially identified. Subsequently, the pressure distribution and flow pattern will be investigated. The comparison between the results for steady state and those for pseudo-steady state flow behaviours will follow. The main outcome of this section will be the formulations of effective wellbore radius. Finally, the effect of face damage and choked damage, including the new proposed skin correlations for estimation of these damages, will be discussed.

3.3.1 Important parameters for flow around HFWs

As mentioned earlier in Section 3.1, the HFW system investigated in this section is an HFW located in the centre of a square or circular drainage area, Figure 3.2. In single-phase Darcy flow systems, the important parameters which can affect the productivity of the wellbore at steady or pseudo-steady state conditions are:

1- Fracture permeability, k_f.
2- Fracture Thickness, w_f.
3- Fracture half length, x_f.
4- Matrix permeability, k.
5- Drainage area half length, x_e.

The basic dimensionless parameter in HFW systems is the absolute fracture conductivity, which is the ratio of absolute conductivity inside the fracture over that in the matrix (Cinco-Ley *et al.*, 1978). This parameter, which for simplicity is called fracture conductivity and shown by C_{fD}, controls the productivity of an HFW in single-phase Darcy flow systems:

$$C_{fD} = \frac{k_f w_f}{k x_f}. \tag{3.16}$$

The other parameter which can affect the performance of an HFW is the non-radiality of flow in the unfractured zone. When considering the geometry of a fractured well system, it can be concluded that the non-radial flow effect in the unfractured zone is affected by the relative size of the fracture compared with that of drainage area, expressed by the following dimensionless number:

$$I_X = \frac{x_f}{x_e}. \tag{3.17}$$

Here, I_X is called the fracture penetration ratio.

In the following sections, the effects of these two dimensionless parameters on the performance and the effective wellbore radius of HFWs will be investigated.

3.3.2 Effective wellbore radius

Figures 3.5-7 show the steady state pressure drop contour maps in a quarter of drainage area of HFW systems with low penetration ratio (I_x=0.16) but with different fracture conductivity. Here pressure drop percent is defined as:

$$pressure \quad drop\% = \frac{P - P_w}{P_e - P_w} \times 100\%. \tag{3.18}$$

In all these three figures, iso-pressure drop curves are almost circular in the unfractured zone ($r > x_f$). However, they convert to ellipses near to the wellbore. Figures 3.5-7 clearly show that in HFWs, flow geometry is strongly dependent on the fracture conductivity. According to these figures, flow in a fractured zone is more elliptical in high conductive hydraulically fractured systems. In other words, flow around the hydraulically fractured wells is elliptical, however, it meets radial flow as the fracture conductivity decreases. It is expected that for zero fracture conductivity, there is no fracture (w_f=0); the flow is completely radial. Figure 3.8 shows the same pressure drop contour maps for HFW systems with the same fracture conductivity of the HFW system of Figure 3.6 (C_{fD}=2, I_x=0.22), however, with lower penetration ratio (I_x=0.05). There is no significant difference between the two plots. However, the shape of iso-pressure drop curves in

Figure 3.9, which is the pressure drop contour map around an HFW with C_{fD}=2 and I_x=0.88, is different. This shows fracture penetration ratio can influence the performance of an HFW when fracture length is comparable with reservoir length, which is in line with the reported results in the literature (Cinco Ley, 1978).

Using the analytical method, Prats (1961) reported similar isopressure curves and concluded that the flow around hydraulically fractured wells is elliptical. He also equalized elliptical flow around the HFW with radial flow around an open-hole system, and introduced the idea of effective wellbore radius. This is defined as the wellbore radius of an open-hole system which under the same drawdown provides the same flow rate as that of an HFW. In other words, the effective wellbore radius of an HFW is the radius of an open-hole system, which provides the same flow resistance or the same dimensionless productivity index of the HFW.

Steady state dimensionless productivity index of an HFW, without damage, based on the total pressure difference between external boundary and wellbore, is defined as:

$$J_D = \frac{1}{\ln \frac{r_e}{x_f} + S_f^{'}} = \frac{1}{\ln \frac{r_e}{r_w^{'}}} \tag{3.19}$$

In this equation, r_e is the exterior radius of the circular drainage area. In the case of a square drainage area, this value can be calculated as the result of equating the circular area with the square area, i.e.

$$r_e = \frac{2}{\sqrt{\pi}} x_e \tag{3.20}$$

In Equation 3.19, $S_f^{'}$ is the pseudo fracture skin and $r_w^{'}$ is the effective wellbore radius; these are simply related by:

$$r_w^{'} = x_f e^{-S_f^{'}} \tag{3.21}$$

The single-phase Darcy flow at the bottomhole can be estimated as follows:

$$q_w = \frac{2\pi kh}{\mu} \times J_D \times \Delta P \tag{3.22}$$

Or,

$$q_w = \frac{2\pi kh}{\mu} \times \frac{\Delta P}{\ln \frac{r_e}{x_f} + S_f^{'}} \tag{3.23}$$

Rearranging Equation 3.23 in the form of Equation 3.24 illustrates the physical meaning of pseudo fracture skin:

$$q_w = \frac{\Delta P}{\frac{\mu}{2\pi kh} \ln\left(\frac{r_e}{x_f}\right) + \frac{\mu S_f^{'}}{2\pi kh}} = \frac{\Delta P}{R_{mz} + R_{fz}}, \tag{3.24}$$

where R_{mz} ($\mu \ln(r_e/x_f)/2\pi kh$) is the radial flow resistance in the unfractured zone. Therefore R_{fz} ($\mu S_f^{'}/2\pi kh$) mainly represents the flow resistance in the fractured zone, although it also contains non-radial effect in the unfractured zone. These regions are schematically shown in Figure 3.2.

After Prats (1961) introduced the concept of effective wellbore radius ($r_w^{'}$) and showed that for HFW systems with infinite fracture conductivity, $r_w^{'}$ is half of the fracture half length (valid only for low I_X), many investigators followed this subject and tried to develop some formulae for the calculation of the productivity index, pseudo fracture skin or effective wellbore radius. However, almost all these formulae are set up for pseudo-steady state conditions. Raghavan (1978) compared the performance of an HFW with infinite conductivity located in the centre of a square drainage area at steady state with that at pseudo- steady state conditions. He concluded that for small fracture penetration ratios the two performances are almost the same, however, with increasing value of I_x, the exterior boundary conditions affect the fracture performance.

To demonstrate the same phenomena for all ranges of fracture conductivities, the results of two in-house simulators - steady state and pseudo-steady state simulators - were compared. The basic theory and the numerical form of the governing equations of the in-house simulators were presented in Section 3.2.

In Figure 3.10, the results of the two states of flow for finite fracture conductivity (C_{FD}=1) and almost infinite fracture conductivity (C_{fD}=1000) have been compared. It can be stated that, similar to the results of Raghavan, when penetration ratio is less than 0.2 the pseudo skin factor of the two systems is almost the same, however, for I_X>0.2 the results are different. It is also noticed that with decreasing fracture conductivity the difference is decreased.

Therefore, it can be concluded that: *the formulae, available in the literature, for determination of the effective wellbore radius at pseudo-steady state should be suitable for determination of effective wellbore radius at steady state, provided that the fracture penetration ratio is less than 0.2.*

Meyer and Jacot (2005) conducted a thorough study of pseudo-steady flow in HFWs, and introduced the following semi-analytical equation for estimating the Darcy flow pseudo fracture skin of an HFW, located in the centre of a rectangular drainage area with the aspect ratio of $\lambda=x_e/y_e$.

$$S_f^{'} = \ln\left(\xi_\infty + \frac{\pi}{g(\lambda)C_{fD}}\right) \quad , \tag{3.25}$$

where g(λ) is a geometrical function and ξ_∞ is the ratio of fracture half length over the effective wellbore radius if the fracture conductivity was infinity; $\frac{x_f}{r_{w,\infty}^{'}}$. The value of this parameter can be calculated by the modified Gringarten equation. The details of the equations of g(λ) and ξ_∞ can be found in the SPE paper published by Meyer and Jacot (2005).

For square drainage area, g(λ) is 1.0, and for I_x less than 0.2, ξ_∞ can be approximated as 2.0 (Meyer and Jacot, 2005). Therefore, for square drainage area with I_x less than 0.2, where the performance of HFWs at steady state and pseudo-steady state is the same, Equation 3.25 is simplified as:

$$S_f^{'} = \ln\left(2 + \frac{\pi}{C_{fD}}\right). \tag{3.26}$$

This semi-analytical equation is valid for both steady state and pseudo-steady state conditions but with the restriction of I_X being less than 0.2.

Figure 3.11 compares the results of the SS in-house simulator with the results of this equation for I_X less than 0.2. A close conformity is noted between the results of this semi-analytical equation and those of the numerical based in-house simulator. These results also confirm the integrity of the grid structure used in this study.

The author modified Equation 3.26 to a more general equation valid for all I_X values. Figure 3.12 shows the variation of $S_f^{'}$, at steady state conditions, versus I_X at different C_{fD}. As expected for greater values of C_{fD}, where π/C_{fD} approaches zero, the effect of I_X is more significant. This notification suggested that constant 2 in Equation 3.26 must be replaced with a function, which approaches 2 as I_X approaches zero. In other words, Equation 3.26 should be modified as follows to be applicable for all ranges of I_X in square drainage area at steady state conditions:

$$S_f^{'} = \ln\left(2 \times A + \frac{\pi}{C_{fD}}\right), \tag{3.27}$$

where A is a function of I_X. To find this function, the results of the SS in-house simulator for many different values of I_X were analysed. In other words the SS in-house simulator were used to calculate pseudo fracture skin of many hydraulically fractured wells with different fracture penetration ratios but with almost infinite fracture conductivity (C_{fD}=10,000). These values of pseudo fracture skin then were used in Equation 3.27 to estimate A and produce a Table of A versus fracture penetration ratio. A simple curve fitting, described in Appendix A, provides the optimum values of the unknown constants but before that the structure of the equation should be selected based on the shape of the variation of A and the impact of fracture penetration ratio. Considering these points and performing data analysis resulted in the following equation for the estimation of A:

$$A = \ln\left(e^{1} - \frac{0.17}{r_{eD} - 0.87} \right). \tag{3.28}$$

In this Equation, r_{eD} is the dimensionless outer radius, which represents the effect of fracture penetration ratio on S'_f.

$$r_{eD} = \frac{r_e}{x_f} = \frac{2}{\sqrt{\pi}} \frac{1}{I_X} \tag{3.29}$$

Figure 3.13 shows the variation of A with I_X. As expected, A approaches 1.0 as I_X approaches zero. The minimum value of A is 0.723, which occurs at unit value of I_x. When I_X is equal to 0.2, A is 0.983 and the maximum possible difference between the results of Equations 3.26 and 3.27, occurring at infinite C_{fD}, is approximately 2.5%, whilst the corresponding difference between their predicted value at I_x=1 is approximately 47%.

Figure 3.14 shows the high level of accuracy of Equation 3.27 by comparing its results with the outcomes of the steady state in-house simulator, for a wide range of variation of the pertinent parameters as follows:

Fracture width (w_f): 2, 6, 10, 14 mm
Fracture half length (x_f): 24, 59 and 146 m
Fracture permeability (k_f): 10, 50, 90, 130, 170, 210 D
Reservoir permeability (k): 0.1, 1, 9, 25, 48, 81 mD
r_{eD} range: $1.2 < r_{eD} < 10$
C_{fD} range: $0.2 < C_{fD} < 888$
Number of data points: 15900

Here the Average Absolute Deviation (AAD%) is less than 1.3%, confirming the applicability of Equation 3.27 for the calculation of pseudo fracture skin at steady state conditions.

Combining Equations 3.21 and 3.27 introduces the following equation for estimation of an effective wellbore radius of an HFW at steady state conditions.

$$r_w^{'} = \frac{x_f}{2\times A + \frac{\pi}{C_{fD}}} \tag{3.30}$$

As mentioned earlier, for PSS, Meyer and Jacot (2005) have introduced a general formula for pseudo fracture skin and effective wellbore radius in rectangular drainage area (Equation 3.25). However as the general equation of ξ_∞ is not simple to use, attempts were made for developing a simpler equation for estimation of ξ_∞ in square drainage areas. In other words, it is intended to develop simple equations, similar to Equations 3.27-3.30, for PSS.

Before formulating ξ_∞ there is a need to discuss a small but important point about the pseudo-steady state productivity. For a producing well, without damage and located in the centre of a square or cylindrical drainage area, it is mathematically derived that PSS productivity index is calculated by the following equation (Dake, 1978):

$$J_D = \frac{\mu}{2\pi kh}\times\frac{q}{\overline{P} - P_w} = \frac{1}{\ln\frac{r_e}{r_w^{'}} - \frac{3}{4} + \frac{r_{wD}^2}{2} + \frac{r_{wD}^4}{4}} \tag{3.31}$$

Where $r_w^{'}$ is the effective wellbore radius and r_{wD} is the dimensionless effective wellbore radius.

$$r_{wD} = \frac{r_w^{'}}{r_e} \tag{3.32}$$

Normally $r_w^{'}$ is much smaller than r_e so the third and fourth terms in the denominator of Equation 3.31 are neglected and it is simplified as follows,

$$J_D = \frac{\mu}{2\pi kh}\times\frac{q}{\overline{P} - P_w} = \frac{1}{\ln\frac{r_e}{r_w^{'}} - 3/4} \tag{3.33}$$

However for HFWs with considerable penetration ratio this simplification could cause some errors especially for high fracture conductivities. This is especially true for

estimation of ξ_∞, as this parameter is the ratio of fracture half length over the effective wellbore radius when the fracture conductivity is infinity; $\frac{x_f}{r'_{w,\infty}}$. For infinite conductive fractures at I_X=1.0, r_{wD} is about 0.3 and neglecting this parameter results in the overestimation of ξ_∞. This point is important in the conversion of productivity index to ξ_∞ at PSS, which has been taken into account in this formulation.

Figure 3.15 shows ξ_∞ of PSS for square drainage area as a function of fracture penetration ratio estimated by three methods, which are (i) Equation D.3 of Meyer and Jacot paper, (ii) Digitizing Figure D.3 of the same paper and (iii) the results of the in-house PSS simulator. These simulation results have been obtained by varying Ix at very large C_{fD} of 10000. The solution of each case has been mapped to Equation 3.33 to calculate r'_w, which was then converted to ξ_∞ using $\xi_\infty = \frac{x_f}{r'_{w,\infty}}$ expression.

Figure 3.16 contains the same information with a difference that for the third case Equation 3.31, instead of Equation 3.33, has been used for converting J_D to ξ_∞. It can be seen that using a more correct equation has slightly reduced ξ_∞ when I_X approaches 1.0. These values of ξ_∞ have been used for the new formulation.

Similar to what explained for Equation 3.28, analysis of the results of the in-house simulator resulted in the following equation for the estimation of ξ_∞ in a square drainage area at PSS.

$$\xi_\infty = 2 \times B \,, \tag{3.34}$$

where:

$$B = \ln\left(e^1 + \frac{0.64}{(r_{eD} - 0.746)^{1.283}} \right). \tag{3.35}$$

The constants of the above equation have been adjusted based on the data analysis (described in Appendix A) of the results of more than 360 simulation results of HFWs under PSS conditions with the following dimensions:

Fracture width (w_f): 5, 10, 20, 40 mm
Fracture half length (x_f): 5, 11, 24, 50, 70 and 140 m
I_X range: $0.05 < I_X < 0.96$
$C_{fD} = 10{,}000$

Figure 3.17 shows again ξ_∞ versus I_X but also including the results of Equation 3.35. According to this figure, the accuracy of Equation 3.35 seems good.

Now the more general forms of the equations of pseudo fracture skin and effective wellbore radius of an HFW, located in the centre of a square or circular drainage area, applicable for both SS and PSS can be written as follows,

$$S_f^{'} = \ln\left(2\times\delta + \frac{\pi}{C_{fD}}\right) \quad , \tag{3.36}$$

and

$$r_w^{'} = \frac{x_f}{2\times\delta + \frac{\pi}{C_{fD}}}, \tag{3.37}$$

where for steady-state conditions: $\delta = A = \ln\left(e^1 - \frac{0.17}{r_{eD} - 0.87}\right)$

and for pseudo-steady state conditions: $\delta = B = \ln\left(e^1 + \frac{0.64}{(r_{eD} - 0.746)^{1.283}}\right)$.

The difference between the performance of an HFW at SS and that at PSS depends on the absolute value of δ and also its relative magnitude compared to π / C_{fD}. When I_X is less than 0.2, δ has the same value for both SS and PSS ($A \approx B \approx 2$) so effective wellbore radius for both SS and PSS is almost the same. The same situation also occurs

when $2\times\delta$ is much smaller than π / C_{fD}, i.e. the effect of I_X on effective wellbore radius is negligible compared to the effect of C_{fD}. Therefore, it can be concluded that for small value of either I_X or C_{fD}, the performance of an HFW at SS and PSS is almost the same. In other words when the Propped Number, defined by Equation 3.38 (Valko *et al.*, 1998), is small, there is not a significant difference between the performance of a HFW at SS or PSS.

$$N_P = I_X^2 C_{fD} \tag{3.38}$$

It noted that based on Equation 3.38, N_p is two times the ratio of the propped volume to the reservoir volume weighted by their permeability contrast. The concept of Np and its application for fracture design will be discussed further in the next chapter.

It is also important to look at the slope of ξ_∞ versus I_X as *Ix* approaches 1.0. As shown in Figure 3.15, the slope of Figure D.3 is smaller than that of Equation D.3. This difference is not important in the estimation of ξ_∞ or effective wellbore radius. However, in the optimization of fracture design, where the slope of the effective wellbore radius with I_X plays a key role, this small difference becomes important, which will be discussed in Chapter 4, Section 4.3.

The introduced formulae in this section were derived for single phase Darcy flow systems. In the future Sections (Sections 3.4 and 3.5) non-Darcy flow and then gas condensate flow will be investigated to formulate effective fracture conductivity for these types of flow systems. Then it will be shown that replacing absolute fracture conductivity with effective fracture conductivity will extend the applicability of the formula for effective wellbore radius to gas condensate systems.

However, before closing this section the subject of damage in HFWs (for Darcy flow systems) will be investigated briefly in the following subsection.

3.3.3 Skin factors for damages

The investigation of the damage effect on the productivity of an HFW in multiphase flow systems has not defined as one of the purposes of this study. However, for single-phase Darcy flow systems, the author has taken advantage of the in-house simulators to

make some modification on the formulation of damage skin factors available in the literature.

Damage skin represents the difference between the resistance of the damaged layer and its resistance without any damage. The two most common kinds of damage in hydraulic fractured wells are fracture face and choked damage.

Fracture face damage

Fracture face damage expresses the matrix permeability reduction, adjacent to the fracture. Increasing the matrix resistance caused by this damage can be represented with the fracture face damage skin factor, shown by S_{fd}.

The total flow resistance of an HFW system (R_T) can be calculated by the following equation:

$$R_t = \frac{\mu}{2\pi kh}\left(\ln\frac{r_e}{x_f} + S_f^{'} + S_{fd}\right) = \frac{\mu}{2\pi kh}\ln\frac{r_e}{x_f} + \frac{\mu}{2\pi kh}S_f^{'} + \left(R_{damaged} - R_{undamaged}\right), \quad (3.39)$$

where $R_{damaged}$ is the damaged layer resistance and $R_{undamaged}$ is its resistance without damage. If it is assumed that the damaged layer has a constant thickness and permeability, and flow from the matrix to the fracture is uniform and normal to the fracture face, it can be written:

$$R_{damaged} = \frac{\mu w_d}{4k_d x_f h} \quad and \quad R_{undamaged} = \frac{\mu w_d}{4k x_f h}. \quad (3.40)$$

Combining Equations 3.39 and 3.40 will result in:

$$S_{fd}\frac{\mu}{2\pi kh} = \frac{w_d\mu}{4x_f k_d h} - \frac{w_d\mu}{4x_f kh} \Rightarrow S_{fd} = \frac{\pi}{2}\frac{w_d}{x_f}\left(\frac{k}{k_d} - 1\right). \quad (3.41)$$

This equation was described first by Cinco-Ley (1978). However, in practice, damaged layer thickness is not usually constant but probably decreases, almost linearly, toward the tip of the fracture (Diego *et al.,* 2003). In this case, the negative effect of the damaged layer could be less, especially for large values of the fracture conductivity. That is, most flow enters the fracture through the regions near the tip of the fracture, where the damage thickness and its resistance is less.

To simulate this, in the in-house simulator, the width of the grid blocks in the second row was set equal to the maximum thickness of the damaged layer, however, the average permeability of the blocks of this row was calculated with the following equation:

$$\bar{k} = \frac{kk_d}{k(1-\frac{x}{x_f}) + k_d \frac{x}{x_f}}, \tag{3.42}$$

where x is the distance from the well towards the fracture tip.

This equation is the result of equating the equivalent flow resistance of each block to the summation of flow resistances of the damaged and undamaged layers of that block.

Analysis of a large data bank (more than 8000 cases) obtained from the in-house simulator resulted in Equation 3.43 for calculation of fracture face damaged skin.

$$S_{fd} = \left(0.48 + \frac{1}{C_{fD}}\right)\left(\frac{w_d}{x_f}\right)^{0.82}\left(\frac{k}{k_d} - 1\right)^{0.7}. \tag{3.43}$$

The coefficients of the above correlation have been obtained, by conducting a multi-regression exercise for a wide range of variation of pertinent parameters as follows:

Fracture half-length (x_f): 25, 59, 146 m
Fracture width (w_f): 2, 4, 6, 8, 10 mm
Fracture permeability (k_f): 10, 30, 50, 70, 90, 110D
Reservoir permeability (k): 1, 10, 20, 30, 40, 50 mD
k/k_d: 10, 20, 30, 40, 50

Maximum damage thickness: 3, 12, 21, 30, 39 Cm

C_{fD} range: $0.3< C_{fD}< 47$

Figure 3.18 compares the results of Equation 3.43 with those of the in-house simulator, confirming accuracy of this correlation. Here the standard error of estimate is 0.01.

Figure 3.19 demonstrates that for acceptable conductive fractured systems ($C_{fD}>2$) the effect of this damage could be negligible. This figure also shows the prediction of Equation 3.41, proposed by Cinco-lay, which is independent of variation of C_{fD}. The data of Figure 3.19 have been obtained by varying $k_f w_{f,}$ while the following parameters were kept constant:

$$\frac{w_{d,\max}}{x_f}=2\frac{\overline{w}_d}{x_f}=0.02 \quad and \quad \left(\frac{k}{k_d}-1\right)=50.$$

Choked fracture damage

This damage refers to the presence of a damaged zone inside each fracture wing at the entrance to the wellbore, which causes a reduction of fracture conductivity. The damage could be the result of either an over-displacement of the proppant or fine migration and accumulation at the entrance of the fracture to the wellbore during production (Diego *et al*., 2003). This damage can be expressed by a reduced fracture permeability, $k_{f,ck}$. If it is assumed that all flow passes through the whole length of the damaged zone (x_{ck}), a simple mathematical expression can be obtained for choked fracture skin (Equation 3.44).

$$S_{ck}\frac{\mu}{2\pi kh}=\frac{1}{2}\left(\frac{x_{ck}\mu}{w_f k_{f,ck} h}-\frac{x_{ck}\mu}{w_f k_f h}\right)\Rightarrow$$
$$S_{ck}=\frac{\pi x_{ck} k}{w_f k_f}\left(\frac{k_f}{k_{f,ck}}-1\right) \qquad (3.44)$$

S_{ck} represents the difference between real resistance of the fractured zone and its resistance without damage, and was obtained following a procedure similar to that for Equation 3.41, as follows:

$$R_t = \frac{\mu}{2\pi kh}\left(\ln\frac{r_e}{x_f} + S_f^{'} + S_{ck}\right) = \frac{\mu}{2\pi kh}\ln\frac{r_e}{x_f} + \frac{\mu}{2\pi kh}S_f^{'} + \left(R_{damaged} - R_{undamaged}\right), \quad (3.45)$$

Where

$$R_{damaged} = \frac{\mu x_{ck}}{2k_{f,ck}w_f h}$$
$$R_{undamaged} = \frac{\mu x_{ck}}{2k_f w_f h}.$$

Equation 3.44 is different from the following Equation, reported by Diego *et al.* (2003), as follows:

$$S_{ck} = \frac{\pi x_{ck} k}{x_f k_f}\left(\frac{k_f}{k_{f,ck}} - 1\right). \quad (3.46)$$

In this equation, S_{ck} depends on the fracture half-length instead of the fracture width as found in Equation 3.44. In their paper, it has not been explained why choked skin is a function of fracture length, which should not relate to the flow resistance in the choked layer. Since all other parameters in both equations are the same, there must be a typing error in their formula, Equation 3.46.

Figure 3.20 shows the accuracy of Equation 3.44 by comparing its results with those of the in-house simulator. As this figure shows this equation could overestimate the values of $S_{ck,}$ especially for the high values of x_{ck}. This is because Equation 3.44 is based on the assumption that all flow passes though the whole length of the damaged (choked) area. However, for high values of $x_{ck,}$ a considerable portion of flow enters from the sides of the damaged zone and does not pass through the entire damaged zone.

For a more accurate calculation of choked skin, Equation 3.47 can be used as:

$$S_{ck} = 0.43\left(\frac{\pi x_{ck} k}{w_f k_f}\right)^{0.51}\left(\frac{k_f}{k_{f,ck}} - 1\right)^{0.7}. \quad (3.47)$$

This correlation is structurally similar to Equation 3.44 but with a different coefficient and power exponents. These coefficient and exponents have been obtained by conducting a multi-regression exercise using a large data bank produced by the in-house simulator. This data bank contained more than 7000 data points, with the following conditions:

Fracture width (w_f): 4, 6, 8, 10 mm
Fracture permeability (k_f): 20, 60, 100, 140, 180D
Reservoir permeability (k): 1, 10, 20, 30, 40, 50 mD
$k_f/k_{f,ck}$: 2, 4, 7, 10
$x_{ck}/x_f < 0.15$
Fracture half-length (x_f): 24, 59, 146m

Figure 3.21 shows the accuracy of Equation 3.47. In this comparison the standard error of estimate is about 0.06.

3.4 Single-Phase Non-Darcy Flow Systems

3.4.1 Introduction

Darcy's law states that the pressure drop inside the porous media varies linearly with fluid velocity, as follows:

$$\vec{v} = -\frac{\overline{\overline{k}}}{\mu} \bullet \nabla P, \tag{3.48}$$

where ∇ is the gradient operator, $\vec{v}$ is the velocity vector and $\overline{\overline{k}}$ is the permeability tensor. For isotropic formations with zero non-diagonal elements of permeability tensor, Equation 3.48 can be simplified to the following equation.

$$\vec{v} = -\frac{k}{\mu} \nabla P \tag{3.49}$$

where k is the scalar value of the absolute permeability.

At high velocities according to the Forchheimer equation, pressure drop through the porous media is a second order function of the superficial fluid velocity, as follows:

$$-\overline{\overline{k}} \bullet \nabla P = \mu\vec{v} + \rho\left(\overline{\overline{k}} \bullet \overline{\overline{\beta}}\right) \bullet \vec{v}|v| \tag{3.50}$$

Here $|v|$ is the scalar absolute value of flow velocity.

This tensorial form of the Forchheimer equation was proposed and verified by Wang *et al.* (1999). In this equation $\overline{\overline{\beta}}$ is a non-Darcy coefficient tensor.

In isotropic formations and when the non-diagonal elements are negligible, $\overline{\overline{k}}$ and $\overline{\overline{\beta}}$ tensors are the products of the scalar value of k and β and the unit matrix respectively. For this case, the above equation can be simplified as:

$$\nabla P = \frac{\mu}{k}\vec{v} + \beta\rho|v|\vec{v}\,, \tag{3.51}$$

The difference between this equation and the Darcy Equation (3.49) is the second term on the right hand side, $\rho\beta|v|\vec{v}$, which represents pressure drop or fluid energy lost owing to inertial effect. Therefore, this term is called the 'inertia term' and β is called the 'inertia factor'.

Equation 3.51 can be rearranged to take the following form:

$$\vec{v} = -\frac{k}{\mu}\nabla P \frac{1}{1 + \rho k\beta|v| \Big/ \mu} \tag{3.52}$$

Therefore,

$$\vec{v} = -\frac{k \times F_{ND}}{\mu}\nabla P\,, \tag{3.53}$$

where F_{ND} is called a non-Darcy function and is related to the Reynolds number as follows:

$$F_{ND} = \frac{1}{1+\mathrm{Re}}; \quad \mathrm{Re} = \frac{\rho|v|k\beta}{\mu} \tag{3.54}$$

By comparing Equation 3.53 with the Darcy Equation, it is noted that the effective permeability caused by the non-Darcy or inertial effect is $k \times F_{ND}$. In other words, F_{ND} is the relative permeability of a single-phase as a result of the non-Darcy flow regime.

In an HFW, inside the matrix (as will be shown) the inertial effect is not significant because of the low velocity. However, inside the fracture, fluid (gas or even oil) commonly flows with high velocities, so the inertial effect could be very important and reduce the effective fracture conductivity significantly.

Many investigators have studied this subject and introduced some correlations for predicting the inertial effect. Guppy *et al.* (1982) studied inertial effect in hydraulically fractured wells. They simulated a series of draw down tests and developed the following correlation:

$$C_{fD-eff} = \frac{C_{fD}}{1+0.31\times Q_D}. \tag{3.55}$$

Here, Q_D is the dimensionless flow constant defined as:

$$Q_D = \frac{k_f \rho\beta q_w}{h w_f \mu} = 2\,\mathrm{Re}_w, \tag{3.56}$$

where q_w is the total flow rate from both wings of the fracture.

Equation 3.55 can be rewritten in terms of Re as follows:

$$C_{fD-eff} = \frac{C_{fD}}{1+0.62\times \mathrm{Re}_w}. \tag{3.57}$$

In another paper, Guppy *et al.* (1982) simulated a fractured well for a build-up test and introduced this correlation:

$$C_{fD-eff} = \frac{C_{fD}}{1+0.55\times Q_D} = \frac{C_{fD}}{1+1.1\times \mathrm{Re}_w}. \tag{3.58}$$

Gidely (1991) proposed that inertial effect reduces effective fracture conductivity as follows:

$$C_{fD-eff} = \frac{C_{fD}}{1+\mathrm{Re}_w}, \tag{3.59}$$

where Re_w is estimated based on the flow properties at the wellbore.

Settari *et al.* (2002) tried to develop a correlation for the calculation of non-Darcy flow skin, by simulating a hydraulically fractured well at pseudo-steady state conditions. They compared the results of their simulations with Equation 3.58 (basically developed for build-up test), demonstrating that this equation overestimates the non-Darcy effect. They also suggested that the non-Darcy skin factor should be a function of two additional parameters (i.e., $k_f w_f$ and k) in addition to dimensionless parameters C_{fD} and Re. Smith *et al.* (2004) confirmed Settari's finding that Equation 3.58 overestimates inertial effect. The authors of these two papers have not compared their results with the equation derived for drawdown, Equation 3.57, which can describe their simulations more closely.

Although all the above studies have confirmed the importance of inertial effect in the reduction of fracture conductivity the results of the introduced formulae could be very different. In the next subsection after evaluation the impact of inertial effect the correct formula will be selected.

3.4.2 Impact of inertial effect for HFWs

As mentioned earlier, relative permeability of the single-phase flow, F_{ND}, defined by Equation 3.54, represents how inertial effect decreases the effective permeability.

Figures 3.22a and b show single-phase relative permeability distribution around a HFW. These plots show the results of simulating the HFWS-1 system with the properties as described in Table 3.1a.

Figures 3.22 indicates two important points:

First, it can be seen that F_{ND} in the matrix is almost 1.0, while in the fracture it is significantly less than 1.0. That is, the inertial effect inside the matrix is negligible compared with this effect inside the fracture. In other words, it is a good assumption to neglect inertial effect inside the matrix.

Another HFW model (HFWS-2) was simulated, whereby its inertial effect in the matrix had been increased by using a higher permeable rock. In the new model the matrix was Clashach with permeability of 553 mD and single-phase inertial factor of $1.035*10^{8}$ m^{-1}. The fracture permeability was also increased to 1460 Darcy to keep the fracture conductivity in an acceptable range, however, in order to keep kβ of the fracture constant, the proppant beta factor was decreased 10 times. The rest of parameters were the same as that in the previous example. As shown in Figures 3.23a and 3.23b, even in this highly permeable rock with very high well productivity, the inertial effect in the matrix is negligible.

The second important point in Figures 3.22 and 3.23 is the variation of F_{ND} inside the fracture. As these figures show, the inertial effect inside the fracture is not constant but, as expected, it increases toward the wellbore and it has its maximum value, minimum F_{ND}, at the wellbore. Therefore, assuming that inertial effect is constant could not be a good assumption.

In Equations 3.58 and 3.59, the coefficient of 'Re' at the wellbore, is 1.1 and 1.0, respectively. According to these two equations, the average inertial effect in the fracture is equal to 1.1 or 1.0 times that at the wellbore, whilst it is clear from Figures 3.22 and 3.23 that this effect is at its maximum at the wellbore. In other words, for drawdown cases in the formulation of $\overline{F}_{ND}$, because Re is determined based on the wellbore conditions, its coefficient should definitely be less than one and henceforth $\overline{F}_{ND}$ can represent the average inertial effect inside the fracture. Furthermore, it should be noticed

that Equation 3.58 was developed for a build-up test and is not applicable for a producing well, which is more in line with a drawdown test.

The author compared the results of the correlation derived by Guppy *et al*. (1982), introduced for drawdown test, Equation 3.57, with the results of the in-house simulator for many different cases of single-phase flow. It was concluded that this correlation can predict the impact of inertial effect on the fracture conductivity with good accuracy (Gas Condensate Progress Report, September 2006). A similar verification has also been reported recently by Huang *et al.* (2007).

Using Equation 3.57 suggests that the average inertial effect in the fracture (represented by Reynolds number) is 62% of that at the fracture entrance to the wellbore. Therefore, in single-phase non-Darcy flow systems, the effective fracture conductivity can be calculated as follows:

$$C_{fD-eff} = C_{fD} \times \overline{F}_{ND}; \quad \overline{F}_{ND} = \frac{1}{1 + 0.62 \times \mathrm{Re}}, \tag{3.60}$$

The equation of effective fracture conductivity has two main applications. One application, as explained by Guppy *et al.* (1988), is in the well test analysis to identify the fracture parameters. The other application is in the formulation of effective wellbore radius in non-Darcy flow systems. In Section 3.5.4, it will be shown that for non-Darcy flow systems effective wellbore radius can be calculated with Equation 3.38, provided that, instead of absolute fracture conductivity, effective fracture conductivity is used.

3.5 Gas condensate flow systems

3.5.1 Introduction

In gas condensate reservoirs, when pressure falls below the dew point, condensate build-up plays a key role in controlling well productivity. This parameter depends on the pressure profile around the wellbore. The important parameters, which can control pressure profile and consequently the condensate saturation distribution in the drainage area, are:

1- Fluid composition.

2- Reservoir temperature and pressure.

3- Flowing bottomhole pressure.

4- Rock's Flow resistance.

In HFW systems, the problem becomes more complex because rock physical properties and flow behaviour in matrix and fracture are totally different.

In Section 3.3.2, it was shown that pressure distribution around an HFW strongly depends on the fracture conductivity. However, in gas condensate reservoirs, the effective fracture conductivity could be very different from absolute fracture conductivity. In Section 3.4, it was shown how velocity effect inside the fracture can affect the effective fracture conductivity for single-phase flow systems. In gas condensate reservoirs, velocity could affect the flow behaviour as a result of both inertial and coupling effects albeit to a different extent. Moreover, condensate build-up changes the mobility of gas and condensate in both fracture and matrix to a different extent. Therefore, gas condensate flow in the fracture and around that in the matrix can have complex effects on effective fracture conductivity, owing to interactions between flow velocity and condensate build-up. For example, in an HFW at constant bottomhole pressure, a production rate decrease owing to condensate build-up may increase effective fracture conductivity as a consequence of a reduction of the inertial effect, resulting in decreasing rock's flow resistance around the wellbore. If the bottomhole, reservoir and dew point pressures are constant, decreasing flow resistance causes less pressure drop around the wellbore; i.e. dew point is reached deeper into the reservoir, and therefore a greater two-phase region. Enlarging a two-phase region, on the other hand, increases flow resistance.

3.5.2 Two-phase region around wellbore

In order to investigate the important parameters controlling effective fracture conductivity in gas condensate reservoirs, first there is a need to inspect the shape and extent of the two-phase region by looking at condensate saturation or GTR distribution around HFWs, and evaluate their dependency on fracture conductivity.

Figure 3.24a shows pressure profiles around an un-fractured well (r_w= 0.1m) and around an HFW (HFWS-3 in Table 3.1a) in the same reservoir. Bottomhole flowing pressure for both cases is 90 bar, and dew point pressure is 117 bar. Fracturing improves well

productivity by decreasing flow resistance or pressure drop around the wellbore. Consequently, if well bottomhole pressure is constant for both cases after fracturing the region where its pressure is below the dew point pressure, the two-phase flow region is expanded deeper into the reservoir (see Figure 3.24b). This is more pronounced for higher fracture conductivity.

Figures 3.25a and 3.25b show the shape of the two-phase regions in a quarter of the drainage area (of HFWS-3 defined in Table 3.1a) and also its dependency on fracture conductivity. These figures also show the condensate saturation distribution around the HFW with k_f = 146 D and k_f = 14.6 D respectively. A reduction of fracture absolute permeability reduces absolute fracture conductivity from 9.6 to 0.96.

Figures 3.26-29 show the steady state GTR contour maps around the HFWS-4 to HFWS-7, defined in Table 3.1b.

Basically, the shape of GTR contour maps, as expected, are similar to the pressure or pressure drop contour maps, shown in Figures 3.5 to 3.9. The curves become more elliptical approaching the wellbore. In Figure 3.26, corresponding to HFWS-4, wellbore pressure is 20 psi less than the dew point pressure, however, the exterior boundary pressure is 30 psi greater than the dew point pressure. Thus there is both a single-phase region and two-phase region in this system. Here, as shown in Figure 3.26, the extent of the two-phase region is smaller than the fractured zone. In other words, the half length of the fracture is 106 m, while the two-phase flow region is ended at the depth of less than 40 m from the wellbore.

HFWS-5 is the same as HFWS-4 but its fracture thickness is double. Therefore, the effective fracture conductivity is increased whilst the fracture thickness is kept constant. It results in the expansion of two-phase flow region (Figure 3.27). Moreover, owing to the increase in effective fracture conductivity, GTR constant curves are more elliptical.

In HFWS-6 (see Figure 3.28) the exterior pressure is just 5 psi greater than the dew point pressure. Decreasing drawdown has also decreased the flow rate and accordingly the inertial effect, resulting in an increase in effective fracture conductivity. Therefore, the extent of two-phase flow is greater than that in the previous system and the entire

fractured zone is within the two-phase region. Here GTR contour curves are almost circular in the unfractured zone but become more elliptical in the fractured zone.

An HFW system containing a very small two-phase region is studied by modelling HFWS-7, with its GTR contour map shown in Figure 3.29. The flowing bottomhole pressure is just 5 psi below the dew point pressure, henceforth, the two-phase region is very small and the condensate bank has surrounded just about three metres of each fracture wing.

An important observation that can be made from the above discussion, is that the shape and extent of the two-phase region in an HFW system depends on the fracture conductivity and bottomhole pressure. The two-phase region around HFWs is more elliptical for more conductive fractures and its length can be smaller or bigger than the fracture length.

This consideration raises a serious question about the approach of considering a gas condensate region as a damaged layer with constant thickness around the whole fracture.

3.5.3 Effective Fracture Conductivity

In Section 3.4, the right formula for effective fracture conductivity for single-phase non-Darcy systems, Equation 3.60, was selected. This can be rewritten as:

$$C_{fD-eff} = \frac{w_f k_f \times \overline{F}_{ND}}{x_f k \times 1} = \frac{w_f k_{f-eff}}{x_f k_{eff}}, \tag{3.61}$$

where $k_{f\text{-}eff}$ and k_{eff} are the effective permeability of the fracture and matrix in the single-phase flow system, respectively. A comparison of the expression of effective fracture conductivity (Equation 3.61) with that of absolute fracture conductivity (Equation 3.16) suggests that: *if the absolute permeability is replaced with effective permeability, the absolute fracture conductivity converts to the effective fracture conductivity*. This statement is an important conclusion for single-phase systems, however, not good enough for multiphase systems where relative mass mobility (a combination of relative permeability density and viscosity) plays the key role. In other words, in multiphase flow systems in addition to the relative permeability, the ratio of density over viscosity

of each phase also affects the relative mobility of that phase. This point is clearly seen from the flow equation (Equation 3.5). In this equation $\rho k_r / \mu$ group, referred to as relative mass mobility of each phase, is the multiplication factor next to the pressure gradient of that phase (in this study capillary pressure has been neglected so the pressure of both phases is the same). The impact of fluid properties in this parameter becomes important when there is a significant difference between ρ / μ of different phases.

Thus there is a need to relate absolute fracture conductivity with effective fracture conductivity by the relative mobility.

Equation 3.61 can also be rewritten based on mobility as follows:

$$C_{fD-eff} = \frac{w_f k_f \times \overline{F}_{ND}}{x_f k \times 1} = \frac{w_f k_f \left(\overline{F}_{ND} \rho / \mu \right)}{x_f k \left(1 \times \rho / \mu \right)} \tag{3.62}$$

Here $k_f \left(\overline{F}_{ND} \rho / \mu \right)$ is the effective mass mobility in the fracture or, in other words, $\left(\overline{F}_{ND} \rho / \mu \right)$ is the relative mass mobility in the fracture. Similarly $k\left(1 \times \rho / \mu \right)$ is the effective mass mobility in the matrix. The definition of absolute fracture conductivity can also be rewritten as:

$$C_{fD} = \frac{w_f k_f}{x_f k} = \frac{w_f k_f \left(\rho / \mu \right)}{x_f k \left(\rho / \mu \right)} \tag{3.63}$$

Where $k_f \left(\rho / \mu \right)$ and $k\left(\rho / \mu \right)$ are absolute mass mobilities in the fracture and matrix respectively. Now, by comparing Equations 3.62 and 3.63, it can be concluded that *if the absolute mobility of fracture and matrix are replaced with their effective mobility, the absolute fracture conductivity will change to the effective fracture conductivity*. That is, the following equation may be used for the estimation of effective fracture conductivity:

$$C_{fD-eff} = \frac{w_f k_f \times \overline{\mathrm{M}}_{rf}}{x_f k \times \overline{\mathrm{M}}_{rm}} = C_{fD} \frac{\overline{\mathrm{M}}_{rf}}{\overline{\mathrm{M}}_{rm}} \tag{3.64}$$

In this equation $\overline{\mathrm{M}}_{rf}$ and $\overline{\mathrm{M}}_{rm}$ are the average relative mass mobility in the fracture and matrix respectively. For gas condensate flow systems, these parameters are defined as:

$$\overline{\mathrm{M}}_{rf} = \left(\frac{\rho_g}{\mu_g} k_{rg-f} + \frac{\rho_c}{\mu_c} k_{rc-f} \right)_{av} \tag{3.65}$$

$$\overline{\mathrm{M}}_{rm} = \left(\frac{\rho_g}{\mu_g} k_{rg-m} + \frac{\rho_c}{\mu_c} k_{rc-m} \right)_{av} \tag{3.66}$$

These formulae for relative mobility are applicable for both single-phase flow and gas condensate flow, but they are not straight forward to use. The first difficulty is the method of averaging: i.e. what is the best averaging method that can represent the effective mobility inside the fracture and matrix. It definitely depends on the flow regimes and it can not be a simple geometrical averaging because the flow is not homogenous within the entire fracture or the entire matrix of the fractured zone. The second difficulty is raised because of the unavailability of some data. For instance, the fracture base relative permeability curve can be measured in the laboratory, however, it is different from the relative permeability affected by velocity (required for use in the above formula).

Thus, the main purpose here is the development of more practical formulae that use more easily available data at wellbore conditions to estimate effective fracture conductivity.

Relative mass mobility in the fracture

In Section 3.4 it was shown that, for single-phase systems, inertia can seriously affect effective permeability inside the fracture. For gas condensate systems, velocity could have two possible effects (Danesh *et al.,* 1994); whilst inertial effect has a negative effect on the relative permeability; coupling effect, which is a combination of velocity and interfacial effect, can improve it.

The author evaluated the impact of variations of coupling and inertia by conducting a series of simulations on gas condensate flow inside the HFWs, for many different fracture and reservoir designs. Figure 3.30 shows the variation of gas relative permeability and also base gas relative permeability along the fracture of an HFW system; the case is labelled as HFWS-8 in Table 3.1c. In Figure 3.30, base relative permeability is the relative permeability measured in the laboratory at very low velocity and high IFT.

Variation of k_r curves and the difference between them in the fracture, shown in Figure 3.30, highlight a very important point: *inside the fracture, owing to high flow velocities, the inertial effect is dominant and coupling effect is negligible.*

The fact that the coupling effect inside the fracture is negligible, lead the author to develop a simple relationship between base gas relative permeability of the proppant and its gas relative permeability (affected by inertial effect), which is:

$$k_{rg-f} = \frac{k_{rgb-f}}{1+\mathrm{Re}} \tag{3.67}$$

where b refers to base. Different definitions of the Reynolds number were checked, and it was concluded that if the Reynolds number contains inertial effects of both gas and condensate, the results of the above equation and the generalized HW permeability correlation (Jamiolahmady *et al.* 2006) become almost the same, Figure 3.31.

Thus Reynolds number is defined as:

$$\mathrm{Re} = \frac{\bar{\rho} v k_f \beta_f \left(k_{rgb-f} + k_{rcb-f}\right)}{\bar{\mu}} \tag{3.68}$$

Here, average density and viscosity are estimated by the volumetric average of the properties of two phases.

$$\begin{aligned} \bar{\rho} &= GTR \times \rho_g + (1-GTR)\rho_c \\ \bar{\mu} &= GTR \times \mu_g + (1-GTR)\mu_c \end{aligned} \tag{3.69}$$

Although the volumetric averaging is not the best method for the estimation of the average viscosity it is not expected that it will cause significant errors. This is because usually fractional flow of condensate is much less than that of gas phase.

Figure 3.31 shows the good agreement between the results of general HW correlation and Equation 3.67 for HFWS-8. If, in the calculation of the Reynolds number, condensate inertial force element is neglected, by ignoring k_{rcb-f} compared with k_{rgb-f}, relative permeability will be slightly overestimated as shown in Figure 3.31.

The high level of agreement between Equation 3.67 and the HW generalised relative permeability correlation is because, coupling effect in the fracture is not important and also the HW generalised relative permeability correlation uses a similar approach for taking into account the inertial effect on relative permeability. The good agreement of the predicted k_r values by the HW generalised relative permeability correlation with the corresponding measured values for two propped fractures with permeability of 15D and 146 D has recently been verified (Jamiolahmady *et al,* 2008).

The discussion in section 3.4.2 suggested that for the case of single-phase flow average inertial effect in the fracture can be estimated using Reynolds number estimated at wellbore conditions, provided that the coefficient of Reynolds number is 0.62 (see Equation 3.60).

Now the use of this equation is extended to that of a two-phase flow. That is:

$$\bar{k}_{rg-f} = \frac{\bar{k}_{rgb-f}}{1 + 0.62 \times \mathrm{Re}_w} \tag{3.70}$$

In this Equation $\bar{k}_{rgb-f}$ is the average base gas relative permeability in the fracture. In the case of single-phase flow, $\bar{k}_{rgb-f}$ is equal to one and Equation 3.60 is obtained.

In Equation 3.70, Re_w refers to Reynolds number at wellbore conditions, calculated as:

$$\mathrm{Re}_w = \frac{\overline{\rho}_w v_w k_f \beta_f \left(k_{rgb-f} + k_{rcb-f}\right)_w}{\overline{\mu}_w}, \tag{3.71}$$

where $\overline{\rho}_w$ and $\overline{\mu}_w$, average density and viscosity, similar to other parameters, are estimated at wellbore conditions.

$$\begin{aligned} \overline{\rho}_w &= GTR_w \times \rho_{g_w} + (1 - GTR_w)\rho_{c_w} \\ \overline{\mu}_w &= GTR_w \times \mu_{g_w} + (1 - GTR_w)\mu_{c_w} \end{aligned} \tag{3.72}$$

In Equation 3.71, β_f is the fracture single-phase inertia factor and v_w is the velocity at the entrance of the fracture to the wellbore:

$$v_w = \frac{q_w}{2hw_f} \tag{3.73}$$

where q_w is the wellbore flow rate at the bottomhole conditions.

After calculation of average gas relative permeability, average condensate relative permeability can be calculated with the following equation (Jamiolahmdy *et al.,* 2006).

$$\overline{k}_{rc-f} = \overline{k}_{rg-f} \frac{1 - GTR}{GTR} \times \frac{\mu_c}{\mu_g} \tag{3.74}$$

Combining the above equation with Equation 3.70 results in:

$$\overline{k}_{rc-f} = \frac{\overline{k}_{rgb-f}}{1 + 0.62\,\mathrm{Re}_w} \frac{1 - GTR}{GTR} \times \frac{\mu_c}{\mu_g} = \frac{\overline{k}_{rcb-f}}{1 + 0.62\,\mathrm{Re}_w} \tag{3.75}$$

Here GTR and viscosity should be average GTR and viscosity along the fracture, which is difficult to estimate. However, as will be shown in the next section, all the parameters can be estimated at the wellbore conditions.

Now combining Equations 3.65, 3.70 and 3.75 will give the following equation for estimation of average relative mass mobility in the fracture.

$$\overline{\mathrm{M}}_{rf} = \frac{\left(\frac{\rho_g}{\mu_g} k_{rgb-f} + \frac{\rho_c}{\mu_c} k_{rcb-f}\right)_{av}}{1 + 0.62\,\mathrm{Re}_w} = \frac{\overline{\mathrm{M}}_{rbf}}{1 + 0.62 \times \mathrm{Re}_w} \tag{3.76}$$

Here subscript b refers to base. $\overline{\mathrm{M}}_{rbf}$ is the average relative base mobility in the fracture. The sole difficulty when using Equation 3.76 is the estimation of average values of flow properties which will be removed.

Relative mass mobility in the matrix

Figure 3.32 shows the variation of gas relative permeability and base gas relative permeability in the matrix of the case referred to as HFWS-8 in Table 3.1c. This figure also shows k_{rg} in the EOH system. The procedure for estimation of the wellbore radius of the EOH system, which is the main purpose of this section, will be explained in Section 3.5.4. Figure 3.32 shows the following 3 important points:

1. Far away from the wellbore (further than 20m in Figure 3.32), relative permeability is almost constant and parallel to the base relative permeability. The difference is the result of the impact of IFT.

2. Near to the wellbore (closer than 20m in Figure 3.32) the increase in velocity improves gas relative permeability, however, its effect on the average gas relative permeability inside the matrix does not seem particularly significant.

3. The shape of variation of k_{rg} in the matrix of the HFW system and that in the EOH system is the same, and the difference between their values is negligible.

Since the effect of IFT on gas relative permeability (as shown in Figure 3.32) is significant, it needs to be investigated further. Basically, in gas condensate reservoirs IFT depends on the richness of the reservoir fluid. For richer gas condensate reservoirs, the dew point is higher and the reservoir can be in a two-phase region in higher pressures. Thus, as IFT decreases with the increase in pressure, high IFT ratios, i.e. ratio of base value of IFT (3 mNm^{-1}) to local IFT , are more possible in the richer gas

condensate formations. The IFT effect shown in Figure 3.32 is for the case, HFWS-8, that the fluid is C_1-C_{10}, representing a very rich gas condensate fluid. Here the flowing bottomhole pressure is 55 psi below the dew point and IFT ratio is about 400. Now we consider a similar system except the reservoir fluid is a mixture of C_1-C_4 containing 77% methane at 100 ^{o}F, representing a lean gas condensate system. The dew point pressure is 1865 psi and the flowing bottomhole pressure is 1810 psi, 55 psi below P_D (the same as the last case), however, for this system the IFT ratio at the wellbore is about 30. The variation of gas relative permeability in the matrix is shown in Figure 3.33. Two curves of k_{rg} and k_{rgb} are almost the same.

As the coupling effect is a complex function of both velocity and IFT (Jamiolahmady *et al.,* 2006), finding an IFT ratio above which, the IFT effect on the gas relative permeability in the matrix is significant is not an easy task. However some experimental studies in the Gas Condensate Recovery research group at Heriot-Watt University (Final Report, 2002-2005) have shown that when IFT ratio is less than 50, IFT effect on gas relative permeability can be neglected.

To summarize this section, it could be said that average relative mass mobility in the matrix should be estimated based on the IFT affected gas and condensate relative permeability, although when the IFT ratio at the wellbore is less than 50 it could be estimated (with an acceptable accuracy) using matrix base relative permeability. In other words:

$$\overline{\mathrm{M}}_{rm} = \left(\frac{\rho_g}{\mu_g} k_{rg-m} + \frac{\rho_c}{\mu_c} k_{rc-m} \right)_{av} \tag{3.77}$$

$$\overline{\mathrm{M}}_{rm} = \left(\frac{\rho_g}{\mu_g} k_{rgb-m} + \frac{\rho_c}{\mu_c} k_{rcb-m} \right)_{av} \quad if \quad IFT)_{wellbore} > 0.06 \ mN.m \tag{3.78}$$

Approximation of average relative mass mobility ratio to wellbore relative mass mobility ratio

Based on what has been discussed so far, effective fracture conductivity can be estimated using the following formula:

$$C_{fD-eff} = C_{fD} \times \frac{1}{1+0.62\times \mathrm{Re}_w} \times \frac{\overline{\mathrm{M}}_{rbf}}{\overline{\mathrm{M}}_{rm}} \tag{3.79}$$

Or in other words:

$$C_{fD-eff} = C_{fD} \times \frac{1}{1+0.62\times \mathrm{Re}_w} \times MR_{av} \tag{3.80}$$

where MR_{av} is the ratio of average relative mass mobility, which is the ratio of average relative base mobility in the fracture over average relative mobility in the matrix.

$$MR_{av} = \frac{\left(\frac{\rho_g}{\mu_g} k_{rgb-f} + \frac{\rho_c}{\mu_c} k_{rcb-f}\right)_{av}}{\left(\frac{\rho_g}{\mu_g} k_{rg-m} + \frac{\rho_g}{\mu_g} k_{rc-m}\right)_{av}} \tag{3.81}$$

This parameter is still not easy to estimate, because it should be evaluated based on average values. As mentioned earlier, estimation of average relative mobility in the fracture and matrix (which strongly depends on the flow behaviour) is not a straightforward task.

Therefore, attempts were made to find a relationship between this parameter and wellbore relative mass mobility ratio which can be easily estimated at wellbore conditions.

In order to investigate the variation of relative mass mobility ratio, at this stage, it is assumed that the condensate mobility is small compared to the gas mobility. This assumption is applicable when gas relative permeability is much greater than that of condensate and there is an insignificant difference between kinematic viscosity of gas and condensate. However it is notable that this simplifying assumption has only been made in this part of the study. Thus Equation 3.81 could be written as follows:

$$MR \approx \frac{\frac{\rho_g}{\mu_g} k_{rgb-f}}{\frac{\rho_g}{\mu_g} k_{rg-m}} = \frac{k_{rgb-f}}{k_{rg-m}} \tag{3.82}$$

In other words the shape of the variation of *MR* is almost the same as the shape of the variation of $\frac{k_{rgb-f}}{k_{rg-m}}$ which depends on the extent of two-phase region and its relative size to the fractured zone. It also depends on whether the IFT effect on k_{rg-m} is significant or not. To survey the shape of the variation of $\frac{k_{rgb-f}}{k_{rg-m}}$, there is a need to draw the distributions of k_{rgb-f} and k_{rg-m} for different cases and see the variation of their ratio. Here, for simplicity, it is assumed that the distribution of k_{rg-m} along the diagonal can represent the average of its two dimensional distribution.

When the IFT effect is not important and fracture zone is smaller than the two-phase region the ratio of $\frac{k_{rgb-f}}{k_{rg-m}}$ will be equal to $\frac{k_{rgb-f}}{k_{rgb-m}}$, which is more or less constant. Figure 3.34 shows k_{rgb-f} of HFWS-9 as a function of x-distance from the wellbore and also its k_{rg-m} as a function of diagonal distance from the wellbore. This latter curve has been plotted in the domain of effective wellbore radius, which will be formulated in the next subsection, and fracture half length.

In HFWS-9, the fractured zone is smaller than the two-phase region and also the IFT effect is not important. Here the two curves are almost parallel and the ratio of $\frac{k_{rgb-f}}{k_{rg-m}}$ varies between 2.52 and 2.53: i.e. almost constant. Many other similar cases were investigated and it was proved that when fractured zone is smaller than the two-phase region and IFT ratio is less than 50, the ratio of $\frac{k_{rgb-f}}{k_{rg-m}}$ is almost constant. Thus $\frac{(k_{rgb-f})_{av}}{(k_{rg-m})_{av}}$ is almost equal to $\frac{(k_{rgb-f})_{w}}{(k_{rg-m})_{w}}$; consequently MR_{av} can be approximated with relative mass mobility ratio estimated at wellbore conditions; MR_w.

When the IFT effect on the gas relative permeability in the matrix is significant, the coupling effect around the wellbore becomes more pronounced; thus two curves of k_{rgb-f} and k_{rg-m} are not in good parallel alignment. These curves for HFWS-8 have been shown in Figure 3.35. As mentioned earlier, the IFT ratio at the wellbore of this system is about 400, so the improving coupling effect on k_{rg-m} around the wellbore is more pronounced. Therefore, at the wellbore $\frac{k_{rgb-f}}{k_{rg-m}}$ has its minimum value which is 1.18, whilst this ratio for other points could be at most 1.43 (18% difference). That is to say, the maximum possible difference between $\frac{(k_{rgb-f})_{av}}{(k_{rg-m})_{av}}$ and $\frac{(k_{rgb-f})_{w}}{(k_{rg-m})_{w}}$ for this case must be less than 18%. Investigation of some other similar cases resulted in similar ranges of differences between these ratios. However, it is expected that the real difference between $\frac{(k_{rgb-f})_{av}}{(k_{rg-m})_{av}}$ and $\frac{(k_{rgb-f})_{w}}{(k_{rg-m})_{w}}$ should be much less than the maximum possible difference, because the flow properties at the wellbore plays the key role in controlling average flow behaviour. Thus average relative mobility ratio should be extremely close to the relative mobility ratio at the wellbore rather than other local relative mobility ratios in the fractured zone.

The variation of the relative mobility ratio becomes more significant when the two-phase region lies inside the fractured zone. In this case, k_{rgb-f}, k_{rg-m} and consequently their ratio are 1.0 at the outer boundary of the fractured zone, where there is single-phase, however, the ratio is definitely different from 1.0 at the wellbore. However, since the two-phase region, which provides the major resistance within the flow pattern and controls it, is near to the wellbore, it can be assumed that even in this case, the average relative mobility ratio is very close to the relative mobility ratio at the wellbore. The validity of this assumption will be verified in Section 3.6.1, where the results of modelling equivalent open-hole system are compared with the results of simulating fine grid block models. For instance, simulating HFWS-7, which contains a very small two-phase region (see Figure 3.29), predicts a mass production rate as 7280 kg/d, while mass production rate estimated from the simulation of its EOH system is 7550 kg/d. In other words, the absolute deviation between the results of two models is about 3.5%. This indicates the good accuracy of the formula for effective wellbore reduce which strongly depends on the precision on the estimated effective fracture conductivity at wellbore

conditions. The corresponding deviation for HFWS-4, containing a greater two-phase region but still smaller than the fractured zone, is just about 1%.

In summary, average relative mobility ratio can be approximated to the wellbore relative mobility ratio and therefore, effective fracture conductivity in gas condensate systems can be estimated by the following equation:

$$C_{fD-eff} = C_{fD} \times MR_w \times \frac{1}{1+0.62\times \mathrm{Re}_w}, \tag{3.83}$$

where:

$$MR_w = \frac{\mathrm{M}_{rbf}\big|_w}{M_{rm}\big|_w} = \frac{\left(\frac{\rho_g}{\mu_g}k_{rgb-f} + \frac{\rho_c}{\mu_c}k_{rcb-f}\right)_{well-bore}}{\left(\frac{\rho_g}{\mu_g}k_{rg-m} + \frac{\rho_c}{\mu_c}k_{rc-m}\right)_{well-bore}} \tag{3.84}$$

All data required for using in Equations 3.83 and 3.84 are estimated at the wellbore conditions. It should be noted that gas and condensate relative permeability in the matrix becomes almost equal to the base values, measured in the laboratory, if the IFT effect at the wellbore is negligible (IFT at the wellbore is greater than 0.06); if not, it should be estimated by the correlations of relative permeability (Jamiolahmady *et al.* 2006) using base relative permeability and wellbore IFT, velocity and pressure gradient.

3.5.4 Pseudo Fracture skin and effective wellbore radius

In gas condensate systems, SS pseudo fracture skin is defined by the following equation:

$$\dot{m} = 2\pi kh \frac{\Delta\Psi}{\ln\left(\frac{r_e}{x_f}\right) + S_f^{'} + S_d} \tag{3.85}$$

In this equation, S_d is the summation of mechanical damage skins and $\Delta\psi$ is the pseudo pressure difference, defined as:

$$\Delta\Psi = \int_{P_w}^{P_e}\left(\frac{\rho_g}{\mu_g}k_{rg} + \frac{\rho_c}{\mu_c}k_{rc}\right)dP, \tag{3.86}$$

where k_{rg} and k_{rc} are the gas and condensate relative permeability in the matrix, respectively. Equation 3.85 can be written based on an effective wellbore radius as follows:

$$\dot{m} = 2\pi kh\frac{\Delta\Psi}{\ln\left(\frac{r_e}{r_w^{'}}\right) + S_d} \tag{3.87}$$

It should be noted that pseudo pressure depends on the flow velocity in the matrix; hence, $\Delta\psi$ in Equations 3.85 and 3.87 could be different (Jamiolahmady et al. 2005). However, as in HFW systems normally an effective wellbore radius is not small it is expected that velocity and its impact on relative permeability is not significant. Therefore, the two $\Delta\psi$ in Equations 3.85 and 3.87 would not be very different. Hence, the relationship between pseudo fracture skin and effective wellbore radius, similar to single-phase, is as follows:

$$r_w^{'} = x_f e^{-S_f^{'}} \tag{3.88}$$

In Section 3.3.2, the formula for an effective wellbore radius of a HFW at steady or pseudo-steady state was introduced for single-phase Darcy flow conditions. The author proposes extending the use of this formulation for gas condensate systems by replacing the absolute fracture conductivity by the effective fracture conductivity (introduced in the last section). Therefore, the corresponding equations for estimation of pseudo fracture skin and effective wellbore radius located in the centre of a square or circular gas condensate reservoirs at steady or pseudo-steady state conditions are:

$$S_f^{'} = \ln\left(2\times\delta + \frac{\pi}{C_{fD-eff}}\right) \tag{3.89}$$

$$r_w^{'} = \frac{x_f}{2\times\delta + \pi / C_{fD-eff}}, \tag{3.90}$$

where, as mentioned before,

for steady-state conditions: $\delta = A = \ln\left(e^1 - \frac{0.17}{r_{eD} - 0.87}\right)$

and for pseudo-steady state conditions: $\delta = B = \ln\left(e^1 + \frac{0.64}{(r_{eD} - 0.746)^{1.283}}\right)$.

3.5.5 The Iterative Method for Estimation of Effective Well-Bore Radius

The formulation introduced in this chapter can be used in an iterative method for estimation of an effective wellbore radius of the EOH system as follows:

1- As a first estimate, the effective wellbore radius is calculated based on a Darcy effective wellbore radius as follows:

$$r_w^{'} = \frac{x_f}{2\times\delta + \pi / C_{fD}}.$$

2- Pressure distribution and well flow calculation are conducted based on the above effective wellbore radius.

3- Effective fracture conductivity is calculated using the following equations:

$$C_{fD-eff} = C_{fD} \times MR_w \times \frac{1}{1 + 0.62 \times \mathrm{Re}_w},$$

where

$$MR_w = \frac{\mathrm{M}_{rbf}\big|_w}{M_{rm}\big|_w} = \frac{\left(\frac{\rho_g}{\mu_g} k_{rgb-f} + \frac{\rho_c}{\mu_c} k_{rcb-f}\right)_{well-bore}}{\left(\frac{\rho_g}{\mu_g} k_{rg-m} + \frac{\rho_c}{\mu_c} k_{rc-m}\right)_{well-bore}},$$

$$\mathrm{Re}_w = \frac{\overline{\rho}_w v_w k_f \beta_f \left(k_{rgb-f} + k_{rcb-f}\right)_w}{\overline{\mu}_w},$$

$$k_{rcb-f}\Big|_w = \left(k_{rgb-f}\,\frac{1-GTR}{GTR} \times \frac{\mu_c}{\mu_g}\right)_w \quad ,$$

$$\overline{\rho} = GTR \times \rho_g + (1-GTR)\rho_c\Big|_{at\ well-bore}$$
$$\overline{\mu} = GTR \times \mu_g + (1-GTR)\mu_c\Big|_{at\ well-bore} \quad ,$$

$$v_w = \frac{q_w}{2hw_f}.$$

4- A new effective wellbore radius is calculated using the following equation:

$$r_w^{'} = \frac{x_f}{2\times\delta + \pi / C_{fD-eff}}.$$

5- If the difference between the successive effective wellbore radius values is not negligible, the effective wellbore radius is readjusted and the calculations are repeated from step 2, otherwise calculated pressure distribution and other flow parameters are reported.

As it will be shown in Section 3.6.1, this iterative method converges to the almost accurate solution, i.e. less than 1 mm difference between two successive calculated $r_w^{'}$, on average, with around 6 iterations.

3.5.6 CPU Time

One of the main applications of the developed method for calculation of effective wellbore radius, is the simulation of an EOH system in a commercial simulator, as opposed to simulation of an HFW system, which needs to use very fine grid blocks. Owing to the iterative nature of the method, questions may be raised about the convergence speed and also the relative running time of both methods. To answer these questions, 10 HFW systems (HFWS-10 in Table 3.1c) were modelled with both the 2D HFW in-house simulator and the OH in-house simulator. It was noticed that the 1D OH in-house simulator, using the proposed iterative method, reached the converged solution

at least 4 times faster than the HF simulator. It should also be noted that the in-house 2D HFW simulator simulates just a quarter of the drainage area. However, in simulating a real field with a commercial simulator, the whole drainage area of all HFWs is simulated, so the running time ratio of two approaches should be considerably more than 4. In these runs, the required number of iterations to reach a high accuracy of 1 mm for the wellbore radius values in the last two successive iterations was 4 or 5. The issue of the required number of iterations will also be investigated further in the next section.

3.6 Verification

The main outcomes of this study have been the formulation of effective fracture conductivity, Equation 3.83, and formulation of effective wellbore radius, Equation 3.90 for practical purposes. In this section the applicability of these formulae are verified for both single-phase (including cases affected by inertia) and gas condensate (affected by both coupling and inertia), either at steady state or pseudo state conditions using the in-house and commercial ECLIPSE 300 simulators. The fluid properties used in this part have been shown in Tables 3.2a and 3.2b. Table 3.3 shows base relative permeability values for different rocks, and proppant. The constants and core exponent values, used for the keywords of VELDEP, VDKRG and VDKRO in Eclipse 300, have been shown in Table 3.4. The core exponent values of VDKRG and VDKRO keyword required for the correlation available in ECLIPSE 300 to estimate variation of relative permeability with velocity and IFT are those measured experimentally as part of Gas Condensate Recovery research project at HW University.

3.6.1 Using the in-house simulators

The in-house simulators (explained in Section 3.2) are useful tools for verifying the applicability of the introduced formulae, for steady state conditions. In Section 3.3.2 the proposed formulation was verified for single-phase Darcy flow systems. It was shown that the AAD% for about 16000 comparisons was less than 1.3%.

To verify the accuracy of the developed formulation for single-phase non-Darcy flow and also gas condensate systems, many simulations were conducted for five different series of hydraulically fractured systems. Tables 3.1c and 3.1d summarize the prevailing flow conditions for different cases simulated with both the in-house 2D HFW simulator and 1D OH simulators.

It is noted that the internal radius of the open-hole model is the effective wellbore radius of the HFW, calculated by the iterative method explained earlier. All other parameters of the open-hole model (e.g. matrix physical properties, reservoir extent, pressure difference and reservoir fluid) are the same as those of the HFW model.

In the set of the HFWS-11 simulations, the fluid is a mixture of C_1-C_4 with the methane mole fraction of 73.6% at 311 K (100°F). This fluid can represent a lean gas condensate fluid system with a small retrograde zone. For this fluid at the above temperature, the dew point pressure is 1865 psi. Since the outer boundary pressure (P_e) is 1855 psi (10 psi below the dew point pressure), the whole drainage area lies in the two-phase region. In this set of simulations, flowing bottomhole pressure varies between 1350-1850 psi (5-515 psi below the dew point pressure), and as a result GTR at the wellbore varies between 0.62-0.84. The matrix rock is Texas cream core - a carbonate rock with k=9.1 mD - and proppant absolute permeability is 146 D.

Figure 3.36 compares the results of the two simulators, estimated production rate by the in-house HFW simulator (using the fine grid model) and that by the in-house 1D OH simulator. A high level of accuracy of the developed method for these 198 different cases can be seen from this figure. The average absolute deviation in percentage (AAD%) is 1.8% and the standard error of estimate (SEE) is 0.004.

Figure 3.37 shows the number of iterations required to have a high accuracy of 1 mm for the wellbore radius values in the last two successive iterations. According to this figure, the required number of iterations increases with decreasing effective fracture conductivity. For $C_{fD\text{-}eff}$=0.1, it could be as high as 14, but in this study the average number of iterations is 6.

To investigate rich gas condensate systems, in the set of cases of HFWS-12, Table 3.1c, the fluid was changed to a mixture of C_1-C_{10} with the methane mole fraction of 80% at 500 K (440°F) with the dew point pressure of 3542 psi. The theoretical properties of this system are calculated with the EOS PR3 by the PVTi software, shown in Table 3.2b. The dew point pressure of this fluid is 3541.5 psi. Here the flowing bottomhole pressure varies between 2977 to 3536.5 psi (5 - 546.5 psi below the dew point pressure); thus GTR at the wellbore is something between 0.8 to 0.983. For the simulations whose external outer boundary is 3642 psi (about 100 psi greater than the dew point pressure),

there are both single-phase and two-phase regions in the system. This set of simulations also includes the cases that a two-phase region is smaller than the fractured zone (cases with long fractures, low effective fracture conductivity and bottomhole pressure near to dew point pressure). Figure 3.38 shows the high level of accuracy of the developed method for 194 different cases with AAD% of 1.32% and SEE of 0.007.

In the set of HFWS-13 simulations, the accuracy of the method for a very tight matrix, RC1b (k=0.18mD), was verified by simulating 469 different cases. Different geometrical designs and also different pressure boundaries were covered in this set of study. Here again, as shown in Figure 3.39, the accuracy of the method is acceptable with AAD% and SEE of 1.18% and 0.00021, respectively.

In the set of HFWS-14 simulations, the applicability of the method for a high permeable matrix, Berea (k=110 mD) was conformed. The number of simulations in this study was 204. It should also be noted that, to keep the effective fracture conductivity above 0.01, the proppant was 10 times more permeable than those of the previous cases (i.e. k=1440 Darcy); its beta factor was also 10 times smaller but its base relative permeability was the same.

Figure 3.40 shows that the accuracy of the method is acceptable for this system as well, with AAD% and SEE of 3.78% and 0.01, respectively.

To see the applicability of the method for single-phase non-Darcy flow systems, the set of HFWS-15 and their EOH system have been simulated for 174 different operating conditions. In all conditions, flowing bottomhole pressure is kept above the dew point pressure, resulting in single-phase flow within the model. According to Figure 3.41, which compares the results of two simulators, the AAD% is less than 0.8%, verifying the application of the method for single-phase systems.

3.6.2 Using ECLIPSE 300

By now the accuracy of the method for steady state conditions has been verified. As shown in Figure 3.17 PSS formula for effective wellbore radius for single-phase Darcy flow systems is almost the same as Meyer *et al.* formula. The latter is in a very good agreement with other methods available in the literature such as UFD method.

Therefore, there might still be a question about the accuracy of the developed method for gas condensate flow at PSS and also its applicability in a commercial simulator, which basically simulates the model at unsteady state conditions. In late transient conditions, all parameters change with time, but the system approaches either pseudo-steady state or steady state, depending on the exterior boundary condition. This issue was discussed in more detail in section 3.3.2, and it was shown that for fracture penetration ratio greater than 0.2 the equations of effective wellbore radius for steady state and pseudo-steady state are different. It is expected that: *for late transient state, when pressure drop response reaches the external boundary, if the pressure at the exterior boundary is kept constant the performance of HFW is close to that at SS condition, and when there is a closed exterior boundary the equation of pseudo-steady state is more practical*. In the following section this statement will also be verified.

Constant pressure boundary

In a drainage area containing a producer well with constant production rate, if the exterior pressure is kept constant, the well performance will approach steady state and it is expected that the steady state formula should be applicable for estimation of an effective wellbore radius.

Figure 3.42 show the variations of the drawdown $(P_e - P_w)$ of HFWS-16 (see Table 3.1e) and its EOH systems with time. In this figure, and the other subsequent figures, EOH SS refers to EOH with the wellbore radius estimated by steady state formula $(\delta = A)$, whilst EOH PSS refers to EOH with the wellbore radius estimated by pseudo-steady state formula $(\delta = B)$.

In HFWS-16, the flow is single-phase under Darcy flow conditions (β_f is set equal to zero) and the exterior pressure is kept constant and equal to 200 bar (2900 psi). Since the flow rate is also constant, the performance approaches steady state and drawdown becomes constant after almost 30 days. As expected, the performance of the HFW with exterior constant pressure, even at transient conditions, is the same as the EOH system with the effective wellbore radius estimated by SS formula.

The same verification for non-Darcy flow systems is noticed in Figures 3.43 showing the results of simulating the HFWS-17. Here again a high level of conformity between the performance of fine grid model (HFW) and its EOH SS models is observed.

The point should be made clear that in a transient state because the bottomhole pressure is time dependent, the fluid property and hence the Reynolds number and consequently the effective wellbore radius all vary with the progression of time. This variation could be more significant in two-phase cases, which will be discussed later in this section. However, just for simplicity in all the reported results of this section (except for Figure 3.44) this variation has been ignored. The effective wellbore radius has then been calculated based on the conditions at 60 days after the beginning of production, when the rate of variation of bottomhole pressure and, as a result, effective fracture conductivity is not significant. Needless to say, this simplification may decrease the accuracy of the results. To obtain more accurate results, at transient state, the effective wellbore radius should be re-calculated at each transient state.

Figure 3.44 shows the same verification for gas condensate flow in HFWS-18 In Figure 3.44, the effective wellbore radii of EOH systems are calculated at three time steps. In these three time steps, the drawdown of steady state EOH systems is the same as that of the HFW system.

In short, the results of this section, Figures 3.42-3.44, show that: *when the exterior boundary of the drainage area is maintained at constant pressure, even in late transient state, SS formulation of effective wellbore radius has satisfactory accuracy*.

Closed boundary

As mentioned earlier, the performance of an HFW in a closed boundary drainage area approaches pseudo-steady state conditions. In the previous sections, a general formula for the estimation of effective fracture conductivity in gas condensate systems was developed; subsequently it was shown that, for steady state or constant pressure boundary, using this parameter (effective fracture conductivity) instead of absolute fracture conductivity will extend the application of formulation to gas condensate reservoirs. Now it is intended to show that this approach is also applicable for pseudo-steady state, i.e. closed boundary conditions.

First the developed method is tested for single-phase Darcy flow systems at closed boundary conditions. Figure 3.45 compares drawdown predicted for HFWS-21 and its EOH systems. This figure shows the acceptable accuracy of applying PSS formula for an HFW in closed drainage area under single-phase Darcy flow regime.

Now this verification is extended to single-phase non-Darcy flow and also gas condensate systems. In Figure 3.46 (HFWS-20) absolute fracture conductivity is 11, however, owing to the considerable production rate, effective fracture conductivity is 2.5. Here again the performance of EOH-PSS is the same as that of HFW.

For gas condensate reservoirs also, a high level of accuracy is noticed from Figure 3.47 (HFWS-21).

The important point shown here is the fact that the correctness of PSS formulation of effective wellbore radius for three cases of single-phase Darcy flow, single-phase non Darcy flow and gas condensate flow is almost the same, which conforms to the following important conclusions:

1- *When the exterior boundary of the drainage area is closed, even in late transient state, the PSS formula for effective wellbore radius has acceptable accuracy.*

2- *The developed formula for effective fracture conductivity is also valid for unsteady steady state conditions.*

3- *Using effective fracture conductivity instead of absolute fracture conductivity extends the applicability of formulae of the effective wellbore radius to gas condensate reservoirs.*

3.7 Conclusions

In this chapter, after describing the basic theory behind the 2D and 1D in-house simulators, single-phase and gas condensate flow around HFWs at steady and pseudo-steady states were studied. The main conclusions can be summarized as follows:

1. By presenting pressure drop contour maps around HFWs, it was shown that flow near to the wellbore is elliptical, although it converges to radial flow with decreasing fracture conductivity.

2. It was shown that for small propped numbers the performance of an HFW at steady-state conditions is the same as that at pseudo-steady state conditions, however, for large propped numbers when fracture penetration ratio is greater than 0.2, an HFW can have two different performances at SS and PSS.

3. New formulae were developed for estimation of effective wellbore radius of an HFW at SS and PSS.

4. It was explained that the dominant velocity effect inside the fracture is an inertial effect; whilst inside the matrix (except for the cases that IFT at the wellbore conditions is less than 0.06), velocity effect is not significant.

5. Some of the formulae available in the literature for estimation of non-Darcy effect in single-phase flow systems were discussed, and it was shown that Guppy's correlation (developed for drawdown) can predict inertial effect with high levels of accuracy.

6. It was shown that, inside the matrix, the main source for the difference between k_{rgb} and k_{rg} is IFT effect.

7. After investigating the variation of relative mobility inside the fracture and matrix of the fractured zone, a new formula for estimation of effective fracture conductivity in gas condensate reservoirs was introduced (Equations 3.83, 3.84 and 3.71). This formula is applicable for both SS and PSS conditions.

8. It was shown that the introduced equations for estimation of an effective wellbore radius in single-phase Darcy flow systems can still be used for gas condensate reservoirs if the effective fracture conductivity is used instead of absolute fracture conductivity.

9. An iterative method for using the developed formula for effective wellbore radius was proposed, and its convergence rate was found to be acceptable.

10. The accuracy of the formula for steady state conditions was verified for different fluid systems, matrix cores and flow conditions (over 1000 simulations), which confirmed the integrity of the approach.

11. For unsteady state conditions, when I_X is less than 0.2, both SS and PSS formulae are the same and can predict the effective wellbore radius. However, when I_X is greater than 0.2, the most suitable formula should be selected according to the exterior boundary condition.

12. It was shown that the SS and PSS formulae can predict the effective wellbore radius of an HFW, even in late transient condition with acceptable accuracy for the cases of constant exterior pressure and closed exterior boundary, respectively.

References

Carvajal G.A., Danesh A., Jamiolahmady M. and Sohrabi M.: "The Impact of Pertinent Parameters on the Design of Hydraulic Fracturing in Gas Condensate Reservoirs" SPE 94074, presented at SPE Europech/EAGE annual Conference, Madrid, Spain, 2005.

Cinco-Ley, H., Samaniego-V. F.: "Effect of Wellbore storage and Damage on the Transient Pressure behaviour of vertically fractured Wells", SPE 6752, presented at 52nd Annual Fall Technical Conference, Denver, USA, 1977.

Cinco-Ley, H., Samaniego-V. F. and Dominguez A. N.: "Transient Pressure Behaviour for a well with a Finite Conductivity Vertical Fracture", SPE 6014, SPE Journal, pp. 253-264, Sep-1978.

Cinco-Ley, H. and Samaniego-V.: "Transient Pressure Analysis Finite Conductivity Fracture Case versus Damaged Fracture Case," SPE 10179, 1981.

Cinco-Ley, H.: "Evaluation of Hydraulic Fracturing by Transient Pressure Analysis Methods" SPE 10043, presented at International Petroleum Exhibition and Technical Symposium, Beijing, China, 1982.

Cinco-Ley, H., Ramey Jr., H., Samaniego-V. F. and Dominguez A. N.: "Behaviour of Wells with Low-Conductivity Vertical Fractures" SPE 16776, presented at SPE Annual Technical Conference and Exhibition, Dallas, USA, 1987.

Danesh A., Khazam M., Henderson G.M., Tehrani D. and Peden G.M: "Gas Condensate Recovery Studies" DTI Improved Oil Recovery and Research Dissemination Seminar, London, June 1994.

Dake, L.P.: Fundamentals of Reservoir Engineering, Elsevier Science B.V., Amsterdam, Netherland, 1978.

Economides, M., Oligney, R., and Valko, P.: Unified Fracture Design, Orsa Press, Alvin, Texas, USA, (2002).

Forchheimer, P.: Hydraulik, Chapter15, pp. 116-8, Leipzik and Berlin, 1914.

Gas Condensate Recovery Project (1999-2002) Final Report, IPE, Heriot Watt University, UK, 2002.

Gas Condensate Recovery Project (2002-2005) Final Report, IPE, Heriot Watt University, UK, 2005.

Gas Condensate Recovery Project (Jan. 2007- Sep. 2007) Progressing Report, IPE, Heriot Watt University, UK, Sep. 2007.

Gas Condensate Recovery Project (2005-2008) Final Report, IPE, Heriot Watt University, UK, 2008.

Giddley J.L.: "A Method for Correcting Dimensionless Fracture Conductivity for Non-Darcy Flow Effects" SPE 20710, SPE Production Engineering Journal, pp.391-394, Nov-1991.

Gringarten, A. C., Ramey, H.J., and Raghavan, R.: "Unsteady State Pressure Distributions Created by a Well with a Single Infinite-Conductivity Fractures" SPE Journal, pp 347-360, 1974.

Guppy K.H., Cinco-Ley H., Ramey Jr. H.J. and Samaneigo-V. F.: "Non-Darcy Flow in Wells with Finite-Conductivity vertical Fractures" SPE 8281, SPE Journal, pp. 681-698, Oct-1982.

Guppy K.H., Cinco-Ley H., and Ramey Jr. H. J.: "Pressure Build-up Analysis of Fractured Wells Producing at High Flow Rate" JPT, pp. 2656-2666, Nov-1982.

Hashemi A. and Gringarten A. C.: "Comparison of Well Productivity between Vertical, Horizontal and Hydraulically Fractured Wells in Gas Condensate Reservoirs" SPE 94178, presented at SPE Europech/EAGE Annual Conference, Madrid, Spain, 2005.

Holditch, S.A. and Morse, R.A.: "The Effects of Non-Darcy Flow on the Behaviour of Hydraulically Fractured Gas Wells," Journal of Petroleum Technology, pp 1169-1178, Oct. 1976.

Huang H. and Ayoub J.A.: "Modeling Non-Darcy Flow and Perforation Convergence for Vertically Fractured Wells" SPE 107853, presented at European Formation Damage Conference, Scheviningen, Netherland, 2007.

Jamiolahmady, M., Danesh, A., Rezaei, A., Ataei, R. and Sohrabi, M.: "Calculation of productivity of a gas condensate well: application of skin with rate dependent pseudo-pressure" SPE 94718, presented at Proceedings of the SPE European Formation Damage Conference, May 2005.

Jamiolahmady, M., Danesh, A., Tehrani, D.H., and Sohrabi, M.: "Variations of Gas Condensate Relative Permeability with Production Rate at Near Wellbore Conditions: A general Correlation" SPE Reservoir Engineering and Evaluation Journal, **9** (6), pp.688-697, 2006.

Jamiolahmady, M., Sohrabi, M. and Ireland, S.: "Gas Condensate Relative Permeabilities in Propped Fracture Porous Media: Coupling Versus Inertia", SPE 115726, Colorado, USA, September 2008.

Mahdiyar H., Jamiolahmady M., Danesh A.: "New Mechanical and Damage Skin Factor Correlations for Hydraulically Fractured Wells" SPE 107634, presented at European Formation Damage Conference, Scheviningen, Netherland, 2007.

McGuire, W. and Sikora V.: "The Effect of Vertical Fractures on Well Productivity" paper SPE 1618-G, JPT, **12**(10), pp.72-74, 1960.

Meyer B.R. and Jakot R.H.: "Pseudo-Steady State Analysis of Finite Conductivity Vertical Fractures", SPE 95941, Presented at SPE Annual Technical Conference, Texas, USA, 2005.

Mohan J., Pope G.A. and Sharma M. M.: "Effect of Non-Darcy Flow on Well Productivity of a Hydraulically Fractured Gas/Condensate Well" SPE 103025, presented at Gas Technology Symposium, Texas, USA, 2006.

Prats M.: "Effect of Vertical Fractures on Reservoir Behaviour-Incompressible Fluid Case", SPE Journal, **222**, pp. 105-118, June 1961.

Raghavan, R., Hadinoto, N.: "Analysis of Pressure Data for Fractured Wells: The Constant Pressure Outer Boundary" SPE 6015, SPE Journal, pp.139-149, April 1978.

Raymond, L.R., and Binder, G.G.: "Productivity of Wells in Vertically Fractured, Damaged Formations," JPT, pp 120-130, Jan. 1967.

Riley, M.F., Brigham, W.E., and Horne, R.N.: "Analytical Solutions for Elliptical Finite-Conductivity Fractures," SPE 22656, presented at SPE Annual Technical Conference and Exhibition, Dallas, USA, Oct. 1991.

Romero D. J., Valko P. P. and Economides M. J.: "Optimization of the Productivity Index and the Fracture Geometry of a Simulated Well with Fracture Face and Choked Skins", SPE 81908, Journal of SPE Production and facilities, **18**(1), pp. 57-64, 2003.

Rostami-Ravari R., Wettenbarger R. A., Rezaei-Doust A. and Amani M.: "Analytical Evaluation of Gas/Condensate Skin in Hydraulically Fractured Wells" SPE 108016, presented at Latin America and Caribbean Conference, Argentina, 2007.

Settari A., Bale A., Batchman R.C., Floisand V.: "General Correlation for the Effect of Non-Darcy Flow on Productivity of Fractured Wells" SPE 75715, presented at Gas Technology Symposium, Calgary, Canada, 2002.

Smith M. B., Bale A. and Bitt L.K.: "An Investigation of Non-Darcy Flow Effects on Hydraulic Fractured Oil and Gas Well Performance", SPE 90864, presented at Annual Technical Conference, Texas, USA, 2004.

Valko Peter P. and Economides, Micheal J.: "Heavy Crude Production from Shallow Formations: Long Horizontal Wells Versus Horizontal Fractures" SPE 50421, presented at SPE International conference on Horizontal Well Technology, Calgary, Canada, 1998.

Wang, X., Thauvin, F., Mohanty, K.K.: "Non-Darcy flow through anisotropic porous media", Journal of Chemical Engineering Science, **54**, pp 1859-1869, (1999).

Wang X., Indriati S., Valko P.P and Economides, M. J.: "Production Impairment and Purpose Built Design of Hydraulic Fracture in Gas Condensate Reservoirs," SPE 64749, presented at International Oil and Gas Conference and Exhibition, Beijing, China, November 2000.

	HFWS-1	**HFWS-2**	**HFWS-3**
Matrix core	Texas Cream k=9.1mD β=3.927E+9	Clashach k=553 mD β=1.035E+8	Texas Cream k=9.1mD β=3.927E+9
Fluid	C_1-C_4 (Z_{C1} =73.6%) T=311K, P_D=1865 psia	C_1-C_4 (Z_{C1} =73.6%) T=311K, P_D=1865 psia	C_1-C_4 (Z_{C1} =91%) T=311K, P_D=1697 psia
Number of Data Points	1	1	1
Formation Thickness/m	30	30	30
x_f/m	105	105	67
w_f/mm	10	11	40
k_f/D	146	1460	146
β_f/m^{-1}	3.511E+5	3.511E+4	3.511E+5
$I_x=x_f/x_e$ (range)	0.1835	0.1835	0.085
P_{wf}/psia (range)	1915	1915	1305
GTR_w	1.0	1.0	--
P_e/psia	2015	2015	1740
C_{fD}	1.53	0.2746	9.6
$C_{fD\text{-}eff}$	0.267	0.2	--
Comment	Single Phase	Single Phase	Two Phase

Table 3.1 a: Parameters of different HFWS, studied in this work.

	HFWS-4	**HFWS-5**	**HFWS-6**	**HFWS-7**
Matrix core	Texas Cream k=9.1mD β=3.927E+9	Texas Cream k=9.1mD β=3.927E+9	Texas Cream k=9.1mD β=3.927E+9	Texas Cream k=9.1mD β=3.927E+9
Fluid	C_1-C_{10} (Z_{C1} =80%) T=500K, P_D=3541.5 psia	C_1-C_{10} (Z_{C1} =80%) T=500K, P_D=3541.5 psia	C_1-C_{10} (Z_{C1} =80%) T=500K, P_D=3541.5 psia	C_1-C_4 (Z_{C1} =73.6%) T=311K, P_D=1865 psia
Number of Data Points	1	1	1	1
Formation Thickness/m	30	30	30	30
x_f/m	105.7	105.7	105.7	105.7
w_f/mm	8	16	8	8
k_f/D	146	146	146	146
β_f/m^{-1}	3.511E+5	3.511E+5	3.511E+5	3.511E+5
$I_x=x_f/x_e$ (range)	0.1835	0.1835	0.1835	0.1835
P_{wf}/psia (range)	3521.5	3521.5	3521.5	1860
Prod. Rate (kg/d)	9.4E+04	1.1E+05	4.75E+04	7.28E+04
GTR_w	0.941	0.941	0.941	0.7655
P_e/psia	3571.5	3571.5	3546..5	1895
C_{fD}	1.2138	2.428	2.428	1.214
$C_{fD\text{-}eff}$	0.37	1.05	1.72	0.375
Comment	Two Phase zone is ended within the fractured zone	Two Phase zone is ended within the fractured zone	Two Phase zone is ended outside of the fractured zone	Two Phase zone is very small

Table 3.1 b: Parameters of different HFWS, studied in this work.

	HFWS-8	**HFWS-9**	**HFWS-10**	**HFWS-11**	**HFWS-12**
Matrix core	Texas Cream k=9.1mD β=3.927E+9	Texas Cream k=9.1mD β=3.927E+9	Texas Cream k=9.1mD β=3.927E+9	Texas Cream k=9.1mD β=3.927E+9	Texas Cream k=9.1mD β=3.927E+9
Fluid	C_1-C_{10} (Z_{C1} =80%) T=500K, P_D=3541.5 psia	C_1-C_4 (Z_{C1} =73.6%) T=311K, P_D=1865 psia	C_1-C_4 (Z_{C1} =73.6%) T=311K, P_D=1865 psia	C_1-C_4 (Z_{C1} =73.6%) T=311K, P_D=1865 psia	C_1-C_{10} (Z_{C1} =80%) T=500K, P_D=3541.5 psia
Number of Data Points	1	1	10	198	194
Formation Thickness/m	30	30	30	30	30
x_f/m	106	106	106	17, 42, 106	17, 42, 106
w_f/mm	4	4	4,8,…,40	2, 6, 10, 14	2, 6, 10, 14
k_f/D	146	146	146	146	146
β_f/m^{-1}	3.511E+5	3.511E+5	3.511E+5	3.511E+5	3.511E+5
$I_x=x_f/x_e$ (range)	0.36	0.36	0.1835	0.04—0.7	0.04—0.7
P_{wf}/psia (range)	3486.5	1810	1810	1350—1850	2977—3536.5
GTR_w (range)	0.885	0.653	0.653	0.62—0.84	0.8—0.983
P_e/psia	3536.5	1860	1860	1855	3532, 3642
***$C_{fD\text{-}eff}$* (range)**	0.23	0.95	0.95	0.1—29	0.02—11.8

Table 3.1 c: Parameters of different HFWS, studied in this work.

	HFWS-13	**HFWS-14**	**HFWS-15**
Matrix core	Rc1b k=0.18mD β=1.056E+12	Berea k=110mD β=1.854E+8	Texas Cream k=9.1mD β=3.927E+9
Fluid	C_1-C_{10} (Z_{C1} =80%) T=500K, P_D=3541.5 psia	C_1-C_{10} (Z_{C1} =80%) T=500K, P_D=3541.5 psia	C_1-C_{10} (Z_{C1} =80%) T=500K, P_D=3541.5 psia
Number of Data Points	469	204	174
Formation Thickness/m	30	30	30
x_f/m	42, 106, 259	42, 106, 259	17, 42, 106
w_f/mm	2, 4, 12, 20	2, 6, 10, 12, 14	2, 12, 22, 32, 42
k_f/D	146	1460	146
β_f/m^{-1}	3.511E+5	3.511E+4	3.511E+5
$I_x=x_f/x_e$ (range)	0.06—0.84	0.06—0.7	0.09—0.59
P_{wf}/psia (range)	2677—3538	2677—3527	3890, 3790, 3690, 3590
GTR_w (range)	0.8—0.986	0.8—0.95	1.0
P_e/psia	3532, 3642	3532	3990
$C_{fD\text{-}eff}$ (range)	0.02—11.8	0.05— 4.6	0.01--18

Table 3.1 d: Parameters of different HFWS, studied in this work.

	HFWS-16	**HFWS-17**	**HFWS-18**
Matrix core	Texas Cream k=9.1mD	 k=0.91mD β=3.927E+9	Texas Cream k=9.1mD β=3.927E+9
Fluid	C_1-C_4 (Z_{C1} =77%) T=311K	C_1-C_4 (Z_{C1} =77%) T=311K	C_1-C_4 (Z_{C1} =77%) T=311K
Number of Data Points	1	1	1
Formation Thickness/m	30	30	30
x_f/m	292.6	292.6	292.6
w_f/mm	20	20	40
k_f/D	146	146	146
β_f/m^{-1}	0	3.511E+5	3.511E+5
$I_x=x_f/x_e$ (range)	0.866	0.866	0.866
P_{wf}/psia (range)	--	--	--
Prod. Rate (Sm3/d)	400,000	400,000	200,000
GTR_w	1.0	1.0	--
P_e/psia	2900	2900	1740
C_{fD}	1.1	11	2.2
$C_{fD\text{-}eff}$	1.1	2.15	0.98
Comment	Single Phase Darcy Flow	Single Phase non-Darcy Flow	Gas Condensate flow

Table 3.1 e: Parameters of different HFWS, studied in this work.

	HFWS-19	**HFWS-20**	**HFWS-21**
Matrix core	Texas Cream k=9.1mD	 k=0.91mD β=3.927E+9	Texas Cream k=9.1mD β=3.927E+9
Fluid	C_1-C_4 (Z_{C1} =77%) T=311K	C_1-C_4 (Z_{C1} =77%) T=311K	C_1-C_4 (Z_{C1} =77%) T=311K
Number of Data Points	1	1	1
Formation Thickness/m	30	30	30
x_f/m	292.6	292.6	292.6
w_f/mm	20	20	40
k_f/D	146	146	146
β_f/m^{-1}	--	3.511E+5	3.511E+5
$I_x=x_f/x_e$	0.866	0.866	0.866
P_{wf}/psia (range)	--	--	--
Prod. Rate (Sm3/d)	160,000	400,000	200,000
GTR_w	1.0	1.0	--
P_e/psia	Closed Boundary	Closed Boundary	Closed Boundary
P_i/psia			1739
C_{fD}	1.1	11	2.2
$C_{fD\text{-}eff}$	1.1	2.5	0.9
Comment	Single Phase Darcy Flow	Single Phase non-Darcy Flow	Gas Condensate flow

Table 3.1 f: Parameters of different HFWS, studied in this work

P/psi	x_j	y_j	$\rho_{c/kgm^{-3}}$	$\rho_{g/kgm^{-3}}$	$\mu_{c/CP}$	$\mu_{g/CP}$	IFT/mN.m
1865	0.4195	0.4195	223.3	223.3	0.0261	0.0261	0.0000
1850	0.3521	0.5049	307.50	220.50	0.0398	0.0255	0.0080
1840	0.3430	0.5146	317.40	211.40	0.0405	0.0249	0.0360
1800	0.3069	0.5535	341.10	188.70	0.0431	0.0211	0.1120
1790	0.3018	0.5583	345.10	184.80	0.0437	0.0206	0.1490
1750	0.2814	0.5776	359.50	171.30	0.0462	0.0195	0.2809
1700	0.2609	0.5944	374.70	157.40	0.0491	0.0184	0.4318
1650	0.2444	0.6088	387.00	146.50	0.0520	0.0176	0.5785
1600	0.2279	0.6232	397.80	137.80	0.0549	0.0170	0.7329
1565	0.2192	0.6297	404.00	132.60	0.0570	0.0166	0.8520
1500	0.2030	0.6418	421.76	118.39	0.0608	0.0160	1.1106
1400	0.1821	0.6550	438.62	106.44	0.0669	0.0152	1.5938
1250	0.1540	0.6664	459.64	91.27	0.0762	0.0144	2.3971
1200	0.1452	0.6690	466.06	86.68	0.0793	0.0141	2.6907
1000	0.1136	0.6712	487.63	69.89	0.0908	0.0133	3.9239
800	0.0859	0.6640	505.63	54.71	0.1015	0.0126	5.2907
600	0.0604	0.6335	522.29	41.17	0.1121	0.0120	6.8104
500	0.0484	0.6050	530.06	34.86	0.1173	0.0117	7.6186
400	0.0368	0.5636	537.53	28.78	0.1234	0.0114	8.4582
300	0.0257	0.4985	544.48	22.93	0.1283	0.0111	9.3119
200	0.0152	0.3948	551.22	17.16	0.1330	0.0106	10.2085
150	0.0100	0.3128	554.66	14.33	0.1356	0.0101	10.6795
100	0.0049	0.1901	557.94	11.55	0.1383	0.0094	11.1500
80	0.0029	0.1230	559.11	10.45	0.1393	0.0090	11.3299
60	0.0008	0.0408	560.48	9.35	0.1405	0.0083	11.5268
51.61	0.0000	0.0000	560.87	8.9000	0.1411	0.0080	11.5950

Table 3.2 a: important properties of the mixture C_1-C_4, %C_1: 73.6%, P_{Dew}=1865 psia

P/psi	x_j	y_j	$\rho_{c/kgm^{-3}}$	$\rho_{g/kgm^{-3}}$	$\mu_{c/CP}$	$\mu_{g/CP}$	IFT/mN.m
3541.537	0.2383	0.3238	320.5259	250.7587	0.0390	0.0306	0.0017
3530	0.2341	0.3284	324.1658	247.1800	0.0395	0.0302	0.0025
3520	0.2307	0.3321	327.1002	244.3360	0.0399	0.0299	0.0033
3500	0.2246	0.3387	332.4373	239.1790	0.0406	0.0293	0.0054
3480.894	0.2194	0.3446	337.0365	234.7541	0.0413	0.0289	0.0078
3440	0.2097	0.3554	345.7472	226.4137	0.0425	0.028	0.0144
3380.868	0.1978	0.3687	356.5403	216.1560	0.0441	0.0270	0.0277
3330	0.1890	0.3789	364.7034	208.4539	0.0454	0.0262	0.0426
3280.84	0.1814	0.3877	371.8961	201.7067	0.0465	0.0256	0.0601
3230	0.1742	0.3962	378.7836	195.2800	0.0476	0.025	0.0814
3180.817	0.1677	0.4038	385.0191	189.4897	0.0486	0.0245	0.1053
3130	0.1615	0.4111	391.0992	183.8700	0.0497	0.024	0.1332
3080.791	0.1559	0.4178	396.6908	178.7248	0.0506	0.0236	0.1634
2980.765	0.1454	0.4303	407.3214	169.0010	0.0526	0.0228	0.2348
2880.740	0.1358	0.4416	417.1584	160.0714	0.0544	0.0221	0.3196
2780.714	0.1271	0.4519	426.3642	151.7733	0.0562	0.0214	0.4181
2680.688	0.1190	0.4612	435.0527	143.9930	0.0580	0.0209	0.5306
2580.662	0.1115	0.4696	443.3070	136.6476	0.0598	0.0204	0.6572
2480.637	0.1044	0.4773	451.1902	129.6740	0.0616	0.0199	0.7982
2380.611	0.0978	0.4845	458.7513	123.0233	0.0633	0.0195	0.9538
2280.585	0.0915	0.4908	466.0296	116.6563	0.0651	0.0191	1.1242
2180.560	0.0855	0.4962	473.0568	110.5415	0.0669	0.0187	1.3096
2080.534	0.0798	0.5011	479.8591	104.6526	0.0686	0.0184	1.5104
1980.508	0.0743	0.5051	486.4585	98.9678	0.0704	0.0181	1.7265
1880.483	0.0691	0.5083	492.8735	93.4687	0.0722	0.0178	1.9584
1780.457	0.0642	0.5107	499.1200	88.1396	0.0740	0.0175	2.2061

Table 3.2 b: important properties of the mixture C_1-C_{10}, %C_1: 80%, P_{Dew}=3541.5 psia

GTR	**0**	**0.71**	**0.91**	**0.97**	**0.99**	**0.995**	**1.0**
$k_{rgb,}$Texas Cream	0	0.0744	0.1927	0.3309	0.5945	0.7379	1.0
Ncb,Texas Cream	-	1.33E-5	6.56E-6	4.08E-6	2.32E-6	1.87E-6	-
$k_{rgb,}$ RC1b	0	0.11	0.175	0.237	0.283	0.4	1
Ncb, RC1b	-	1.07E-5	8.58E-6	6.78E-6	5.72E-6	3.68E-6	1
$k_{rgb,}$ Berea	0	0.039	0.095	0.25	0.65	0.746	1.0
Ncb, Berea	-	3.04e-5	1.59e-5	6.44e-6	3.30e-6	2.21E-6	-
$k_{rgb,}$ Proppant	0	0.187	0.495	0.525	0.651	0.695	1.0
Ncb Proppant	-	0.0022	0.00158	0.0015	0.00128	0.00122	-

Table 3.3: Base gas relative permeability of proppant and Texas Cream core as a function of GTR, used for simulation of the hydraulically fractured system.

VELDEP						
1	1	0	2	0/		
VDKRG						
2	4.0	0	1.41e-6	2* -0.3	-1.2	555.78 /Texas C.
0	0	0	9.37E-6	2* -0.3	-1.2	5529 / Proppant
VDKRO						
0.0	14.4	0	1.41e-6 / Texas Cream			
0.0	0.0001	0	9.37e-6/ Proppant			

Table 3.4: Items used for keywords of VELDEP, VDKRG and VDKRO in ECLIPSE-300.

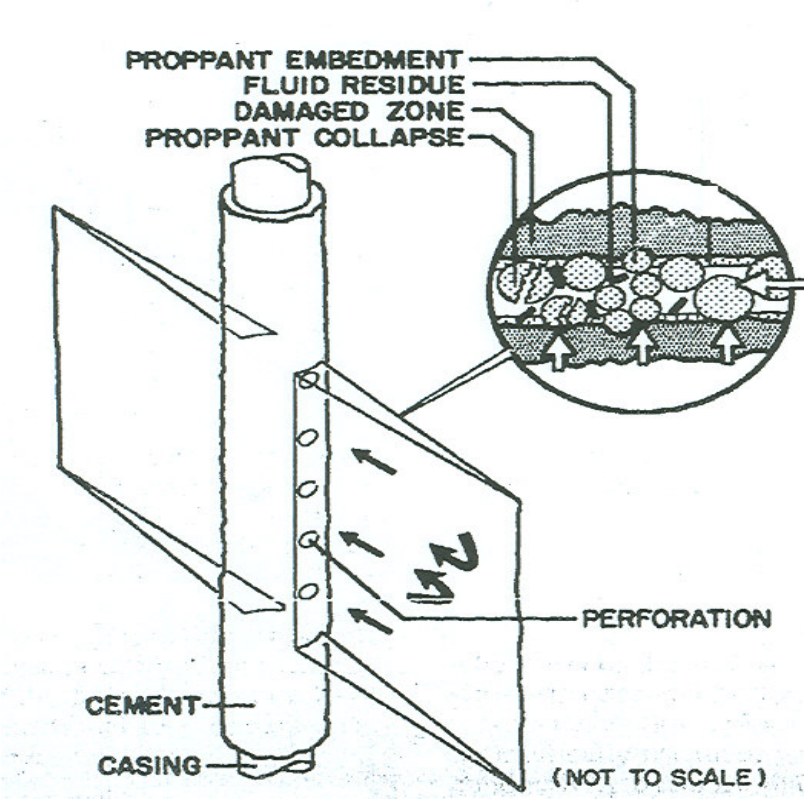

Figure 3.1: A symmetrical hydraulically fractured well.

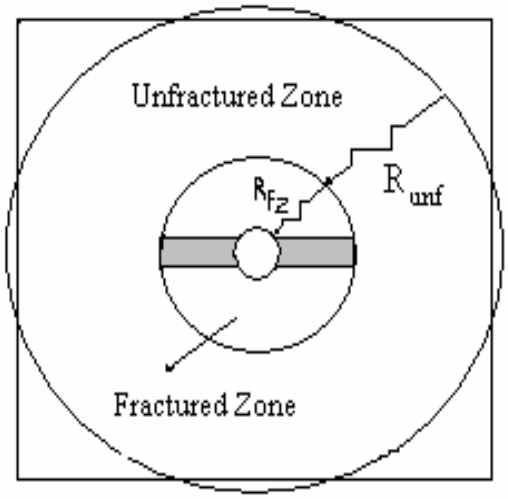

Figure 3.2: An HFW located in the centre of square or circular drainage area.

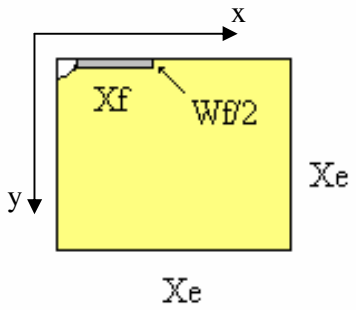

Figure 3.3: A quarter of a hydraulically fractured drainage erea, studied in this work.

Figure 3.4: Grid blocks of a simulated quarter drainage area.

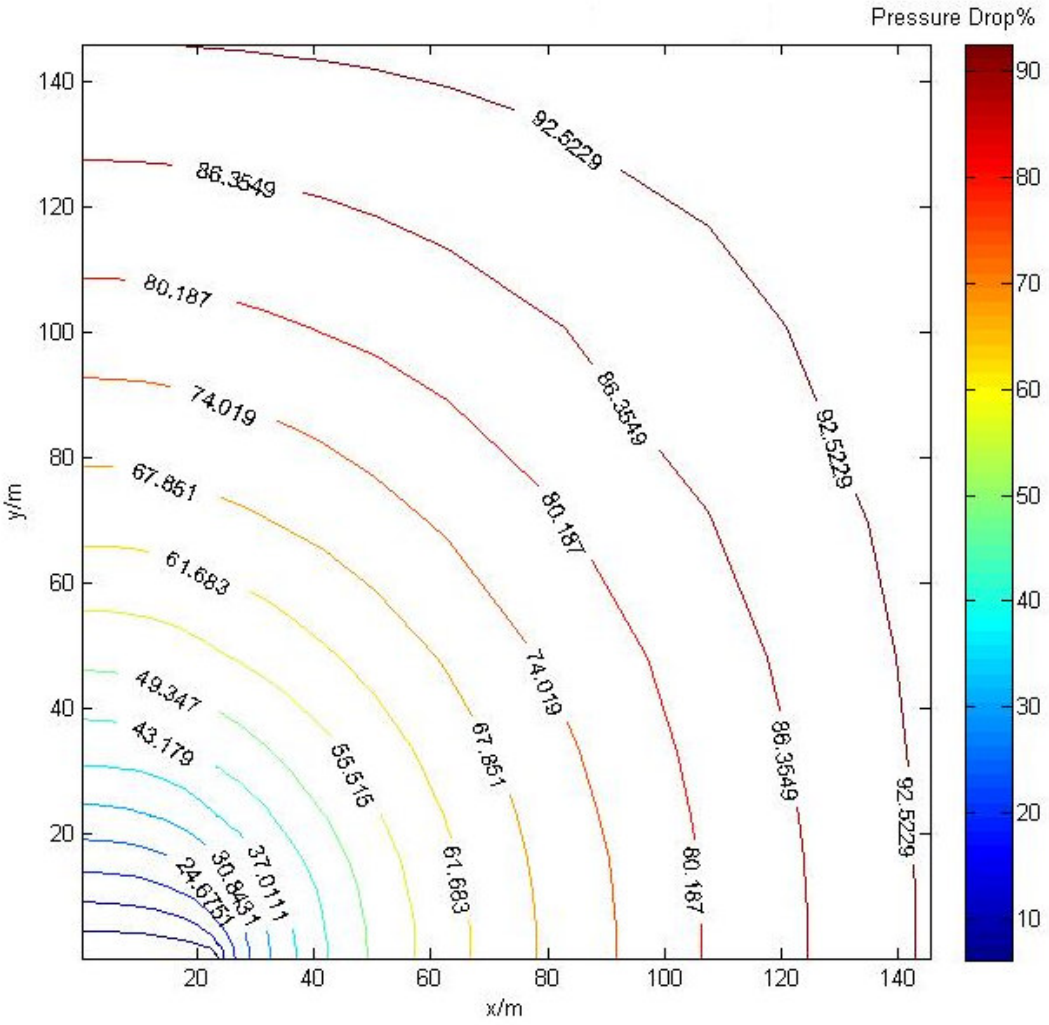

Figure 3.5: Pressure-drop% contour map in a quarter of drainage area of an HFW in single phase Darcy flow system with C_{fD}=200, I_X=0.22 and x_f=23.6 m.

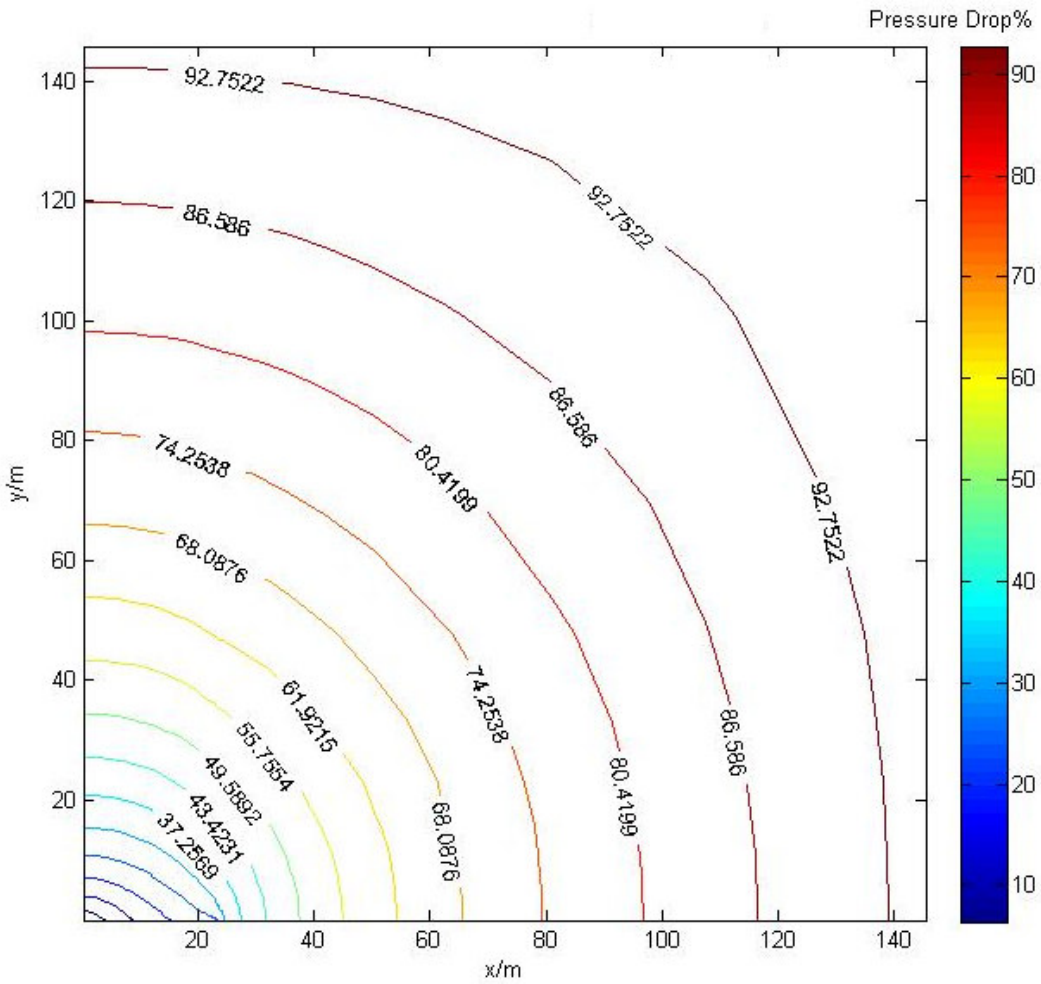

Figure 3.6: Pressure-drop% contour map in a quarter of drainage area of an HFW in single phase Darcy flow system with C_{fD}=2, I_X=0.22 and x_f=23.6 m.

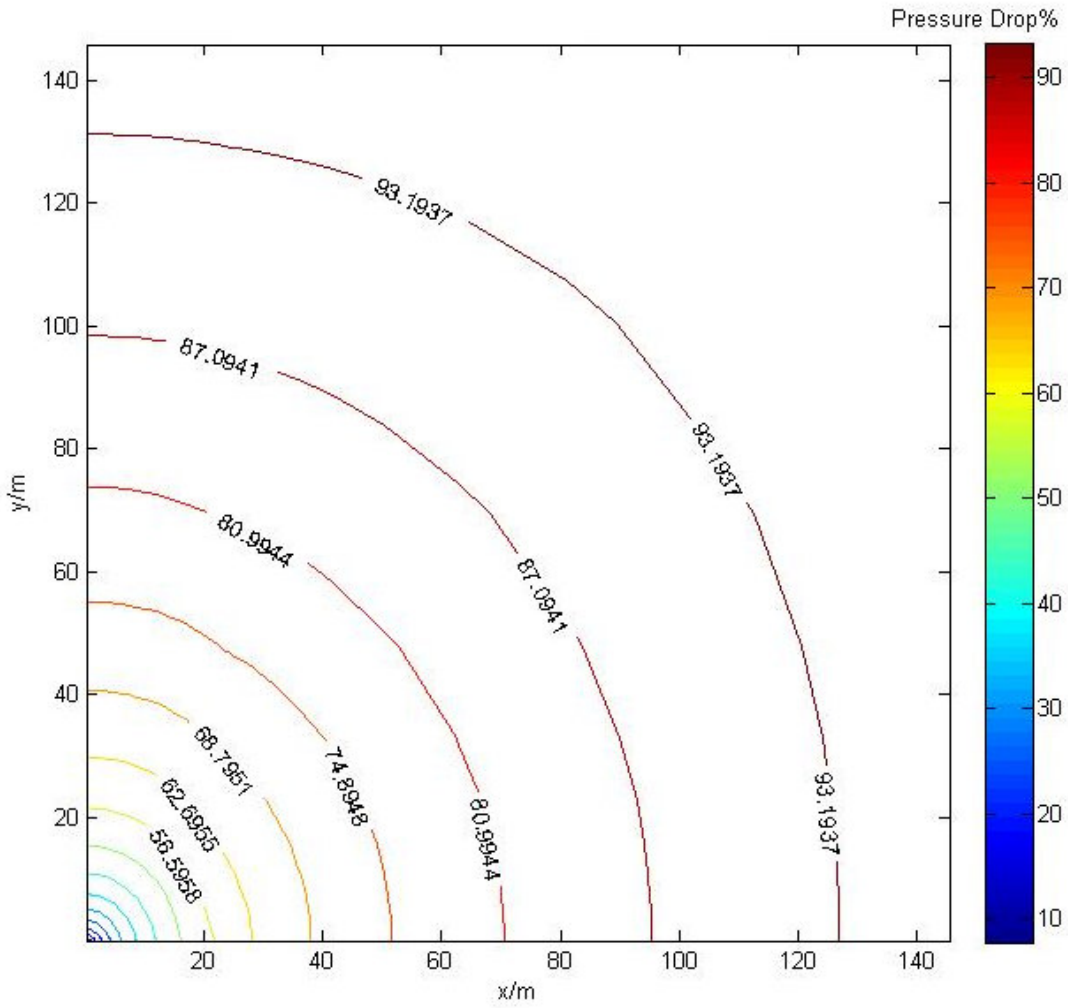

Figure 3.7: Pressure-drop% contour map in a quarter of drainage area of an HFW in single phase Darcy flow system with C_{fD}=0.2, I_X=0.22 and x_f=23.6 m.

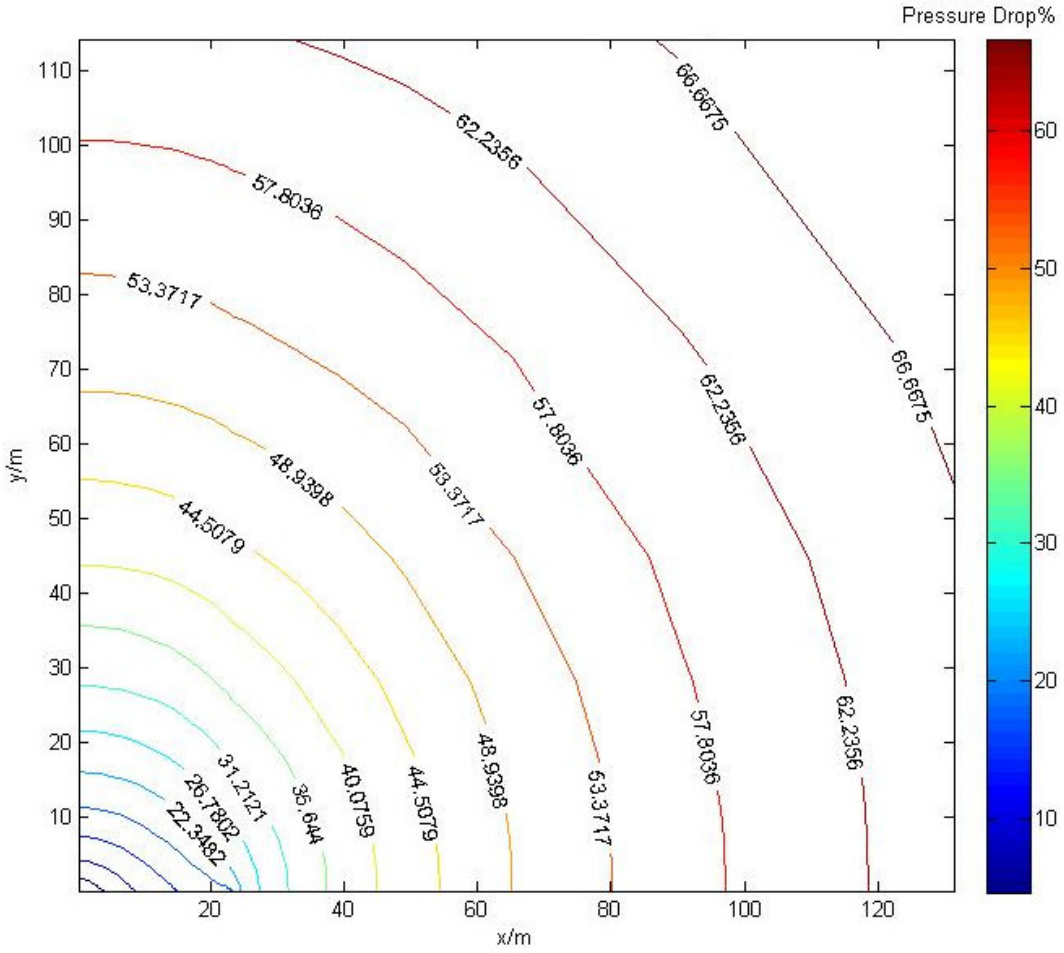

Figure 3.8: Pressure-drop% contour map in a quarter of drainage area of an HFW in single phase Darcy flow system with C_{fD}=2, I_X=0.05 and x_f=23.6 m.

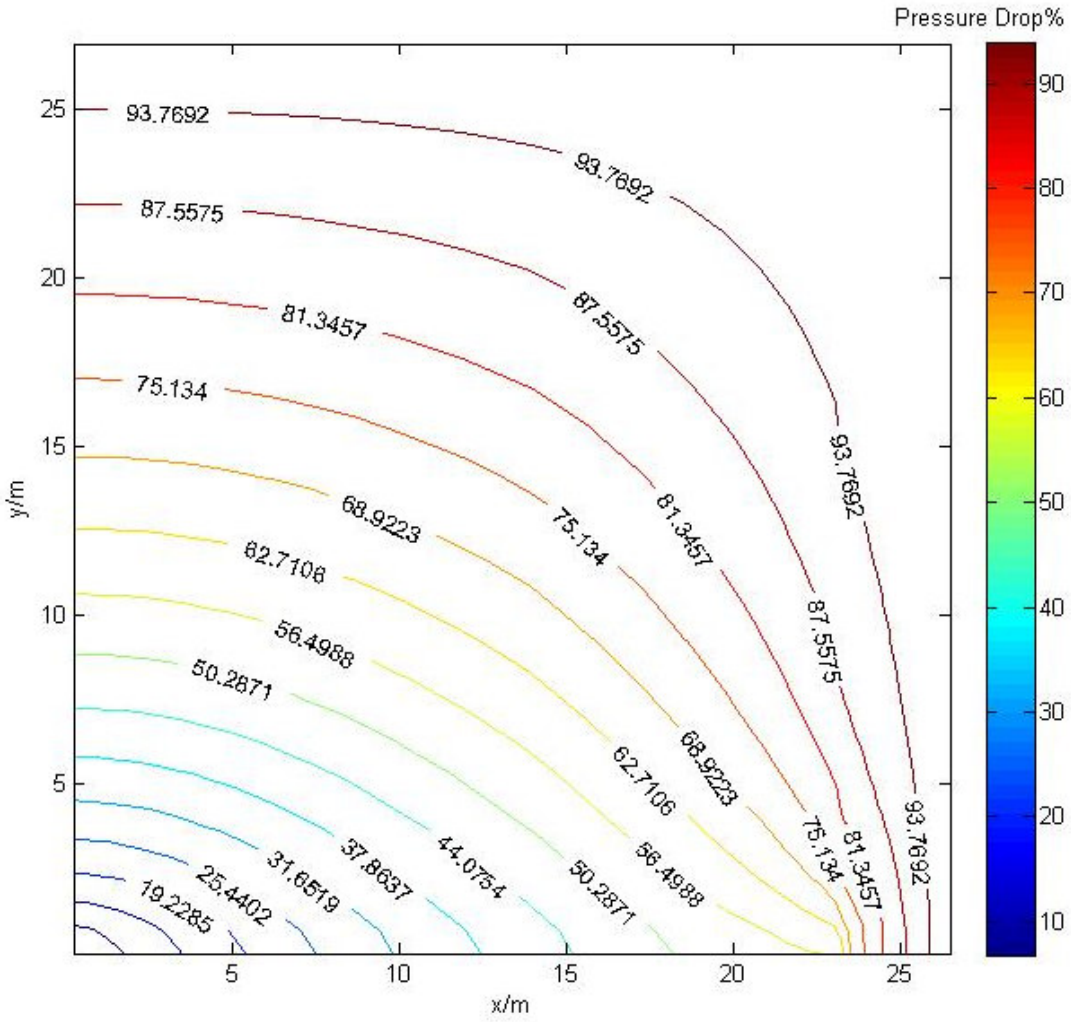

Figure 3.9: Pressure-drop% contour map in a quarter of drainage area of an HFW in single phase Darcy flow system with C_{fD}=2, I_X=0.88 and x_f=23.6 m.

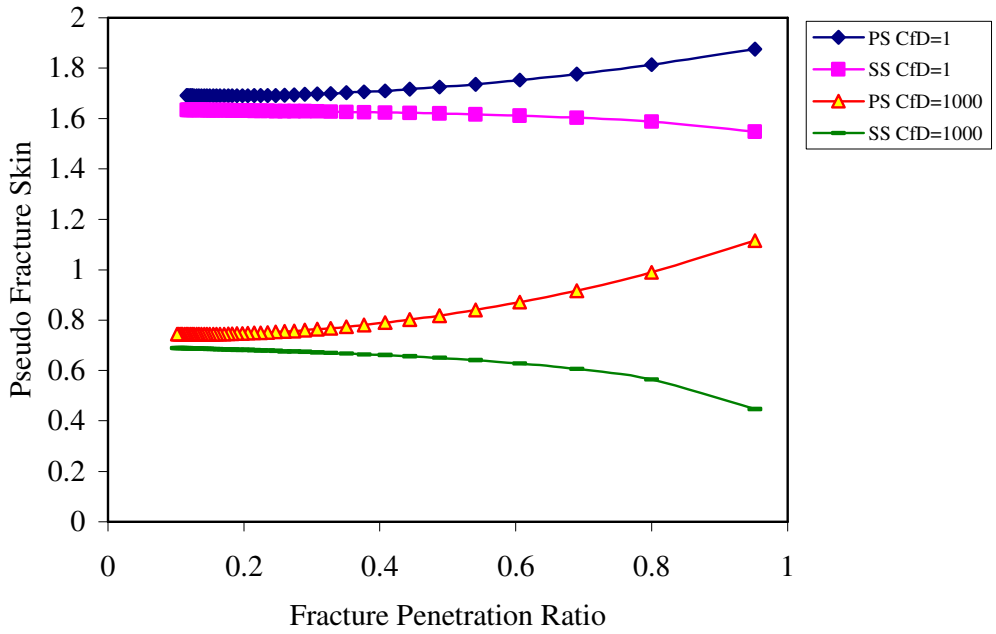

Figure 3.10: Variation of pseudo fracture skin with fracture penetration ratio ($I_x=x_f/x_e$) at pseudo-steady state (PPS) and steady state (SS) conditions. It can be seen that at small values of I_x the values of pseudo-fracture skin are very close in PPS & SS conditions.

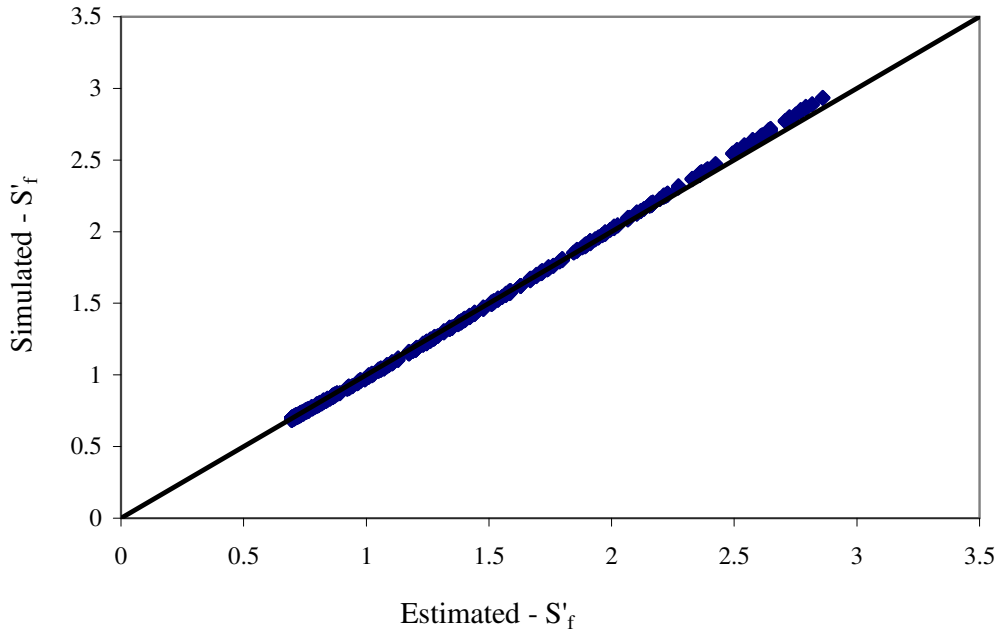

Figure 3.11: Pseudo fracture skin values obtained by the developed simulator versus those estimated using Equation 3.26, at $I_X<0.2$, AAD%=1.25%.

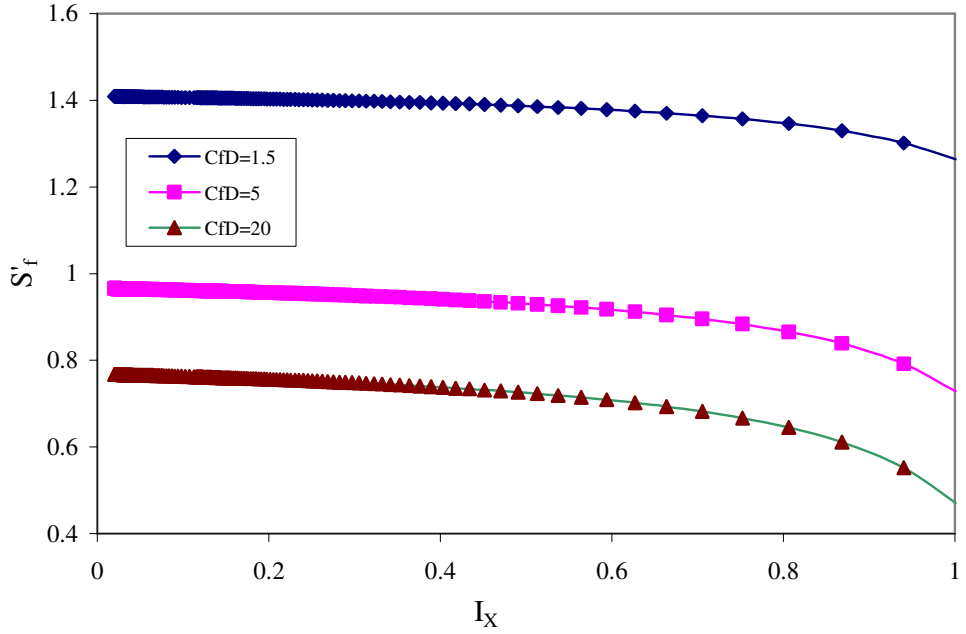

Figure 3.12: Variation of pseudo fracture skin with I_X at three different C_{fD}.

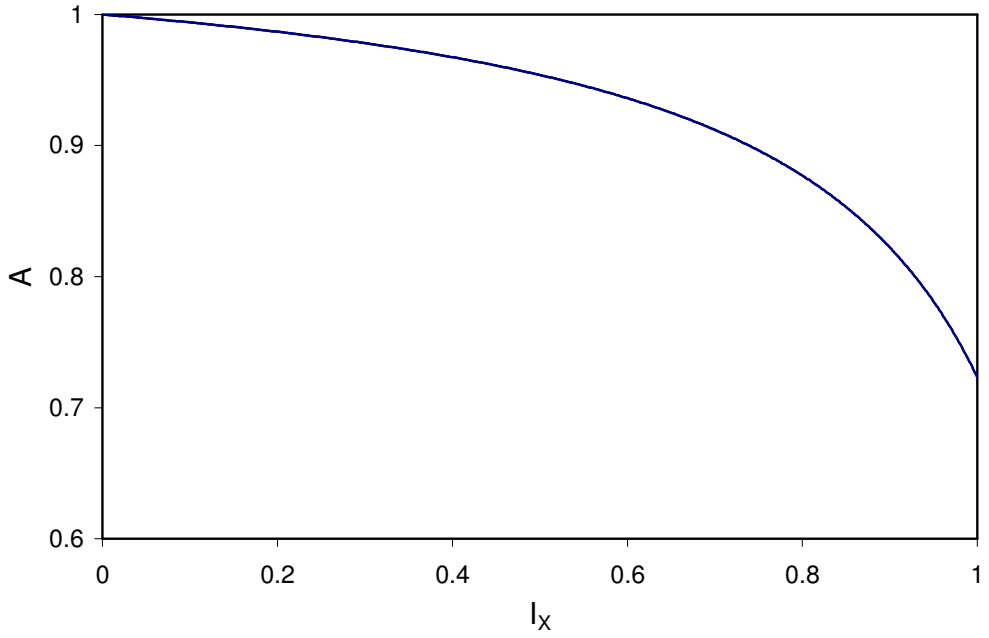

Figure 3.13: Variation of A, defined in Equation 3.27, with fracture penetration Ratio.

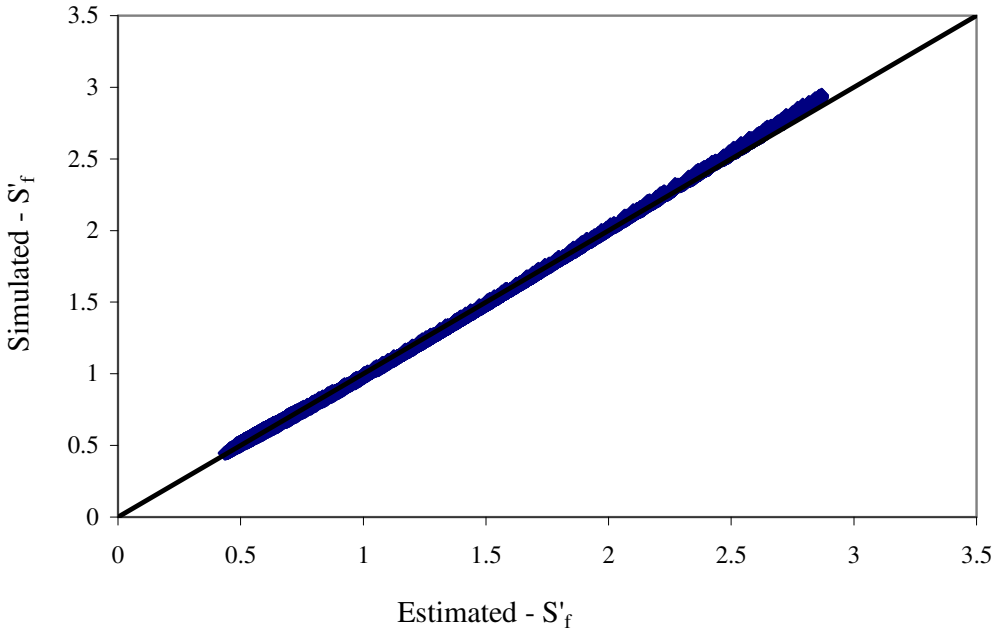

Figure 3.14: Pseudo fracture skin values obtained by the developed simulator versus those estimated using Equation 3.27 for I_X<0.94, AAD%=1.3%.

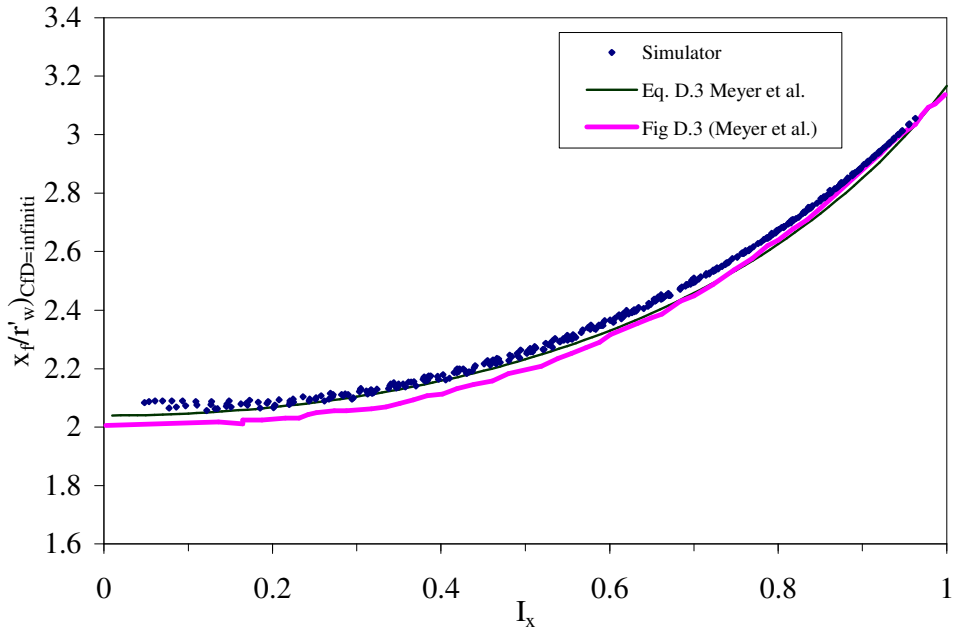

Figure 3.15: ξ_∞ as a function of I_X. The results of the developed simulator have been used as an input to the common formula for productivity index, Equation 3.33.

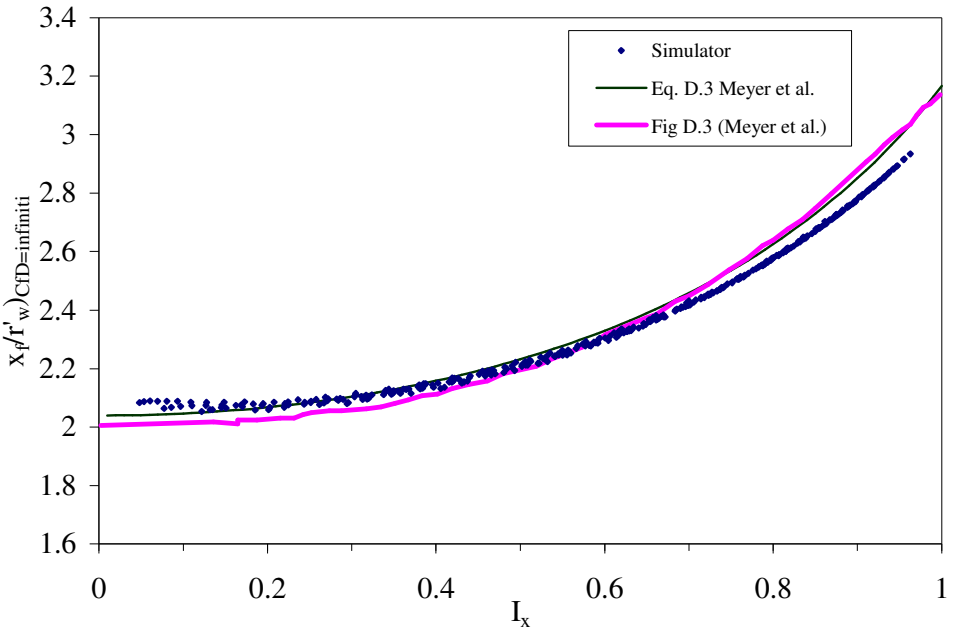

Figure 3.16: ξ_∞ as a function of I_X. The results of the developed simulator have been used as an input to the more accurate formula for productivity index, Equation 3.31.

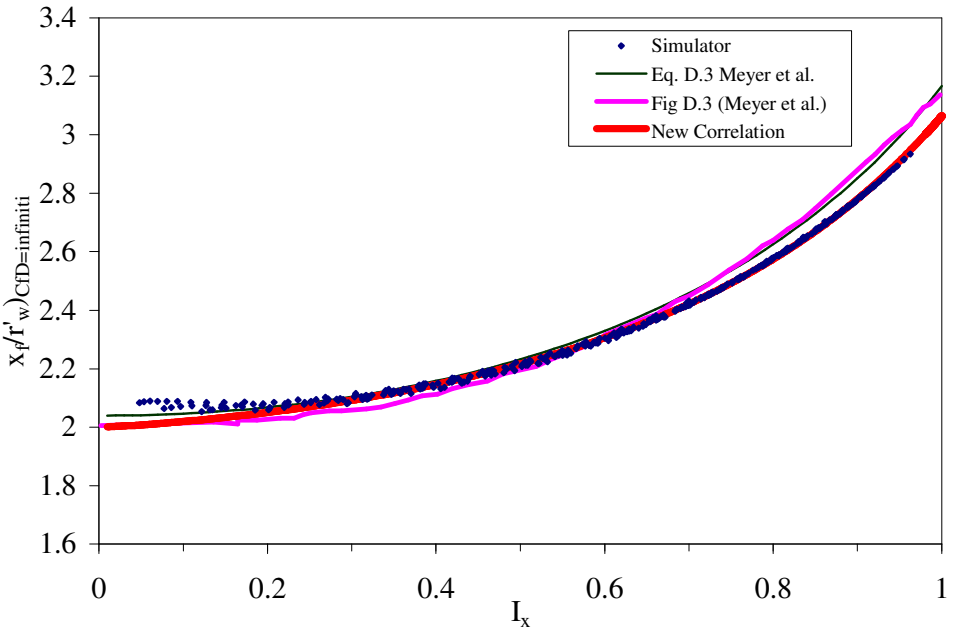

Figure 3.17: ξ_∞ as a function of I_X. The results of the developed simulator, matches very well the new correlation, Equations 3.34-5, which has been developed based on the using of the more accurate formula for productivity index, Equation 3.31.

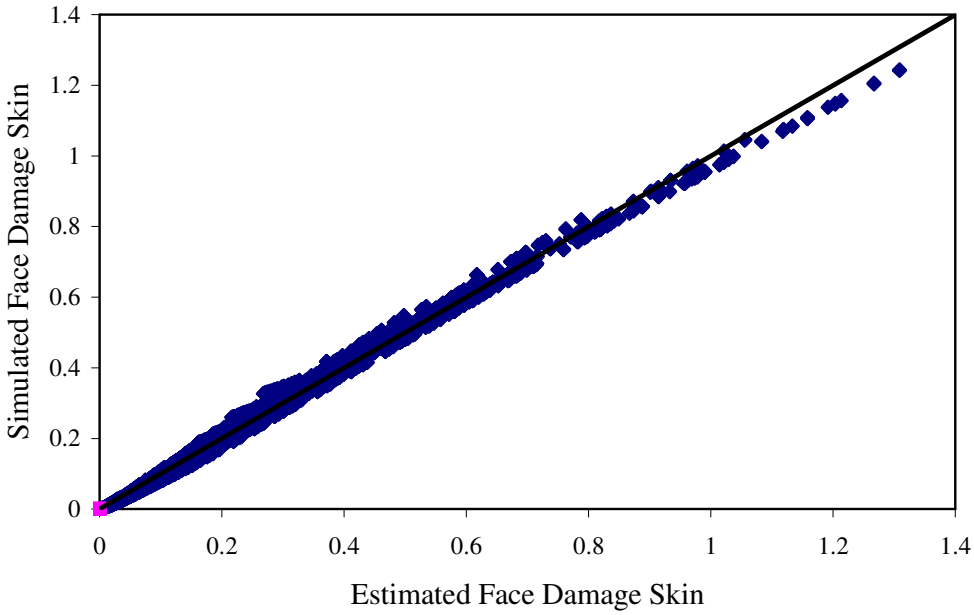

Figure 3.18: Face damage skin values obtained by the developed in-house simulator versus those estimated using the proposed formula, Equation 3.43, when damage thickness decreases linearly towards the fracture tip.

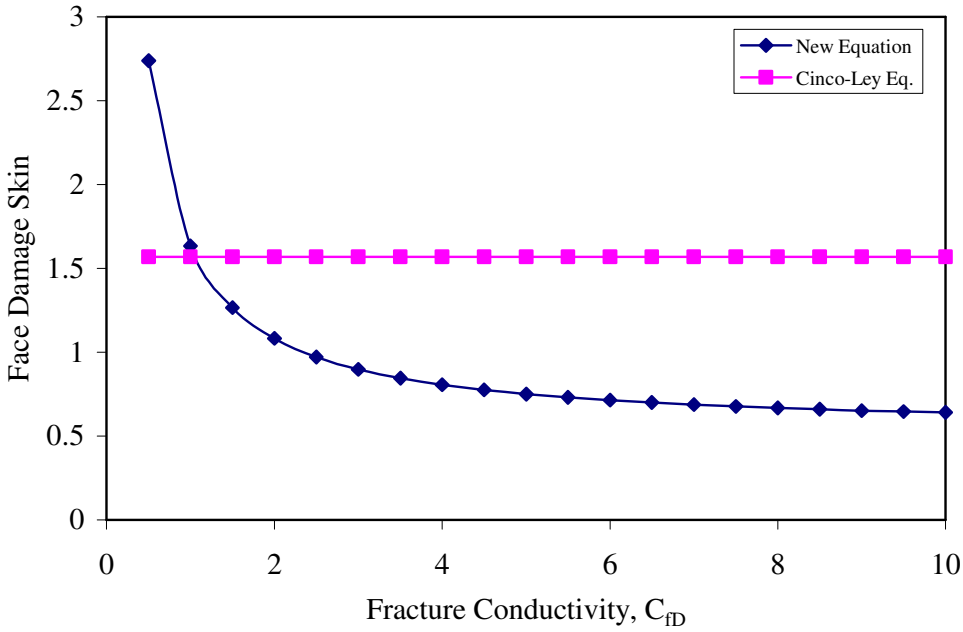

Figure 3.19: Face damage skin vs fracture conductivity for constant damage thickness, Cinco-ley Equation, 3.41, and the new developed equation based on decreasing damage thickness, Equation 3.43.

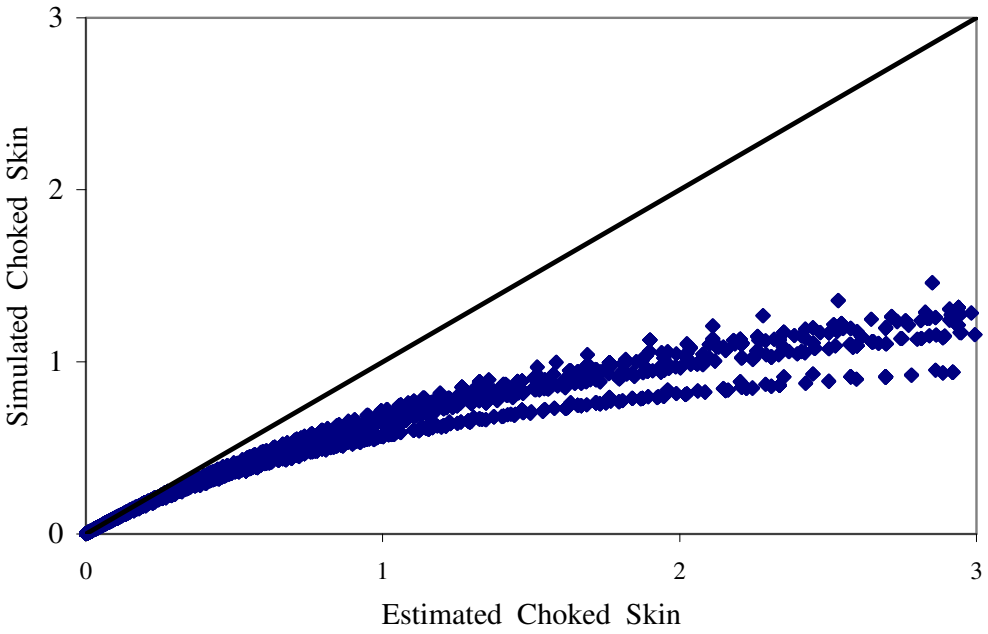

Figure 3.20**:** Choked damage skin values obtained by the developed simulator versus those estimated by Equation 3.44.

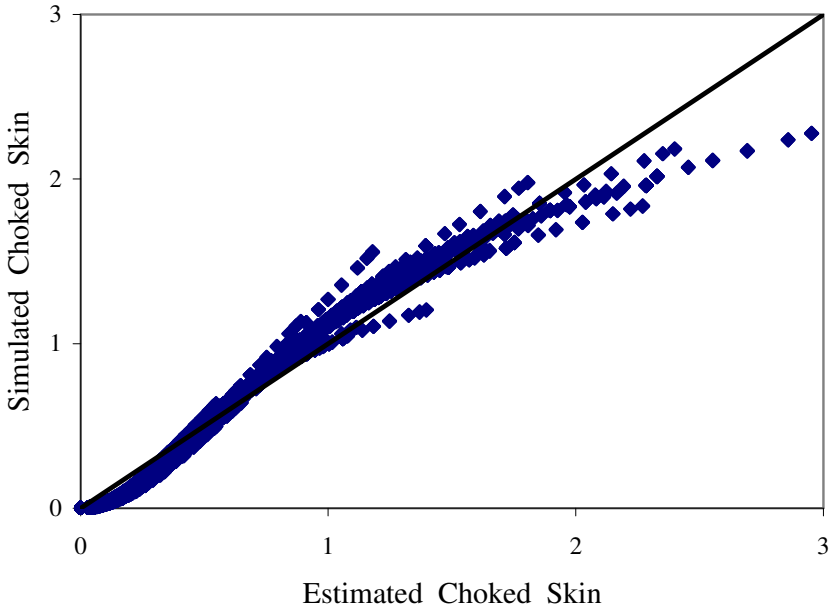

Figure 3.21: Choked damage skin values obtained by the developed simulator versus those estimated by the proposed formula, Equation 3.47.

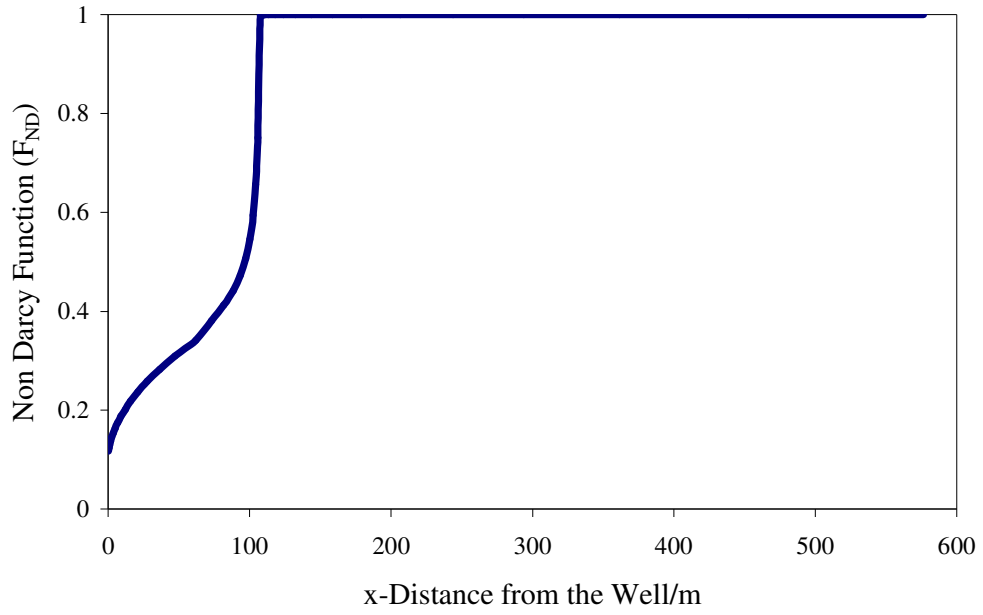

(a)

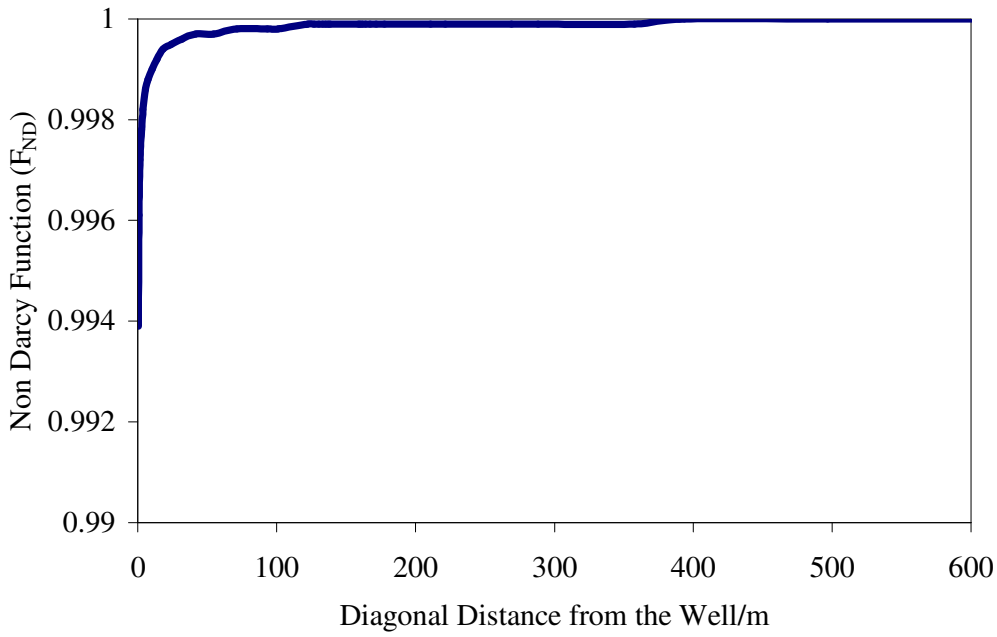

(b)

Figure 3.22: Single-phase relative permeability distribution in the HFWS-1 defined in Table 3.1a: (a) along x-distance from the well, in the fracture and matrix, (b) along diagonal-distance from the well, in the matrix.

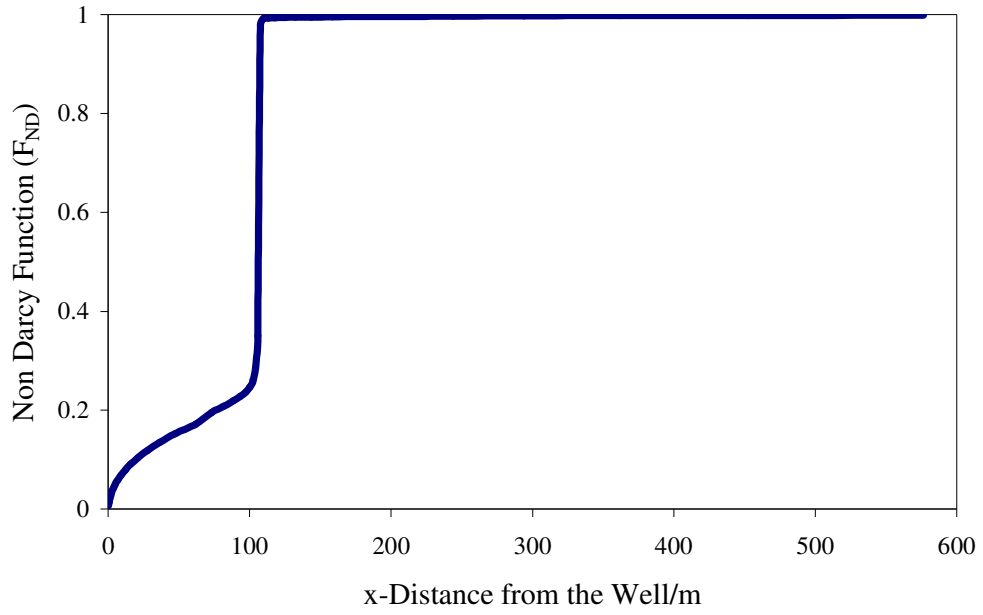

(a)

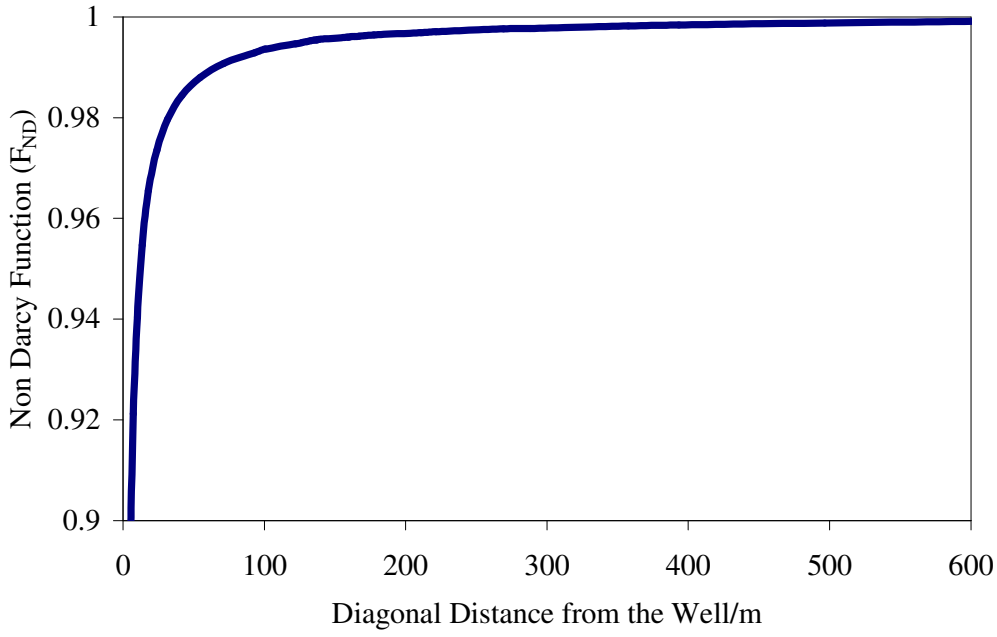

(b)

Figure 3.23: Single-phase relative permeability distribution in the HFWS-2 defined in Table 3.1a: (a) along x-distance from the well in the fracture and matrix, (b) along diagonal-distance from the well in the matrix.

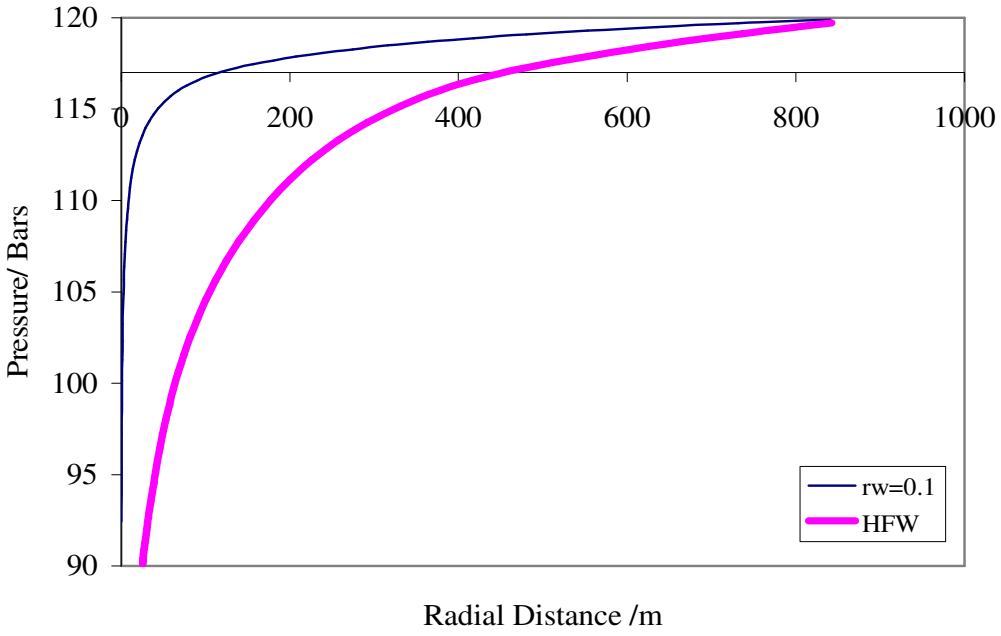

(a)

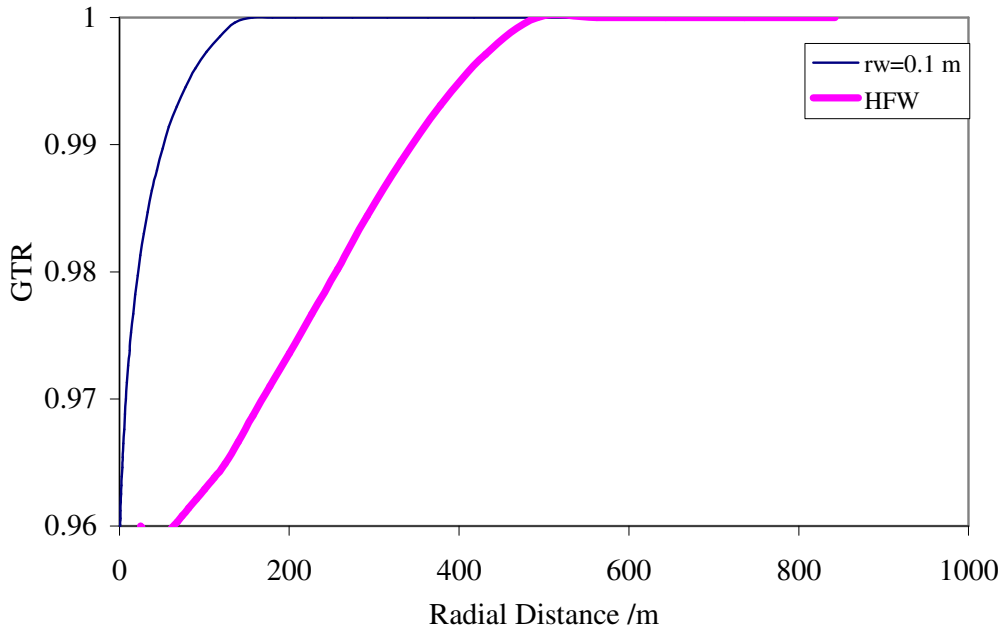

(b)

Figure 3.24: SS Pressure distributions (a) and SS GTR distributions (b) around a HFW (HFWS-3 defined in Table 3.1a) and an un-fractured well in the same reservoir.ew Point Pressure: 117 bar.

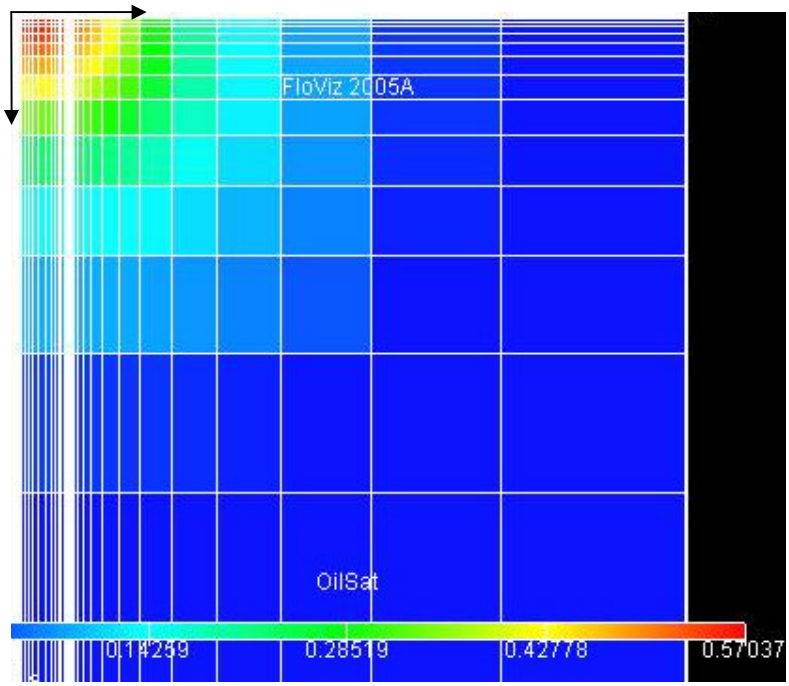

(a)

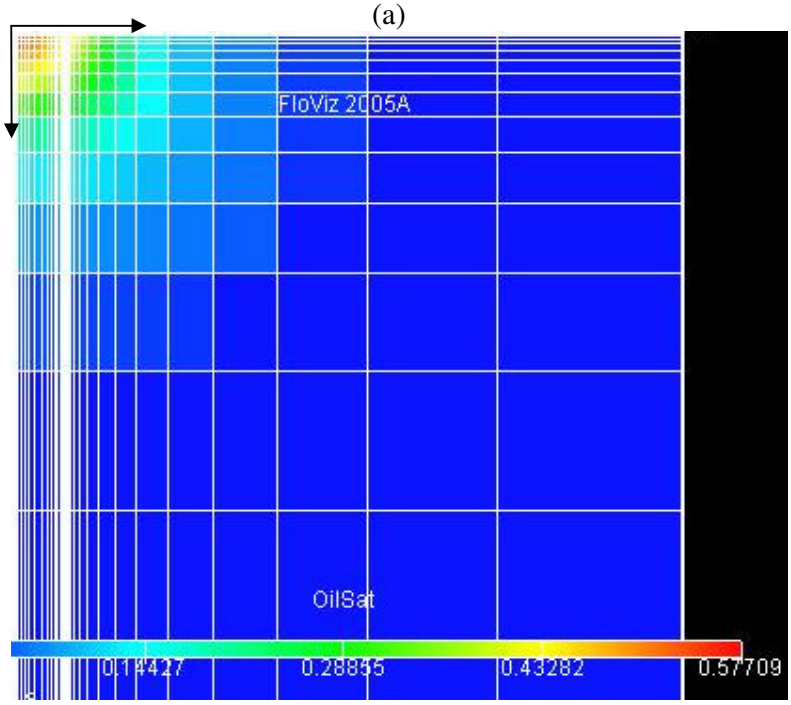

(b)

Figure 3.25: Distribution of condensate saturation in HFWS-3 defined in Table 3.1a:

a) The HFW with $k_f = 146$ D ($C_{fD} = 9.1$)
b) The HFW with $k_f = 14.6$ D ($C_{fD} = 0.91$)

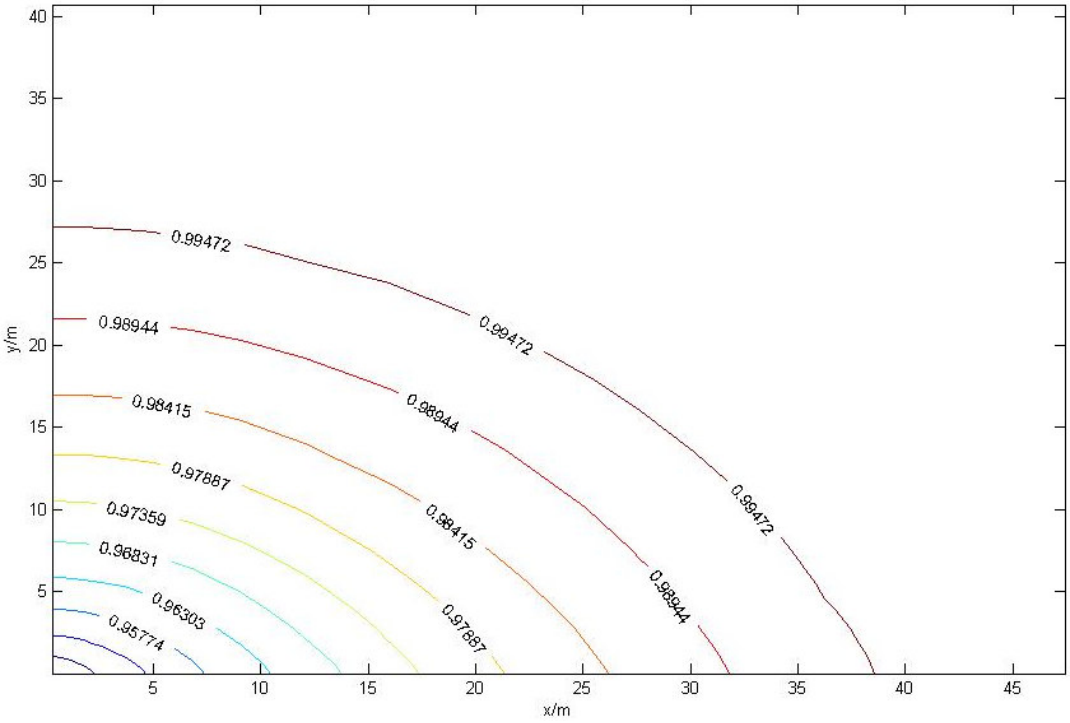

Figure 3.26: GTR contour map in a quarter of drainage area of a HFW in a gas condensate flow system with $C_{fD\text{-}eff}$=0.37, I_X=0.1835 and x_f=105.7 m, FHWS-4 defined in Table 3.1b. Two phase zone is smaller than the fractured zone.

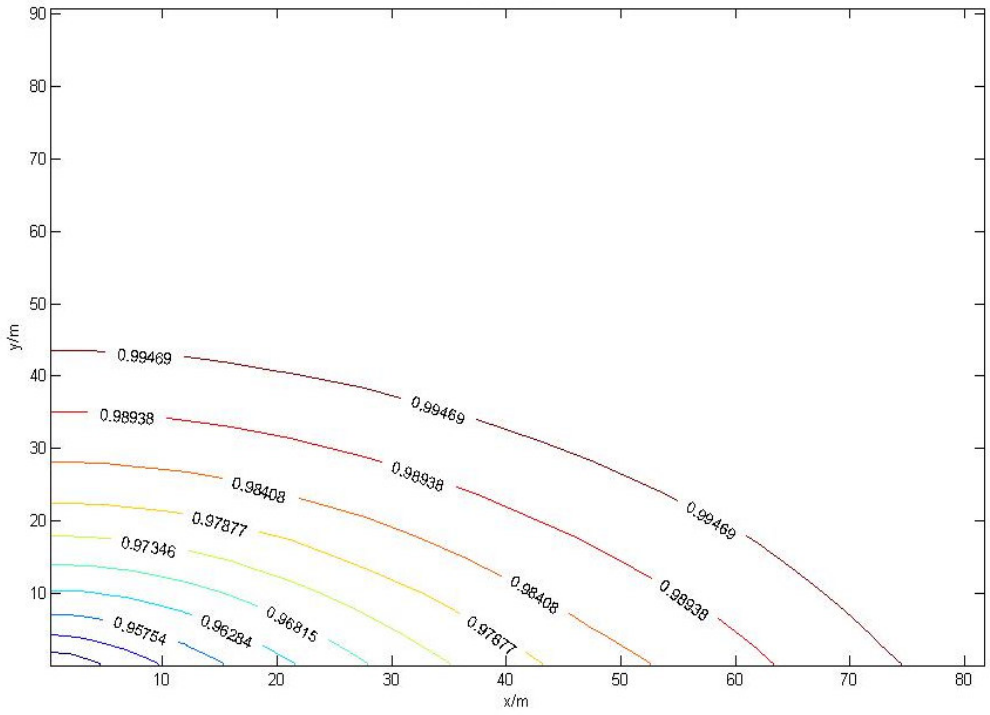

Figure 3.27: GTR contour map in a quarter of drainage area of a HFW in a gas condensate flow system with $C_{fD\text{-}eff}$=1.05, I_X=0.1835 and x_f=105.7 m, FHWS-5 defined in Table 3.1b. Two phase zone is smaller than the fractured zone.

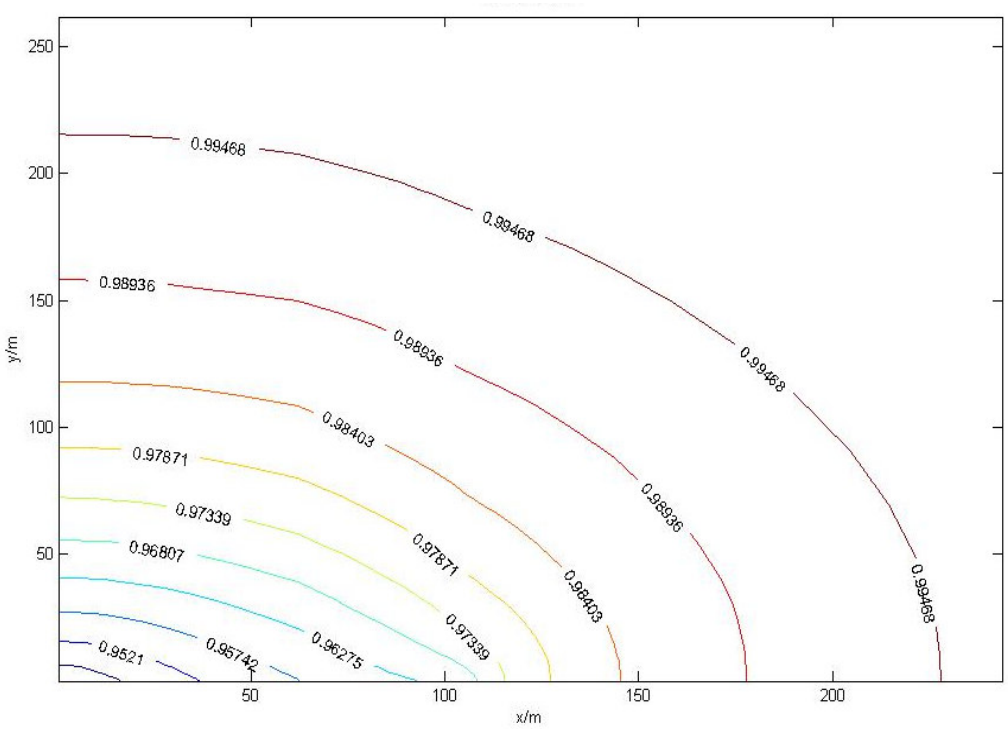

Figure 3.28: GTR contour map in a quarter of drainage area of a HFW in a gas condensate flow system with $C_{fD\text{-}eff}$=1.72, I_X=0.1835 and x_f=105.7 m, FHWS-6 defined in Table 3.1b. Two phase zone is greater than the fractured zone.

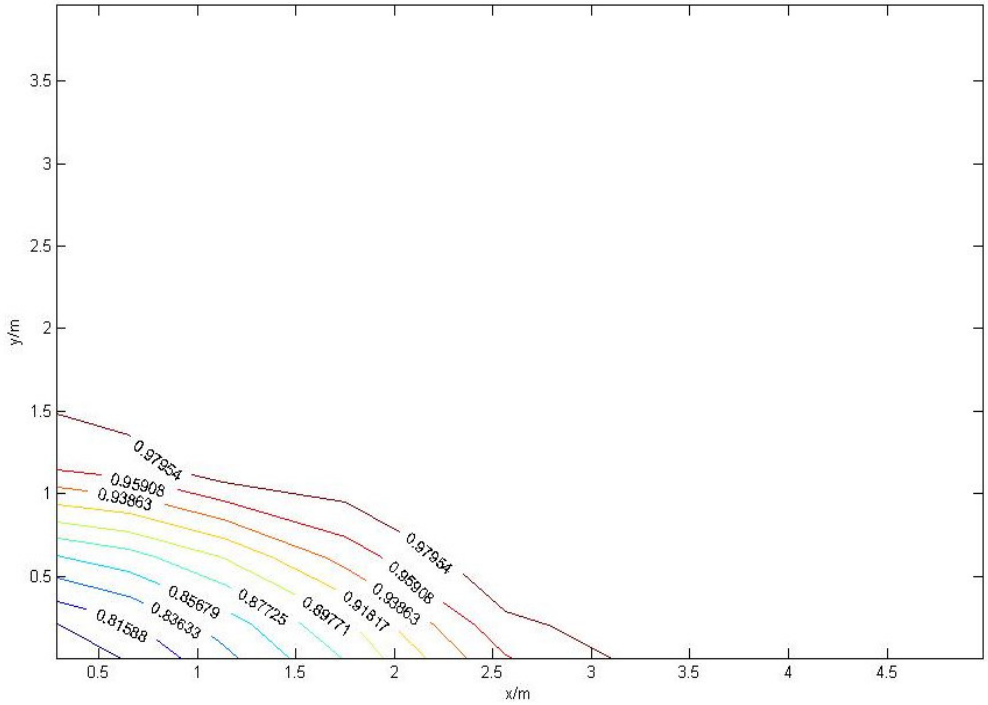

Figure 3.29: GTR contour map in a quarter of drainage area of a HFW in a gas condensate flow system with $C_{fD\text{-}eff}$=0.375, I_X=0.1835 and x_f=105.7 m, FHWS-7 defined in Table 3.1b. Two phase zone is much smaller than the fractured zone.

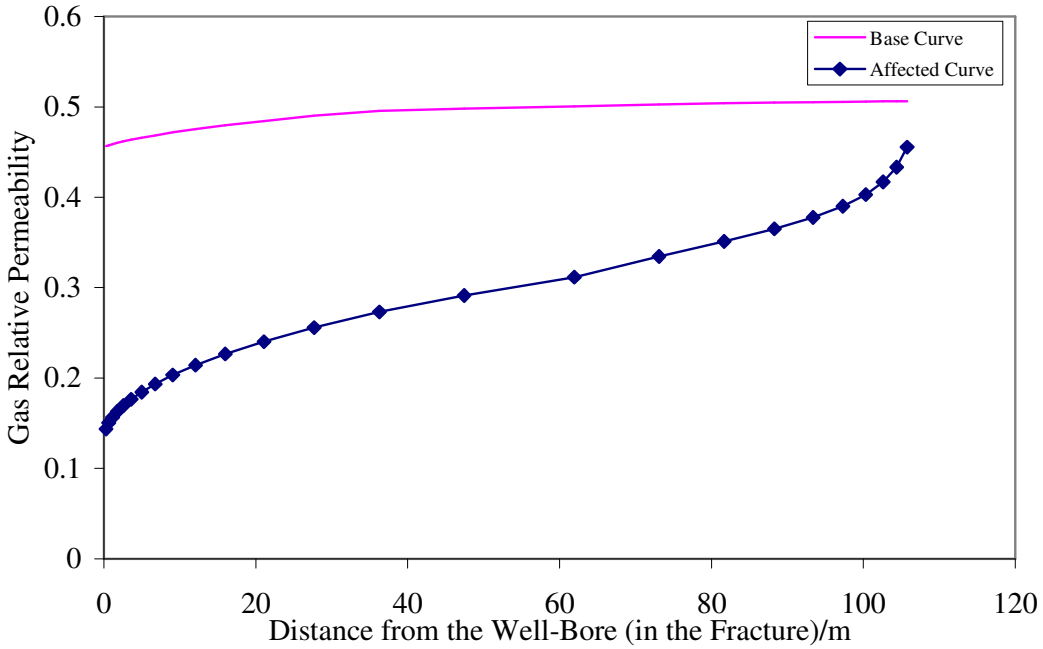

Figure 3.30: Variation of base and affected gas relative permeability inside the fracture, HFWS-8 defined in Table 3.1c.

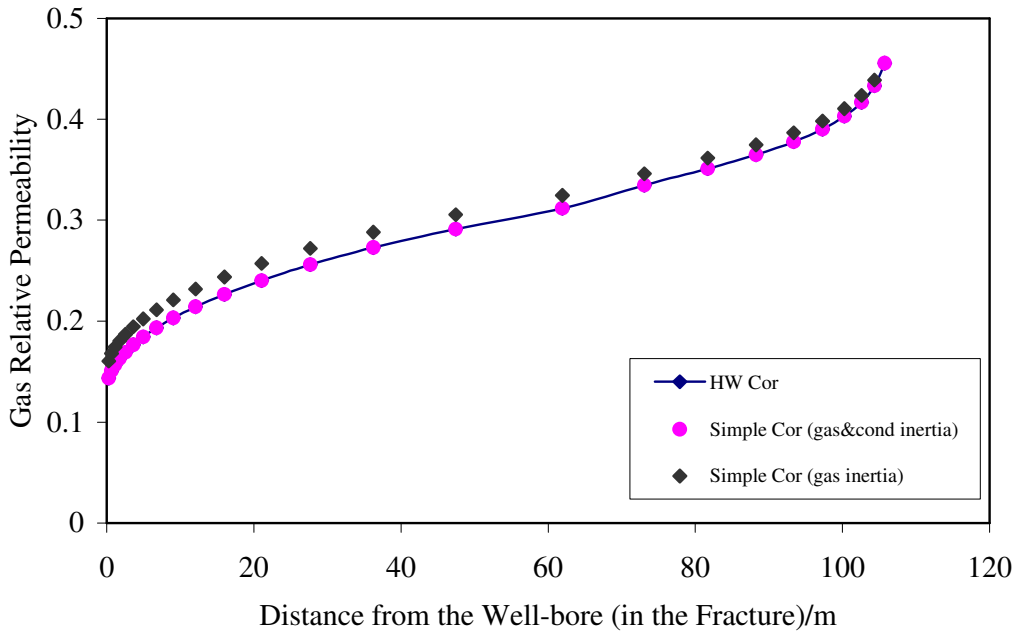

Figure 3.31: Gas relative permeability inside the fracture predicted by HW generalized correlation, the developed Formula (Equations 3.67 and 3.68) and the developed equation but with ignoring $k_{rbc\text{-}f}$ in Reynolds number. HFWS-8 defined in Table 3.1c.

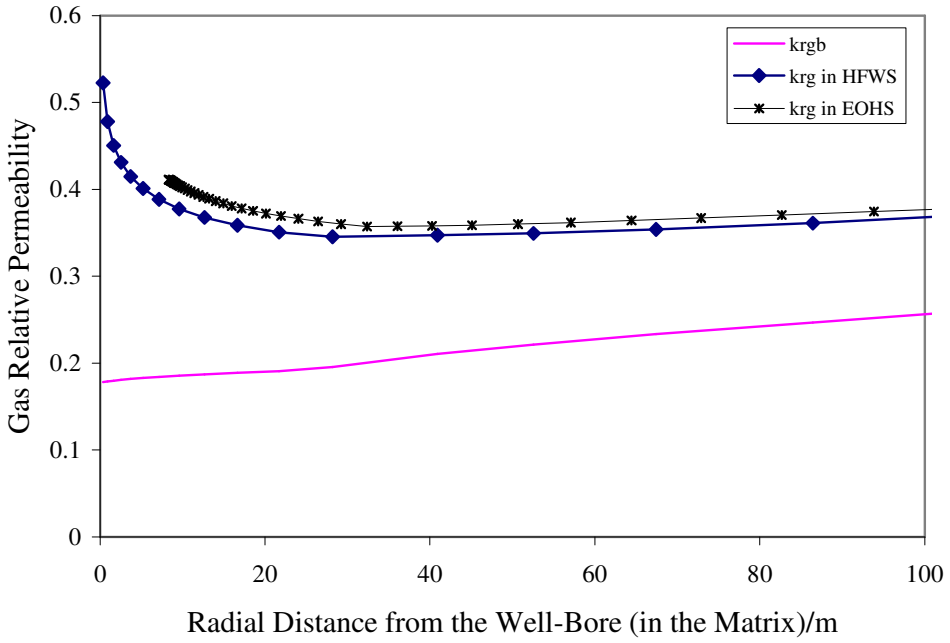

Figure 3.32: Variation of base and affected gas relative permeability inside the matrix, HFWS-8 defined in Table 3.1c.

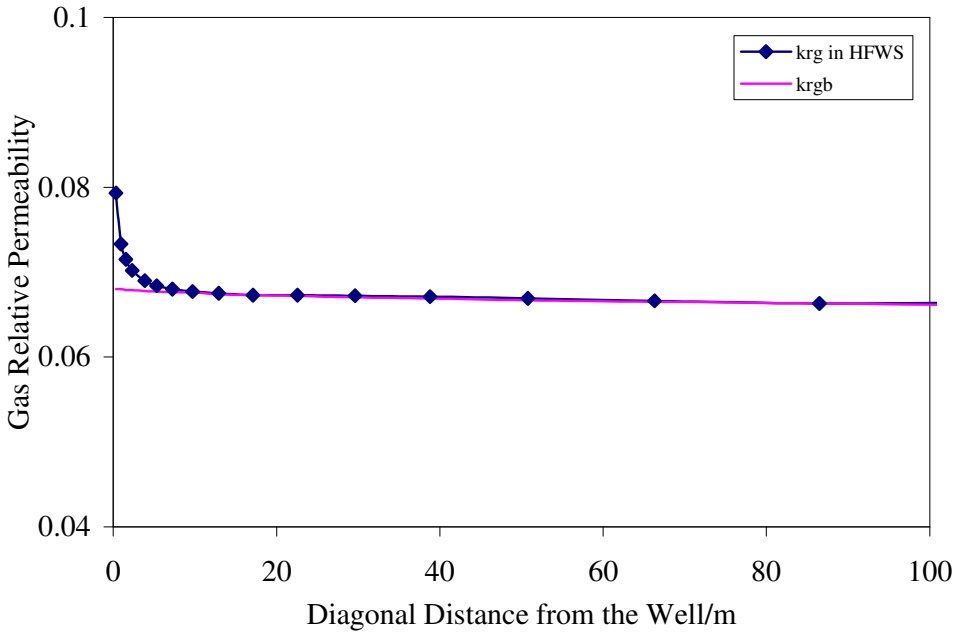

Figure 3.33: Variation of base and affected gas relative permeability inside the matrix, HFWS-9 defined in Table 3.1c.

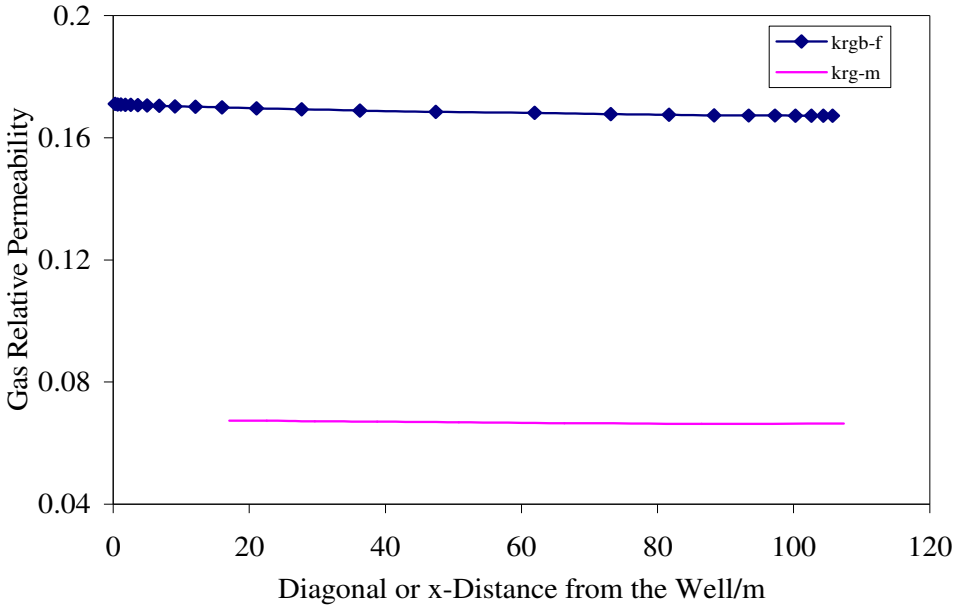

Figure 3.34: Base gas relative permeability in the fracture versus x-distance from the wellbore and gas relative permeability in the matrix versus diagonal distance from the wellbore for HFWS-9, defined in Table 3.1c.

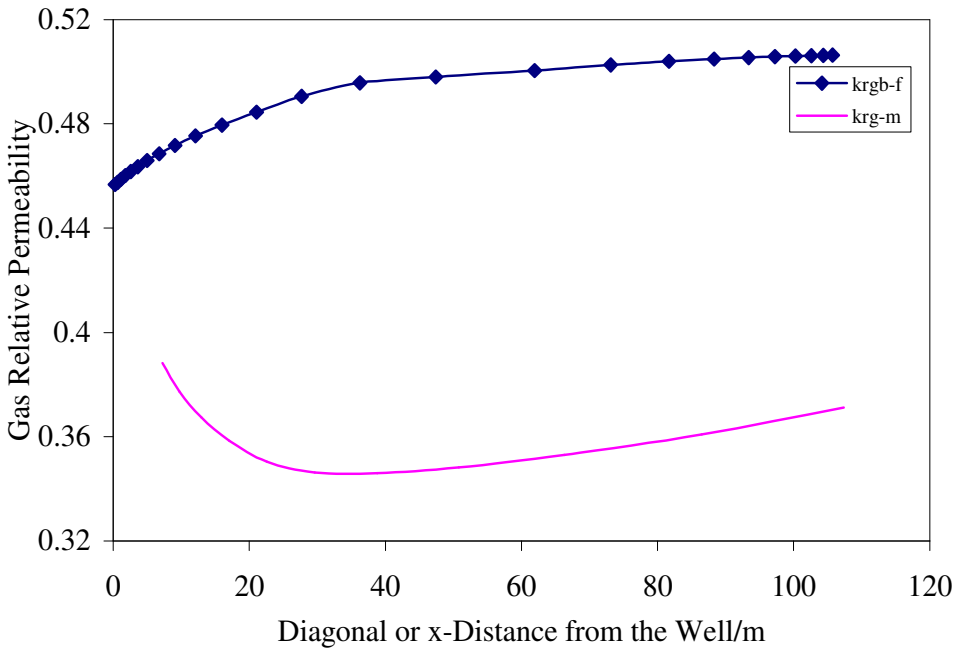

Figure 3.35: Base gas relative permeability in the fracture versus x-distance from the wellbore and gas relative permeability in the matrix versus diagonal distance from the wellbore for HFWS-8 defined in Table 3.1c.

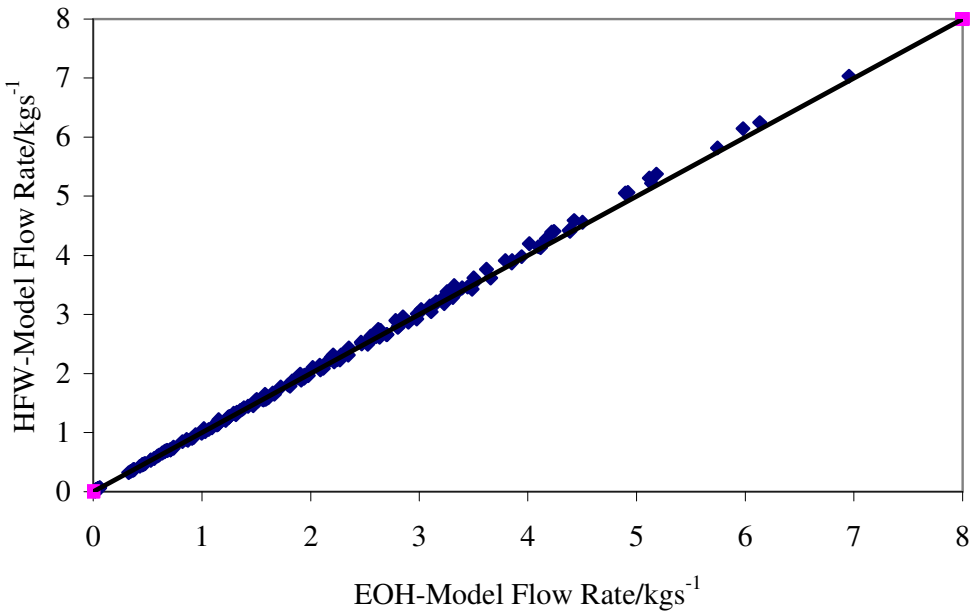

Figure 3.36: Estimated production rate by the in-house HFW simulator versus that by the in-house OH simulator. HFWS-11 defined in Table 3.1c. AAD% = 1.8%.

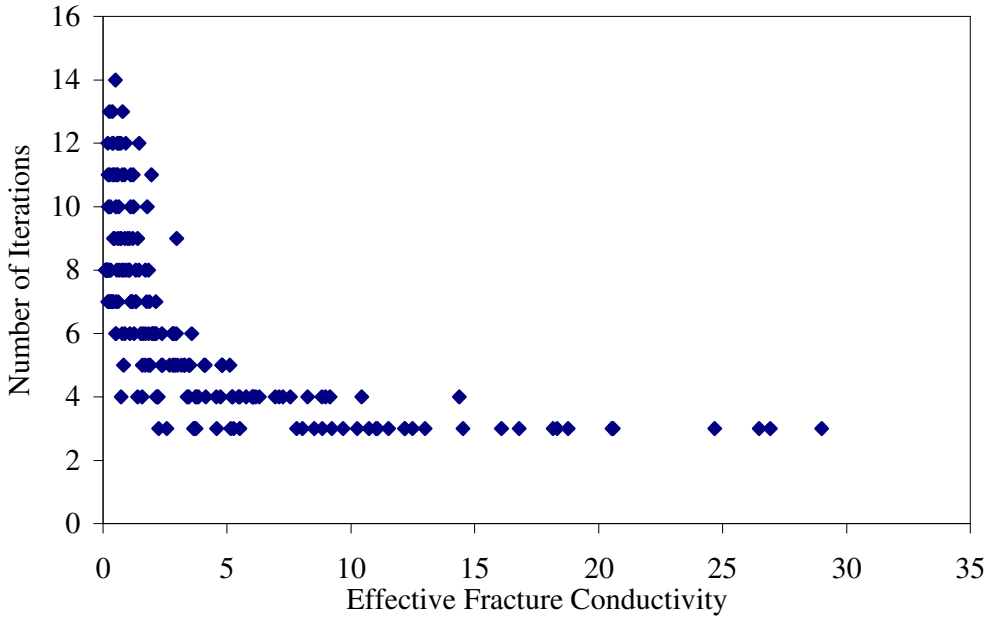

Figure 3.37: Number of iterations against effective fracture conductivity, HFWS-11 defined in Table 3.1c.

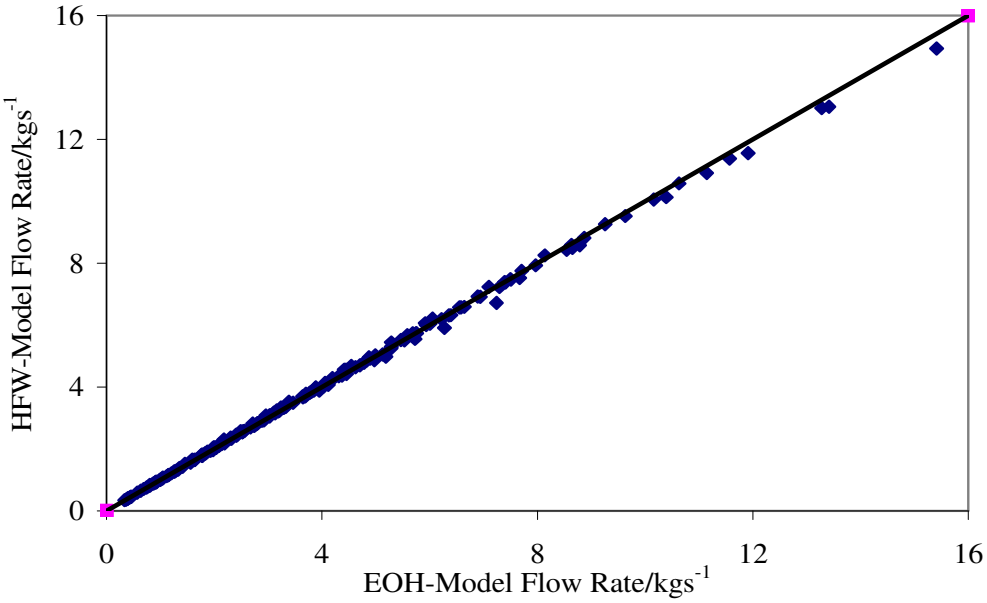

Figure 3.38: Estimated production rate by the in-house HFW simulator versus that by the in-house OH simulator. HFWS-12 defined Table 3.1c. AAD% = 1.32%.

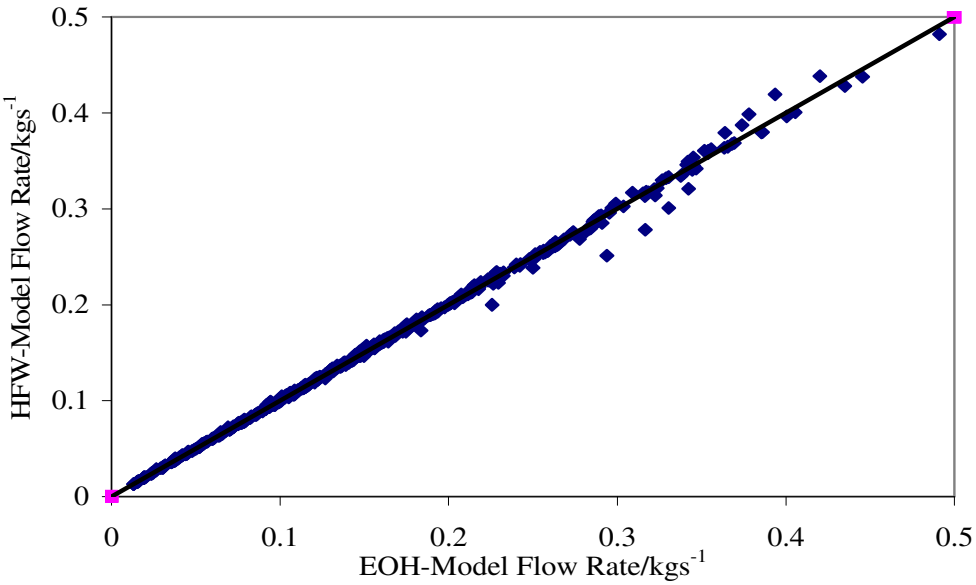

Figure 3.39: Estimated production rate by the in-house HFW simulator versus that by the in-house OH simulator. HFWS-13 defined in Table 3.1d. AAD%=1.2%.

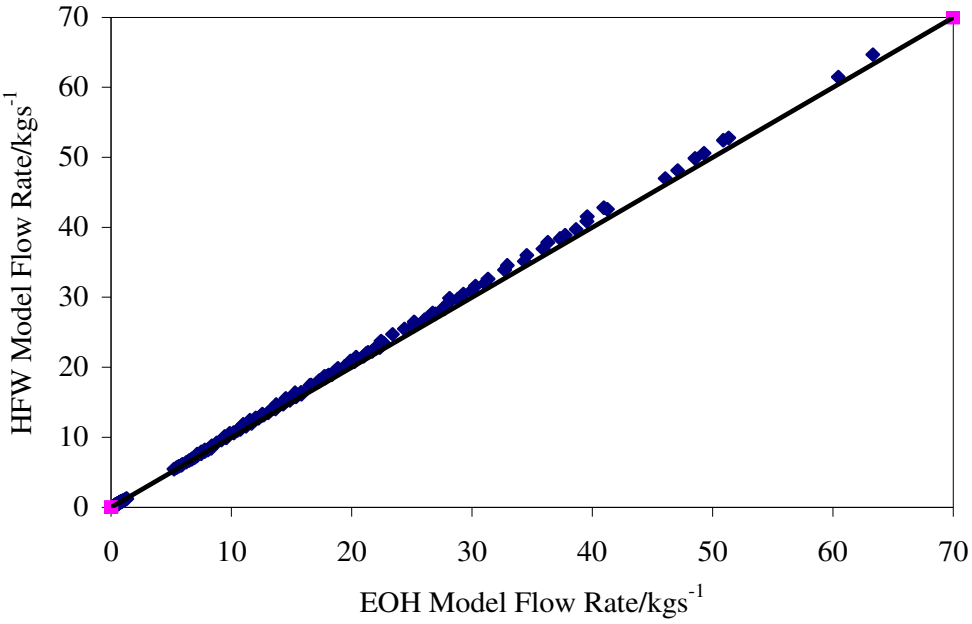

Figure 3.40: Estimated production rate by the in-house HFW simulator versus that by the in-house OH simulator. HFWS-14 defined in Table 3.1d. AAD%= 3.8%.

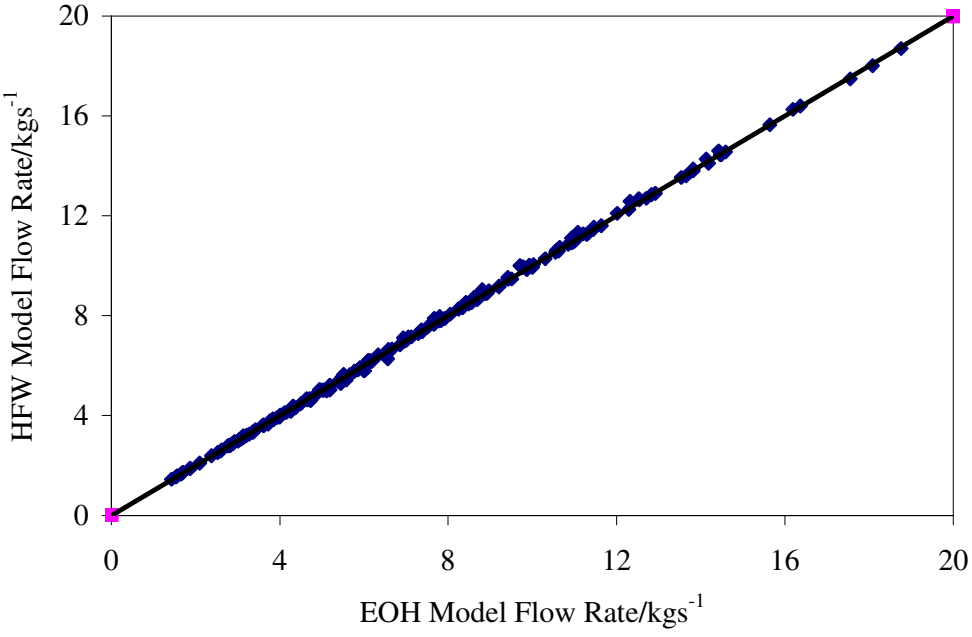

Figure 3.41: Estimated production rate by the in-house HFW simulator versus that by the in-house OH simulator. HFWS-15 defined in Table 3.1d. AAD%=0.78%.

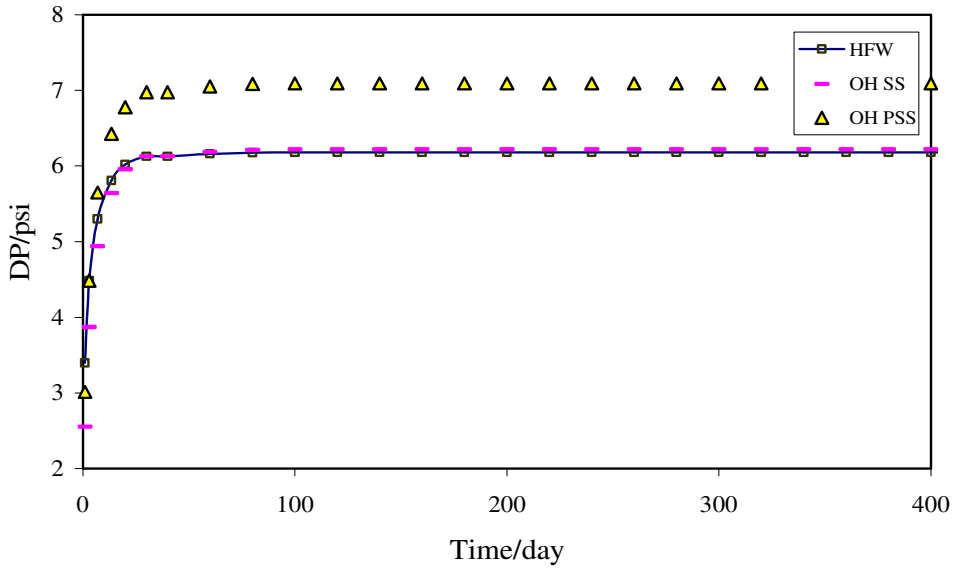

Figure 3.42: Draw down, $DP = P_e - P_w$, as a function of the production time. For a single phase Darcy flow system with constant exterior pressure, HFWS-16 defined in Table 3.1e.

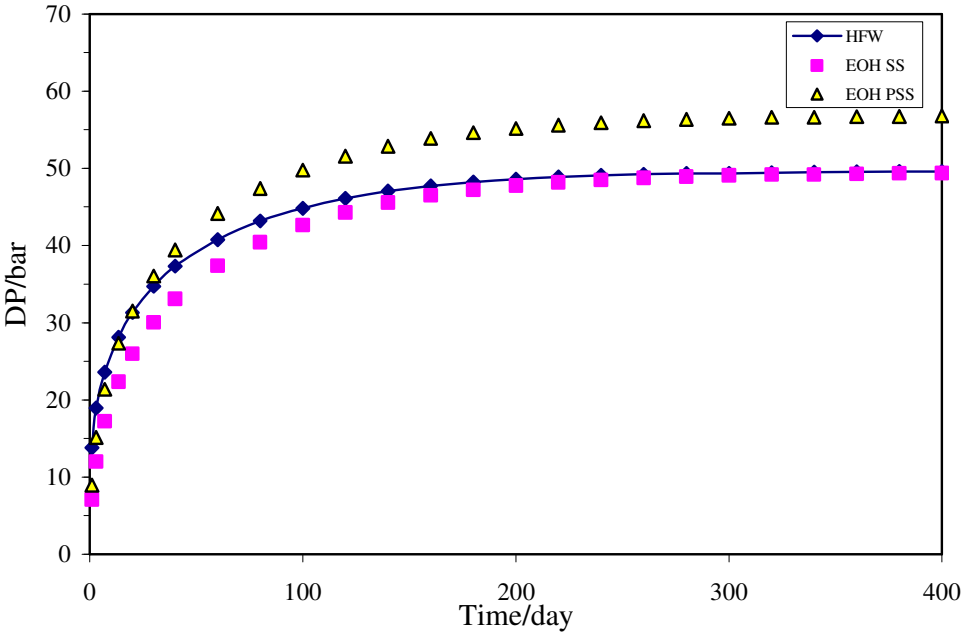

Figure 3.43: Draw down, $DP = P_e - P_w$, as a function of the production time. Single phase non-Darcy flow system with constant exterior pressure, HFWS-17, defined in Table 3.1e.

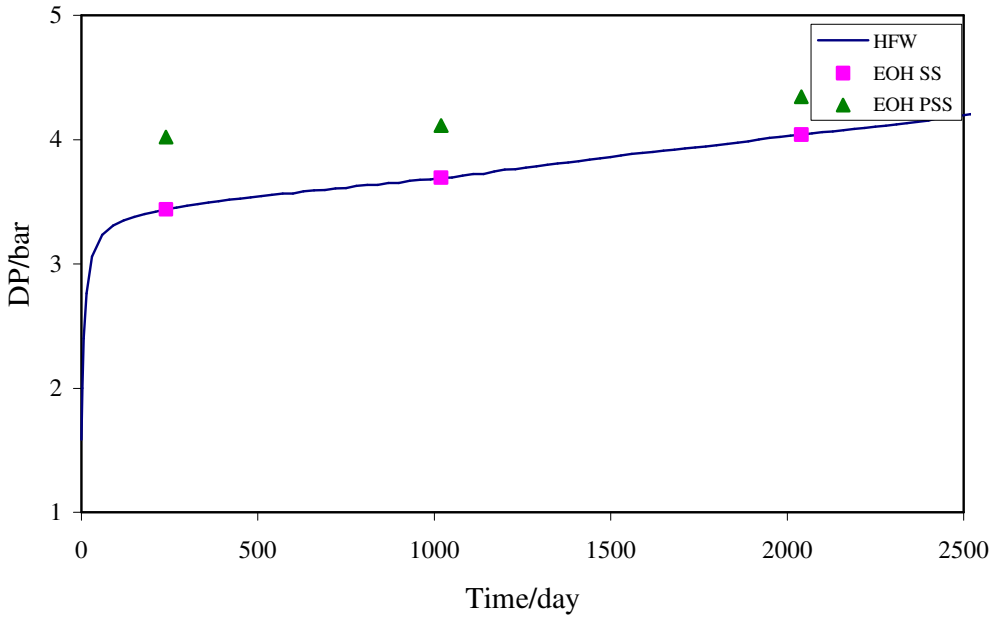

Figure 3.44: Draw down, $DP = P_e - P_w$, as a function of the production time. Gas Condensate flow system with constant exterior pressure, HFWS-18 defined in Table 3.1e.

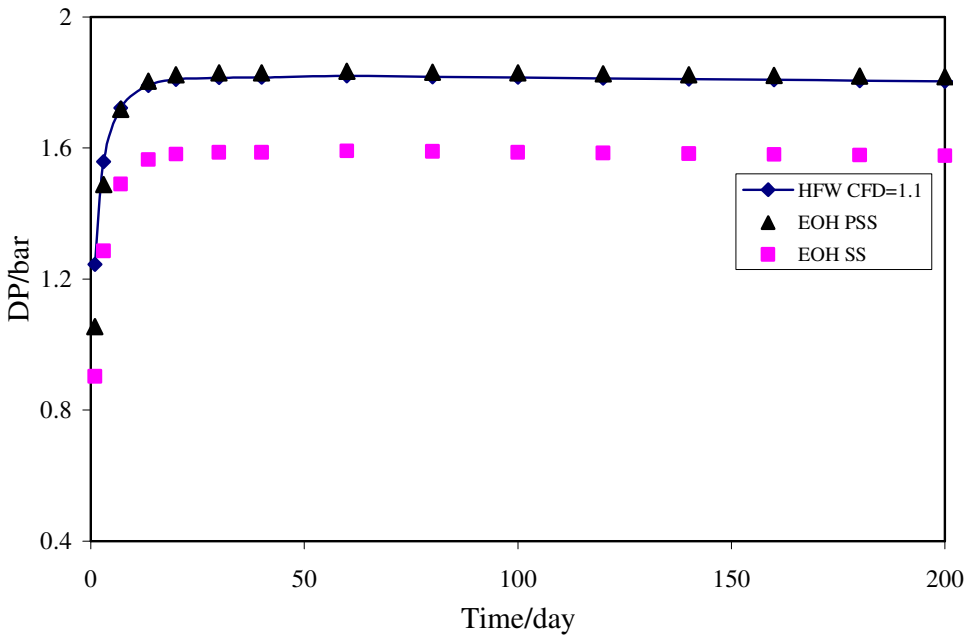

Figure 3.45: Draw down, $DP = \overline{P} - P_w$, as a function of the production time. Single phase Darcy flow system with closed exterior boundary, HFWS-19 defined in Table 3.1f.

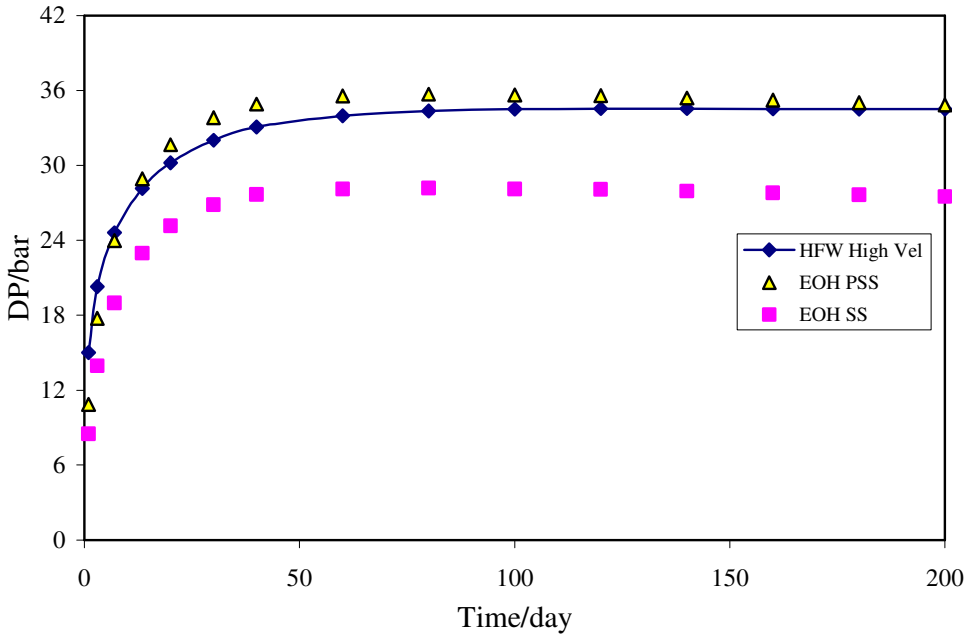

Figure 3.46: Draw down, $DP = \overline{P} - P_w$, as a function of the production time. Single phase non-Darcy flow system with closed exterior boundary, HFWS-20 defined in Table 3.1f.

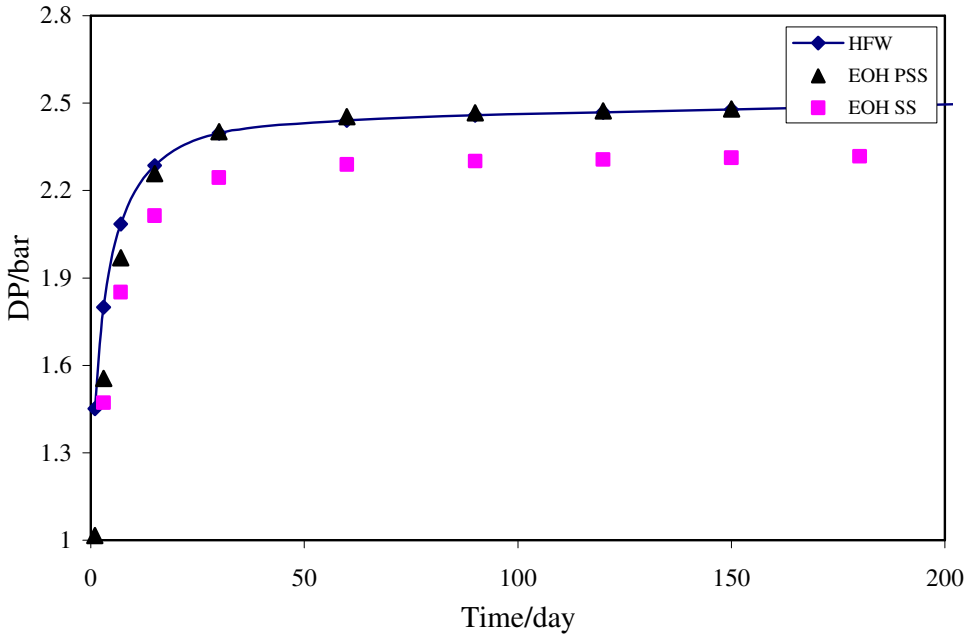

Figure 3.47: Draw down, $DP = \overline{P} - P_w$, as a function of the production time. Gas Condensate flow system with closed exterior boundary, HFWS-21 defined in Table 3.1f.

Chapter 4 Optimization of Hydraulic Fracture Geometry

4.1 Introduction

In the last chapter, the flow around hydraulically fractured wells was investigated and the formulae of effective wellbore radius for gas condensate reservoirs were developed. In this chapter, those formulae will be utilized to find the optimum geometry of a Hydraulic Fracture (HF) with a definite volume.

Two important geometrical parameters which can have significant effects on the well-productivity are fracture thickness and fracture half-length; these are related together by the constraint of fracture volume as follows:

$$V_f = 2w_f x_f \tag{4.1}$$

Here V_f is the fracture volume per the unit height of the fracture. Obviously, for a fixed fracture volume, increasing the fracture half length results in the decrease of the fracture thickness and vice versa. The effect of variation of these parameters on the well productivity can be distinguished easily for single phase, non-damaged, Darcy flow systems. In these systems, for a constant fracture volume, flow resistance in the fractured and un-fractured zones is, respectively, increased and decreased with the increase in fracture length (see Section 3.3). Obviously, there is an optimum value for the fracture half length at which the summation of these flow resistances reaches a minimum, and consequently well productivity is maximized. Finding the optimum fracture half length, but in the presence of gas condensate flow complexities, is the main purpose of this chapter.

Prats (1961) was the first to introduce the issue of the optimum fracture length, or geometry. According to his results, optimum fracture design for an HFW in a square drainage area and with small fracture penetration ratio under the Darcy flow regime is gained at C_{fD}=1.26.

Because of the importance of the optimization of fracture geometry, many investigators have put a great deal of effort on that. Valko *et al.* (1998) presented a physical optimization approach called Unified Fracture Design (UFD). They have emphasized that "*the key to formulating a meaningful technical optimization problem is to realize that penetration and dimensionless fracture conductivity are competing for the same source; the propped volume*". In the UFD method, the Propped number is introduced as two times of the ratio of the propped volume to the reservoir volume weighted by their permeability contrast. Valko *et al.* presented some charts of the dimensionless productivity index of Hydraulically Fractured Wells (HFWs) at Pseudo-Steady State (PSS) as functions of Propped number and fracture conductivity. In these graphs, it is clearly shown that for each Propped number there is an optimum fracture conductivity at which the productivity index is a maximum.

Economides *et al*. (2002) presented a discussion on optimal design. They claimed that *"…In reality the existence of a transient flow period does not change the previous conclusions on optimal dimensions. Our calculations show that there is no reason to depart from the optimum compromise derived for the pseudo-steady state, even if the well will produce in the transient regime for a considerable time (say months or years). Simply stated, what is good for maximizing pseudo-steady state flow is also good for maximizing transient flow"*.

Meyer and Jacot (2005) developed a semi-analytical formula for the estimation of effective wellbore radius of an HFW in a rectangular closed drainage area for single-phase Darcy flow at PSS. They also presented a chart which correlates the optimum fracture conductivity with rectangular aspect ratio with a restriction for fracture penetration ratio; i.e. the chart is applicable for HFWs with fracture penetration ratio less than 0.2. According to the results of Meyer *et al.* (2005) and also Valko *et al.* (1998), optimum fracture conductivity in square drainage areas (with I_x less than 0.2) is about 1.57 which is a little higher than the Prats result (1.26).

The optimization of hydraulic fracture in a non-Darcy flow system has also been the subject of study by some investigators.

Lopez-Hernandez *et al.* (2004) introduced the concept of using effective Propped number in the UFD method for estimation of optimum fracture length for non-Darcy flow systems. In this concept, as the inertial effect reduces absolute fracture permeability to the effective value, effective permeability should be used in the calculation of Propped number and fracture conductivity. In this paper, the Gildey approximation (Equation 3.59) has been used for the estimation of effective fracture permeability. Lopez-Hernandez *et al.* have used the same charts of the UFD method, developed by Valko and Economides (1998) for single phase systems, to optimize fracture design in the presence of non-Darcy effects. The low accuracy of Gildey's approximation for estimation of inertial effect was discussed in some detail in Section 3.4, and it was concluded that the inertial effect is overestimated by the Gildey equation.

Zeng and Zhao (2008) simulated Transient non-Darcy flow around hydraulically fractured wells, and developed a correlation for optimum fracture half length. As even this correlation cannot satisfy the case of Darcy flow, its reliability is under question.

There are also some papers available in the literature on optimization of fracture design for gas condensate systems. However, to the best knowledge of the author, in all these studies two phase region is behaved as a damaged layer with constant thickness around the whole fracture, and gas condensate flow behaves as single phase flow in a face-damaged HFW system. For instance, Wang, Valko and Economides (2000) used this approach. They used the Cinco-Ley Equation (Equation 3.41), developed basically for estimation of face damage skin, for estimation of condensate build-up damage. In this approach, the absolute permeability of the damaged layer is set equal to kk_{rg} and the thickness of the damaged layer is replaced with the extent of the two-phase region, which - it is assumed - is a constant layer around the fracture. For estimation of two-phase region thickness, Wang *et al.* have recommended that: "*For any fracture length and a given flowing bottomhole pressure that is known to be inside the retrograde condensation zone of a two-phase envelop the pressure profile normal to the fracture face and into the reservoir will delineate the points where the pressure is equal to the dew point pressure from this pressure profile the fracture face skin distribution along the fracture face is determined.*" Needless to say this difficult, almost impractical,

approach could result in very rough estimations. In Section 3.5, the two-phase region around the wellbore and fracture was investigated, and it was demonstrated that two-phase region is elliptical and becomes radial when the effective fracture conductivity approaches zero; besides, its length could be equal to, smaller or larger than the fracture length. However, in the study of Wang *et al.* (2000), the shape of the two-phase region is assumed as a rectangle with the length equal to the fracture length. They have not explained what type of pressure profile can predict such an unreal two-phase region, because a correct pressure profile will provide an elliptical two-phase region, which could be much smaller or much larger than the fracture length (see Figures 3.25-3.29). Neglecting two-phase flow and also the inertial effect inside the fracture are some of the other weak points of the paper published by Wang *et al.* (2000).

There are some other studies about optimization of fracture geometry in gas condensate reservoirs (such as those of Indriati *et al.* (2002) and Mohan *et al.* (2006)) but as they are all based on the same assumptions, they are not explained here.

Carajaval (2006) by conducting a limited number of numerical sensitivity study using the ECLIPSE 300 compositional commercial reservoir simulator proposed to simply modify the absolute fracture conductivity (C_{fD}) and use the current optimized fracture technique (UFD method), which is based on Darcy flow regime. In his approach C_{fD} has been modified for the effect of coupling in the matrix and that of inertia in the fracture.

To the best of author's knowledge there is not an appropriate methodology for optimizing fracture design in gas condensate reservoirs.

Here it is shown that the formula for effective wellbore radius of HFWs, introduced in the last chapter, provides a good tool for finding the optimum fracture length.

As was shown in Chapter 3, the formula for an effective wellbore radius is dependent on the exterior boundary condition: constant pressure or closed boundary. Thus, optimum design of a fracture could also be dependent on the external boundary condition; in other words, optimum fracture geometry at Steady State (SS) could possibly be different from that at Pseudo-Steady State (PSS). This subject will be shown better in Section 4.1, where the similar curves of the UFD method are developed for SS conditions.

In section 4.2, two sets of formulae for estimation of the optimum fracture conductivity and the optimum fracture length for SS and PSS will be developed. These formulae, which are applicable for both gas and gas condensate square reservoirs, are developed mathematically, based on the maximization of an effective wellbore radius for a fixed fracture volume.

The developed formulae will be verified in section 4.4, where several different illustrations confirm their applicability for finding an optimum fracture design at different operating conditions.

4.2 UFD Method

Valko *et al.* (1998) introduced Unified Fracture Design (UFD) method, to find the optimum fracture design for single phase Darcy flow systems (at pseudo-steady state). In their method, they defined the Propped number as follows:

$$N_P = I_X^2 C_{fD} = \frac{k_f}{k}\frac{w_f x_f}{x_e^2} = 2\frac{k_f}{k}\frac{V_f}{V_e} \tag{4.2}$$

where V_f and V_e refer to fracture and drainage volume, respectively. In fact, the Propped number represents the ratio of the fracture volume over the drainage volume, times their permeability ratio. The importance of the Propped number in fracture optimization for single phase Darcy flow systems is owing to the fact that for a certain Propped number, the productivity index reaches maximum possible value at a certain fracture width-length ratio.

Figure 4.1 is one of the charts developed by Valko *et al.* (1998), which shows the PSS productivity index ($J_{D\text{-}PSS}$) of an HFW in a square or cylinder drainage area as a function of fracture conductivity and Propped number. In the UFD method, $J_{D\text{-}PSS}$ is defined as follows:

$$J_{D-PSS} = \frac{1}{\ln\left(\frac{r_e}{x_f}\right) + S_f^{'}\Big|_{PSS} - 0.75} \tag{4.3}$$

In this chart for small Propped numbers optimum fracture conductivity, $C_{fD\text{-}opt}$, which provides the maximum $J_{D\text{-}PSS}$ for a certain fracture volume, is constant and equal to 1.6. However, for bigger Propped numbers, $C_{fD\text{-}opt}$ is dependent on the Propped number, and it increases with increasing N_p. Figure 4.1 also shows that, for very big Propped numbers (N_p>6), the theoretical optimum fracture conductivity occurs in the region of I_X>1.0, which is impossible. In these cases, optimum practical design can be gained at I_X=1.0 where fracture and reservoir lengths are equal.

4.2.1 Developing UFD method for steady state systems

Although the formulae for optimum fracture design, introduced in the next section, are sufficient for both single phase and gas condensate flow systems, just to emphasize this fact that Valko's charts would not be applicable to constant exterior pressure systems for big Propped numbers, here similar charts for constant exterior pressure systems are developed.

In Section 3.3, it was shown that when the fracture is penetrated in a reservoir with a constant exterior pressure boundary, the performance approaches SS conditions and the well productivity - even at the late transient state - can be estimated with an SS formula for an effective wellbore radius.

The dimensionless productivity index of an HFW for SS conditions is defined as:

$$J_{D-SS} = \frac{1}{\ln\left(\frac{r_e}{x_f}\right) + S_f^{'}\Big|_{SS} - 0.5} \tag{4.4}$$

In Section 3.3, it was shown (see Figure 3.10) that $S_f^{'}$ at PSS is greater than that at SS, and the difference is more significant when I_X approaches one, especially for higher conductive fractures. Moreover, the shape of variation of $S_f^{'}$ with I_X is different in these two systems, i.e. with an increase in I_X: $S_f^{'}\Big|_{PSS}$ increases while $S_f^{'}\Big|_{SS}$ decreases. Therefore it is expected that the shape of variation of $C_{fD\text{-}opt}$ with N_p for SS will be different from what was seen for PSS.

The developed formula for the $S_f^{'}\big|_{SS}$ (Equation 3.27) can be used to develop similar charts of the UFD method but applicable for constant exterior pressure systems.

Figure 4.2 shows five curves of $J_{D\text{-}SS}$ as a function of fracture conductivity for five different Propped numbers. In this figure, for small values of N_p (less than 0.3), optimum fracture conductivity is $\pi/2$ but it decreases with increasing N_p, unlike the variation in PSS systems.

A comparison of Figure 4.1 with 4.2 shows that for PSS systems, optimum fracture conductivity increases with the increase in I_X, whilst for SS systems $C_{fD,opt}$ decreases with the increase in I_X.

Figure 4.3 could also be used for the optimization of fracture penetration ratio. In this Figure, $J_{D\text{-}SS}$ has been plotted versus I_X for different Propped numbers.

4.3 Maximum Effective Well-Bore Radius

Optimum fracture design can be defined as the geometry of a given fracture volume that provides the maximum possible dimensionless productivity.

Ignoring $r_w^{'2}/2r_e^2$ and $r_w^{'4}/4r_e^4$ in the formula for J_D (see Equation 3.31), dimensionless productivity is defined as:

$$J_D = \frac{1}{\ln\left(\frac{r_e}{x_f}\right) + S_f^{'} + S - c} = \frac{1}{\ln\left(\frac{r_e}{r_w^{'}}\right) + S - c} \tag{4.5}$$

Here S could represent the summation of damage and shape skin factor. Shape skin factor, depending only on the shape of the drainage area and the well location, is zero for cylindrical or square drainage areas. c is a constant which is ½ for steady-state systems and ¾ for pseudo-steady systems.

If there is no damage or if the effects of variation of fracture dimensions on damage skin are negligible, it can be stated that the maximum productivity index is achieved when

effective wellbore radius reaches its maximum possible value. That is, for the optimization of fracture design, the following equation should be solved.

$$\left.\frac{\partial r_w^{'}}{\partial x_f}\right)_{V_f, P_w} = 0 \tag{4.6}$$

Where V_f is the fracture volume per the unit height of the fracture. According to this equation, we are looking for an HF design which, for a certain fracture volume and at a certain bottomhole pressure, provides the maximum possible effective wellbore radius.

According to Equation 3.36, which is applicable to square reservoirs at both steady-state and pseudo-steady state, effective wellbore radius can be calculated as:

$$r_w^{'} = \frac{x_f}{2\times\delta + \frac{\pi}{C_{fD-eff}}}, \tag{4.7}$$

where,

for SS systems: $$\delta = A = \ln\left(e^1 - \frac{0.17}{r_{eD} - 0.87}\right) \tag{4.8}$$

and for PSS systems: $$\delta = B = \ln\left(e^1 + \frac{0.504}{(r_{eD} - 0.783)^{1.255}}\right). \tag{4.9}$$

The formula for effective fracture conductivity is also defined as follows:

$$C_{fD-eff} = C_{fD} \times MR_w \times \frac{1}{1 + 0.62\,\mathrm{Re}_w}. \tag{4.10}$$

where:

$$MR_w = \frac{\mathrm{M}_{rbf}\big|_w}{M_{rm}\big|_w} = \frac{\left(\frac{\rho_g}{\mu_g}k_{rgb-f} + \frac{\rho_c}{\mu_c}k_{rcb-f}\right)_{well-bore}}{\left(\frac{\rho_g}{\mu_g}k_{rg-m} + \frac{\rho_c}{\mu_c}k_{rc-m}\right)_{well-bore}} \tag{4.11}$$

$$C_{fD} = \frac{k_f w_f}{k x_f} = \frac{k_f V_f}{2k x_f^2} = \frac{C_1}{x_f^2} \tag{4.12}$$

$$\text{Where } C_1 = \frac{k_f V_f}{2k} \tag{4.13}$$

$$V_f = 2 x_f w_f \tag{4.14}$$

In Equation 4.10, Reynolds number, depending on the flow velocity, is an implicit function of fracture length.

$$\mathrm{Re}_w = \frac{\overline{\rho}_w v_w k_f \beta_f \left(k_{rgb-f} + k_{rcb-f}\right)_w}{\overline{\mu}_w} \Rightarrow$$

$$\mathrm{Re}_w = \left(k_{rgb-f} + k_{rcb-f}\right)_w \frac{\overline{\rho}_w}{\overline{\mu}_w} k_f \beta_f \frac{q_w}{2hw_f} = C_2 q_w x_f, \tag{4.15}$$

Where,

$$C_2 = \left(k_{rgb-f} + k_{rcb-f}\right)_w \frac{\overline{\rho}_w}{\overline{\mu}_w} \frac{k_f \beta_f}{h V_f} \tag{4.16}$$

Substituting from Equation 4.7 and 4.10 into Equation 4.6 and ignoring the variation of fluid properties with variation of x gives the following equation:

$$\frac{\partial}{\partial x_f}\left(\frac{x_f}{2\times\delta + \frac{\pi}{MR_w}\frac{1}{C_{fD}}\left(1+0.62\,\mathrm{Re}_w\right)}\right)_{V_f, P_w} = 0 \tag{4.17}$$

Therefore:

$$\frac{2\delta+\frac{\pi}{MR_w}\frac{1}{C_{fD}}\left(1+0.62\,\mathrm{Re}_w\right)-x_f\left(2\frac{d\delta}{dx_f}+\frac{\pi}{MR_w}\frac{\partial}{\partial x_f}\left(\frac{1+0.62\,\mathrm{Re}_w}{C_{fD}}\right)\right)}{\left(2\delta+\frac{\pi}{MR_w}\frac{1}{C_{fD}}\left(1+0.62\,\mathrm{Re}_w\right)\right)^2}=0 \tag{4.18}$$

While:

$$\frac{\partial}{\partial x_f}\left(\frac{1+0.62\,\mathrm{Re}_w}{C_{fD}}\right)=\left(1+0.62\,\mathrm{Re}_w\right)\frac{\partial}{\partial x_f}\left(\frac{1}{C_{fD}}\right)+\frac{1}{C_{fD}}\frac{\partial}{\partial x_f}\left(1+0.62\,\mathrm{Re}_w\right) \tag{4.19}$$

According to Equations 4.12 and 4.15, it can be said:

$$\frac{\partial}{\partial x_f}\left(\frac{1}{C_{fD}}\right)=\frac{2x_f}{C_1} \tag{4.20}$$

And

$$\frac{\partial\,\mathrm{Re}_w}{\partial x_f}=\frac{\partial\left(C_2 q_w x_f\right)}{\partial x_f}=C_2\left(q_w+\left(x_f\,\frac{\partial q_w}{\partial x_f}\right)\right) \tag{4.21}$$

At the optimum point for a fixed drawdown the flow rate is the maximum, $\frac{\partial q_w}{\partial x_f}=0$, therefore Equation 4.21 can be simplified as follows:

$$\frac{\partial\,\mathrm{Re}_w}{\partial x_f}=C_2 q_w \tag{4.22}$$

Combining Equations 4.18, 19, 20 and 22 will result in:

$$2\left(\delta-x_f\,\frac{d\delta}{dx_f}\right)-\frac{\pi}{MR_w C_{fD,opt}}\left(1+2\times0.62\,\mathrm{Re}_w\right)=0 \tag{4.23}$$

Solving the above equation for $C_{fD,opt}$ gives:

$$C_{fD,opt} = \frac{\pi}{2\left(\delta - x_f \frac{d\delta}{dx_f}\right)MR_w}\left(1 + 2\times 0.62\,\mathrm{Re}_w\right) \tag{4.24}$$

Since δ has different equations for SS and PSS, further steps of this part will come in two parallel sections for SS and PSS systems.

4.3.1 Steady state systems

For steady state systems, δ is equal to A and Equation 4.24 is rewritten as:

$$C_{fD,opt} = \frac{\pi}{2\left(A - x_f \frac{dA}{dx_f}\right)MR_w}\left(1 + 2\times 0.62\,\mathrm{Re}_w\right) \tag{4.25}$$

On the other hand:

$$x_f \frac{dA}{dx_f} = \frac{x_f}{x_e}\frac{dA}{dI_X} = I_X \frac{dA}{dI_X} \tag{4.26}$$

Thus Equation 4.25 will convert to:

$$C_{fD,opt} = \frac{\pi}{2 f_A MR_w}\left(1 + 2\times 0.62\,\mathrm{Re}_w\right) \tag{4.27}$$

where,

$$f_A = A - I_X \frac{dA}{dI_X} \tag{4.28}$$

Where A is a function of fracture penetration (See Equation 4.8). Figure 4.4 shows f_A as a function of A for the complete range of I_X ($0 \le I_X \le 1.0$).

According to this Figure, the following second order polynomial function can represent f_A exactly for the whole domain of A [0.723, 1.00]; i.e.:

$$f_A = 14.592A^2 - 29.166A + 15.573 \tag{4.29}$$

For small fracture penetration ratios, where A is about one, f_A should be 1.0 while it is estimated as 0.999 by Equation 4.28, verifying high percision of this Equation.

Figure 4.5 shows the plot of the steady state optimum fracture conductivity of an HFW for single phase systems (MR_w=1.0) as a function of fracture penetration ratio (I_X) and Reynolds number.

From Equation 4.27, optimum effective fracture conductivity can be calculated as follows:

$$C_{fD-eff,opt} = C_{fD,opt}\frac{MR_w}{1+0.62\,\mathrm{Re}_w} = \frac{\pi}{2f_A}\frac{\left(1+2\times 0.62\,\mathrm{Re}_w\right)}{1+0.62\,\mathrm{Re}_w} \Rightarrow$$

$$C_{fD-eff,opt} = \frac{\pi}{2f_A}\left(1+\frac{0.62\,\mathrm{Re}_w}{1+0.62\,\mathrm{Re}_w}\right) \tag{4.30}$$

The above Equation is plotted for some different values of I_X in Figure 4.6. From Figures 4.5 and 4.6, it is seen that for HFW systems with constant exterior pressure, optimum absolute and effective fracture conductivities decrease with increasing fracture penetration ratio. This decrease becomes more significant when I_X approaches one. It is also seen that the optimum effective fracture conductivity can vary between 0.785 (for I_X=1.0 and very small Reynolds numbers) and π which occurs at infinite Reynolds number and small fracture penetration ratios.

Substituting $C_{fD\text{-}opt}$ and Reynolds number in terms of $x_{f\text{-}opt}$ in Equation 4.27 results in the following equation, which is a useful tool for finding optimum fracture half-length.

$$a_{SS}\times x_{f-opt}^3 + b_{SS}\times x_{f-opt}^2 + c = 0 \tag{4.31}$$

Where:

$$a_{SS} = \frac{0.62\pi C_2 q_w}{f_A \times MR_w} \tag{4.32}$$

$$b_{SS} = \frac{\pi}{2 \times f_A \times MR_w} \tag{4.33}$$

$$c = -C_1 = -\frac{k_f V_f}{2k} \tag{4.34}$$

This equation can be solved simply by drawing $F_{SS}(x_f)$, defined below, versus x_f or I_X.

$$F_{SS}(x_f) = a_{SS} \times x_f^3 + b_{SS} \times x_f^2 + c \tag{4.35}$$

Optimum fracture length for SS is gained when $F_{SS}(x_f)$ is equal to zero. When none of the roots of Equation 4.31 is between zero and reservoir half length, the plot of $F_{SS}(x_f)$ versus I_X does not intersect the x-axes, and optimum practical fracture design is achieved at I_X=1.

4.3.2 Pseudo-steady state systems

For pseudo-steady state (PSS) systems, δ is equal to B and Equation 4.24 is rewritten as:

$$C_{fD,opt} = \frac{\pi}{2\left(B - x_f \frac{dB}{dx_f}\right) MR_w} \left(1 + 2 \times 0.62 \,\mathrm{Re}_w\right) \tag{4.36}$$

Similar to what was explained in the last section:

$$x_f \frac{dB}{dx_f} = \frac{x_f}{x_e} \frac{dB}{dI_X} = I_X \frac{dB}{dI_X} \tag{4.37}$$

Thus Equation 4.36 will convert to:

$$C_{fD,opt} = \frac{\pi}{2 f_B MR_w} \left(1 + 2 \times 0.62 \,\mathrm{Re}_w\right) \tag{4.38}$$

where,

$$f_B = B - I_X \frac{dB}{dI_X} \tag{4.39}$$

Figure 4.7 shows f_B as a function of B for the complete range of I_X ($0 \le I_X \le 1.0$).Here again a second order polynomial function can represent f_B for the whole domain of B [1.0, 1.57], which is:

$$f_B = -2.9905B^2 + 5.3765B - 1.3789 \tag{4.40}$$

For small fracture penetration ratios, where B should be one, Equation 4.40 estimates f_B as 1.0071 which shows the good accuracy of Equation 4.40. However, it is seen from Figure 4.7 that f_B becomes zero at B=1.488 (I_X=0.972). Similar behaviour is also noticed from data processing of the outcomes of Equation D.3 of the paper of Meyer *et al.* (2005). In fact, both equations slightly overestimate the slope of B versus I_X when I_X approaches 1.0 (see Figure 4.17). When I_X approaches 1.0, the correct slope should be the slope of Figure D.3, which is a little smaller. Meyer, in the communications he had with the author, recommended digitizing Figure D.3 instead of using Equation D.3. However, as explained in Section 4.3.2, this figure is gained based on using Equation 4.33 for estimation of ξ_∞ from the productivity index, which causes a little overestimation of this parameter. In other words, when I_X is about 1.0 Figure D.3 (of Meyer and Jacot's paper) has a more accurate slope of ξ_∞ versus I_X than that of the new developed formula (Equation 4.9). However it slightly overestimates ξ_∞ which results in the underestimation of an effective wellbore radius. Therefore, the author decided to use the new developed formula for estimation of *B* because it is more accurate than Figure D.3 and its impracticality zone is just for $I_X > 0.97$, where its slope is a little greater than that of Figure D.3.

As f_B becomes zero and then negative for $I_X \ge 0.97$, producing unreasonable results, there is a need to put a restriction for the applicability of the results of this part. That is, I_X should be less than or equal to 0.95.

From Equation 4.38, the optimum effective fracture conductivity can be calculated as follows:

$$C_{fD-eff,opt} = C_{fD,opt}\frac{MR_w}{1+0.62\,\mathrm{Re}_w} = \frac{\pi}{2f_B}\frac{\left(1+2\times 0.62\,\mathrm{Re}_w\right)}{1+0.62\,\mathrm{Re}_w} \Rightarrow$$

$$C_{fD-eff,opt} = \frac{\pi}{2f_B}\left(1+\frac{0.62\,\mathrm{Re}_w}{1+0.62\,\mathrm{Re}_w}\right) \tag{4.41}$$

Equation 4.38, for single phase systems, and Equation 4.41 are plotted for some different values of I_X in Figures 4.8 and 4.9, respectively. It is seen that for HFW systems with a closed exterior boundary, optimum effective fracture conductivity is increased with the increase in fracture penetration ratio, and this increase becomes more significant when I_X approaches one, unlike what was seen from Figures 4.5 and 4.6 for SS systems. In fact, the top curves in Figures 4.5 and 4.6 are almost the same as the bottom curves in Figures 4.8 and 4.9, respectively. For PSS systems, the range of optimum fracture conductivity is much wider than the same parameter for SS systems. According to Figure 4.9, optimum effective fracture conductivity for PSS could be in the range of π/2 (for Darcy flow with small fracture penetration ratio), and 22.6 (for very high Reynolds number and I_X=0.95).

Substituting $C_{fD\text{-}opt}$ and Reynolds number in terms of $x_{f\text{-}opt}$ in Equation 4.38 results in the following equation, which is a useful tool for finding optimum fracture length in PSS systems:

$$a_{PSS}\times x_{f-opt}^3 + b_{PSS}\times x_{f-opt}^2 + c = 0 \tag{4.42}$$

Where:

$$a_{PSS} = \frac{0.62\pi C_2 q_w}{f_B \times MR_w} \tag{4.43}$$

$$b_{PSS} = \frac{\pi}{2\times f_B \times MR_w} \tag{4.44}$$

$$c = -C_1 = -\frac{k_f V_f}{2k} \tag{4.45}$$

Here again drawing $F_{PSS}(x_f)$, defined below, versus fracture penetration ratio provides optimum fracture penetration ratio for PSS systems.

$$F_{PSS}(x_f) = a_{PSS} \times x_f^3 + b_{PSS} \times x_f^2 + c \tag{4.46}$$

4. 4 Illustrations

In order to show the application of the newly developed method, introduced in this chapter, and to testify to its accuracy, the geometry of some different Hydraulic Fractures (HF) are optimized in this section, and the results will be compared with the results available in the literature or simulation results.

Illustration 1

Optimization of a small HF under Darcy flow regime (HFWS-O1)

The details of this HF are described in Table 4.1. Here the Propped number is 0.02 and well production rate is 10^{-6} m^3/s which does not result in the non-Darcy effect inside the Fracture. Figure 4.10 shows the result of optimization of this HF. In this figure, effective wellbore radii, Equation 4.7, and F (x_f), Equations 4.35 and 4.46, versus fracture penetration ratio have been drawn for both steady sate (SS) and pseudo-steady state (PSS) systems. Optimum fracture penetration ratio for both cases is 0.1128, and because of the small Propped number (N_p=0.02) the curves of both systems overlap. For both systems at optimum point, Reynolds Number is 0.0015, absolute fracture conductivity is 1.57, the same as the literature (Meyer et al. (2005)), and effective fracture conductivity, as expected, is almost the same (1.569), which is close to the corresponding value for absolute fracture conductivity, showing the negligible inertia effect.

Illustration 2

Optimization of a big HF under Darcy flow regime (HFWS-O2)

In this system, flow is the same as the last system so there is Darcy flow inside the fracture; however, the fracture volume and consequently the Propped number are increased 100 times: N_p=2.0. Figure 4.11 shows the optimization curves of this system. Obviously, where I_X is greater than 0.2, the performances of the HFW at SS and PSS are different. For SS, optimum fracture length is equal to the reservoir length, while for PSS, optimum fracture penetration ratio is 0.82.

The importance of using the correct formulation in optimization is clearly observed from Figure 4.11. For instance, if for a constant exterior pressure, PSS optimum point is selected incorrectly, the effective wellbore radius will be 17% less than the maximum possible value.

The optimum point calculated by the UFD method (Valko *et al.* (1998)) is also shown in Figure 4.11. According to this method for PSS, optimum I_X is 0.733. This is about 10.6% less than the optimum I_X predicted by the new method. However, as the variation of effective wellbore radius with I_X around the optimum point is not very considerable, there is no significant difference between the optimum PSS wellbore radii calculated by these two methods (AD%=4.6%).

Illustration 3

Optimization of a big HF under non-Darcy flow regime (HFWS-O3)

The characteristics of this system, as written in Table 4.1, are almost the same as the last system (HFWS-O2), but the flow rate is much greater (0.05 m^3/s) to see the effect of inertia on the optimization results. Figure 4.12 shows the optimization curves of this system. The absolute Propped number is 2, but inertia seriously decreases the effective Propped number. For PSS, optimum fracture penetration ratio, absolute fracture conductivity and effective fracture conductivity are 0.478, 8.8 and 2.9, respectively. Whilst for SS the corresponding values of these parameters are 0.504, 7.9 and 2.5, respectively.

A comparison of the results of illustrations 2 and 3 clearly shows how inertial effect decreases the optimum length of the fracture for a fixed fracture volume. In other words, in these examples the optimum fracture length in the presence of inertial effect is about 50% shorter than that if inertial effect were to be neglected.

Illustration 4

Optimization of a HF in Gas Condensate reservoir (the whole drainage area lays in two-phase region)

In order to verify the applicability of the new developed optimization method for gas condensate flow systems, the geometry of an HF was optimized for HFWS-O4 (see Table 4.2). In this system, the fluid is a mixture of C_1-C_{10} $\left(Z_{C_1} = 80\%\right)$. The fluid properties have been shown in Table 3.2b. The bottomhole pressure and exterior

pressure are 3486.5 psi and 3536.5 psi which are 55 and 5 psi below the dew point pressure respectively; thus there is two-phase gas condensate flow within the whole system. Figure 4.13 shows the results of the optimization of this HF by three approaches, which are i) drawing production rate, ii) effective wellbore radius and iii) $F_{SS}(x_f)$ versus fracture penetration ratio.

In this problem production rate is a dependent variable, depending on the drawdown and the fracture dimensions. Here, the curve of production rate versus I_X has been produced using the in-house simulator; i.e. the curve of production rate for a fixed fracture volume but different fracture penetration ratios have been calculated using the in-house 2D HFW simulator.

In Figure 4.13 (and also Figures 4.14 and 4.16 of the two next illustrations) the curves of $F_{SS}(x_f)$ and effective wellbore radius have been plotted using the production rate at optimum point (15.97 m^3/hr), estimated from the curve of production rate versus I_X. However, as will be discussed in Section 4.5 when the production rate is unknown its value is assumed and an iterative procedure should be followed to find the optimum fracture design.

A very good agreement is noticed amongst the results of the three approaches in Figure 4.13. In this illustration the predicted optimum parameters are:
Optimum fracture penetration ratio: 0.585
Optimum absolute fracture conductivity: 2.35
Optimum effective fracture conductivity: 1.98
Optimum Reynolds number: 0.78

Illustration 5

Optimization of a HF in Gas Condensate reservoir (The length of the two-phase region is almost the same as fracture length)

The independent parameters of this illustration, except the exterior pressure, are the same as the last illustration. Here the exterior pressure is 100 psi above the dew point pressure whilst the bottomhole pressure is still 55 psi below the dew point pressure. Thus there are both two-phase flow and single-phase flow regions within the system. Moreover as the drawdown is increased the optimum production rate should increase resulting in further inertial effect. Figures 4.14 and 4.15 show the optimization curves of

this system, and the GTR contour map around the wellbore of the optimum design, respectively. Here again a good agreement is seen between the results of different approaches for optimization, and all three curves show almost the same point as the optimum point. The characteristics of HFWS-O5 and some of the estimated parameters are shown in Table 4.2.

In this illustration optimum production rate is estimated as 80.9 m^3/hr, about 5 times more than that of the last illustration. Thus, as expected the increase in inertia has decreased the optimum fracture length from 146 m to 80 m.

The other optimum parameters are predicted to be:
Optimum fracture penetration ratio: 0.32
Optimum absolute fracture conductivity: 7.71
Optimum effective fracture conductivity: 2.46
Optimum Reynolds number: 2.17

It has to be emphasised that optimization of the fracture geometry based on the methodology developed for single phase Darcy flow systems could result in significant errors. For instance, for this case using the single phase Darcy flow concept will predict optimum fracture penetration ratio equal to 0.8. It results in the production rate of around 65 m^3/hr which is about 20% less than the production rate gained at the correct optimum I_X value of 0.32

Illustration 6

Optimization of a HF in Gas Condensate reservoir (The length of two-phase region is smaller than the fracture length)

In order to show the applicability of the developed method for the cases in which the two-phase flow region is smaller than the fractured zone, the exterior pressure is increased to 3741.5 psi, 200 psi above the dew point pressure, whilst the bottomhole pressure is still kept at 55 psi below the dew point pressure. Thus the drawdown is increased to 255 psi (100 psi more than that of the last illustration). The new system is called HFWS-O6, and its features and some of the results of optimization have been written in Table 4.2.

Figure 4.16 shows the optimization curves of this system. According to all three curves of this figure, the optimum fracture penetration ratio is 0.27; i.e. optimum fracture half-length is 67m which is 13m shorter than that of HFWS-O5 as a result of the increase in inertial effect.

The GTR contour map around the optimum design of this HF system is shown in Figure 4.17. Here the half length of the two-phase region is almost 36 metres, about half of the fracture half length.
The optimum parameters of this illustration are estimated as follows,
Optimum fracture penetration ratio: 0.27
Optimum absolute fracture conductivity: 11
Optimum effective fracture conductivity: 3
Optimum Reynolds number: 3

The illustrations of this part confirm the applicability of the semi-analytical developed method which can be simply applied for gas or gas condensate flow systems with square drainage areas where mechanical damage does not affect the optimum geometry.

For this case using the single phase Darcy flow optimization concept will predict optimum fracture penetration ratio equal to 0.8. It results in the production rate of around 100 m^3/hr which is about 30% less than the production rate gained at the correct optimum I_X value of 0.27.

4.5 Optimum Fracture Design Problems

The method introduced in the last section helps the production engineer to design the optimum fracture geometry for the desired operating conditions. In a fracture design problem, when the physical properties of the fracture and matrix (k, β, k_{rb}), the required correlations or EOS for fluid properties (μ, ρ, GTR,…) and average (or external) pressure of the drainage area are identified, there are five variables left: fracture length (x_f), fracture thickness (w_f), fracture volume (V_f), production rate ($\dot{m}$) and drawdown $\left(\Delta P = \overline{P} - P_w\right)$. There are also three equations available which combine these variables, the equations of optimum fracture design, production rate and fracture volume.

Therefore, among these five variables just two are independent variables. That is, two variables can be selected as the goals of the fracturing, and the other variables are calculated using the available equations. Owing to the dependency of the variables on each other, the procedure of solving the design problem is an iterative method and dependent on which variables are known. In the following sections, the solutions of three important possible types of the optimum fracture design problems are explained.

Type I- Production rate and drawdown are the known parameters and the minimum fracture volume and its optimised dimensions must be found.

For solving this kind of problems the following stepwise procedure can be followed.

1- Assume fracture volume.
2- Calculate optimum fracture length and thickness.
3- Calculate optimum effective wellbore radius.
4- Simulate the drainage area and calculate the production rate.
5- Check if the difference between the calculated production rate and the known value is less than the acceptable value.
   YES: Go to step 6.
   NO: Readjust the assumed value for fracture volume and go back to step 2.
6- Report the designed fracture geometry.

Type II- Production rate and fracture volume are the known parameters and the optimised fracture geometry giving the lowest drawdown must be found.

This type of problems can be solved by the following stepwise procedure:

1- Assume the bottomhole pressure (P_w).
2- Estimate fluid properties and then mobilities at P_w.
3- Calculate optimum fracture length and thickness.
4- Calculate optimum effective wellbore radius.
5- Simulate the drainage area and calculate the bottomhole pressure.
6- Check if the difference between the calculated bottomhole pressure and the assumed value is less than the acceptable value.
   YES: Go to step 7.

NO: Readjust the assumed value for P_w and go back to step 2.

7- Report the designed fracture geometry and bottomhole pressure.

Type III- Bottomhole pressure and fracture volume are the known parameters, and the optimised fracture geometry giving the highest production rate must be found.

Here the procedure is very similar to the last one, but the production rate must be assumed instead of bottomhole pressure.

1- Assume the production rate (q_w).
2- Calculate optimum fracture half-length and thickness.
3- Calculate optimum effective wellbore radius.
4- Simulate the drainage area and calculate the production rate.
5- Check if the difference between the calculated production rate and the assumed value is less than the acceptable value.
   YES: Go to step 6.
   NO: Readjust the assumed value for q and go back to step 2.
6- Report the designed fracture geometry and bottomhole pressure.

4.6 Summary and Conclusions

In HFWs with big propped number and penetration ratio greater than 0.2, the well performance and hence, optimum fracture geometry depend on the exterior boundary condition. This issue was discussed as the first topic of this chapter, and some graphs were developed to extend the applicability of UFD method, originally developed for Darcy flow regime and under PSS conditions, to both SS and PSS conditions.

The developed formulae for estimation of effective wellbore radius of a gas condensate HFW in the last chapter were used to develop the required formulae semi analytically for estimation of optimum values of absolute/effective fracture conductivity at SS and PSS.

The above equations were then rearranged into the shape of 3rd order polynomial equations which can be solved to estimate optimum fracture half-length.

Several illustrations confirmed the applicability of the new developed formulae for single phase and gas condensate systems.

Some of the important notifications can be summarized as follows:
Optimum effective fracture conductivity is independent of the mobility ratio but depends on the Reynolds number and fracture penetration ratio.

1. When optimum fracture penetration ratio is less than 0.2, the optimum fracture design is the same for both SS and PSS and optimum effective fracture conductivity, depending on the Reynolds Number, can be between $\pi/2$, for low velocity systems ($Re \approx 0$), and π for very high velocity systems ($Re >> 1$).

2. For HFW systems with constant exterior pressure, optimum absolute/effective fracture conductivities are decreased with increasing fracture penetration ratio.

3. For HFW systems with a closed exterior boundary, optimum absolute/effective fracture conductivity is increased with the increase in fracture penetration ratio.

References

Carvajal, G.: Numerical Simulation of Gas Condensate Flow in Induced Fractured Wells, MPhil Thesis, Heriot-Watt University, Submitted for examination, June 2006.

Economides, M., Oligney, R., and Valko, P.: Unified Fracture Design, Orsa Press, Alvin, Texas, USA, 2002.

Giddley J.L.: "A Method for Correcting Dimensionless Fracture Conductivity for Non-Darcy Flow Effects" SPE 20710, SPE Production Engineering Journal, pp.391-394, Nov-1991.

Indriati, Sh., Wang, X., Economides, M., J.: "Adjustment of Hydraulic Fracture Design in Gas Condensate Wells" SPE 73751, presented at International Symposium and Exhibition on Formation Damage Control, Louisania, USA, 2002.

Lopez-Hernandez, H., D., Valko, P. P., Pham, T., T.: "Optimum Fracture Design Minimizes the Impact of Non-Darcy Flow Effects" SPE 90195, presented at SPE Annual Technical Conference and Exhibition, Houston, USA, 2004.

Meyer B.R. and Jakot R.H.: "Pseudo-Steady State Analysis of Finite Conductivity Vertical Fractures", SPE 95941, presented at SPE Annual Technical Conference, Texas, USA, 2005.

Mohan J., Pope G.A. and Sharma M. M.: "Effect of Non-Darcy Flow on Well Productivity of a Hydraulically Fractured Gas/Condensate Well" SPE 103025, presented at SPE Gas Technology Symposium, Texas, USA, 2006.

Prats M.: "Effect of Vertical Fractures on Reservoir Behaviour-Incompressible Fluid Case", SPE Journal, pp. 105-118, June 1961.

Valko Peter P. and Economides, Micheal J.: "Heavy Crude Production from Shallow Formations: Long Horizontal Wells Versus Horizontal Fractures" SPE 50421, Presented at SPE International conference on Horizontal Well Technology, Calgary, Canada, 1998.

Wang X., Indriati S., Valko P.P and Economides, M. J.: "Production Impairment and Purpose Built Design of Hydraulic Fracture in Gas Condensate Reservoirs," SPE 64749, Presented at SPE International Oil and Gas Conference and Exhibition, Beijing, China, 2000.

Zeng, F., Zhao, G.: "The Optimal Hydraulic Fracture Geometry Under Non-Darcy Flow Effect" SPE 114285, presented at CIPC/SPE Gas Technology Symposium 2008 Joint Conference, Calgary, Canada , 2008.

	HFWS-O1	HFWS-O2	HFWS-O3
Matrix core	Texas Cream k=9.1mD β=3.927E+9	Texas Cream k=9.1mD β=3.927E+9	Texas Cream k=9.1mD β=3.927E+9
Fluid Kinematic Viscosity	$\frac{\mu}{\rho}=1E-7\ \ m^2/s$	$\frac{\mu}{\rho}=1E-7\ \ m^2/s$	$\frac{\mu}{\rho}=1E-7\ \ m^2/s$
k_f/D	146	146	146
β_f/m^{-1}	3.511E+5	3.511E+5	3.511E+5
Reservoir Half length	500	500	500
Formation Thickness/m	30	30	30
Propped Volume (m^3/m)	0.625	62.5	62.5
Absolute Propped number	0.02	2.00	2.00
Wellbore production rate (m^3/s):	1E-06	1E-06	0.05
PSS optimum I_x	0.1128	0.819	0.478
PSS optimum C_{fD}	1.57	2.99	8.8
PSS optimum $C_{fD\text{-}eff}$	1.57	2.99	2.9
SS Optimum I_X	0.1128	1.0	0.504
SS optimum C_{fD}	1.57	2.0	7.9
SS optimum $C_{fD\text{-}eff}$	1.57	2.0	2.5

Table 4.1: Parameters of HFWS (in single-phase flow systems), optimized in this chapter.

	HFWS-O4	HFWS-O5	HFWS-O6
Matrix core	Texas Cream k=9.1mD β=3.927E+9	Texas Cream k=9.1mD β=3.927E+9	Texas Cream k=9.1mD β=3.927E+9
Fluid	C_1-C_{10} (Z_{C1} =80%) T=500K, P_D=3541.5 psia	C_1-C_{10} (Z_{C1} =80%) T=500K, P_D=3541.5 psia	C_1-C_{10} (Z_{C1} =80%) T=500K, P_D=3541.5 psia
k_f/D	146	146	146
β_f/m^{-1}	3.511E+5	3.511E+5	3.511E+5
Reservoir Half length	250	250	250
Formation Thickness/m	30	30	30
Propped Volume (m^3/m)	6.25	6.25	6.25
Absolute Propped number	0.8	0.8	0.8
Optimum Production Rate (m^3/hr):	15.97	80.9	133.16
P_w/psi	3486.5	3486.5	3486.5
P_e/psi	3536.5	3641.5	3741.5
GTR_w	0.885	0.885	0.803
MR_w	1.25	0.75	0.803
SS Optimum I_X	0.585	0.32	0.27
SS Optimum C_{fD}	2.35	7.71	11
SS Optimum $C_{fD\text{-}eff}$	1.98	2.46	3
SS Optimum Reynolds Number	0.78	2.17	3

Table 4.2: Parameters HFWS (in gas condensate flow systems), optimized in this chapter. Base relative permeability and fluid properties are shown in Tables 3.2 and 3.3.)

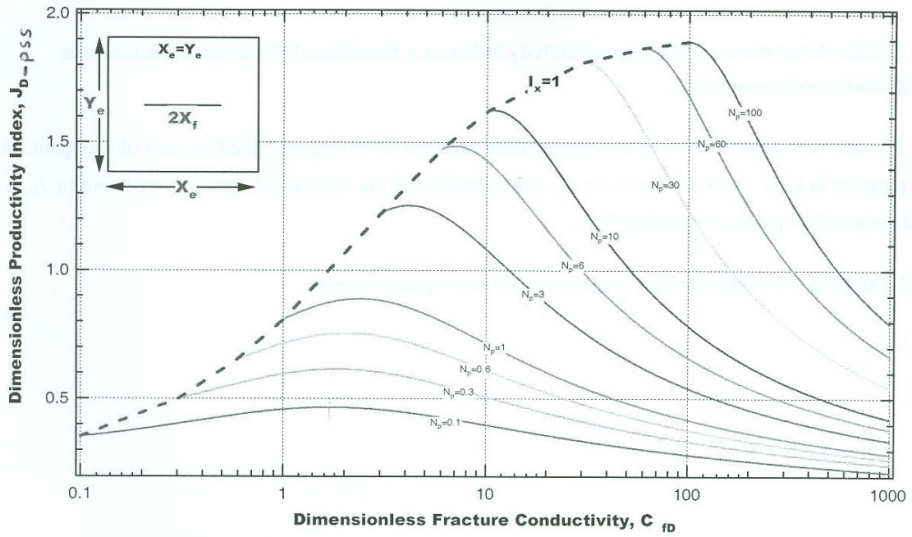

Figure 4.1: Pseudo-steady state productivity index of a square drainage area (shown in the inside box) as a function effective fracture conductivity and Propped numbers, developed by Valco *et al.* (1998).

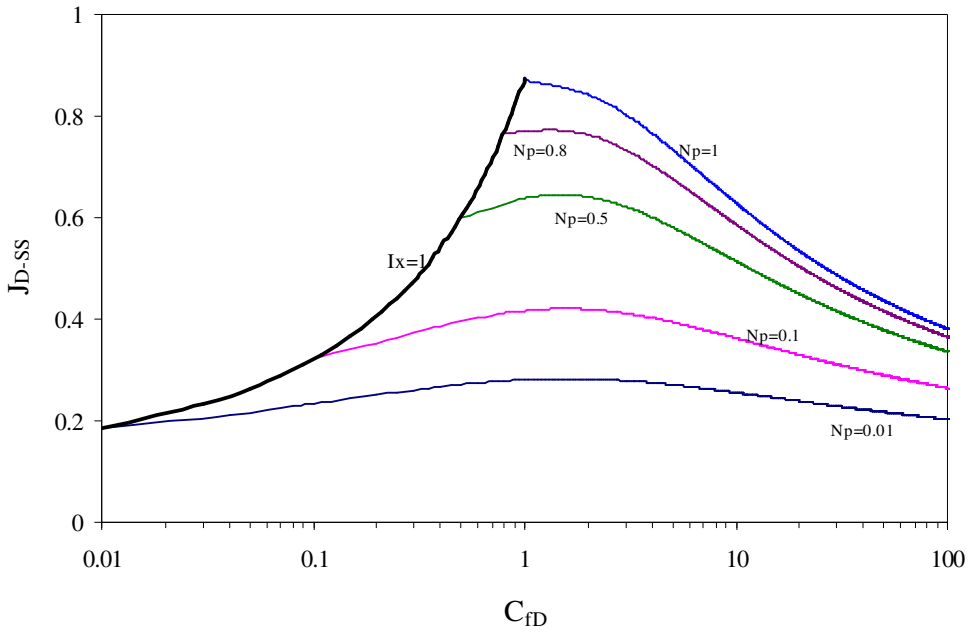

Figure 4.2: Steady state productivity index as a function of fracture conductivity and Propped number.

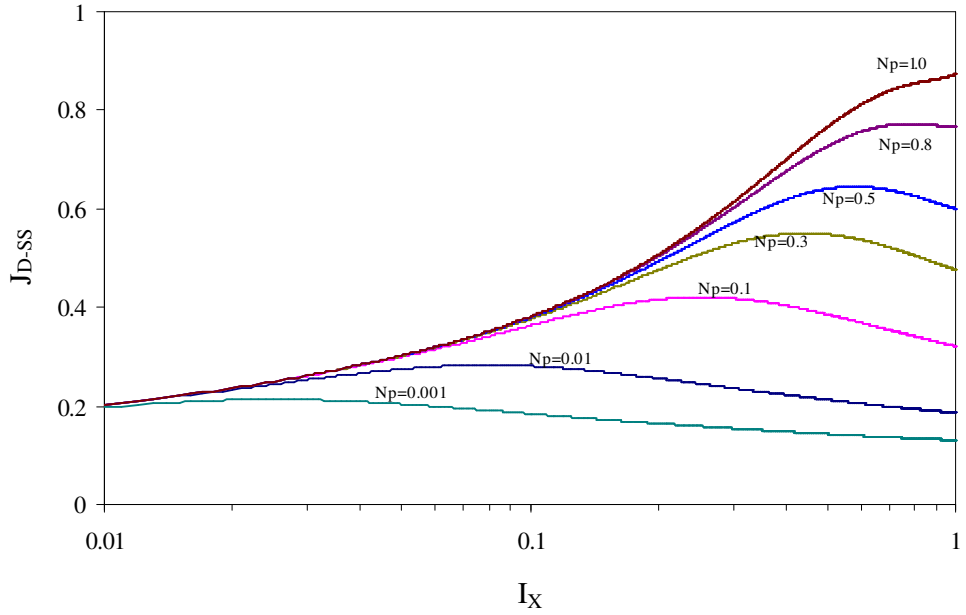

Figure 4.3: Steady state productivity index as a function of fracture penetration ratio and Propped number.

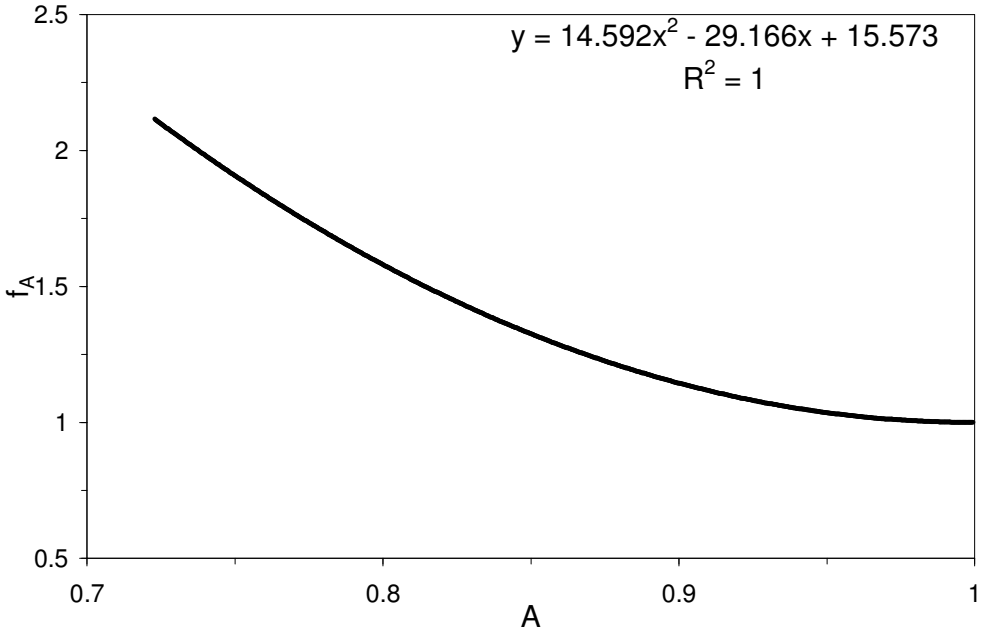

Figure 4.4: Variation of f_A versus A. $\left(f_A = A - I_X \frac{dA}{dI_X} \right)$

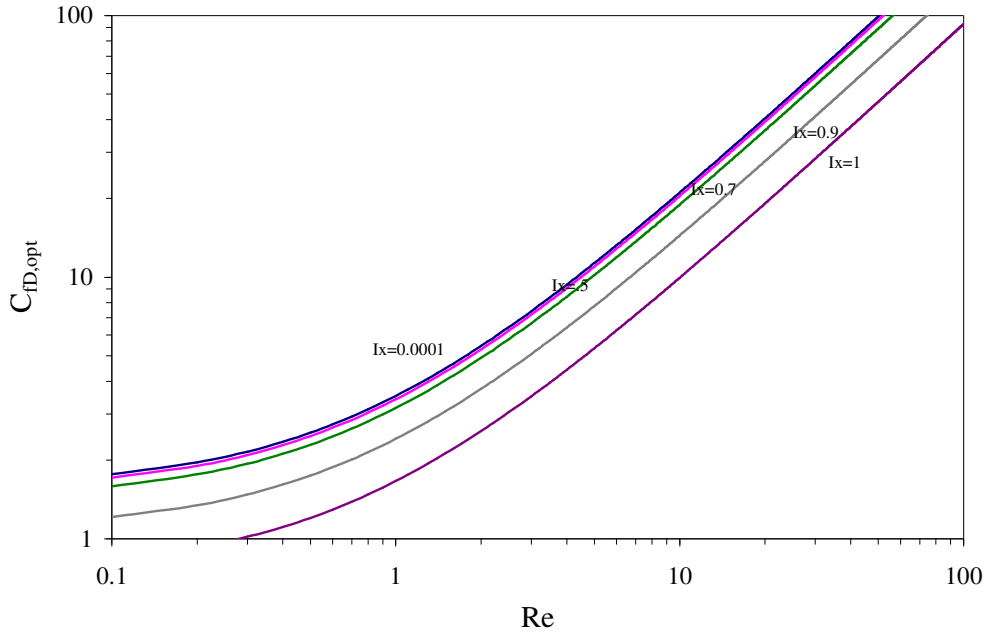

Figure 4.5: Optimum fracture conductivity, for single phase systems, as a function of Reynolds number and fracture penetration ratio for steady state conditions.

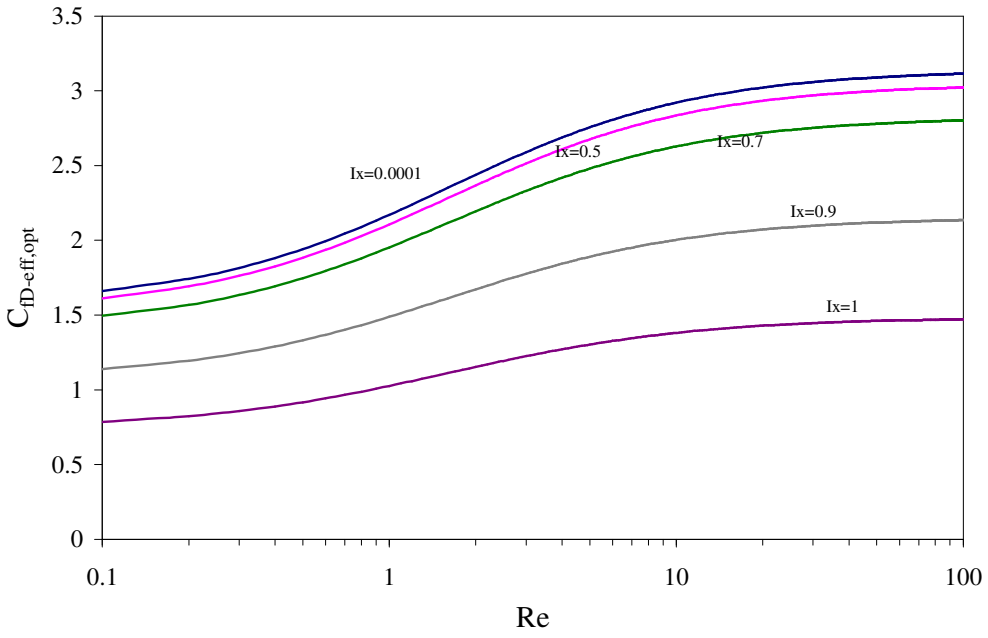

Figure 4.6: Optimum effective fracture conductivity as a function of Reynolds number and fracture penetration ratio for steady state conditions.

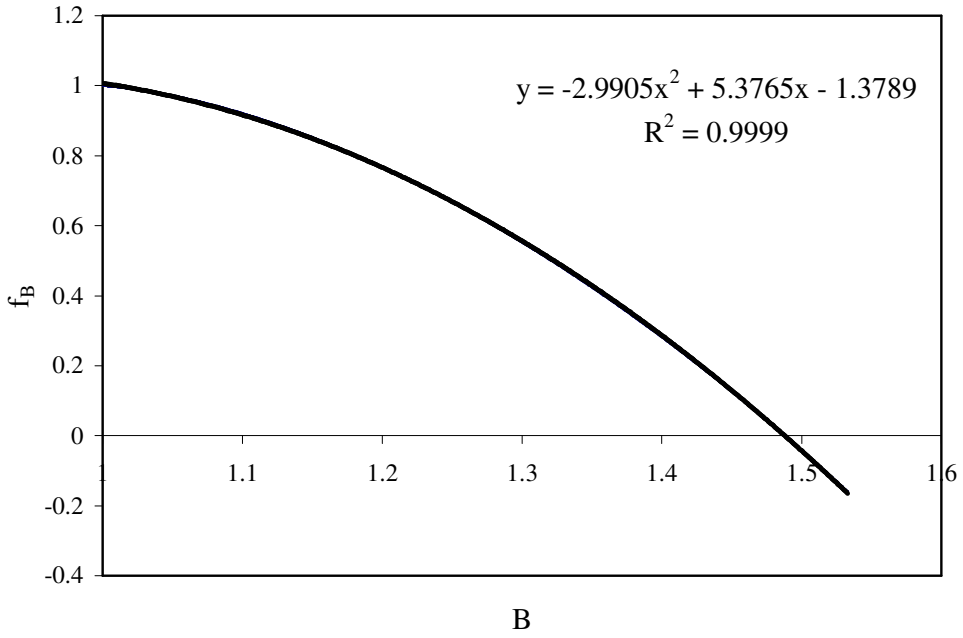

Figure 4.7: Variation of f_B versus B. $\left(f_B = B - I_X \frac{dB}{dI_X} \right)$

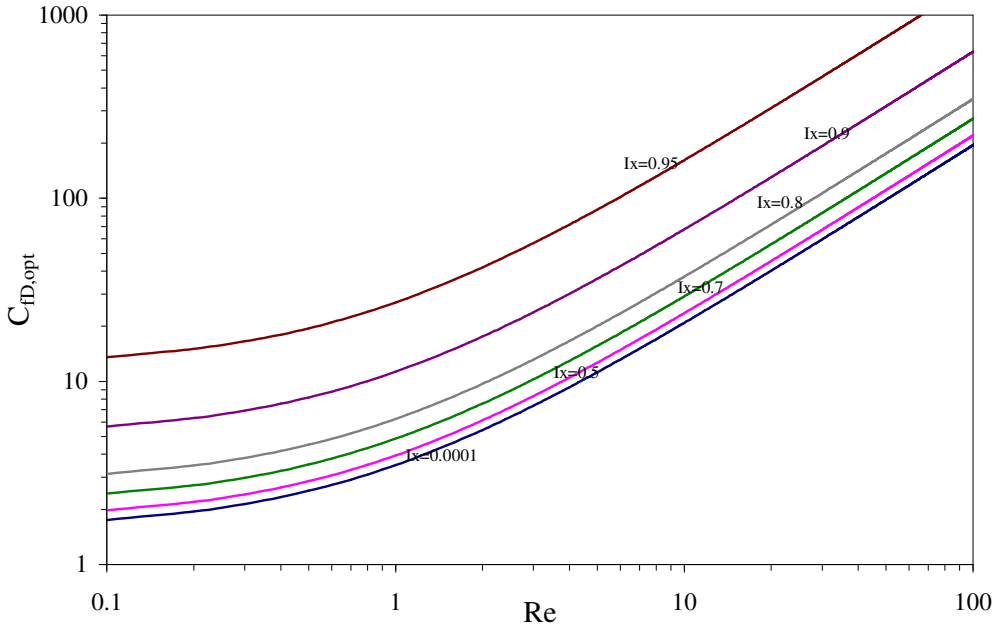

Figure 4.8: Optimum fracture conductivity, for single phase systems, as a function of Reynolds number and fracture penetration ratio for pseudo-steady state conditions.

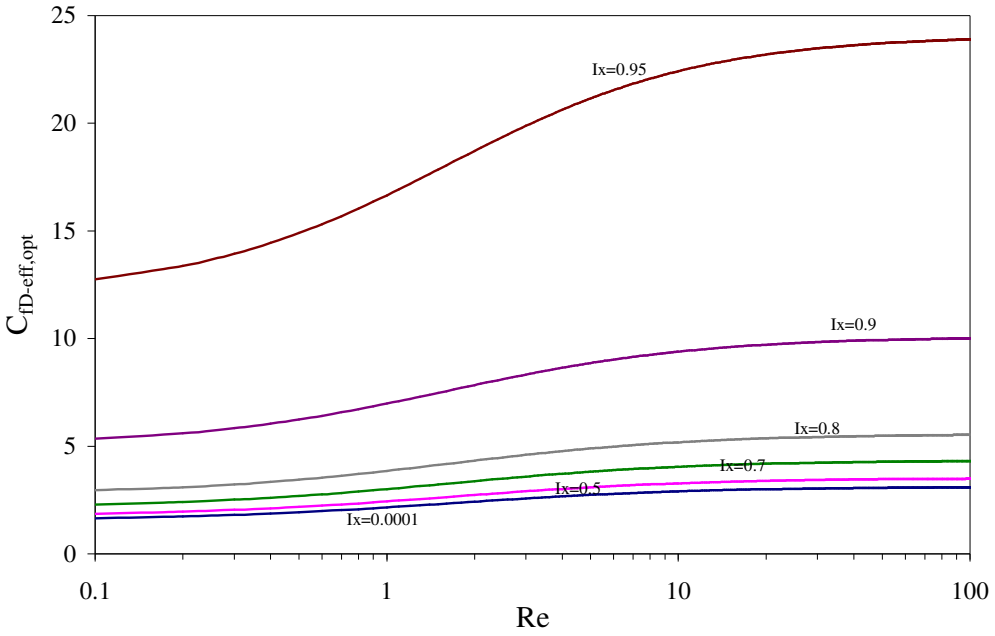

Figure 4.9: Optimum effective fracture conductivity as a function of Reynolds number and fracture penetration ratio for pseudo-steady state conditions.

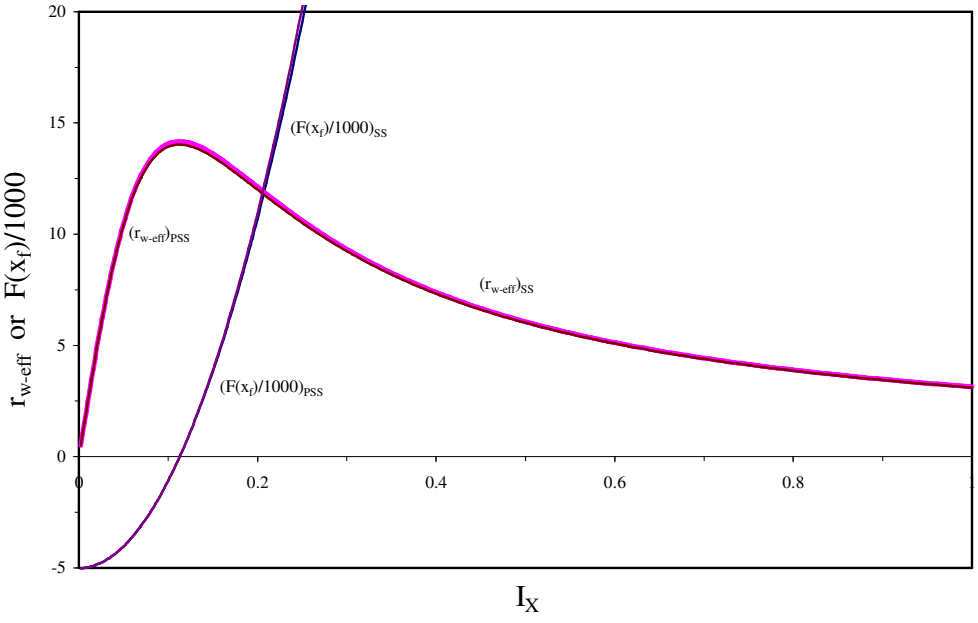

Figure 4.10: Variation of $F(x_f)$ and effective wellbore radius with I_X for HFWS-O1 defined in Table 4.1. Optimum fracture penetration ratio is 0.1128 where $F(x_f)$ becomes zero and effective wellbore radius has its maximum value.

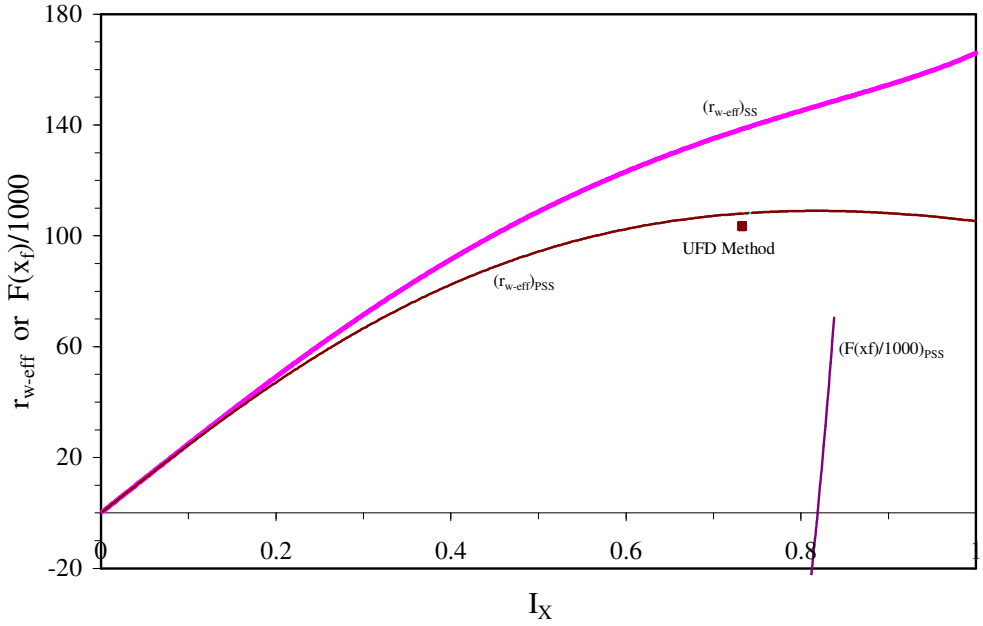

Figure 4.11: Variation of $F(x_f)$ and effective wellbore radius with I_X for HFWS-O2 defined in Table 4.1. For PSS optimum fracture penetration ratio is 0.8189, where $F_{PSS}(x_f)$ becomes zero, but for SS system it is 1.0 and $F_{SS}(x_f)$ does not cut the x-axes.

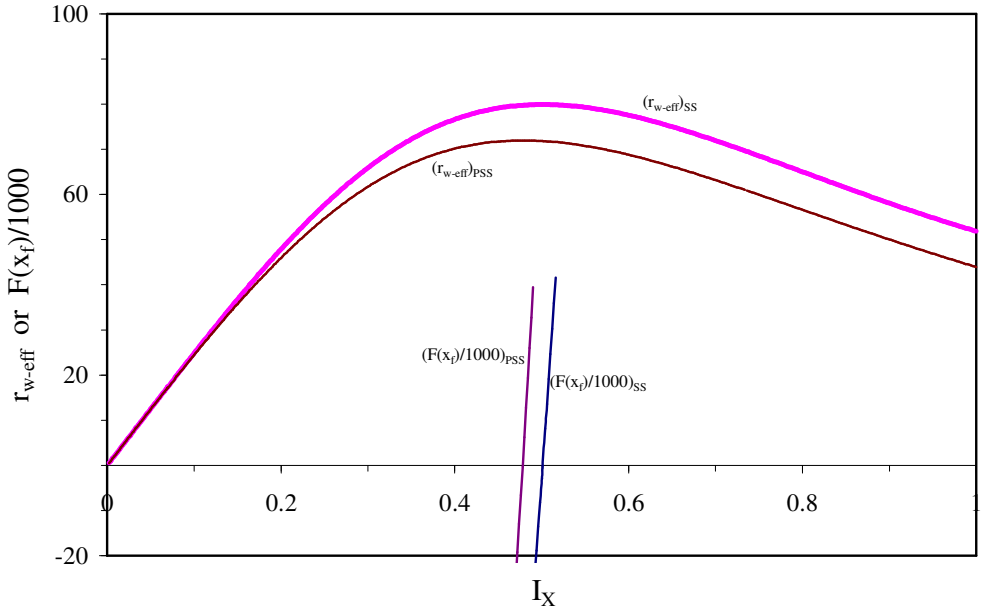

Figure 4.12: Variation of $F(x_f)$ and effective wellbore radius with I_X for HFWS-O3 defined in Table 4.1. Inertial effect has significantly decreased the effective propped number.

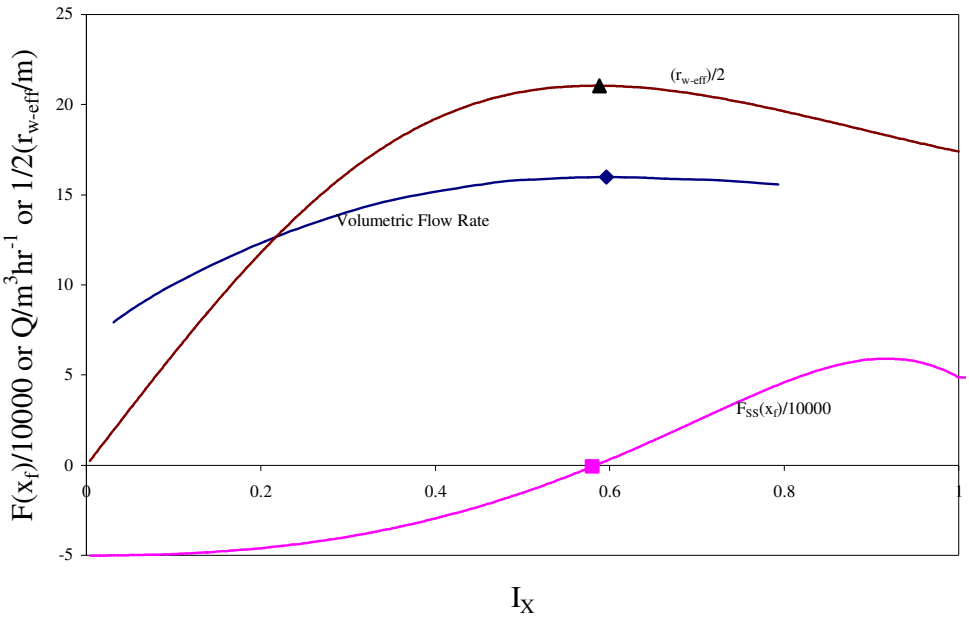

Figure 4.13: Optimization curves of a HF in gas condensate drainage area, HFWS-O4 defined in Table 4.2. There is two-phase flow within the whole drainage area. Production rate, calculated by simulator, and effective wellbore radius become maximum where $F_{SS}(x_f)$ is zero.

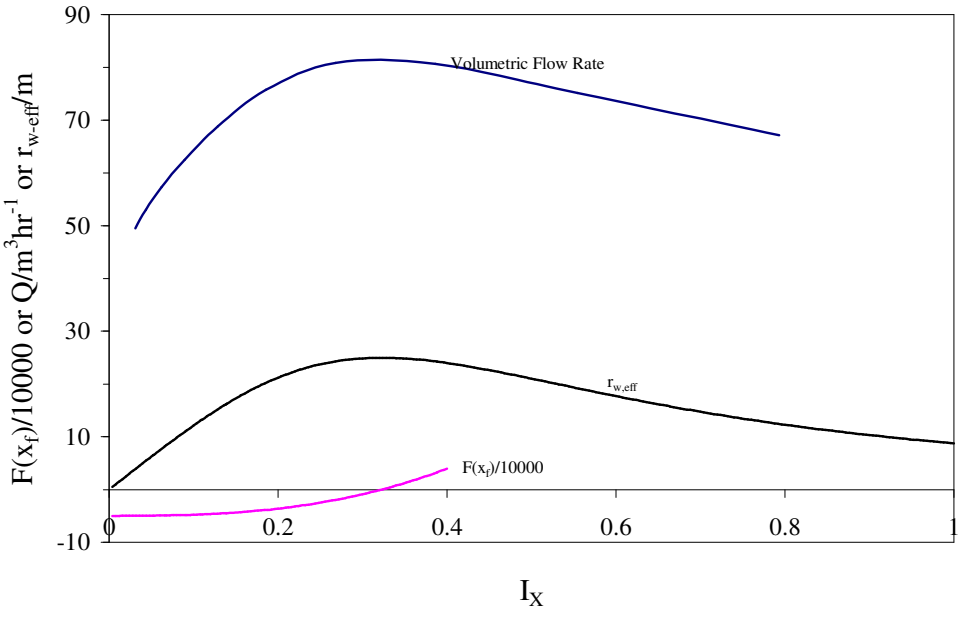

Figure 4.14: Optimization curves of a HF in gas condensate drainage area, HFWS-O5 defined in Table 4.2. The length of two-phase region is almost equal to the fracture length (See Figure 4.15). Production rate, calculated by simulator, and effective wellbore radius become maximum where $F_{SS}(x_f)$ is zero.

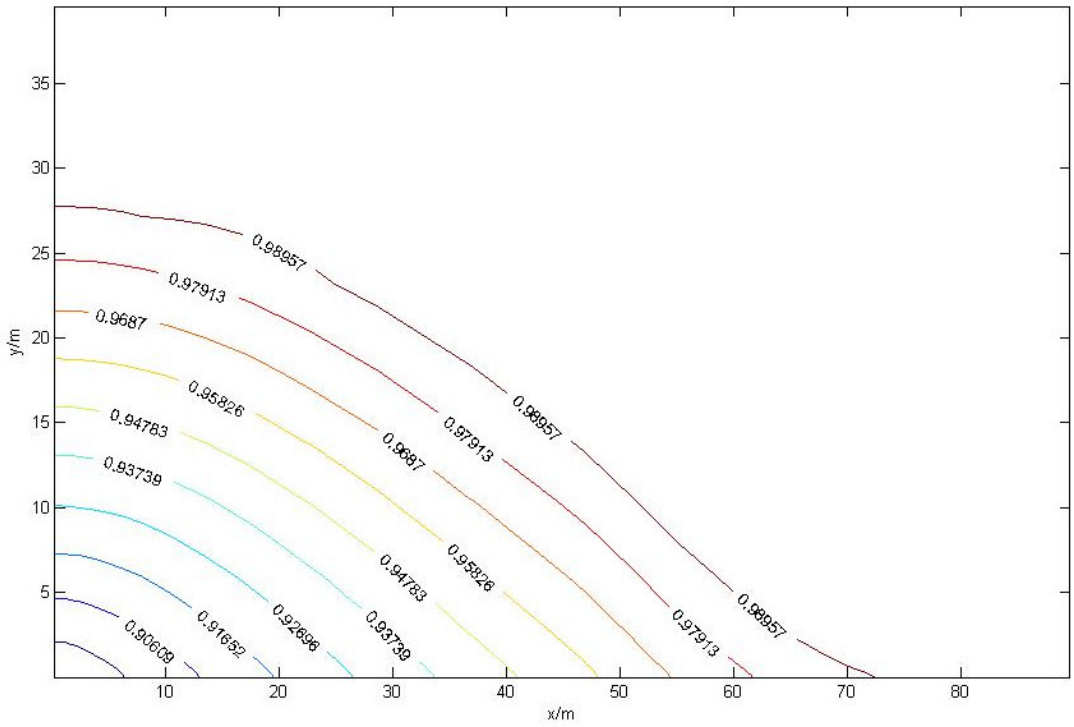

Figure 4.15: GTR contour map around the wellbore of the optimum design of HFWS-O5 defined in Table 4.2. Fracture Half length is about 80m.

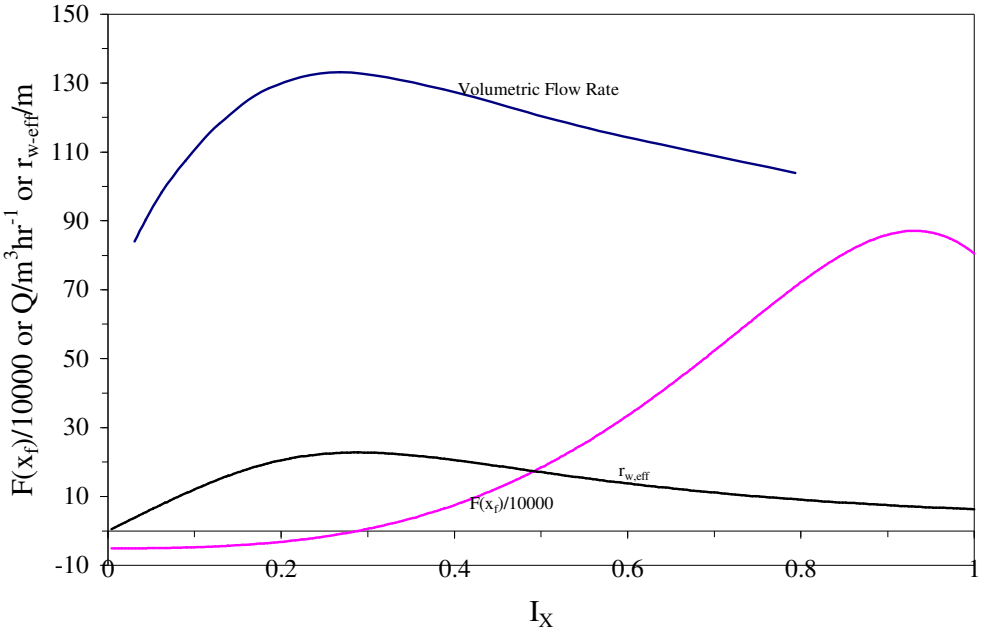

Figure 4.16: Optimization curves of a HF in gas condensate drainage area, HFWS-O6 defined in Table 4.2. The length of two-phase flow region is smaller than the fracture length (See Figure 4.17). Production rate, calculated by simulator, and effective wellbore radius become maximum where $F_{SS}(x_f)$ is zero.

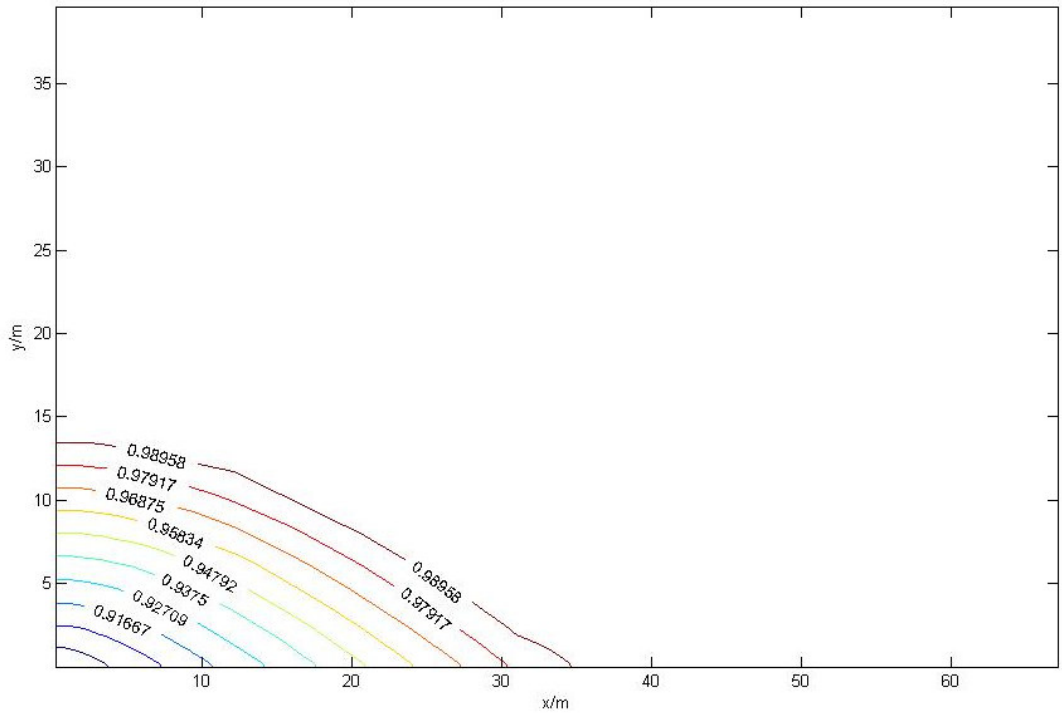

Figure 4.17: GTR contour map around the wellbore of the optimum design of HFWS-O6 defined in Table 4.2. Fracture Half length is about 67m.

Chapter 5 Gas Condensate Flow around Perforated Wells

5.1 Introduction

The wide application of perforation completions and the importance of the accurate estimation of well productivity have made *'flow around perforated wells'* one of the most important subjects in reservoir and production engineering.

In modeling a perforated well, owing to the very small perforation dimensions compared with the reservoir dimensions, the approach of the use of fine grid blocks around the wellbore is almost impractical. Therefore the most convenient way for defining a perforated well in a field model is to define an Equivalent Open-Hole (EOH) system with a skin factor or an effective wellbore radius.

The skin factor shows how the performance of the real well is different from that of the open-hole well. This difference could be because of the presence of mechanical differences and/or flow behaviour differences between two systems. Mechanical differences refer to geometrical or average permeability differences (e.g. because of damage or anisotropic effect), whilst the flow differences come from the differences between flow regimes in two systems. Thus total skin is a combination of mechanical skin, representing the mechanical differences, and flow skin, representing the flow differences.

Many investigators have studied the well productivity of perforated wells and considered the influences of perforated well parameters on productivity however the majority of the studies have focused on single phase systems. Basically, three types of models - electrolyte, numerical and semi/analytical - have been used as the main tools for doing those studies.

The **Electrolytic model** was first used by Mcdowel and Muskat (1950) to measure the effect of perforation length, radius and phasing angle on well productivity. They concluded that, if the perforations are long enough, the productivity of a perforated well might be even higher than that of an open-hole. Howard and Watson (1950) conducted similar experiments and reported similar results. Pan and Tang (1989) conducted a comprehensive set of experiments on a scaled electrolytic apparatus, and developed empirical equations for perforation flow efficiency.

Numerical Models based on finite difference or finite element methods have been proposed in many studies. Harris (1966) investigated the productivity of perforated completions considering a wedge-shaped perforation by a finite difference model. He presented the computed results as an apparent skin effect on a series of dimensionless working curves. Hong (1975) worked with a similar model, and reported the impact of the formation damage and perforation pattern on well productivity.

However, owing to the geometrical irregularities involved in perforation completions, finite difference models were not appropriate to simulate flow into practical-shaped perforations; therefore, with improved computer technology, investigators started using Finite Element Methods (FEM) to simulate flow around perforated wells.

Koltz *et al.* (1974) used a 2D finite element model to investigate the impact of a crushed zone and formation damage around the perforation on the well productivity. Locke (1981) was first to use a 3D finite element model to produce more realistic perforation geometries, and to account for spiral perforation distribution. The limiting dimension of his model was set at 30 times the radius of the bore-hole. Locke presented a monograph to predict perforation skin in isotropic formations.

Tariq (1987), using a general-purpose finite element code, ANSYS, investigated the influence of non-Darcy flow on the flow efficiency of perforated completions. He remarked that Locke's numerical method, and thus his monograph, overestimated the perforated well productivity as a result of insufficient element numbers. Tariq selected the exterior radius of the model as 30-60 times that of the wellbore radius. Tariq (1989) also investigated flow into perforations under the influence of formation anisotropy, shale laminations and natural fractures.

Behi and Settari (1993) and Dogula (1998) proposed the use of hybrid grids and local grid refinement to overcome the shortcomings of finite difference models. Both studies reported that the results from their model do not agree with those from Tariq's work when non-Darcy flow regime is considered.

Ansah *et al.* (2002) chose ANSYS 5.7 as the finite element solver and modelled flow around perforated wells. Their model incorporated the cone-shaped perforation geometry with a tapered tip. They used a full three-dimensional finite element model with over 30,000 elements in each perforation layer. Ansah *et al.* showed the effect of the exterior radius on the perforation skin for isotropic formations, and selected the model size at 100 times the wellbore radius. The productivity ratio predicted by their model for isotropic formation is very close to that of Taiq, whilst for anisotropic formations, their model predicts productivity ratio significantly greater than Tariq's simulator.

Jamiolahmady *et al.* (2005), using COMSOL as a finite element solver, improved the mesh quality around the perforations and increased the number of elements. This simulator has been used as the main tool for investigating different geometrical parameters as well as different gas condensate flow parameters in several studies. In the paper of Jamiolahmady *et al.* (2006), gas condensate flow around a perforation tunnel was studied by performing steady-state core experiments and numerical simulations. The results indicated that different sets of thickness-permeability (h-k) values obtained from matching single phase flow performance could be assigned to the damaged zone around perforation to represent the results of gas condensate flow in their core experiments.

Semi-Analytical models, proposed by some investigators such as Karakas and Tariq (1991) and Brooks (1997), are commonly used because of the simplicity of their proposed methods.

Karakas and Tariq (1991), by integrating the results of Tariq's Finite Element simulator with the analytical results of hydraulically fractured and horizontal wells, constructed a semi-analytical model and presented empirical equations to compute perforation skin. In this model, the perforation skin is assumed to be the linear summation of wellbore skin, horizontal skin and vertical skin. The formulations of these three skins for each phasing

angle contain 7 constants which have been evaluated by matching the results of the finite element simulator with the results of the proposed formula. According to the wide application of this method, its equations are summarized in appendix A.

Brooks (1997) stated that the maximum productivity for a perforated region is achieved when an infinite number of perforations with small phasing angle replace a formation porous medium extending from the wellbore to the perforations tip. Then he defined productivity efficiency as the ratio of productivity of a perforation arrangement to maximum productivity. He also presented some charts correlating the productivity efficiency to a series of dimensionless numbers, which included important perforation parameters, excluding phasing angles. For developing this correlation, Brooks used SPAN software to predict productivity for many different perforation designs, but just for one phasing angle. SPAN uses the Karakas-Tariq method for the computation of perforation skin.

Saleh and Stewart (1996) developed a semi analytical method based on radial flow up to the perforation tip, followed by local spherical flow into individual perforations. The difference between real flow to each perforation and the simplified spherical flow is taken into account using a flow shape factor. This shape factor can be estimated by matching the results of the formula with a Finite Element simulator. Saleh and Stewart did not introduce the required correlations for calculation of spherical shape factors, but concluded that for Darcy flow systems it is approximately around 1.0.

Hagoort (2007) recently presented an **Analytical Model** for the prediction of the productivity of perforated wells in Darcy flow systems. The basic building block of the model is an analytical solution for single-phase Darcy flow to a single perforation in a semi-infinite porous medium. Then he expanded the solution to a well with regularly spaced arrays of equidistant perforations along the wellbore wall. In this method, Anisotropy is taken into account by increasing the distance between two successive perforations, reducing the effective permeability and changing the perforation radius. By comparing the results of this model with those of the KT model, Hagoort concluded that the latter method underestimates the anisotropy effect.

To the best of the author knowledge, all the practical methods for the estimation of perforation skin or well productivity, available in the literature, have been developed for

single-phase Darcy flow systems. For instance among the above semi/ analytical methods only Saleh and Stewart (1996) tried to develop perforation skin for non Darcy flow and gas condensate flow systems however their final formulae were dependent on flow shape factor which had not been formulated. Furthermore, the coupling effect has not been considered in their analysis.

For non-Darcy flow systems, where due to high velocity near the wellbore inertia can control productivity; flow geometry could have a significant effect on the well-performance. This is especially true for perforated well systems where there is a 3 dimensional complex flow geometry flow around the wellbore.

In gas condensate systems, at relatively low interfacial tension (IFT) values, the composite velocity dependency of relative permeability adds even further complexity.

In order to provide a useful tool for a reservoir/production engineer for estimation of the productivity of a perforated well in gas condensate reservoirs a long study started in the Gas Condensate Recovery research group at HW University in 2001. Some of the important results have been published by Jamiolahamdy and his co-authors (2005, 2006 and 2007).

Ataei (2004) in his PhD program simulated some perforated wells with ECLIPSE commercial simulator and compared his results with the HW in-house simulator and noticed a high level of conformity between the results of two simulators.

This chapter of the study is aimed at the development of a practical and convenient method for defining the EOH system of a perforated well in gas condensate flow systems. The new method developed in this chapter is very easy to use and applicable for both single-phase and two-phase gas condensate flow systems.

The HW in-house 3D perforated well simulators have been used to simulate and study single phase and gas condensate flow around perforated wells. A brief introduction about these simulators will come in Section 5.2. The 1D open-hole simulator used in this chapter is the same as the 1D open-hole simulator described in Chapter 3.

Darcy flow around perforated wells is the subject of Section 5.3. In this section, pseudo perforation skin, based on an open-hole at the tip of perforations which can represent flow resistance in the perforated zone, will be defined. As this parameter presents a physically meaningful parameter, i.e. flow resistance, correlating that to the other pertinent parameters is a more straightforward task as described in this section.

Single phase non-Darcy flow around perforated wells will be discussed in Section 5.4. The effects of production rate and geometrical parameters on the well performance are investigated in this section. A similar investigation for gas condensate systems has been done by Jamiolahmady and his co-authors (2006 and 2007). The important conclusions of these papers will come in Section 5.5.

In Section 5.6 a new and simple method will be developed for defining an EOH system in which flow behaviour is very close to that in the real system. The main advantage of this method is that flow skin is negligible and there is no need for its calculation.

One of the main approaches for taking the inertial effect into account is the use of the D-factor. Originally this method could be used only for open-hole completions. However, in practice, it is mistakenly used for perforated wells, which can cause major errors in the estimation of well productivity. In Section 5.7, it will be shown how the D-factor of perforated wells in single-phase flow systems should be calculated so that the non-Darcy effect and consequently well-productivity can be calculated correctly using this approach.

5.2 The in-House 3D Perforated Well Simulator

Figure 5.1 shows schematically a perforated system, the 3D model considered in this study.

The main geometrical parameters in a non-damaged perforated system are:

Phasing angle (θ): the angle between two successive perforations.

Perforation density (N): the number of perforations per unit height of the well. This parameter is the inverse of the vertical distance between the centres of two successive perforations (h_p).

Perforation radius (r_p): the average radius of the perforations.

Wellbore radius (r_w): the outer radius of the cement layer around the liner.

Perforation length (L_p): the main length between r_w and the tip of the perforations.

The 3D perforated well simulators were developed by Jamiolahmady *et al*. (2005 and 2007). The single phase simulator simulates steady-state single phase flow including inertial effect whilst the two phase simulator simulates two-phase flow of gas and condensate accounting for phase change, coupling and inertial effects using the generalized HW relative permeability correlation.

The governing equations of these simulators are the three dimensional forms of the governing equations described earlier in Chapter 3.

In these highly non-linear partial differential equations (PDE), the main dependent variable is the pressure P. The boundary conditions are:

- Pressure at the outer boundary (external pressure) is constant (known).
- There is no inflow or outflow at the wellbore except through perforations.
- Due to high conductivity of perforations compared to that of the porous medium, the pressure inside perforations is constant and equal to the known wellbore pressure. The validity of this assumption has been investigated by Jamiolahmady et al. (2005).

Comsol Multiphysics mathematical software (version 3.2, 2006), which solves PDE systems using finite-elements, was employed to solve the resultant governing equations and the confining boundary conditions.

More details about the 3D Perforated Well Simulators and their verifications can be found in the final report of Gas Condensate Recovery group (2005-2008) and also the papers published by Jamiolahmady and his co-authors (2005 and 2007).

5.3 Single Phase Darcy Flow around Perforated Wells

As mentioned earlier, many investigators have already studied single phase Darcy flow around perforated wells. The main practical outcome of this kind of studies has been the formula for mechanical and perforation skins. Karakas and Tariq (1991) introduced a

semi analytical method (KT method), which is widely used by production engineers for estimation of perforation skin. In the following sections, it will be discussed that the KT method overestimates perforation skin for high anisotropic formations. Thus, in the first step of this chapter of study, attempts were made to formulate perforation skin with better accuracy.

Here, the author of this study introduces and applies a new definition called pseudo perforation skin, which is based on flow resistance. Pseudo perforation skin has a very simple relation with perforation skin, i.e. their formulae are related, but has a more sound physical meaning compared to conventional perforation skin definition.

5.3.1 Pseudo Skin Factor in Perforated Wells

For a single-phase Darcy flow system, the skin factor is defined by the following equation.

$$q = \frac{2\pi kh\ (P_e - P_w)}{\mu\left[\ln(\frac{r_e}{r_w}) + S_t\right]} \tag{5.1}$$

Rearranging Equation 5.1 in the following form gives:

$$q = \frac{2\pi kh(P_e - P_w)}{\mu\left[\ln(\frac{r_e}{r_w}) + S_t\right]} = \frac{P_e - P_w}{\frac{\mu}{2\pi kh}\ln(\frac{r_e}{r_w}) + \frac{\mu S_t}{2\pi kh}}$$
$$\Rightarrow q = \frac{\Delta P}{R_{OH} + \frac{\mu S_t}{2\pi kh}} \tag{5.2}$$

In this equation, q is the flow rate and ΔP is the driving force so the denominator is the total Darcy flow resistance. Here R_{OH} is the radial flow resistance from the outer boundary (r_e) to the wellbore (r_w). Therefore, the second term in the denominator, $\mu S_t/2\pi kh$, is a term for correcting flow resistance in the open-hole system to replicate that in the cased perforated system. In other words, although the skin factor explains how a perforated system performs compared with the open-hole system, it cannot represent a sound physical flow parameter.

As shown in Figure 5.2, a perforated system can be divided into two zones, namely perforated zone and unperforated zone. The perforated zone is the cylindrical medium, containing both perforations and matrix, with the inner radius of r_w and the outer radius of r_w+L_P. The unperforated zone is the cylindrical medium, containing just matrix, behind the perforated zone. The boundary between these two zones, a cylindrical surface at the tip of the perforations with the radius of r_w+L_P, is called the tip cylinder in this chapter.

The pseudo skin factor, S'_t, defined by Equation 5.3, can represent flow resistance in the perforated zone.

$$q = \frac{2\pi kh(P_e - P_w)}{\mu\left[\ln(\frac{r_e}{r_w + L_P}) + S'_t\right]} = \frac{P_e - P_w}{\frac{\mu}{2\pi kh}\ln(\frac{r_e}{r_w + L_P}) + \frac{\mu S'_t}{2\pi kh}}$$

$$\Rightarrow q = \frac{\Delta P}{R_{mz} + \frac{\mu S'_t}{2\pi kh}} \qquad (5.3)$$

Here again the denominator must be total Darcy flow resistance from the exterior boundary to the perforation surface. R_{mz} is the flow resistance in the unperforated zone, assuming radial flow in that zone. Thus the second term in the denominator, $\mu S'_t/2\pi kh$, is the flow resistance in the perforated zone when flow in the unperforated zone is radial.

The main advantage of the pseudo skin factor is that it represents a physically more meaningful parameter, i.e. the flow resistance in the perforated zone. Moreover, the pseudo skin factor is always positive, and a zero value would correspond to the maximum productivity of the perforated system, with a well of radius extending to the perforation tip. These advantages will prove to be important in finding an efficient correlation expressing the impact of pertinent parameters on the perforation skin.

For single-phase systems with negligible non-Darcy effect, there is a simple relation between skin factor and pseudo skin factor. A comparison of Equation 5.3 with Equation 5.1 provides this relation, as follows:

$$S_t = S_t^{'} - \ln\left(\frac{r_w + L_p}{r_w}\right) \tag{5.4}$$

5.3.2 Formulation

In single-phase Darcy flow system, the total skin factor is a function of perforation, damaged and crushed skin factors.

$$S_t = f\left(S_P,\ S_d,\ S_{cr}\right) \tag{5.5}$$

And similarly for the pseudo skin factor:

$$S_t^{'} = f\left(S_P^{'},\ S_d,\ S_{cr}\right) \tag{5.6}$$

Here, $S_P^{'}$ is the pseudo perforation skin, representing Darcy flow resistance in the perforated zone. S_d and S_{cr} are the damaged and crushed skin factors, representing the effect of the damaged region around the wellbore and crushed layer around perforations on flow resistance respectively.

Some authors, such as Yildiz (2006), have reported correlations for the estimation of total skin in the presence of such damage. The main difficulty in using these correlations is the estimation of the permeability and the geometry of the damaged and crushed layers. However a brief description of the required formulae for the estimation of mechanical skin in the presence of crushed and damage layers and how they can be used with the proposed formula here will be presented in appendix B. In other words, this study is concentrated mostly on the perforation skin term.

$S_p^{'}$ mainly represents the Darcy flow resistance of the unit height of the perforated zone, and for an isotropic formation is only a function of geometrical parameters. In anisotropic reservoirs, the anisotropy ratio, k_v/k_h, can also affect pseudo perforation skin. In the proposed method, the effects of geometrical parameters on the flow resistance in the perforated zone are expressed by a dimensionless number for a given phasing angle. The effect of anisotropy is expressed by another dimensionless number. Then these two dimensionless numbers are related to pseudo perforation skin, with the appropriate constants adjusted using the results of the in-house simulator.

Isotropic formations

For a specific phasing angle, the geometrical parameters controlling the flow resistance in the perforated zone are perforation density (N), perforation radius (r_p), wellbore radius (r_w) and perforation length (L_p).

For single phase Darcy flow with constant density and viscosity in isotropic formations, flow resistance in the perforated zone is a function of:

1- The effective area, A_{eff}, available for the flow in the perforated zone.
2- The average distance, λ_{av}, covered by the fluid in the perforated zone.
3- The no-flow wellbore radius.

In the perforated zone, fluid flows from the tip cylinder (Figure 5.2) to the perforations, so the effective area to flow per unit length of the well is a function of an average of the tip cylinder area, $2\pi(L_p+r_w)$, and the perforation area, $N2\pi r_p L_p$. However, wellbore radius (r_w), being much smaller than perforation length (L_p), can be neglected here, without significant effect on the results. Therefore, if it is assumed that the geometrical average (the square of the multiplication products of two areas) is applicable it can be stated that:

$$A_{eff} = f_1\left(Nr_p L_p^2\right) \tag{5.7}$$

The average distance covered by the fluid in the perforated zone, which is the main distance between the tip cylinder and perforations, is proportional to the tip cylinder radius (L_p+r_w) and the distance between two successive perforations, $h_p = 1/N$. Thus by neglecting r_w it may be stated that:

$$\lambda_{av} = f_2\left(\frac{L_p}{N}\right) \tag{5.8}$$

A wellbore provides an obstacle against flow in the perforated zone. For a specific phasing angle, the effect of this obstacle on the flow resistance in the perforated zone, E_{wb}, is proportional to the ratio of the wellbore radius to the perforation length. So:

$$E_{wb} = f_3\left(\frac{r_w}{L_p}\right) \tag{5.9}$$

Because of the complex nature of the flow in the perforated zone, the above qualitative analysis cannot provide the information required about the shape of the functions: $f_1,\ f_2\ and\ f_3$.

If it is assumed that power functions can express these dependencies, it can be written as follows:

$$\begin{aligned} S_p^{'} &= f_4\left\{\frac{(\lambda_{av})^a (E_{wb})^c}{(A_{eff})^b}\right\} \\ \Rightarrow S_p^{'} &= f_5\left\{\left(\frac{L_p}{N}\right)^a \left(\frac{r_w}{L_P}\right)^b \left(\frac{1}{N^2 L_p r_p}\right)^c\right\} \\ \Rightarrow S_p^{'} &= f_5(N_G) \end{aligned} \tag{5.10}$$

where,

$$N_G = \frac{r_w^{C_1}}{N^{(C_2+C_3-C_1)} r_p^{C_2} L_p^{C_3}}. \tag{5.11}$$

N_G is a geometrical dimensionless number, expressing the effects of geometrical parameters on the flow resistance per unit height of the perforated zone, for a specific phasing angle.

In Equation 5.11, exponents of L_p, r_p and r_w depend on the phasing angle. These exponents as well as the other constants which will be introduced in Equations 5.13 and 5.14 have been estimated using curve fitting approach, described in Appendix A. The exponent of perforation density, N, is calculated such that N_G is dimensionless. Thus in calculating N_G, the consistency of units is satisfied.

Figure 5.3 shows the variation of pseudo perforation skin in an isotropic formation for more than 80 different perforation designs with $\theta = 90^o$. Here the values of C_1, C_2 and C_3 are 0.067, 0.5 and 0.69, respectively. As will be described in the following sections

these exponents and other constants of the proposed formula have been determined from matching its results with the results of the in-house simulator.

Figure 5.3 confirms the validity of the assumption that unknown functions f_1, f_2 and f_3 can be expressed by power law functions. It also shows that pseudo perforation skin is a linear function of N_G; i.e. f_5 is a linear function. The intercept of this line is the minimum possible pseudo skin factor for this phasing angle, which is obtained at zero N_G as the result of infinite perforation density with finite perforation radius and length. This issue will be discussed further in the following sections.

For other phasing angles of this study, i.e. θ = 30, 60, 120, 180 and 0 (360) degrees, a similar trend was observed. However, the corresponding values of constants $C_{1\text{-}3}$ for different phasing angles are different, as presented in Table 5.1.

Anisotropic formations

An increase in anisotropy decreases the effective permeability in the perforated zone. Some investigators, e.g. Tariq (1989) and Hagoort (2007), have studied this effect and concluded that it is equivalent to increasing the distance between two successive perforations and consequently decreasing the shot density, N, by a factor of $\sqrt{k_h/k_v}$. However, it will be shown here that this analogy does not apply when k_v is very small, especially at large r_p and/or N values.

The perforated zone can be divided into two series of sub zones, Vertical Flow Sub-zones (VFSZs) and Horizontal Flow Sub-zone (HFSZs), shown in Figure 5.2. Each VFSZ represents a cylindrical region, with the height of $(h_p\text{-}2r_p)$ and the radius of (r_w+L_p), between two successive perforations where fluid must have a vertical flow component to get to the perforations. Each HFSZ, on the other hand, represents a cylinder with the height of perforation diameter and the radius of (r_w+L_p), where the fluid can get to the perforations even without vertical movement. That is, in HFSZ even for the extreme case of zero vertical permeability, i.e. with no vertical flow, fluid can still flow into the perforations horizontally.

The total height of HFSZ and VFSZ per unit height of the well can be calculated as follows:

$$h_{HFSZ} = 2Nr_p$$
$$h_{VFSZ} = 1 - h_{HFS} \tag{5.12}$$

For instance, for a perforated system with N = 12 SPF and r_p = 0.25" the height of both HFSZ and VFSZ is equal to 0.5 ft/ft. h_{HFSZ} reaches its maximum value, 1.0, when h_p, the vertical distance between the centers of two successive perforations, is equal to the perforation diameter.

Now in the extreme case of k_v = 0, the work of Tariq (1989) and Hagoort (2007) suggests that the effective distance between perforations is infinite and/or effective perforation density is zero; i.e. the skin factor is infinity resulting in absolutely no flow. However, as it was explained, there is still flow in the HFSZ and total flow is not zero.
In other words, anisotropy can significantly increase the flow resistance in VFSZ as perceived in the literature, but it cannot affect flow in HFSZ to the same extent. Therefore, the traditional method is not accurate for expressing the impact of anisotropy in perforated regions.

According to the flow resistance concept, the anisotropic effect can increase flow resistance by decreasing the effective permeability, which is equivalent to increasing the average distance. Increasing the distance in the VFSZ is what has been used in the literature, i.e. making the distance proportional to $\sqrt{k_h/k_v}$, but it should be different from that in the HFSZ. Therefore, the overall effect of anisotropy must be a function of k_v/k_h but not directly related to $\sqrt{k_h/k_v}$.

Figure 5.4 shows the variation of pseudo perforation skin with the inverse of anisotropy ratio (k_h/k_v) for two different perforated system designs. As this Figure shows, the pseudo perforation skin factor increases with decreasing anisotropy ratio; however, as explained earlier, it should approach a finite limiting value when k_v/k_h approaches zero. Based on the above discussion and observation made in Figure 5.4, the following dimensionless number could represent the anisotropy effect on the pseudo skin factor.

$$N_K = C_4 + \frac{k_v}{k_h} \tag{5.13}$$

From data analysis, it was found that C_4 is equal to 0.0018 for all phasing angles. The impact of N and r_p on HFSZ is accounted for in the geometrical dimensionless number (N_G). The value of N_K could be between C_4, for reservoirs with zero vertical permeability and C_4+1 for isotropic reservoirs. It is clear that the skin factor decreases with increasing N_K.

Minimum pseudo perforation skin

In a perforated system with an infinite number of perforations (i.e. N_G approaches zero) there is still flow resistance in the perforated zone. Therefore, even for these extreme cases, pseudo perforation skin is not zero but it is at its minimum possible value, which depends on the phasing angle. For instance, when the phasing angle is 180^o with an infinite number of perforations, the system converts to a hydraulically fractured well with infinite fracture conductivity in an infinite reservoir, and with pseudo skin of about 0.69, which can be estimated by the correlations available in the literature such as the one that was introduced in Chapter 3 for estimating the pseudo fracture skin factor.

In short, for each phasing angle there is a minimum value for the pseudo perforation skin, representing the minimum resistance of the perforated zone. This minimum resistance could be achieved theoretically in a perforation system with an infinite number of perforations, resulting in zero value for N_G. This minimum value is represented by a constant, C_5, in the main body of the correlation, and its value for different phasing angles has been calculated from the intercept of the linear correlation between S'_P and N_G. The values of C_5, shown in Table 5.1, demonstrate that C_5 decreases when phasing angle decreases, except for θ=0. The corresponding value of C_5 for $\theta = 180^o$ is 0.62, which is comparable with the fracture pseudo skin of a hydraulically fractured well with infinite fracture conductivity, 0.69.

Correlation

The trend in Figure 5.3 suggests that the pseudo perforation skin must be a linear function of N_G, and the curves in Figure 5.4 show that the pseudo skin is a power function of N_K. The results of many different data analyses confirmed these relationships, and it was concluded that, after calculation of N_G and N_K, the pseudo perforation skin can be estimated simply with the following correlation:

$$S'_P = C_5 + C_6 N_G N_K^{C_7} \tag{5.14}$$

As explained earlier, for a specific phasing angle, C_5 is the minimum possible value of the pseudo perforation skin. In other words, when N_G approaches zero, the pseudo perforation skin reaches its minimum possible value, C_5, and further improvement of the perforation design with increasing N, r_p or L_p will not decrease the pseudo skin factor.

Since S_P is an special case of the total Darcy skin factor, Equation 5.4 can be written for this parameter as follows.

$$S_P = S_P^{'} - \ln\left(\frac{r_w + L_p}{r_w}\right) \tag{5.15}$$

Therefore, Equation 5.16 can be used for calculation of the perforation skin factor.

$$S_P = C_5 + C_6 N_G N_K^{C_7} - \ln\left(\frac{r_w + L_p}{r_w}\right) \tag{5.16}$$

In this method, for each phasing angle, seven constants, $C_{1\text{-}7}$, are required for calculation of the perforation skin factor. The in-house simulator has been used to provide a large data bank comprising the results of simulating many different perforation designs and anisotropic ratios as follows:

Perforation density: 4, 8, 12 shots per foot (4/12, 8/12, 1 shots per inch).
Perforation length: 6, 9, 12, 15, 20, 30, 50 inch.
Perforation radius: 0.15, 0.2, 0.25, 0.5 inch.
Wellbore radius: 1.5, 3, 4.3, 6, 8 inch.
Anisotropy ratio, k_v/k_h: 0.001, 0.002,… 0.01, 0.02… 0.1, 0.2… 1.0

The above cases cover the vast majority of the practical perforation system designs.
The data banks produced have been used for adjusting the coefficients of this new method. Table 5.1 shows the adjusted values of required constants $C_{1\text{-}7}$ for different applicable phasing angles.

Verification

To show the accuracy of this method, its results have been compared with the results of the 3D perforation simulator. Figure 5.5 shows an example of this comparison for a 90^o phasing angle. As this Figure shows, there is a good agreement between the results of this new method and the results of the simulator. For a 90^o phasing angle, the standard error of estimation of S'_p is just 0.06 and AAD% is 3.7%. The accuracy of the method for other phasing angles is also in the same order of magnitude.

5.3.3 Comparison with Karakas-Tariq method

One of the most common methods for calculation of the perforation skin factor is the Karakas-Tariq method, used in some commercial software such as SPAN. In this method, it is assumed that the perforation skin factor is the summation of horizontal, vertical and wellbore skin factors. The corresponding equations for calculation of these skin factors are described in appendix B.

Figure 5.6 compares the results of this new method with those of the Karakas-Tariq method for an isotropic formation. As it can be seen from this figure for isotropic formations, in general, there is a good agreement between the results of the two methods.

However, for very high anisotropic formations, as Figure 5.7 shows, there is not such a good agreement between the results of the two methods. Figure 5.7 shows that for highly anisotropic reservoirs Karakas-Tariq method overestimates $S'_{p,}$ compared with the newly developed method.

In the Karakas-Tariq method, the total skin is a linear summation of vertical, horizontal and wellbore skin factors (Equation B.11), and only vertical skin is affected by anisotropic ratio. In their method, according to Equation (B.8), the dimensionless distance between two successive perforations is proportional to $\sqrt{k_h/k_v}$; therefore, when k_v approaches zero, vertical skin and hence perforation skin approaches infinity, regardless of the values of horizontal and wellbore skin factors. As discussed earlier, ignoring the presence of horizontal flow when k_v approaches 0 is the reason for this method overestimating perforation skin for very highly anisotropic formations.

The above results emphasize that Karakas-Tariq formula does not correctly account for the effect of anisotropy. In other words, instead of Equation B.11, there should be a different relation between these skin factors such that for extreme cases, when there is absolutely no vertical flow ($S_V = \infty$), S_p can still reflect the limiting value of horizontal skin, S_H.

5.3.4 Comparison with Hagoort method

Hagoort (2007) developed an analytical method for estimation of the skin factor of perforated systems, including the effects of anisotropy and damage. He compared some of his results with those of Karakas-Tariq, and stated that the latter underestimates anisotropy effect, contrary to what was stated in the above section.

Hagoort, in developing his analytical model, stated that the anisotropic effect reduces perforation radius, formation permeability, and also distance between two successive perforations to their equivalent values as follows:

$$r_{peq} = r_p \times \left(1 + \sqrt{k_v / k_h}\right) / 2 \tag{5.17}$$

$$k_{eq} = \sqrt{k_h k_v} \tag{5.18}$$

$$h_{peq} = h_p \sqrt{k_h / k_v} \tag{5.19}$$

Based on Equation 5.19 anisotropy increases the distance between two successive perforations, which is equivalent to the decrease of the number of perforations. One result of using this equation is the decrease of the number of HFSZs (Figure 5.2) which causes the underestimation of horizontal flow. Therefore, as stated earlier, using Equation 5.19 results in the overestimation of skin factor or underestimation of flow rate.

Table 5.2 compares the results of the simulator with those of the Hagoort and Karakas-Tariq methods and also the new method for isotropic and two anisotropic formations.

This table shows that for an isotropic formation, the Hagoort method has estimated perforation skin almost 35% higher than the value calculated by the new method, and 45% higher than that obtained by the Karakas-Tariq method.

However, for a moderately anisotropic formation, k_v/k_h = 0.2, the results of the simulator, the new method and Karakas-Tariq method are almost the same, but the Hagoort method estimates perforation skin to be more than three times higher than others.

For very highly anisotropic formation, k_v/k_h = 0.001, the perforation skin predicted by the KT method is about 53% higher than the values estimated by the simulator or the new method.

5.3.5 Impact of geometrical parameters

One of the applications of the developed skin correlation is the evaluation of the effects of different parameters on well productivity.

The dimensionless productivity index of an undamaged perforated system at steady state is defined as follows:

$$J_D = \frac{1}{\ln\left(\frac{r_e}{r_w + L_P}\right) + S'_p} \tag{5.20}$$

The dimensionless productivity index J_D is the inverse of dimensionless flow resistance, which is the summation of dimensionless flow resistance in the unperforated zone, $\ln(r_e/(r_w+L_p))$, and that in the perforated zone, S'_p. S'_p value is affected by all geometrical parameters, i.e. phasing angle, wellbore radius, perforation density, length and radius. However, among these parameters, only wellbore radius and perforation length can change flow resistance in the unperforated zone, $\ln(r_e/(r_w+L_p))$.

Phasing angle

Figure 5.8 demonstrates the variation of the pseudo skin factor with the phasing angle in an isotropic formation. This figure illustrates that when the phasing angle is in a practical range, $30 \le \theta \le 120$, its magnitude does not have a significant effect on the

perforation skin factor, which confirms the assumption of Brooks (1997), which is the effect of phasing angle on the well productivity is negligible. However, for phasing angles larger than 120 and also θ=0, which are not commonly used in practice, the effect of the phasing angle on the skin could be significant.

Wellbore radius

The wellbore radius has two separate effects on the productivity index, i.e. reduction of $\ln(r_e/(r_w+L_p))$ and increase of S'_p; however, the overall effect is usually insignificant (e.g. for L_p=20" there is a maximum increase of 3.6% in J_D for three-fold increase in r_w) (Figure 5.9).

For moderate or long perforations, a variation of r_w does not affect $\ln(r_e/(r_w+L_p))$ significantly; thus it can be concluded that the effect of wellbore radius on the unperforated zone flow resistance is negligible.

The effect of wellbore radius on S'_p is reflected by the exponent of r_w in Equation 5.11, i.e. C_1. The data in Table 5.1 show that, for practical phasing angles $30 \le \theta \le 120$, the value of C_1 is small and the impact of r_w is negligible. The effect of this parameter might be important only for perforated systems with θ=0 at which the wellbore barrier can have a significant effect on the well production.

Perforation radius, length and density

Among these three parameters, r_p is the least important parameter. It does not change flow resistance of un-perforated zone, R_{mz} in Equation 5.3, and in the formula for N_G its exponent is less than the exponents of L_p or N, i.e. its effect on S'_p is also not as significant as L_p or N.

Correlation of the pseudo perforation skin (Equation 5.14) and the geometrical dimensionless number (Equation 5.11) indicate that the effect of perforation density on the pseudo perforation skin is more important than that of perforation length. However, as explained before, increasing perforation length (L_p) can also decrease unperforated zone resistance, $\ln(r_e/(r_w+L_p))$.

Figure 5.10 shows how increasing r_p, N or L_p could increase the dimensionless productivity index in an ideal perforated system. It is noted that the effects of changing

perforation radius or density on the pseudo skin factor and productivity index becomes negligible for low values of N_G (the curves flatten). Here increasing N or r_p would just raise the cost of the perforating operation, without any benefit in well productivity.

However, the perforation length always has a positive effect on improving well productivity because of its beneficial effect on unperforated zone resistance.

In short, the effect of increasing perforation radius and perforation density on well productivity becomes negligible for high values of these parameters, i.e. when N_G approaches zero; however, perforation length is always important and has a significant effect on improving well productivity.

5.4 Single phase Non-Darcy Flow around Perforated Wells

The effect of inertia in the increase of pressure drop and consequently in the decrease of effective permeability were discussed in detail in Chapter 3 (Section 3.4) and it was shown that:

$$\vec{v} = -\frac{k \times F_{ND}}{\mu} \nabla P, \tag{5.21}$$

where F_{ND} is called a non-Darcy function and is related to the Reynolds number as follows:

$$F_{ND} = \frac{1}{1+\mathrm{Re}}; \quad \mathrm{Re} = \frac{\rho |v| k \beta}{\mu} \tag{5.22}$$

It was also noted that the effective permeability caused by the non-Darcy or inertial effect was $k \times F_{ND}$. Thus, F_{ND} is the relative permeability of a single phase as a result of the non-Darcy flow regime.

In low velocity regions, where Reynolds number is much smaller than 1.0, the non-Darcy function (F_{ND}) is around 1.0, and the inertial effect cannot decrease effective permeability; i.e. it is almost the same as absolute permeability.

However, around the wellbore, especially in gas reservoirs, following the decrease in available area for flow, Reynolds number increases and consequently there is a considerable decrease in F_{ND} and effective permeability.

In perforated systems there are different geometrical parameters which can change flow geometry and consequently the extent of inertial effect. In this section, the effects of geometrical parameters (perforation length, perforation radius, shot density, phasing angle, wellbore radius), velocity, fluid property and physical properties of the porous medium under study on the performance of a perforated well in the presence of non-Darcy effect will be investigated.

Figure 5.11 is a plot of productivity ratio (PR) versus velocities at three different perforation radii (r_p). In this chapter, productivity ratio is defined as the ratio of the total mass flow rate in the perforated completion to that of an open-hole well with the same inside diameter and at the same conditions. The former total flow rate is obtained from the 3D simulator, whilst the latter is estimated by the 1D simulator.

It should also be noted that the defined PR is also equal to the ratio of volumetric flow rate of the perforated case to that of the unperforated open-hole at the wellbore conditions. The velocity values on these plots have been calculated by dividing the flow rates by the area of the perforation tunnels. The porous medium has the properties of the Clashach rock (k=553 mD, β=1.035E8 m^{-1}), and fluid has a specific gravity of 0.7, density of 88 kgm^{-3} and viscosity of 0.0133 mPa.s (0.0133 cp) unless otherwise stated. The results show that an increase in r_p improves PR. This improvement is more pronounced at higher velocities, as the increase in flow area reduces the negative impact of inertia in the perforated system to a higher extent at these conditions. It is also noted that there are higher PR values at higher velocities. This is because for these perforation designs with S_p<0, the negative impact of inertia is more pronounced in the open-hole completion compared with the perforated completion.

Figure 5.12 shows that increasing perforation density (N) also improves PR and to a greater extent at higher velocities. A comparison of the results of Figure 5.11 and 5.12 emphasises that N is a more effective parameter in improving productivity compared to r_p. That is, at a velocity of around 1000 m/day for instance, an increase in r_p from 0.15 in to 0.25 in, which results in an increased perforation area by a factor of 1.67, improves

PR by around 0.06 (Figure 5.12). However, an increase in perforation area by a factor of 3 (Figure 5.12) when moving from 4 SPF to 12 SPF increases PR by more than 0.4 at the same velocity.

Figure 5.13 is a plot of PR versus velocity at three different perforation lengths (L_p). The data on this plot show that an increase in L_p can significantly increase PR. That is, at the same velocity of 1000 m/day, the increase in L_p by a factor of five improves PR from 0.7 to over 2.2. The improvement in PR by an increase in velocity, noted in Figure 5.11 and 5.12 which were for L_p=30", is consistent with the data of Figure 5.13. That is, at higher L_p values the improvement in PR is more pronounced for high flow rates.

The effect of wellbore radius (r_w) on PR is shown in Figure 5.14. With increasing r_w of an open-hole completion, its performance is improved, but wellbore acts as no flow boundary for perforated completion; hence, for a given perforation design, increasing r_w decreases PR.

Figure 5.15 is a plot of PR versus velocity at three different phasing angles (θ). Comparing the data for θ=60° with those θ=90° shows that where the phasing angle is in the practical range, the impact of its variation on PR is minimal. However, the PR of the perforated systems with θ=0° is much smaller.

Another interesting point which can be seen from Figure 5.15 is the constancy of productivity ratio (i.e. PR=1.0) of the perforation design of θ=0. The perforation skin of this system is zero; consequently its PR for Darcy flow systems is one. The interesting point is that PR does not change with velocity and remains constant and equal to 1.0. This is because the flow geometry of both open-hole and perforated system is almost the same. This issue will be discussed in more detail in Section 5.6.

The effect of flow velocity on PR has been shown to some extent in Figures 5.11 to 5.15. Figures 5.16 and Figure 5.17 illustrate the impact of velocity for a wider range of velocity variation. The perforation arrangement parameters for these plots are shown in Table 5.3. It is noted that PR approaches a constant value at high velocities, and a further increase of flow rate does not influence PR. That is, the difference between the non-Darcy effect around perforation tunnels and that near the open-hole completion does not vary any more at high velocities.

For the results presented above, rock and fluid properties were constant. Figure 5.18 shows the effect of variation of fluid properties on PR. There is not a significant difference between different curves. This is because the effective fluid property that influences Reynolds number in Equation 5.22 is ρ/μ ratio (the inverse of kinematic viscosity), which has not changed significantly in these simulations (Table 5.4).

The effective rock parameter that influences Reynolds number is the kβ product (Equation 5.22). Generally, for rocks with a high k value, the β value is low and vice versa; hence their product does not vary so much for different rocks. For instance, for Clashach sandstone (k=553 mD, β=1.035E8 m^{-1}) and Texas Cream carbonate rocks (k=9.1 mD, β=3.927E9 m^{-1}) with significant difference between their k and β values, their kβ product are 57.2 μm and 35.7 μm, respectively. Therefore it can be expected that at the same velocity and for the same perforation design, the PR of different formations with these two rock properties, affected by inertial effect, will not be very different (see Figure 5.19).

5.5 Gas Condensate Flow around Perforated Wells

The velocity effect in the gas condensate reservoirs is more complicated than that in single phase systems. In single phase systems, inertial and viscous forces compete to control flow, whilst in gas condensate flow there is a complex competition between inertial, viscous and capillary forces. The inertial effect, similar to that in single phase systems increases pressure drop, or reduces effective permeability, whilst the coupling effect decreases pressure drop, i.e. increases effective permeability (Danesh *et al.,* 1994: Jamiolahmady, 2000).

Previous studies in the Heriot-Watt Gas Condensate Research group have shown that basically the coupling effect is more dominant in low- to medium-velocity ranges, while inertia becomes more important at medium- to high-velocity ranges. However, as these effects are complex functions of fluid and rock properties, there is no simple method or criterion to define the flow regime and the magnitude of the importance of each effect (Jamiolahmady, 2000).

The gas condensate flow around perforated wells has been investigated by Jamiolahmdy and his co-authors in several papers, e.g. Jamiolahmady *et al.* (2005, 2006, and 2007).

In 2007, the authors investigated the effects of production rate, fluid properties and perforation parameters on the well performance and productivity ratio of gas condensate systems. The main conclusion of this study was that, at a certain velocity, the overall velocity effect and consequently the absolute value of the flow skin in gas condensate systems are less than those in single phase systems.

5.6 Equivalent Open-Hole System

In the simulation of cased perforated systems, with commercial simulators, instead of using very fine grids in the scale of perforation radius - which is impractical - an Equivalent Open-Hole (EOH) system is simulated. The effect of perforations on well productivity is usually expressed in an EOH system with either total skin factor, or an effective wellbore radius (with or without damaged skin factor).

For Darcy flow systems, the main difficulty in defining an EOH system with a skin factor can occur only in fine grid models with a negative skin factor. In this case the commercial simulator might shut the well automatically because of the negative estimated well-block transmissibility. Otherwise, there is no significant difference between the two approaches.

However, when the effective permeability depends on flow velocity, the definition of an EOH system which replicates that of perforated completion requires particular attention.

In Section 5.2, the mechanical skin of perforated systems was discussed and formulated. Basically, mechanical skin represents the mechanical differences between the real well and the open-hole well. In other words, it includes geometrical and average permeability differences. When the completion is under the Darcy flow regime, the whole difference is represented by mechanical skin and it is equal to total skin. However, in the presence of a non Darcy flow, where the relation between pressure drop and flow rate is not linear, the velocity differences amongst perforated completion and the open-hole system could result in more differences between the well performances of the two systems. This difference is represented by flow skin. Thus the magnitude and importance of flow skin are dependent on the differences between flow behaviour in the real system and that in the defined open-hole system.

According to the conventional/old definition of flow skin, the flow in the open-hole system is defined as Darcy flow consequently the old-flow skin includes all non-Darcy effects from the exterior boundary to the wellbore; thus it could have a considerable value.

In this chapter, to prevent confusion, this definition of flow skin is called old-flow skin and it is denoted by S_F^{old} .

For dry gas systems, old-flow skin is defined by the following equation.

$$\dot{m} = 2\pi kh \frac{\int_{P_w}^{P_e} \frac{\rho_g}{\mu_g} dP}{\ln \frac{r_e}{r_w} + S_M + S_F^{old}} \tag{5.23}$$

In this equation all the non-Darcy flow effects are included in old-flow skin and the integral of the numerator is the same as that for Darcy flow systems. When this approach is used in a numerical simulator, the non-Darcy factor between grid blocks must not been taken into account.

Jamiolahmady *et al.* (2005) proposed a new definition for flow skin in perforated systems with the following equation for single phase systems.

$$\dot{m} = 2\pi kh \frac{\int_{P_w}^{P_e} F_{ND} \frac{\rho_g}{\mu_g} dP}{\ln \frac{r_e}{r_w} + S_M + S_F}, \tag{5.24}$$

where F_{ND}, defined in Equation 5.22, includes the extra pressure drop owing to the inertial effect. Here flow skin represents only the difference between velocity effect in the real system and that in the open-hole system, resulting from the mechanical differences. Obviously, if the real system were an ideal open-hole system, the flow skin would be zero.

For gas condensate flow systems, the flow skin factor is defined as follows:

$$\dot{m} = \frac{2\pi kh \int_{P_w}^{P_e} \left(\frac{\rho_c k_{rc}}{\mu_g} + \frac{\rho_g k_{rg}}{\mu_g} \right) dP}{\ln \frac{r_e}{r_w} + S_M + S_F} \tag{5.25}$$

Here, similar to Equation 5.24, all velocity effects, both inertial and coupling effect are included in relative permeabilities, and the flow skin represents only the difference between flow effects in the two systems.

The main purpose of this chapter of study is to define an equivalent open-hole system at which the flow effects are the same as those in the perforated system, such that the magnitude of flow skin can be neglected.

In section 5.3, it was discussed that, in the absence of damage and crushed effects, the mechanical (perforation) skin factor is a function of geometrical parameters as well as anisotropic ratio, k_v/k_h. Thus, it can be proposed that the mechanical skin factor is the summation of geometrical skin and permeability skin.

$$S_M = S_G + S_k \tag{5.26}$$

Therefore Equation 5.25 can be rewritten as follows:

$$\dot{m} = \frac{2\pi kh \int_{P_w}^{P_e} \left(\frac{\rho_c k_{rc}}{\mu_g} + \frac{\rho_g k_{rg}}{\mu_g} \right) dP}{\ln \frac{r_e}{r_w} + S_G + S_k + S_F} \tag{5.27}$$

The geometrical skin, S_G, represents the effect of geometrical parameters on mechanical skin; i.e. this factor explains how far the flow geometry of the open-hole system is from the flow geometry of the perforated system.

The permeability skin, S_k, represents the effect of the variation of permeability on mechanical skin, and it explains how far the permeability in the open-hole system is from the average permeability in the perforated system.

In a perforated system, the geometrical skin is equal to the mechanical skin without damage and anisotropic effect. Thus it can be calculated from the formula for perforation skin, Equation 5.16, with N_k (Equation 5.13) having an anisotropic ratio equal to one.

$$S_G = C_5 + C_6 N_G (C_4 + 1)^{C7} - \ln\left(\frac{r_w + L_p}{r_w}\right) \tag{5.28}$$

After calculating mechanical and geometrical skin factors, the permeability skin can be computed using Equation 5.26.

Now it is intended to use these geometrical and permeability skin factors to define an EOH system in which flow behaviour is similar to the flow behaviour in the cased perforated well system, so that the flow skin would be negligible. This approach is first proposed for single phase flow system, and then it is extended to gas condensate flow systems.

As mentioned earlier, in a single flow system affected by inertia the flow behaviour is characterized by the Reynolds number, which is the ratio of inertial force over viscous force as follows:

$$\mathrm{Re} = \frac{\rho v k \beta}{\mu} \tag{5.29}$$

If an EOH can be defined with an average Reynolds number equal to that of the perforated system, it can be expected that the flow behaviour in both systems is almost the same and the flow skin would be negligible.

The Reynolds number can be split into three parts, as follows:

$$\mathrm{Re} = \frac{\rho}{\mu} \times v \times k\beta \tag{5.30}$$

Therefore the conditions for equality of average Reynolds number in perforated and EOH systems are:

$$\mathrm{Re})_{perf} = \mathrm{Re})_{EOH} \Rightarrow \frac{\rho}{\mu} \times v \times k\beta \Big)_{perf} = \frac{\rho}{\mu} \times v \times k\beta \Big)_{EOH} \tag{5.31}$$

Or in other words:

$$\frac{\rho}{\mu} \Big)_{perf} = \frac{\rho}{\mu} \Big)_{EOH} \tag{5.32}$$

$$k\beta)_{perf} = k\beta)_{EOH} \tag{5.33}$$

$$v)_{perf} = v)_{EOH} \tag{5.34}$$

That is to say, three conditions should be satisfied to have an EOH system with a zero flow skin factor.

The first condition, the equality of kinematic viscosity, is satisfied automatically because in both systems the fluid properties are the same considering the pressure drop across the two systems is the same.

The second condition is the equality of kβ in both cases. Obviously, in non damaged-isotropic formations for both perforated and open-hole systems, kβ is the same. However, even in anisotropic and/or damaged systems, this condition is also almost satisfied. As shown for two different rocks in Section 5.4, any decrease (increase) in permeability is in line with an increase (decrease) in the inertial factor and the difference of the product of these two terms (kβ) is normally not considerable.

The third condition for equality of the Reynolds number in perforated and EOH systems (Equation 5.34) is the equality of average velocities in these two systems. For a certain flow rate, the same average velocity could be gained if the average available area for both cases and also the main distance covered by the fluid to get to the wellbore were the same. Therefore, both average available area and the main distance should be the same; i.e. the flow geometry of both cases should be alike.

As mentioned before, the geometrical skin represents the difference between the flow geometries of an open-hole system and perforated system. Thus if the geometry of the

open-hole can be changed in a way that its geometrical skin becomes zero, it can be assumed that its new flow geometry is the same as the flow geometry of the perforated system. In Equation 5.27, the best geometrical parameter of the open-hole system for combining with the geometrical skin is the wellbore radius.

Thus it is assumed that defining the effective wellbore radius of the open-hole system with the following equation provides the flow geometrical conditions close to the real system.

$$r_w^{'} = r_w e^{-S_G} \tag{5.35}$$

As evidence, in section 5.4 (see Figure 5.15), it was noticed that for a perforated well with zero perforation skin in isotropic formation (zero geometrical skin), PR is 1.0 and it does not change with production rate. For this system, the effective wellbore radius is equal to the real wellbore radius.

For a gas condensate, the flow in addition to the Reynolds number is affected by capillary number and interfacial tension. The capillary number is the ratio of viscous force over capillary force.

$$N_C = \frac{\mu v}{\sigma} = \frac{\mu}{\sigma} \times v \tag{5.36}$$

Thus to have the same capillary number in a perforated well and EOH system, the fluid properties and velocity in both systems must be the same, conditions which have been discussed earlier for the single phase flow systems.

Therefore, in the proposed method for making a perforated system equivalent to an EOH system, in either single phase or gas condensate systems, it is suggested that:

1- Mechanical, geometrical and permeability skin factors are calculated.
2- Then an effective wellbore radius with Equation 5.35 is estimated.

In this case, the following equation must be used to calculate the mass flow rate:

$$\dot{m} = \frac{2\pi kh \int_{P_w}^{P_e} \left(\frac{\rho_c k_{rc}}{\mu_g} + \frac{\rho_g k_{rg}}{\mu_g} \right) dP}{\ln \frac{r_e}{r_w'} + S_k + S_F} \tag{5.37}$$

The author's results indicated that for many practical cases, following this procedure resulted in the negligible flow skin in Equation 5.37.

For instance, Figure 5.20 shows the variation of single-phase flow skin for two perforated systems, (refer to designs 9 and 10 in Table 5.5, which shows their characteristics).

The X-axis of Figure 5.20 is the Reynolds number at perforation surface defined by the following equation:

$$\mathrm{Re} = \frac{\rho v k \beta}{\mu} \quad ; \quad \rho v = \frac{\dot{m}}{Nh\left(2\pi r_p L_p\right)} \tag{5.38}$$

According to Figure 5.20, the flow skin is negligible especially for perforated systems with high perforation length (30 inches) and density (when N_G is small).

A better assessment of the developed method for the estimation of flow rate can be done by making a comparison between the results of 3D perforated models with their EOH models. This comparison for some sets of designs has been done, and the results are shown in Figures 5.21 and 5.22.

Figure 5.21 shows the comparison for Designs-11, with the characteristics defined in Table 5.5. In this system, the phasing angle is zero, which has an unfavourable geometry as it exaggerates the difference between open-hole and perforated completions. The bottomhole pressure is kept above the dew point, so there is single phase non-Darcy flow within the drainage area. Here average absolute deviation between the results of 3D perforated model and the results of 1D EOH model is about 3.7%, which shows a very good accuracy of the developed method.

A similar comparison, but for Design-12, is shown in Figure 5.22. As shown in Table 5.5, in these systems the phasing angle is 90 degrees and there is a two-phase gas condensate flow within the whole drainage area. Here a better agreement is seen in Figure 5.22, with AAD% of around 2.4%.

5.7 D-Factor for Single-Phase Non-Darcy Flow Systems

5.7.1 Open-hole systems

As explained in the last section, when the velocity effects are included in the integral of pseudo pressure, the flow skin of an open-hole system is zero. However, in the widely used old method, the inertial effect is not included in pseudo pressure but it is taken into account by the old-flow skin factor (defined in Equation 5.23).

For homogenous open-hole systems, because of its simple geometry, the expression for the old-flow skin factor of Equation 5.23 can be simply derived. In these systems flow is one dimensional radial so according to continuity equation it can be said that:

$$\rho v = \frac{\dot{m}}{2\pi khr} = \frac{C}{r};\;\; C = \frac{\dot{m}}{2\pi kh} \tag{5.39}$$

Thus Forchheimer equation can be written as follows,

$$\frac{dP}{dr} = \frac{\mu}{k}v + \rho\beta v^2 \Rightarrow \frac{dP}{dr} = \frac{\mu}{\rho k}\frac{C}{r} + \frac{\rho\beta C^2}{\rho^2 r^2} \Rightarrow \frac{\rho}{\mu}\frac{dP}{dr} = \frac{1}{k}\frac{C}{r} + \frac{\beta C^2}{\mu r^2} \tag{5.40}$$

The above equation can be used for the calculation of pseudo pressure difference:

$$\Delta\psi = \int_{P_w}^{P_e}\frac{\rho}{\mu}dP = \int_{r_w}^{r_e}\left(\frac{C}{kr} + \frac{\beta C^2}{\mu r^2}\right)dr = \frac{C}{k}\ln\frac{r_e}{r_w} + \frac{\beta}{\mu_w}C^2\left(\frac{1}{r_w} - \frac{1}{r_e}\right) \tag{5.41}$$

Here it is assumed that viscosity is constant, equal to that at wellbore conditions; μ_w.

On the other hand pseudo pressure difference from the well flow equation (Equation 5.23) is as follows:

$$\Delta\psi = \frac{\dot{m}}{2\pi kh}\left(\ln\frac{r_e}{r_w} + S_F\right) = \frac{C}{k}\ln\frac{r_e}{r_w} + \frac{C}{k}S_F^{old} \tag{5.42}$$

Now equating Equations 5.41 and 5.42 results in the following equation for the old-flow skin.

$$S_F^{old} = \frac{k\beta}{\mu_w}C\left(\frac{1}{r_w} - \frac{1}{r_e}\right) = \frac{k\beta}{\mu_w}\frac{\dot{m}}{2\pi h}\left(\frac{1}{r_w} - \frac{1}{r_e}\right) = \frac{\rho_w k\beta v_w}{\mu_w}\left(1 - \frac{r_w}{r_e}\right) \xrightarrow{r_w << r_e} \tag{5.43}$$
$$S_F^{old} = \mathrm{Re}_w$$

where Re_w is the Reynolds number at the wellbore conditions.

$$\mathrm{Re}_w = \frac{\rho_w k\beta v_w}{\mu_w} \tag{5.44}$$

Equation 5.43 is an interesting result stating that the old-flow skin of an open-hole, containing all inertial effect from the exterior boundary to the wellbore, is simply equal to the Reynolds number at the wellbore conditions.

Velocity at the wellbore can be related with the standard gas production rate as follows:

$$v_w = \frac{QB_g}{2\pi r_w h} \tag{5.45}$$

where B_g is the gas formation volume factor. Thus old-flow skin can be calculated as follows,

$$S_F^{old} = \frac{\rho_w k\beta}{\mu_w} \times \frac{B_g}{2\pi r_w h}Q = \frac{\rho_S k\beta}{2\pi h\mu_w r_w}Q = DQ \tag{5.46}$$

Where ρ_S is the gas density at standard conditions and:

$$D = \frac{\rho_s k\beta}{2\pi h\mu_w} \times \frac{1}{r_w} \tag{5.47}$$

Here D is called D-factor and is dependent on the rock and fluid properties as well as the open-hole radius. In field units the equation of D-factor is as follows, (Dake 1978):

$$D = 2.223\times10^{-15}\,\frac{\gamma_g k\beta}{h\mu_w}\times\frac{1}{r_w} \tag{5.48}$$

where γ_g is the gas specific gravity.

Thus, in the absence of permeability skin, well-inflow equation can be rewritten as follows:

$$\dot{m} = 2\pi kh\frac{\int_{P_w}^{P_e}\frac{\rho}{\mu}dP}{\ln\frac{r_e}{r_w}+DQ} \tag{5.49}$$

As mentioned earlier, In Equation 5.49, the integral in the numerator - delta pseudo pressure - does not contain the inertial effect, and all the inertial effect from the exterior boundary to the wellbore is presented by the old-flow skin, which is equal to DQ, whilst in Equation 5.24 the inertial effect is included in delta pseudo pressure and the flow skin factor is zero.

However it is noticeable sometimes these distinctions have not been made. For instance in the current version of ECLIPSE the inertial effect between grid blocks is calculated and included in the transmissibility among blocks and the inertial effect inside the well block is calculated as DQ. That is to say, at SS conditions, for instance, the following equation is numerically calculated:

$$\dot{m} = 2\pi kh\frac{\int_{P_w}^{P_{wb}}\frac{\rho}{\mu}dP+\int_{P_{wb}}^{Pe}F_{ND}\frac{\rho}{\mu}dP}{\ln\frac{r_e}{r_w}+DQ}, \tag{5.50}$$

where P_{wb} shows the well-block pressure. This procedure exaggerates the inertial effect between the exterior boundary and the well-block because, as was shown earlier, DQ itself includes all the inertial effect from the outer boundary to the wellbore.

The magnitude of this overestimation depends on the grid block sizes. In coarse block models, where the well block is large, because the velocity behind the well block most likely is not considerable, the F_{ND} between blocks is normally about 1 and the inertial overestimation should not be significant. However, in fine grid blocks F_{ND} could be significantly less than one, resulting in considerable overestimation of the inertial effect or underestimation of the well inflow.

5.7.2 Cased perforated systems

The important point that should be noticed is that the D-factor formula is basically proved for the simple geometry of open-hole systems, but not for perforated systems.

However, using the results of Section 5.5, the formulation of the D-factor can be simply modified and its application can be extended to perforated well systems.

In Section 5.5, it was shown that the inertial effect in a perforated well is almost equal to that in its equivalent open-hole system, with the wellbore radius equal to the effective wellbore radius based on the geometrical skin, calculated by Equation 5.35. On the other hand it was shown that the inertial effect of any open-hole system is equal to *DQ* where D-factor is estimated based on its radius. Thus the inertial effect of the equivalent open-hole system can be estimated as *DQ* provided that D-factor is estimated based on the radius of equivalent open-hole, which is effective wellbore radius.

Therefore, the D-factor of a perforated well should be estimated based on its effective wellbore radius, not its true wellbore radius, i.e.:

$$D\big|_{perforated-system} = D\big|_{r_w=r_w'} = \frac{\rho_s k\beta}{2\pi h\mu_w}\times\frac{1}{r_w'} = \frac{\rho_s k\beta}{2\pi h\mu_w}\times\frac{e^{S_G}}{r_w} \tag{5.51}$$

Therefore the difference between the D-factor of a perforated well with that of an open-hole well is dependent on the value of the geometrical skin. For instance for a perforated well with $\theta=90^o$, N=8 SPF, L_p=30", r_w=4" and r_p=0.2" the geometrical skin is -1.69 and its D-factor is about 18% of the D-factor of an open-hole well with the same wellbore radius. Thus the wrong estimation of D-factor of a perforated well with the formula for open-hole systems (Equation 5.48) could results major errors in the prediction of well-productivity/injectivity.

5.8 Summary and Conclusions

Based on the concept of flow resistance, a new method for calculation of perforation skin is introduced. Its calculation can be summarized as follows:

1- Compute N_G, expressing the impact of geometrical parameters.

$$N_G = \frac{r_w^{C_1}}{N^{(C_2+C_3-C_1)} r_p^{C_2} L_p^{C_3}}$$

2- Compute N_K, expressing the impact of anisotropy ratio.

$$N_K = C_4 + \frac{k_V}{k_H}$$

3- Compute perforation skin as.

$$S_p = C_5 + C_6 N_G N_K^{C_7} - \ln\left(\frac{r_w + L_p}{r_w}\right)$$

The coefficients and exponents of the above equations, $C_{1\text{-}7}$, are reported in Table 5.1.

A comparison between the results of this method with the outcomes of the in-house simulator confirmed the accuracy of this method for many different perforation geometries and anisotropic ratios.

It is shown that, for isotropic and moderate anisotropic formations, the results of the new method and Karakas-Tariq method are in agreement. However, for highly anisotropic formation the formula proposed here is consistent and gives more reliable results whilst those of Karakas-Tariq overestimate the negative impact of anisotropy.

The Hagoort method overestimates the perforation skin of anisotropic reservoirs even compared to those of Karakas-Tariq.

The effect of increasing perforation radius and perforation density on well productivity becomes negligible when N_G approaches zero.

Increasing perforation radius, perforation length, and shot density improves the performance of the perforation. However, the perforation length is the most important parameter. That is among the geometrical parameters, perforation length has the most important effect on improving well productivity.

The impact of the above pertinent parameters varies with increasing fluid velocity (i.e. increasing steady state pressure drop across perforated region), but approaches a finite value at high velocities.

The productivity ratio at a given velocity does not significantly vary for different rocks types and fluids, because the variations of permeability and inertial factor product ($k\beta$) and density to viscosity ratio (ρ/μ) are not significant for different rocks and fluids, respectively.

Mechanical skin can be divided into permeability and geometrical skin. The geometrical skin represents the geometrical difference between the perforated system and the open-hole system. The permeability skin represents the difference between the average permeability in the perforated system and horizontal permeability in the open-hole system.

Defining the EOH system based on the effective wellbore radius $r_w' = r_w e^{-S_G}$ will provide a system with zero geometrical skin and negligible flow skin.

The applicability of the above method was verified for single phase and gas condensate systems demonstrating a good agreement between the flow rate of the perforated well (estimated by 3D-perforated well simulator) and that of the equivalent open-hole system (estimated by a 1D-open-hole simulator).

Flow skin of a homogenous open-hole system, including all inertial effect from the exterior boundary of the drainage area to the wellbore, is equal to the Reynolds number estimated at wellbore conditions, Equation 5.43.

The inertial effect of a perforated system can be taken into account by the D-factor method, provided that the D-factor is estimated based on the effective wellbore radius.

References

Ataei, A.: Generalization of Near Wellbore Relative Permeability Correlation and Modelling of Gas Condensate Flow in Perforated Region, PhD Thesis, Heriot-Watt University, April 2004.

Ansah, J., Proett, M. A. and Soliman, M.: "Advances in well completion design: A new 3D finite element wellbore inflow model for optimizing performance of perforated completions", SPE 73760, presented at SPE international symposium and exhibition on formation dame control, Louisiana, Feb 2002.

Behie, A. and Settari A.: Perforation design models for heterogeneous, multiphase flow, SPE 25901, presented at SPE Rocky Mountain Regional/Low Permeability Reservoir Symposium, Denver, Colorado, pp 591-602, 1993.

Brooks, J.E.: "A Simple Method for Estimating Well Productivity" SPE 38148, presented at European Formation Damage conference, The Netherland., 1997.

Dake, L.P.: Fundamentals of Reservoir Engineering, Elsevier Science B.V., Amsterdam, Netherland, 1978.

Danesh A.: PVT and phase behaviour of petroleum reservoir fluids, Elsevier Science B.V., Amsterdam, Netherland, 1998.

Dogula, Y.S.: "Modeling of well productivity in perforated completions", SPE 51048, presented at the SPE Eastern regional meeting, Pittsburgh, Pennsylvania, November1998.

ECLIPSE Reference Manuals, version 2006A, Technical Description, Schlumberger, 2006.

Forchheimer, P.: Hydraulik, Chapter15, pp116-118, Leipzik and Berlin, 1914.

Jamiolahmady M., Danesh A., Sohrabi M. and Ataei R.: "Gas Condensate Flow in Perforated Region", SPE Journal, **12** (1), pp.89-99, 2007.

Jamiolahmady, M., Danesh, A., Tehrani, D.H., and Sohrabi, M.: "Variations of Gas Condensate Relative Permeability with Production Rate at Near Wellbore Conditions: A general Correlation" SPE Reservoir Engineering and Evaluation Journal, **9** (6), pp.688-697, 2006.

Jamiolahmady M., Danesh A., Sohrabi M. and Duncan D. B.: "Measurement and Modelling of Gas Condensate Flow Around a Rock Perforation", J. Transport in Porous Media, **63**(2), pp. 323 – 347, May 2006.

Jamiolahmady M., Danesh A., Sohrabi M. and Duncan D. B.: "Flow around a rock perforation surrounded by damaged zone: Experiments vs. Theory", J. Petroleum Society Engineering, **50**, pp.102-114, 2006.

Jamiolahmady M. and Sohrabi M.: "Single-phase flow in and around perforation tunnel" IASME Transactions, Issue 7, **2**, pp.1288-1297, 2005.

Jamiolahmady M. and Danesh A.: "Flow in Perforated Region Including Non-Linear Effects" presented at Proceedings of the 67th EAGE Conference and Exhibition, Spain, June 2005.

Jamiolahmady, M., Danesh, A., Rezaei, A., Ataei, R. and Sohrabi, M.: "Calculation of productivity of a gas condensate well: application of skin with rate dependent pseudo-pressure" SPE 94718, presented at Proceedings of the SPE European Formation Damage Conference, May 2005.

Jamiolahmady, M.: Mechanistic Modeling of Gas Condensate Flow in Porous Media,

PhD Thesis, Heriot-Watt University, April 2001.

Hagoort, J.: "An Analytical Model for Predicting the Productivity of Perforated Wells" Journal of Petroleum Science and Engineering, **56,** pp: 199-218, 2007.

Harris, M.H.: The effect of perforating on well productivity, Trans., AIME 237, Journal of Petroleum Technology, 18, pp 518-28, 1966.

Hong, K.C.: "Productivity of perforated completions in formations with and without damage", Petroleum Transactions AIME 259, Journal of Petroleum Technology, 27(2), pp 1027-1038, **1975**.

Howard, R. A., and Watson Jr., M.S.: "Relative productivity of perforated casing-I", Trans., AIME, **189**, pp179, 1975.

Pan, Y., and Tang, Y.: "Study on under balance deep penetrating perforating technology", Technical report, South-western Petroleum Inst., Nonchong, Sichuan, China, 1989.

Koltz, J.A., Krueger, R. F., and Pye, D.S.: "Effect of perforation damage on well productivity" JPT, **26** (11), pp. 1303, November 1974.

Locke, S.: "An advanced method for predicting the productivity ratio of a perforated well", JPT , **33**(2), pp. 2481-2488, December 1981.

Karakas, S.M., and Tariq, S.M.: "Semi analytical Productivity Models for Perforated Completions". SPE 18247, SPE Journal of Prod Eng. pp 73-82, 1991.

McDowel, J. M., and Muskat, M.: "The effect on well productivity of formation penetration beyond perforated casing," Trans., AIME 189, 309, 1950.

Saleh, A.M., and Stewart., G.: "New approach towards understanding of near wellbore behaviour of perforated completions", SPE 36866, presented at SPE European Petroleum Conference, Milan, Italy, 1996.

Streeter, V.L. and Wylie, E.B.: Fluid mechanics, McGraw-Hill, pp. 243-249, 1983.

Tariq, S.M.: "Evaluation of Flow Characteristics of Perforations Including Non Linear Effects with Finite Elements Methods". SPE 12781 SPE Journal of Production Engineering, pp.104-112, 1987.

Tariq, S.M., Ichara, M.J., and Ayestaran, L.: "Performance of Perforated Completions in the Presence of Anisotropy, Lamination or Natural Fractures". SPE Journal. pp 376-384, 1987.

Wang, X., Thauvin, F. and Mohanty, K.K.: "Non-Darcy flow through anisotropic porous media" Chemical Engineering Science, **54**, pp. 1859-1869, 1999.

Yildiz, T.: "Assessment of Total Skin Factor in Perforated Wells" SPE Journal of Resrvoir Engineering, pp: 64-76, 2006.

θ	C_1	C_2	C_3	C_4	C_5	C_6	C_7
30	0.092	0.417	0.61	0.0018	0.1	0.743	-0.342
60	0.061	0.453	0.665	0.0018	0.193	0.572	-0.386
90	0.067	0.5	0.69	0.0018	0.285	0.439	-0.412
120	0.066	0.535	0.714	0.0018	0.4	0.369	-0.428
180	0.077	0.566	0.762	0.0018	0.62	0.323	-0.44
360 (0)	0.21	0.673	0.93	0.0018	1.56	0.211	-0.459

Table 5. 1: Constants required for calculation of the perforation skin for 6 different phasing angles.

Perforation skin				
Anisotropy ratio k_V/k_H	**Simulator**	**Hagoort**	**Karakas-Tariq**	**New Method**
1.0	-0.4	-0.27	-0.49	-0.42
0.2	0.12	0.46	0.14	0.11
0.001	5.58	--	8.65	5.64

Table 5. 2: Comparison of the values of perforation skin computed by simulator, Hagoort, Karakas-Tariq and the author's new method.

Perforation design: θ = 90°, N=4 SPF, L_p = 12", r_w = 4.37", r_p = 0.25"

Design	θ /degree	R_w /in	L_P /in	N_P /SPF	R_p /in	α
1	90	6	50	12	0.25	8
2	90	6	30	12	0.25	12
3	90	6	30	4	0.15	12
4	90	6	10	4	0.15	12
5	0	6	50	12	0.25	8
6	0	6	30	12	0.25	12
7	0	6	30	4	0.15	12
8	0	6	10	4	0.15	12

Table 5. 3: The perforation parameters for different designs of Figures 5.16 and 5.17. $\alpha = r_e / (r_w + L_p)$

P/ psi	ρ /kgm^{-3}	μ /cp	μ/ρ /m^{2}s^{-1}
1500	77.34	0.145	1.87E-7
3000	157.4	0.019	1.21E-7
5000	229.5	0.025	1.08E-7

Table 5. 4: Fluid properties of a natural gas with specific gravity of 0.7 at T=200^{o}f (Danesh 1998) used in Figure 5.18.

	Design 9	**Design 10**	**Designs 11**	**Designs 12**
Matrix core	Clashach k=553 mD β=1.035E+8	Clashach k=553 mD β=1.035E+8	Clashach k=553 mD β=1.035E+8	Clashach k=553 mD β=1.035E+8
Fluid	C_1-C_4 (Z_{C1} =73.6%) T=311K, P_D=1865 psia	C_1-C_4 (Z_{C1} =73.6%) T=311K, P_D=1865 psia	C_1-C_4 (Z_{C1} =73.6%) T=311K, P_D=1865 psia	C_1-C_4 (Z_{C1} =73.6%) T=311K, P_D=1865 psia
Number of Data Points	4	4	42	49
Formation Thickness/ft	1	1	1	1
Phasing angle/ degree	90	90	0	90
Perforation Density (N)	4	12	4,8	4
Perforation Length (L_p/in)	20	30	9, 12, 15	9, 12, 15
Perforation Radius (r_p/in)	0.15	0.25	0.2, 0.5	0.2, 0.5
Wellbore Radius (r_w/in)	3	3	1.5, 4.3	4.3
Flow regime	Single Phase, non-Darcy	Single Phase, non-Darcy	Single Phase, non-Darcy	Gas Condesate non-Darcy
GTR_w	1.0	1.0	1.0	0.7, 0.95, 0.96, 0.97, 0.98, 0.99

Table 5. 5: The parameters of different perforated completion designs.

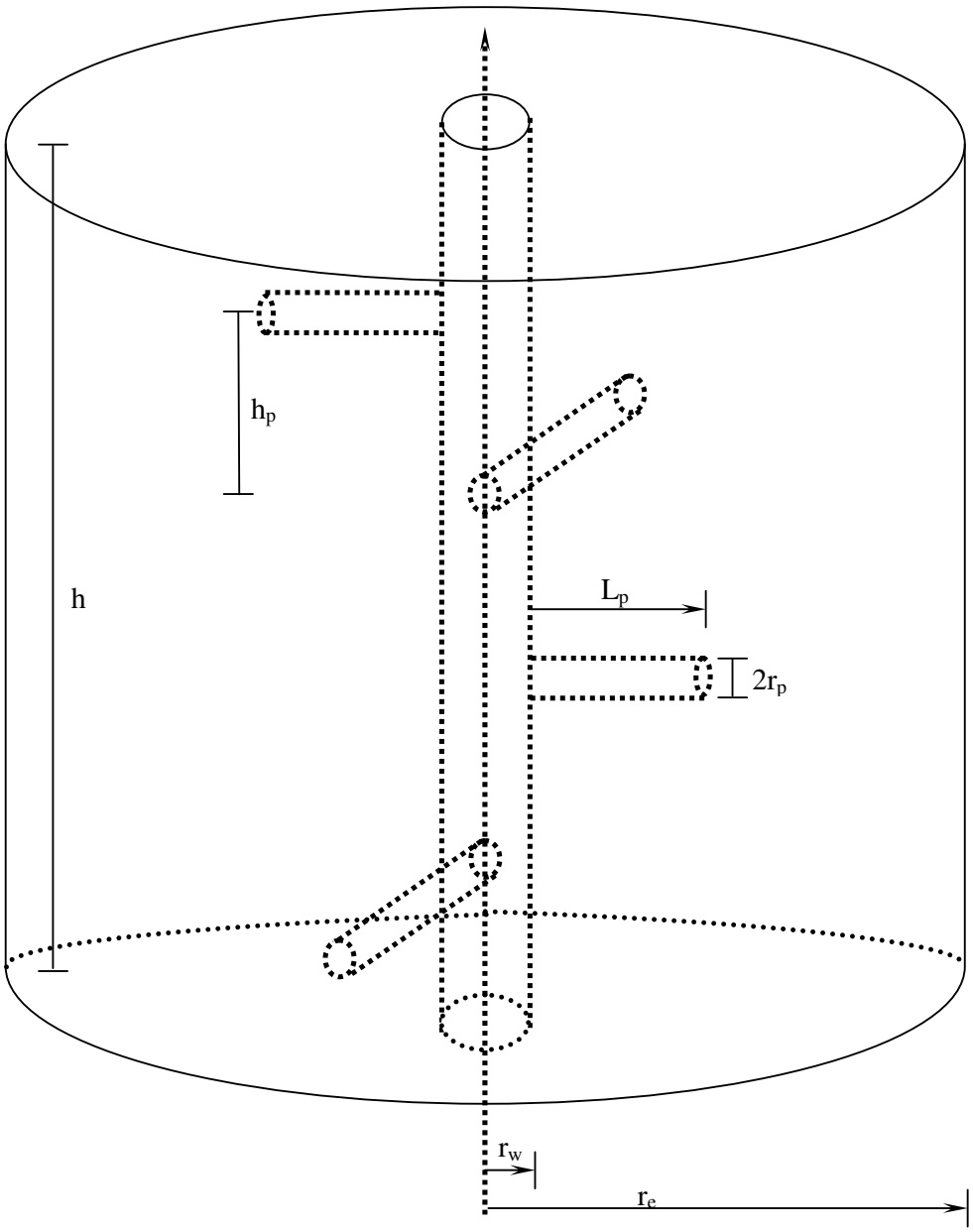

Figure 5.1: A Perforated region with four shots per foot and 90° phasing angle.

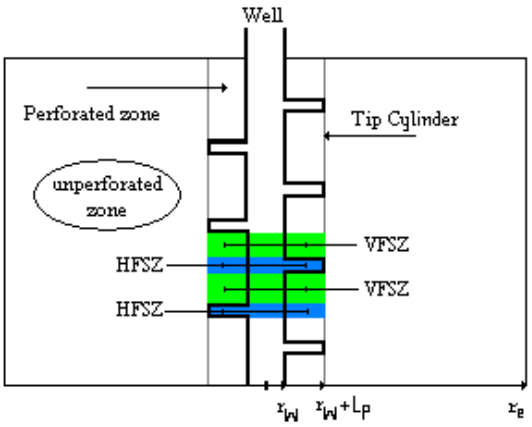

Figure 5.2: Dividing a perforated system into perforated and unperforated zones.

HFSZ = Horizontal Flow Sub-zone

VFSZ = Vertical Flow Sub-zone

Tip Cylinder = Cylinder at the perforation tips

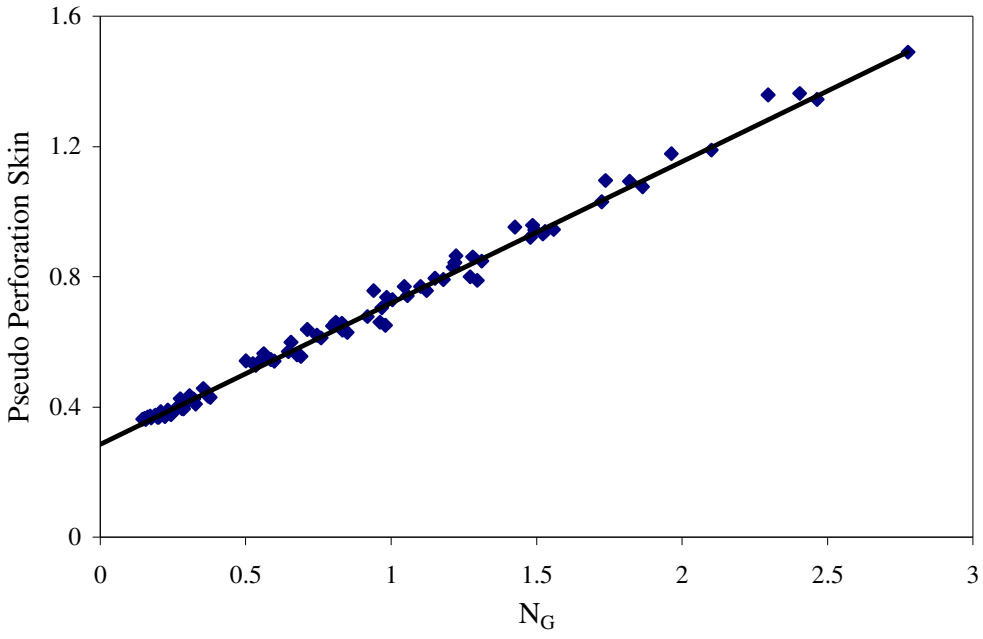

Figure 5.3**:** Variation of pseudo perforation skin, predicted by the HW simulator, versus the geometrical dimensionless number. These results are based on more than 80 different perforation designs with $\theta = 90^o$ in an isotropic formation.

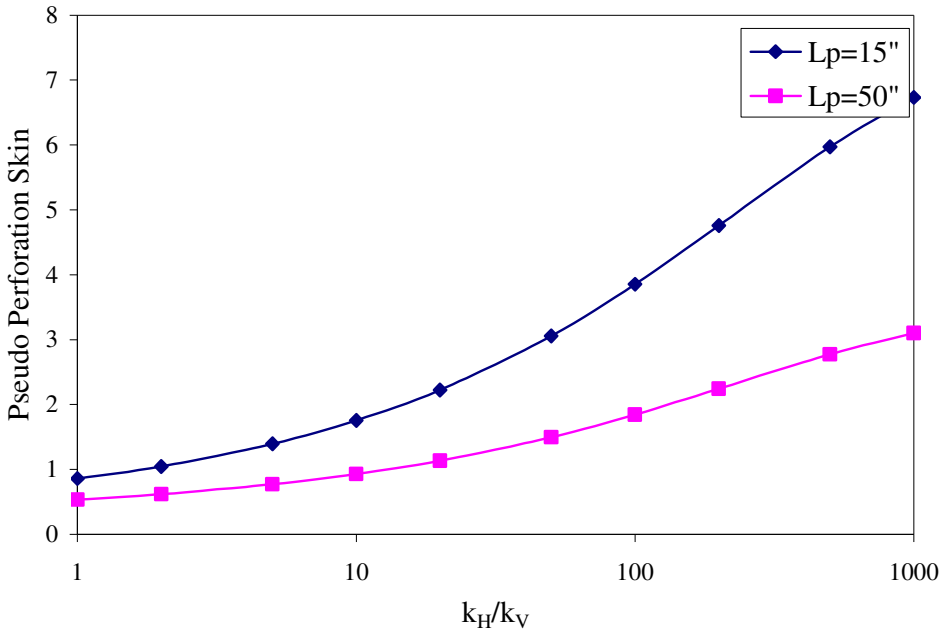

Figure 5.4: Effect of anisotropy ratio on pseudo perforation skin.
System Design: $\theta = 90$, N=4 SPF, $r_w = 4$", $r_p = 0.2$".

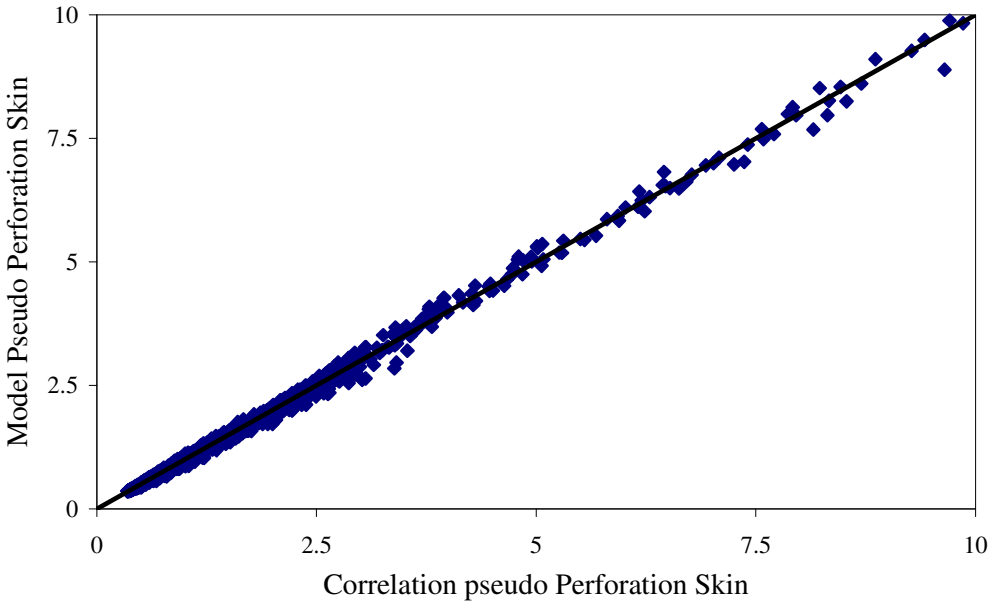

Figure 5.5: Comparison of the predicted skin value by the HW simulator with those by the developed method for 90° phasing angle. The AAD% is 2.8%.

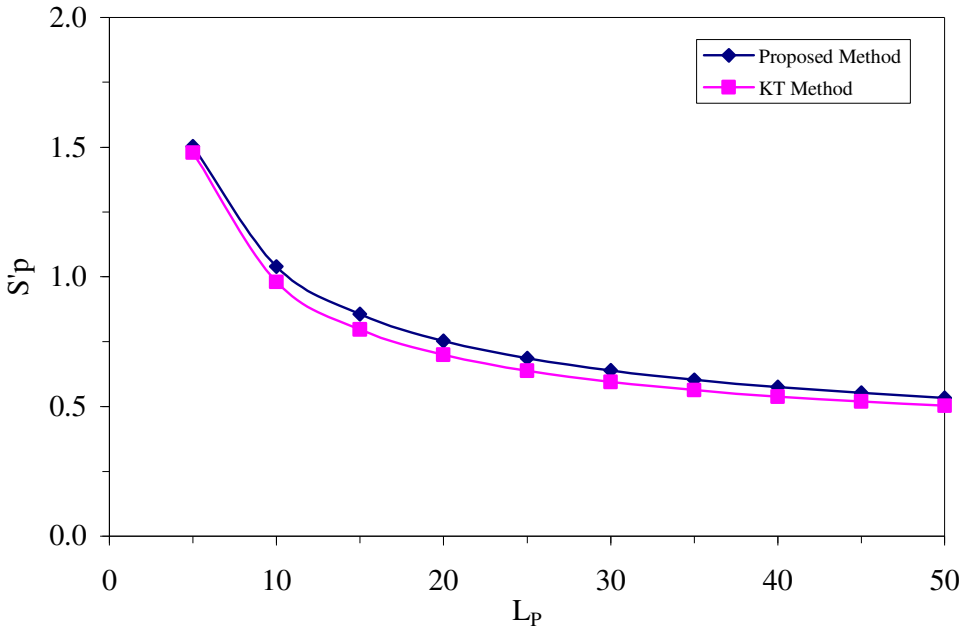

Figure 5.6: Comparison of the results of the proposed method with those of Karakas-Tariq method, isotropic formation, $\theta = 90^o$, N=4 SPF, $r_w = 4$", $r_p = 0.2$".

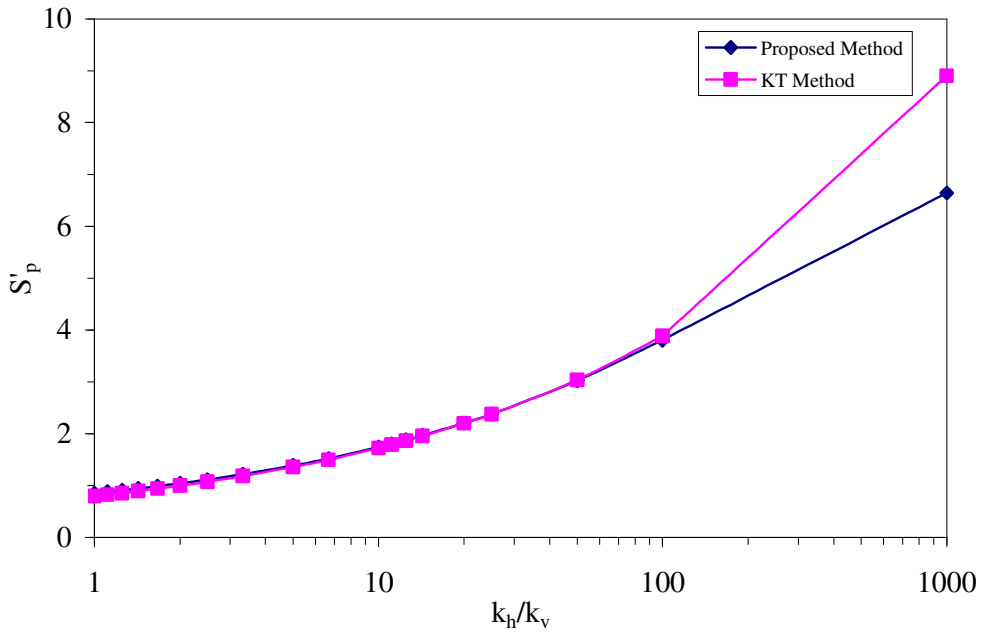

Figure 5.7: Comparison of the results of the proposed method with those of Karakas-Tariq method, anisotropic formation, $\theta = 90^o$, N=4 SPF, $L_p = 15$", $r_w = 4$", $r_p = 0.2$".

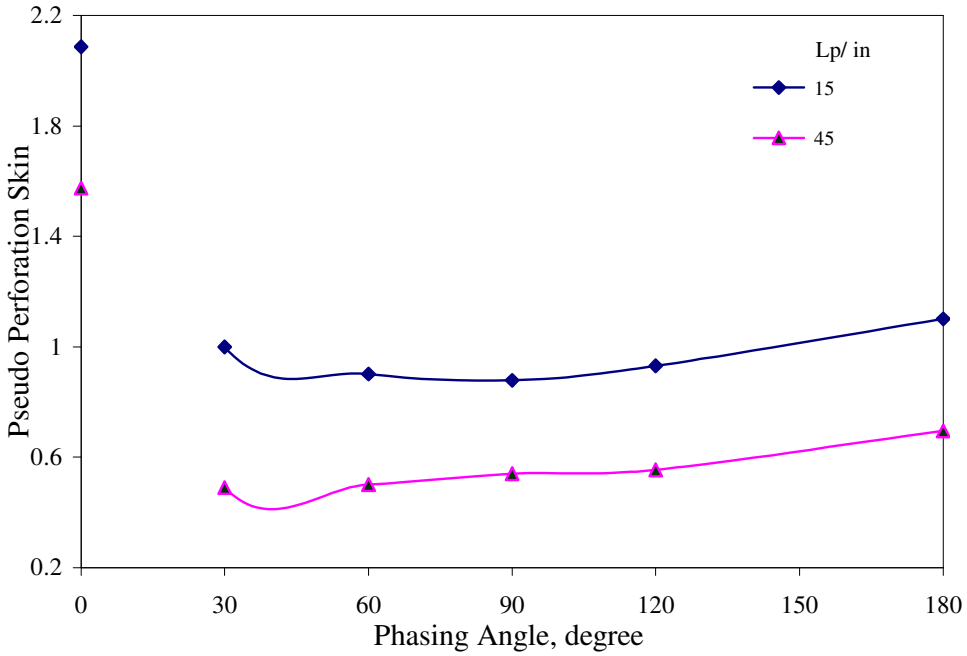

Figure 5.8: Effect of phasing angle on perforation pseudo skin factor in an isotropic formation for two different perforation lengths, N=4 SPF, r_P = 0.2" and r_w =5".

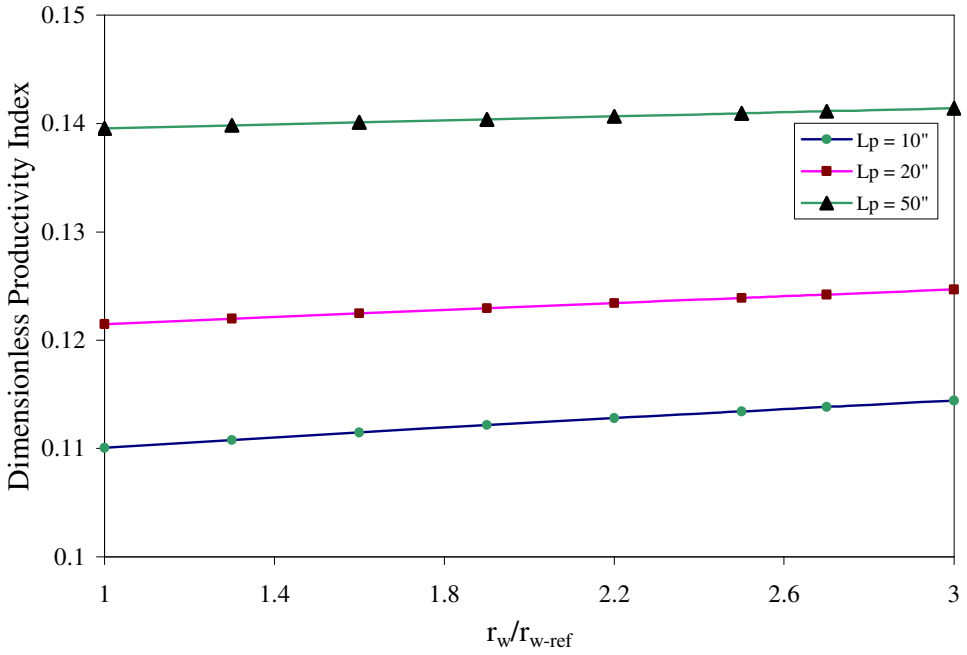

Figure 5.9: Effect of increasing wellbore radius on productivity index, $r_{w\text{-}ref}$ = 3", N = 4 SPF, r_p = 0.2", θ = 90° and r_e= 1000m.

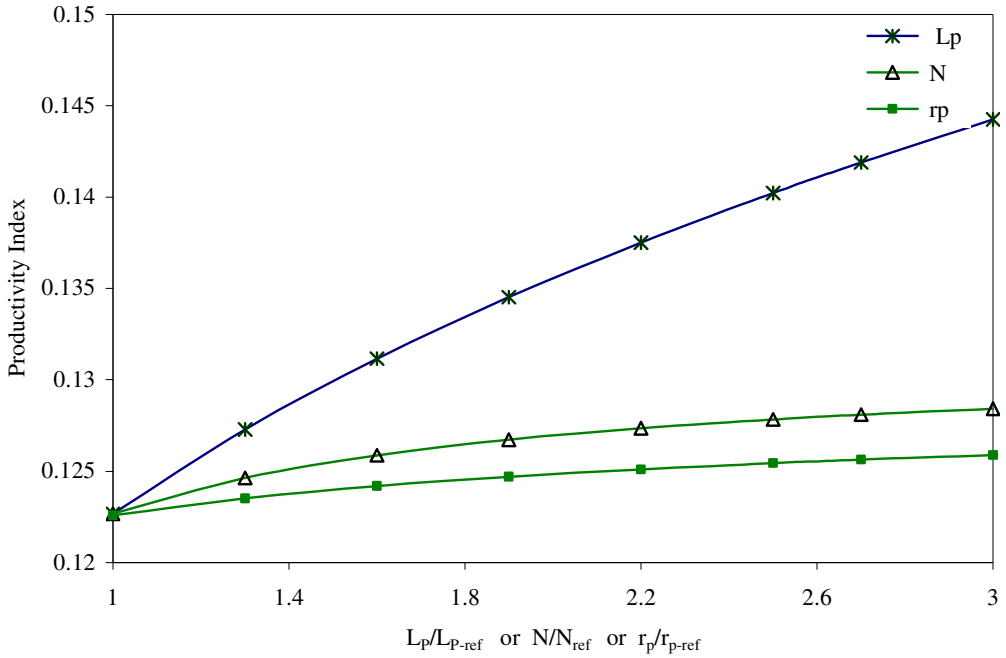

Figure 5.10: Effect of increasing perforation length (L_p), perforation density (N), or perforation radius (r_p) on productivity index.

$L_{p\text{-}ref}$ = 20", N_{ref} = 4 SPF, $r_{p\text{-}ref}$ = 0.2", $\theta = 90^{o}$, r_e= 1000m and r_w= 5".

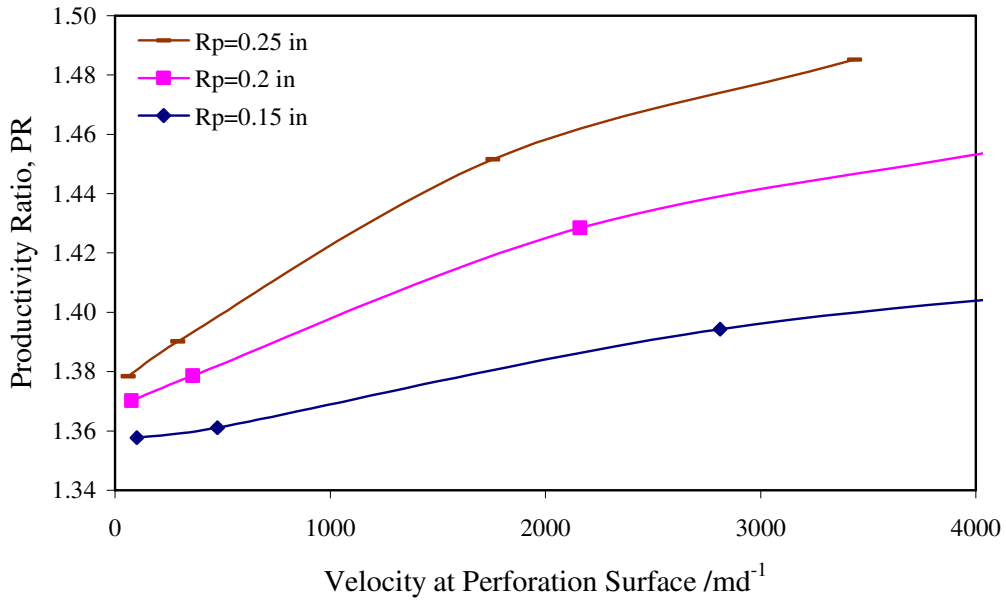

Figure 5.11: The effect of perforation radius on productivity ratio, Clashach core, θ=90°, N_p=4 SPF, R_w=6" and L_p=30".

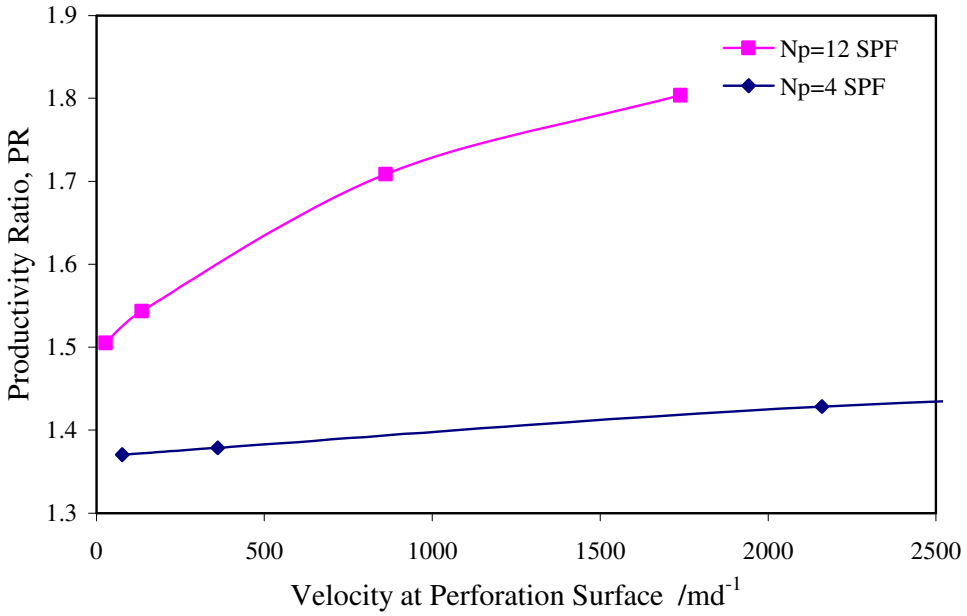

Figure 5.12: The effect of perforation density on productivity ratio, Clashach core, θ=90°, R_p=0.2", R_w=6", L_p=30".

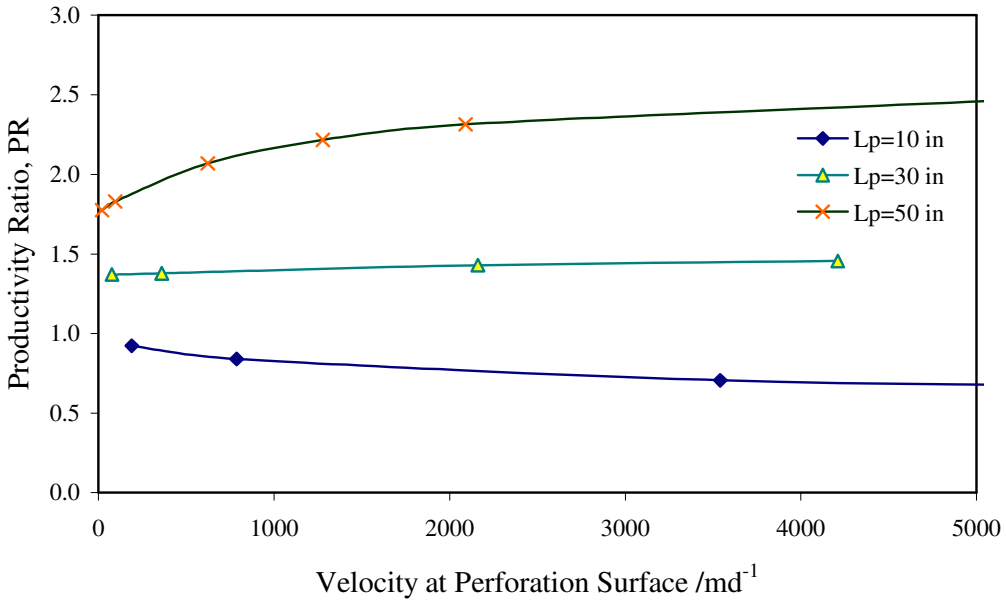

Figure 5.13: The effect of perforation length on productivity ratio, Clashach core, θ=90°, R_p=0.2", R_w=6", N_p=4SPF.

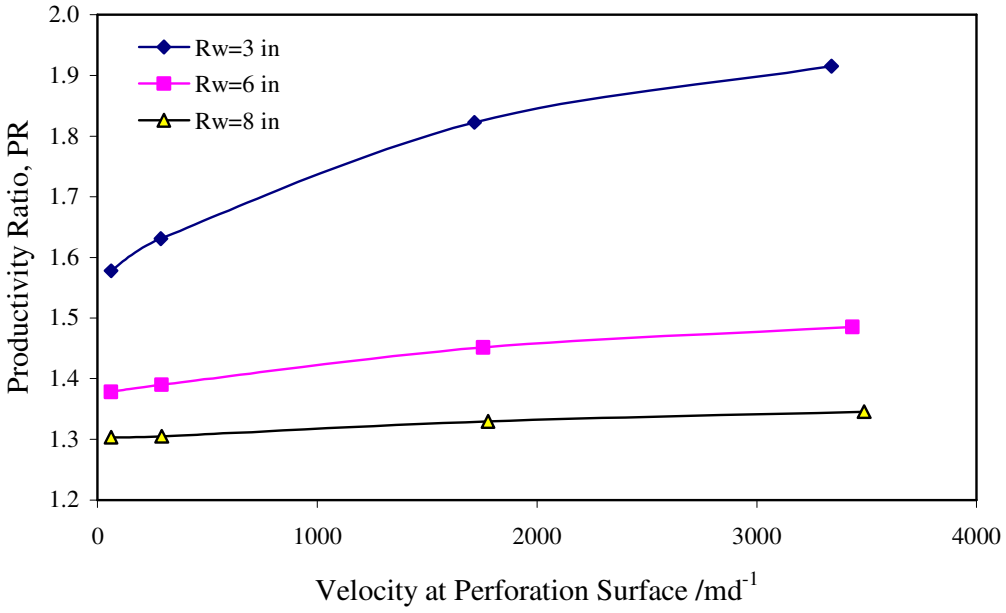

Figure 5.14: The effect of wellbore radius on productivity ratio, Clashach core, θ=90°, N_p=4 SPF, R_p=0.2", L_p=30".

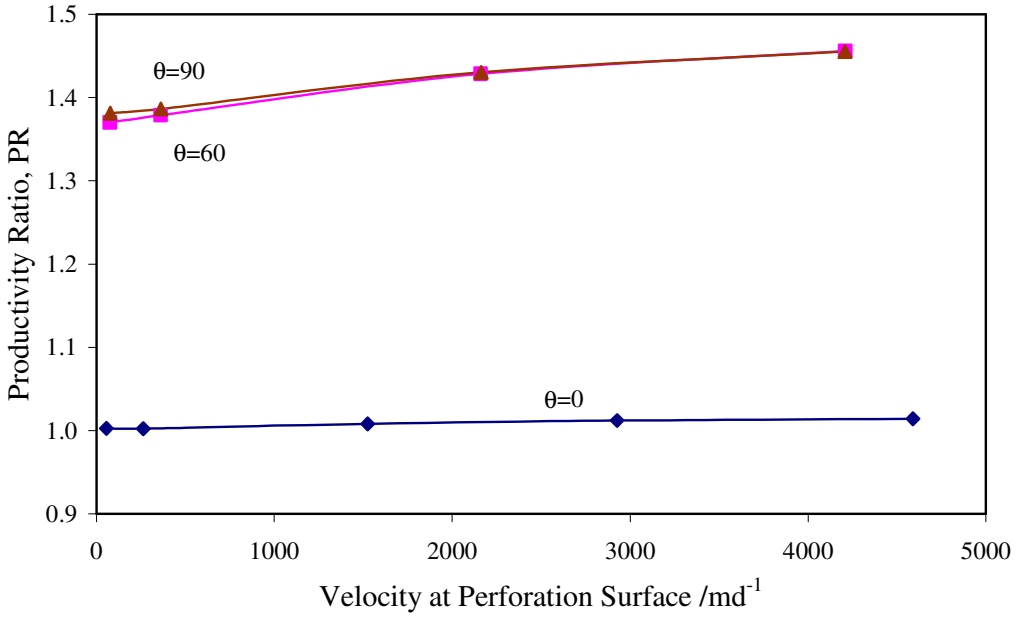

Figure 5.15: The effect of perforation phasing angle on productivity ratio, Clashach core, N_p=4 SPF, R_p=0.2", R_w=6", L_p=30".

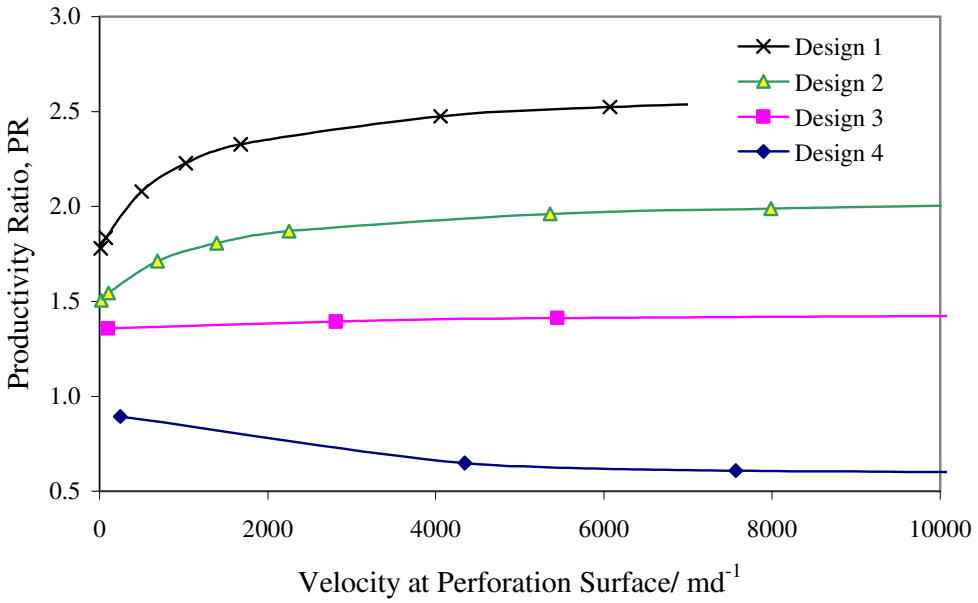

Figure 5.16: Variation of productivity ratio with superficial velocity at the perforations surface, Clashach core, θ=90°, r_w=6", r_e=α*(r_w+L_p), design specifications are given in Table 5.3.

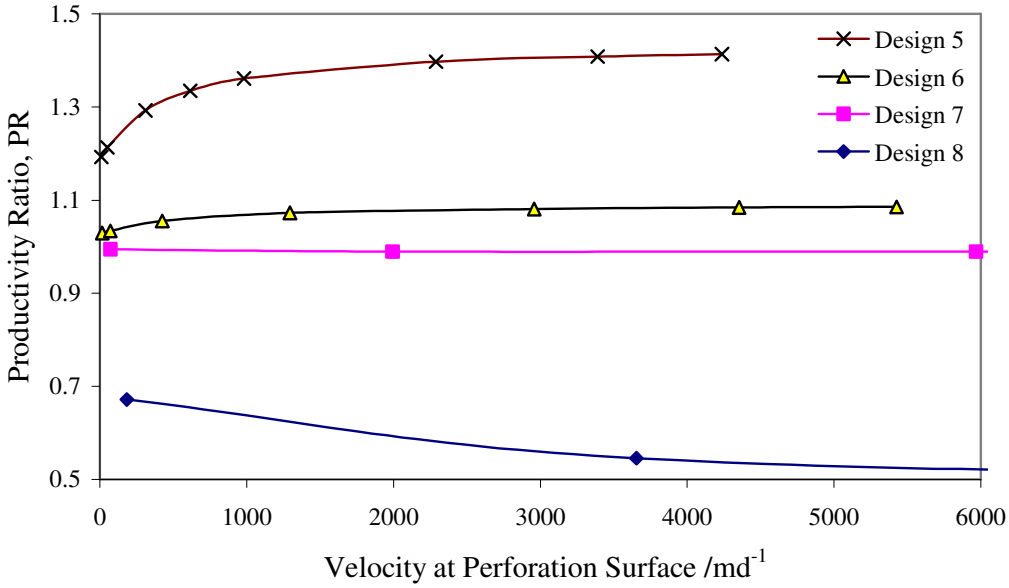

Figure 5.17: Variation of productivity ratio with superficial velocity at the perforations surface, Clashach core, θ=0°, r_w=6", r_e=α*(r_w+L_p), design specifications are given in Table 5.3.

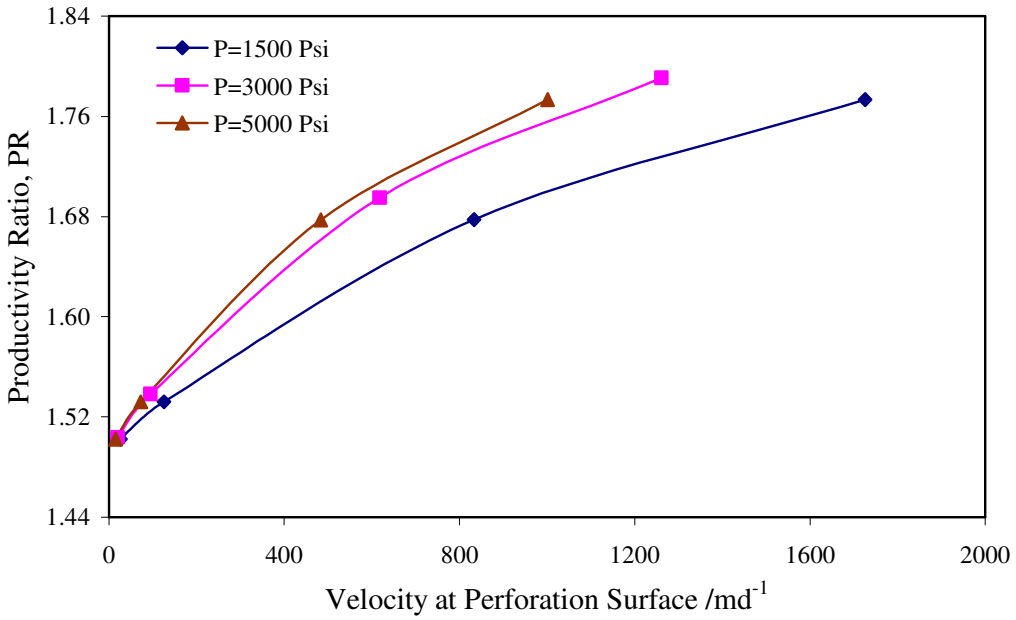

Figure 5.18: The effect of kinematic viscosity on productivity ratio, Clashach core, N=12 SPF, θ=90, r_p=0.2", r_w=6", L_p=30"., natural gas (S=0.7), T=200° F with its fluid properties shown in Table 5.4

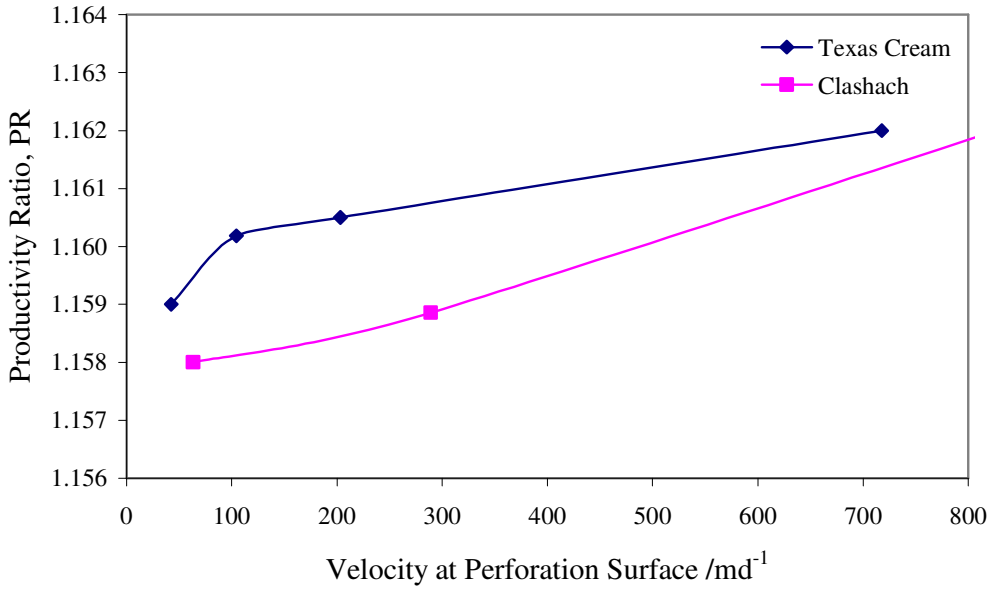

Figure 5.19: The effect of core type on productivity ratio, N=12 SPF, θ=90°, r_p=0.25", r_w=6", L_p=10".

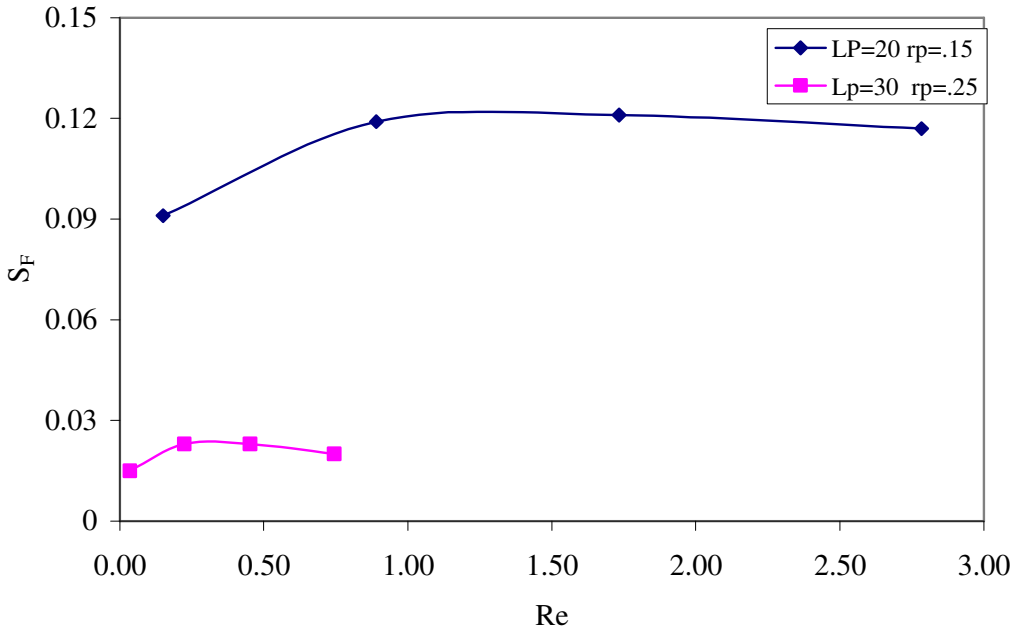

Figure 5.20: Variation of Flow skin in the EOH systems of two perforated wells (Designs 9 and 10 defined in Table 5.5).

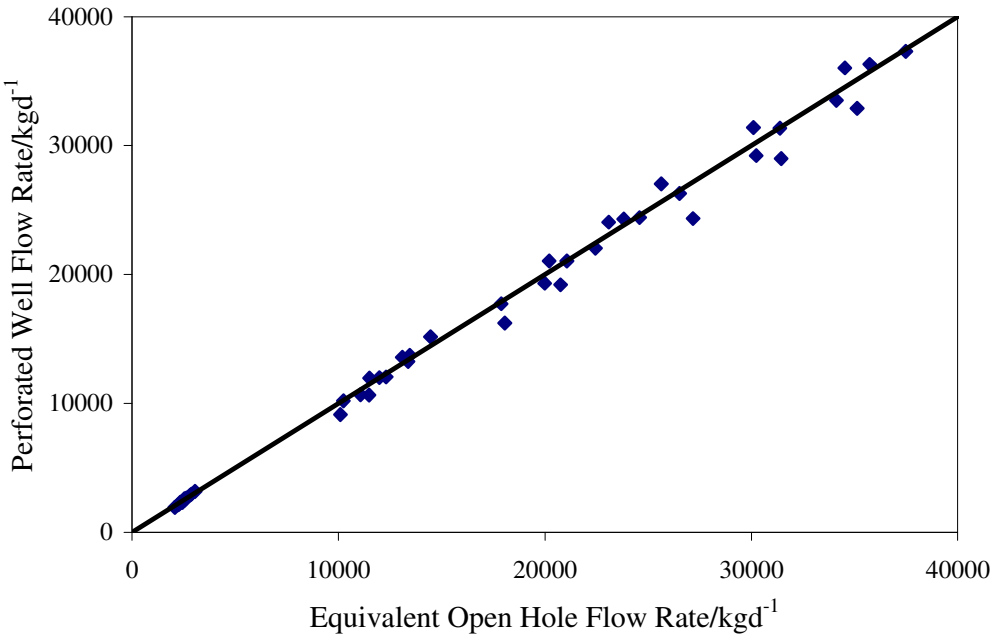

Figure 5.21: Production rate of perforated wells (Systems-11, defined in Table 5.5) versus production rate of their equivalent open-hole wells, Single-phase non-Darcy flow.

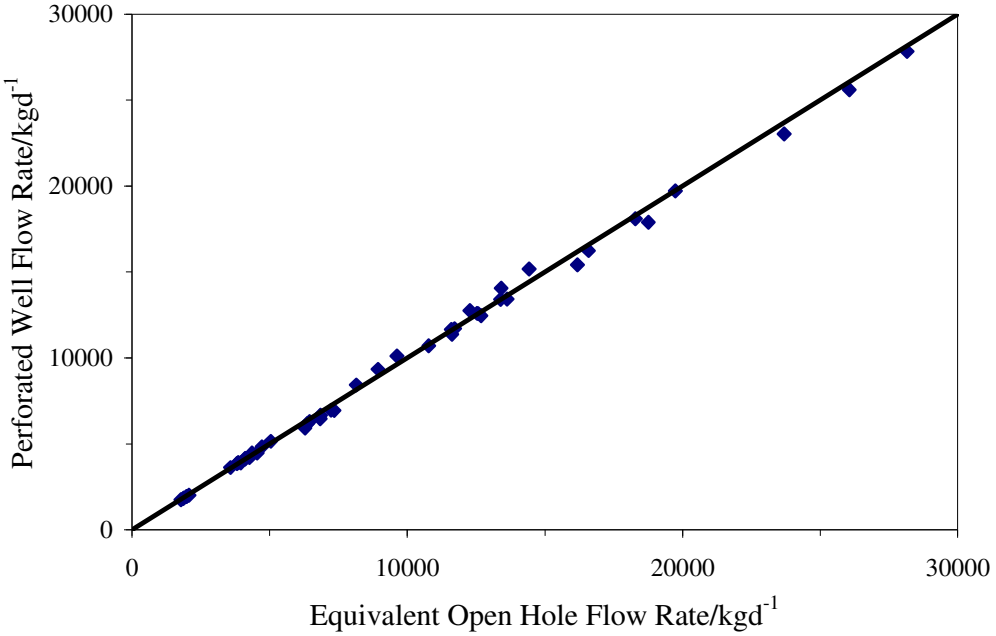

Figure 5.22: Production rate of perforated wells (Systems-12, defined in Table 5.5) versus production rate of their equivalent open-hole wells, two-phase gas condensate flow.

Chapter 6 Conclusions and Recommendations

6.1 Conclusions

This research programme had two different parts: the first part, chapters 3 and 4, was about the study of gas condensate flow around hydraulically fractured wells, while the second part, chapter 5, was about the investigation of gas condensate flow around perforated wells.

The main outcomes of the first part were the development of some new methods for the estimation of effective fracture conductivity, fracture skin, effective wellbore radius, and optimum fracture geometry. The major conclusions can be summarized as follows:

- Flow near to the wellbore of a Hydraulically Fractured Well (HFW) is elliptical, although it converges to radial flow with decreasing fracture conductivity.

- For small propped numbers, the performance of a HFW at steady-state conditions is the same as that at pseudo-steady state conditions; however, for large propped numbers when fracture penetration ratio is greater than 0.2, an HFW perform differently at steady state or pseudo-steady state conditions.

- New formulae were developed for the estimation of effective wellbore radius of an HFW at steady state and pseudo-steady state conditions.

- The dominant velocity effect inside the fracture is the inertial effect whilst inside the matrix (except for the cases in which the IFT ratio is greater than 50) the velocity effect is not significant.

- Guppy's correlation (developed for drawdown) can predict inertial effect on fracture conductivity with high levels of accuracy.

- Inside the matrix, the main source for the difference between k_{rgb} and k_{rg} is the IFT effect.

- A new formula for the estimation of effective fracture conductivity in gas condensate reservoirs was introduced. This formula is applicable for both steady state and pseudo-steady state conditions albeit with different coefficients for each.

- The steady state and pseudo-steady state formulae can predict the effective wellbore radius of an HFW, even in late transient condition, with acceptable accuracy for both cases of constant exterior pressure and closed exterior boundary.

- Different formulae were introduced for the estimation of optimum absolute/effective fracture conductivity and optimum fracture half length for closed boundary and constant exterior pressure drainage area.

- When the optimum fracture penetration ratio is less than 0.2, the optimum fracture design is the same for both steady state and pseudo-steady state, and optimum effective fracture conductivity, depending on the Reynolds Number, can be between $\pi/2$, for low velocity systems ($Re \approx 0$), and π for very high velocity systems ($Re >> 1$).

- For HFW systems with constant exterior pressure, the optimum absolute/effective fracture conductivities are decreased with increasing fracture penetration ratio.

- For HFW systems with a closed exterior boundary, optimum absolute/effective fracture conductivity is increased with the increase in fracture penetration ratio.

The main outcomes of the second part were the development of some new methods for the estimation of perforation skin as well as effective wellbore radius based on the geometrical skin. To be more specific, the major conclusions of this part can be summarized as follows:

- Based on the concept of flow resistance, a new and simple method for calculation of perforation skin was developed.

- It was shown that for isotropic and moderate anisotropic formations, the results of the new method and Karakas-Tariq method are in agreement. However, for highly anisotropic reservoirs, the results could be different.

- The Hagoort method overestimates the perforation skin of anisotropic reservoirs even compared to Karakas-Tariq method.

- The effect of increasing perforation radius and perforation density on well productivity becomes negligible when the geometrical dimensionless number, referred as N_G in chapter 5, approaches zero.

- Increasing perforation radius, perforation length, and perforation density improves the performance of the perforated well. However, the perforation length is the most important parameter. The impact of these pertinent parameters varies with increasing fluid velocity (i.e. increasing steady state pressure drop across perforated region), but approaches a finite value at high velocities.

- The productivity ratio at a given velocity does not significantly vary for different rock types and fluid properties, because the variations of the product of permeability-inertial factor ($k\beta$) and density to viscosity ratio (ρ/μ) are not significant for different rocks and fluids, respectively.

- Perforation (mechanical) skin can be divided into permeability and geometrical skin. Geometrical skin represents the geometrical difference between the perforated system and the open-hole system, while the permeability skin represents the difference between the average permeability in the perforated system and horizontal permeability in the open-hole system.

- Defining an EOH system based on the effective wellbore radius, $r_w' = r_w e^{-S_G}$, will provide a system with zero geometrical skin and negligible flow skin.

- The inertial effect of a perforated system can be taken into account by the D-factor method, provided that the D-factor is estimated based on the effective wellbore radius calculated based on geometrical skin.

6.2 Recommendations

The studies of this research program have been based on some simplifying assumptions; removing some of them would help to bring the results closer to the real situations. Some of these simplifying assumptions which are recommended for removal in future work are:

- *Neglecting the gravity effect on the performance of a perforated well or an HFW.*
- *Neglecting the effect of the perforated case on the performance of an HFW.*

The fracture has been considered as a 2D system with uniform thickness which can be relaxed.

The effect of partial penetration, which has not been investigated here, could also be another area of future research.

A study into the effect of fracture and matrix damages on the productivity of an HFW or a perforated well in gas condensate reservoirs could also be a practical subject.

It is also recommended that the impact of heterogeneity and geological parameters on the performance of hydraulically fractured wells are studied in the future works and the developed equations are modified to be more generalized.

In this study, the approach of an effective wellbore radius for perforated wells based on geometrical skin was developed and verified for gas condensate reservoirs. It is suggested to check if this approach could also be applicable for two phase oil-gas systems and also three phase water-oil-gas in any future work.

It is recommended to evaluate if the formula for effective fracture conductivity presented here could be extended to three-phase flow systems.

In this study, two efficient approaches were followed which provided the formulae for effective wellbore radius of perforated or hydraulically fractured (vertical) wells. Following similar approaches for perforated or hydraulically fractured (horizontal) wells is suggested.

Appendix A: Curve Fitting Method

In this study, the values of the unknown coefficients or exponents of a proposed formula are evaluated based on a curve fitting exercise to match the results of the simulator and those of the proposed formula. In the employed least square method the square of the difference between calculated value by the simulator and that by the proposed formula is computed. Then the summation of these square deviations is minimized to obtain the optimum values of the unknown parameters.

This optimization can be done using the SOLVER option, in the TOOLS Tab, of Microsoft Excel.

The conformity of this curve fitting is evaluated by the percentage of average absolute deviation (AAD%) or standard error of estimate (SEE), which are calculated by the following equations:

$$AAD\% = \frac{\sum_{i=1}^{n} ABS\left(\frac{Z_m - Z_e}{Z_m}\right)_i \times 100}{n} \tag{A.1}$$

$$SEE = \frac{\sum_{i=1}^{n} \left(Z_m - Z_e\right)_i}{n-1} \tag{A.2}$$

Where Z_m and Z_e are the values predicted by the simulator and estimated by the proposed formula, respectively, and n is the number of data points.

For instance to develop Equations 3.28 and 3.35 it is noted that the variation of A and B parameters versus r_{eD} suggests the following two expressions:

$$A = \ln\left(e^1 + \frac{a}{r_{eD} + b}\right) \tag{A.3}$$

$$B = \ln\left(e^{1} + \frac{c}{r_{eD} + d} \right) \tag{A.4}$$

As A and B approaches 1when r_{eD} approaches infinity the exponent of e should be 1.0, with zero uncertainty. However the values of other constants (a, b, c and d) have been evaluated using the above described least square method. In this manuscript while the quality of curve fitting has been reported by AAD% or SEE but the uncertainty of the adjusted constants has not been reported.

Similar procedure has been used for adjusting the exponents in Equation 5.11.

Appendix B: Karakas-Tariq Method for Calculation of Perforation Skin

This method can be summarized in the following steps:

1- Compute horizontal component of skin, S_H:

$$S_H = \ln\left(\frac{r_w}{r_{w_e}}\right) \tag{B.1}$$

Where:

$$r_{w_e} = \frac{L_p}{4} \qquad \text{If} \quad \theta = 0 \tag{B.2}$$

$$r_{w_e} = \alpha(r_w + L_p) \qquad \text{If} \quad \theta \neq 0 \tag{B.3}$$

2- Compute wellbore skin, S_{wb}:

$$S_{wb} = c_1 \exp(c_2 \times r_{w_D}) \tag{B.4}$$

Where:

$$r_{w_D} = \frac{r_w}{r_w + L_p} \tag{B.5}$$

3- Compute vertical skin, Sv, as follows:

$$S_V = 10^a h_D^{b-1} r_{p_D}^b \tag{B.6}$$

Where,

$$r_{p_D} = \left(\frac{r_p}{2h}\right)\left(1 + \sqrt{\frac{k_V}{k_H}}\right) \tag{B.7}$$

$$h_D = \left(\frac{h}{L_P}\right)\sqrt{\frac{k_H}{k_V}} \tag{B.8}$$

$$a = a_1 \log_{10}\left(r_{p_D}\right) + a_2 \tag{B.9}$$

$$b = b_1\left(r_{p_D}\right) + b_2 \tag{B.10}$$

4- Calculate perforation skin as the summation of above skin factors:

$$S_p = S_H + S_V + S_{wb} \tag{B.11}$$

The seven constants required for this method (α, $a_{1\text{-}2}$, $b_{1\text{-}2}$ and $c_{1\text{-}2}$), which are dependent on phasing angle, are reported by Karakas and Tariq (1991).

Appendix C Estimation of Mechanical Skin

When there is Darcy flow regime, the total skin factor can be estimated for three possible cases, as follows:

Case 1: There are just crushed layers with constant thickness present
When there is no damaged layer around the wellbore, the effect of crushed layers around the perforations on increasing flow resistance, represented by the crushed layer skin factor, can be calculated by the following equation:

$$S_{cr} = \frac{1}{NL_P}\left(\frac{k}{k_{cr}}\right)\ln\left(\frac{r_{cr}}{r_p}\right) \tag{C.1}$$

This equation, which is valid for constant thickness crushed layers, can be derived simply using the fact that $\mu S_{Cr}/2\pi kh$ is the difference between the flow resistance of a system with crushed layers and that of a system without crushed layers.

After calculation of perforation and crushed layer skin, the total Darcy skin factor can be calculated by:

$$S_t = S_P + S_{cr} \tag{C.2}$$

Case 2: There are crushed and damaged layers – and perforations terminate inside the damaged layer.
Yildiz (2006) studied this case and concluded that for this case the most accurate way to calculate total Darcy skin factor is by using the following equations:

$$S_{cr} = \frac{1}{NL_P}\left(\frac{k}{k_{cr}} - \frac{k}{k_d}\right)\ln\left(\frac{r_{cr}}{r_p}\right) \tag{C.3}$$

$$S_d = \left(\frac{k}{k_d} - 1\right)\ln\left(\frac{r_d}{r_w}\right) \tag{C.4}$$

$$S_t = \frac{k}{k_d}S_P + S_{cr} + S_d \tag{C.5}$$

These equations are valid just for crushed layers with constant thickness.

Case 3: There are crushed and damaged layers – and perforations extend beyond the damaged layer.

When perforations are longer than the damaged layer thickness, a reasonable way for determination of the skin factors is by using the effective wellbore radius and effective perforation length. As Karakas and Tariq (1991) explained, these parameters can be calculated as follows:

$$L_P^{'} = L_P - \left[1 - \left(\frac{k_d}{k}\right)\right] L_d$$
$$r_w^{'} = r_w + \left[1 - \left(\frac{k_d}{k}\right)\right] L_d \qquad \text{(C.6)}$$

Instead of L_p and r_w these effective parameters (L'_p and r'_w) must be used for calculation of N_G. Besides, if there are crushed layers with constant thickness, $L_p^{'}$ must be used in Equation C.3 to calculate crushed layers skin, S_{cr}. The total Darcy skin factor can then be calculated with Equation C.2.